ESCOLA POLITÉCNICA DA UNIVERSIDADE DE SÃO PAULO

SEGURANÇA EM SISTEMAS METRO-FERROVIÁRIOS

Professor Dr. **Roberto Spinola Barbosa**

São Paulo, 01 Fevereiro de 2017.

ROBERTO SPINOLA BARBOSA

SEGURANÇA EM SISTEMAS METRO-FERROVIÁRIOS

Texto apresentado à Escola Politécnica da Universidade de São Paulo como requisito para obtenção do Título de Professor Livre Docente, junto ao Departamento de Engenharia Mecânica.

São Paulo
2017

ROBERTO SPINOLA BARBOSA

SEGURANÇA EM SISTEMAS METRO-FERROVIÁRIOS

Texto apresentado à Escola Politécnica da Universidade de São Paulo como requisito para obtenção do Título de Professor Livre Docente, junto ao Departamento de Engenharia Mecânica.

Área de concentração: Engenharia Mecânica. Especialidade: Dinâmica e Vibrações.

São Paulo
2017

Catalogação na publicação

BARBOSA, ROBERTO SPINOLA
SEGURANÇA EM SISTEMAS METRO-FERROVIÁRIOS / R. S. BARBOSA - São Paulo, 2017.
270 p.

Tese (Livre-Docência) - Escola Politécnica da Universidade de São Paulo. Departamento de Engenharia Mecânica.

1. DINÂMICA 2. VEÍCULO 3. SEGURANÇA 4. MULTICORPOS 5. FERROVIA I. Universidade de São Paulo. Escola Politécnica. Departamento de Engenharia Mecânica II.t.

DEDICAÇÃO: Ao Gael

AGRADECIMENTOS

Meus sinceros agradecimentos a todos os colegas do Grupo de Dinâmica do Departamento de Engenharia Mecânica da POLI, em particular ao Professor Raul Gonzalez Lima, que generosamente dividiram comigo seu conhecimento desde meu ingresso no grupo.

Agradeço ainda ao Departamento de Engenharia Mecânica da POLI pelo apoio e o suporte financeiro proveniente da FAPESP (projeto de pesquisa nº 2015/25955-9) que com certeza foram bem utilizados.

RESUMO

Este texto é uma sistematização crítica da linha de pesquisa em Dinâmica Veicular, desenvolvida por este autor, ao longo de sua carreira profissional.

A segurança em sistemas metro-ferroviários consiste na capacidade do conjunto veículo/via/operação produzirem o desejado transporte rápido, confortável e seguro. Neste ambiente a dinâmica veicular, a geometria da via e a forma de condução do trem, formam o tripé que estabelece a segurança do sistema metro-ferroviário.

A segurança do veículo metro-ferroviário é a sua capacidade de se adequar às irregularidades da via sem produzir elevada solicitação de guiagem. Quando a relação entre as forças de contato vertical e lateral entre a roda e o trilho (índice *L/V*) é elevada, a probabilidade de descarrilamento aumenta. A possibilidade de estimar este índice permite identificar os locais onde o sistema possui menor nível de segurança. Esta figura de mérito permite direcionar de forma objetiva as ações de manutenção no sistema metro-ferroviário.

A estimação indireta das forças ativas sobre o veículo, requer uma instrumentação especializada para a medição da sua resposta inercial e atitude frente às solicitações externas. Para atender a este desafio, as acelerações translacionais e velocidades angulares de corpo rígido foram medidas utilizando sensores inerciais. Um tratamento de dados especializado para obtenção das acelerações angulares e ângulos foi elaborado. Baseado nas equações da dinâmica de corpo rígido, um algoritmo desenvolvido realiza tal estimativa. Os resultados indicam o nível de segurança contra o descarrilamento do veículo em cada ponto da via para uma determinada velocidade de tráfego.

Na segunda fase deste desenvolvimento sensores complementares distribuídos e de melhor resolução foram empregados para monitorar as acelerações e ângulo de torção longitudinal da suspensão do veículo. Desta forma resultados mais confiáveis do sistema de medição serão obtidos.

O texto descreve de forma sucinta a trajetória desta linha de pesquisa, detalhando seus aspectos tecnológicos e desenvolvimentos realizados e pode ser acompanhado através das publicações produzidas por este autor, contidas nos anexos deste texto. Este trabalho faz parte dos requisitos do concurso de livre docência na Escola Politécnica da Universidade de São Paulo - EPUSP, junto ao Departamento de Engenharia Mecânica.

Palavras-chave: dinâmica, segurança, veículo, ferrovia.

ABSTRACT

This text is a critical systematization of the line of research in Vehicle Dynamics, developed by this author, throughout his professional career.

Safety in railway systems consists of the ability of the vehicle/track/operation assembly to produce the desired fast, comfortable and safe transport. In this environment the vehicular dynamics, the track geometry and the way the train is driven, form the tripod that establishes the safety of the railway system.

The safety of the railway vehicle is its ability to adapt to the track irregularities without producing a high demand for guidance. When the relationship between the vertical and lateral contact forces between the wheel and the rail (L/V index) is high, the probability of derailment increases. The possibility of estimating this index allows to identify the places where the system has a lower level of security. This figure of merit allows to objectively direct maintenance actions in the railway system.

The indirect estimation of the active forces on the vehicle requires specialized instrumentation for the measurement of its inertial response and attitude to external requests. To meet this challenge, translational accelerations and angular velocities of the rigid body were measured using inertial sensors. A specialized data treatment to obtain the angular accelerations and angles was elaborated. Based on the equations of the rigid body dynamics, a developed algorithm makes such an estimate. The results indicate the level of safety against vehicle derailment at each track point for a given traffic speed.

In the second phase of this development, distributed and better resolution complementary sensors were used to monitor the accelerations and longitudinal torsion angle of the vehicle suspension. In this way more reliable results of the measurement system will be expected.

The text briefly describes the trajectory of this line of research, detailing its technological aspects and developments and can be followed through the publications produced by this author, contained in the annexes of this text. This work is part of the requirements of the free teaching contest at the Polytechnic School of the University of São Paulo - EPUSP, within the Department of Mechanical Engineering.

Keywords: dynamic, safety, vehicle, railway.

LISTAS DE ILUSTRAÇÕES E FIGURAS

LISTAS DE ABREVIATURAS

USP - Universidade de São Paulo

EP - Escola Politécnica

PME - Departamento de Engenharia Mecânica

IPT - Instituto de Pesquisa Tecnológica do Estado de São Paulo

CDF - Centro de Desenvolvimento Ferroviário

CBTU – Companhia Brasileira de Transporte Urbano

FEPASA – Ferrovia Paulista S/A

RFFSA – Rede Ferroviária Federal

EFVM - Estrada de Ferro Vitória-Minas

EFC - Estrada de Ferro Carajás

RPC - Remote Parameter Control

AAR - American Associatiation of Railroad

INPI - Instituto Nacional de Propriedade Intelectual

ANTT - Agencia Nacional de Transportes Terrestres

VALE – Companhia VALE S/A

MRS – MRS Logística S/A

UNICAMP - Universidade Estadual de Campinas

ABCM - Associação Brasileira de Ciências Mecânicas

LDSV – Laboratório de Dinâmica e Simulação Veicular

LAC – Laboratório de Automação e Controle

TPN – Tanque de Provas Numérico

CPTM - Companhia Paulista de Trens Metropolitanos

VLT – veículo leve sobre trilhos

TTC – Transportation Test Center

EESC-USP - Escola de Engenharia de São Carlos USP

MBS - *Multibody System*

INRETS - Institut National de Recherche sur le Trasnport et leur Sécurité

MTS – Mineapolis Test Systems Corporation

SAE – Society of Automotive Engineering

UIC – Union Internacionale des Chamin de Fer

FRA – Federal Railway Administration

L/V – razão entre a força lateral e vertical no contato roda/trilho

SI - Safety Index

FFT - fast fourier transform

GPS - Global Positioning System

MEMS - micro eletromechanic measuring systems

IMU – inertial measuring unit

I^2C - protocolo de comunicação

HMI – human machine interface

RAM - random-access memory

A/D – *analogic to digital converter*

AHRS - attitude and heading reference system

DMP - digital motion processor

pitch - movimento de arfagem do corpo

roll - movimento de rolagem do corpo

yaw - movimento de guinada do corpo

LISTAS DE SÍMBOLOS

L – força lateral no contato roda/trilho

V - força vertical no contato roda/trilho

L/V – razão entre a força lateral e vertical no contato roda/trilho

SI – Índice de segurança *(Safety Index)*

m – massa do corpo

a_G - aceleração do centro de massa G do corpo

F_{rodas} - forças ativas nas rodas

g – aceleração da gravidade

G – centro de massa do corpo

$[J]_G$ - matriz de inércia do corpo em relação ao ponto G

α - aceleração angular

ω - velocidade angular

M_G^{ext} – momento das forças externas com respeito ao pólo G

M_{xx} - momento segundo o eixo x-x

SUMÁRIO

1 INTRODUÇÃO

Este texto é uma sistematização crítica da linha de pesquisa em Dinâmica Veicular, desenvolvida por este autor, ao longo de sua carreira profissional de pesquisador, incluindo 20 anos de atuação no Instituto de Pesquisa Tecnológica do Estado de São Paulo – IPT e outros 15 anos no Departamento de Engenharia Mecânica da Escola Politécnica da Universidade de São Paulo – PME/EP/USP. A segurança em sistema veicular consiste na capacidade do conjunto veículo/via/operação produzirem o desejado transporte rápido, confortável e seguro. Neste ambiente a dinâmica veicular, a geometria da via e a forma de condução, formam o tripé que estabelece a segurança do sistema veicular.

O veículo e seus componentes devem ter a capacidade de suportar a carga transportada acrescida dos efeitos dinâmicos. Adicionalmente o veículo deve ter a habilidade de se direcionar adequadamente sobre a geometria e irregularidades impostas pela via. A correlação entre estes dois aspectos decorre da velocidade operacional e seus efeitos longitudinais. Durante a movimentação do veículo as irregularidades da via excitam seus movimentos naturais. A resposta dinâmica do veículo é função da velocidade operacional. Pode haver locais e velocidade de tráfego que excitem modos naturais resultando em fenômeno de ressonância. Este é o ponto focal da linha de pesquisa coroada com a junção destes três aspectos e que será descrita ao longo deste texto.

2 CONTEXTO

Para a contextualização e motivação desta linha de pesquisa alguns aspectos cronológicos e desafios encontrados foram descritos. Foram relatados vários trabalhos precursores realizados por este autor e que contextualizam suas atividades subdivididas em especialidades, independente da data de realização. Descreve as atividades que constituíram as bases para a experiência adquirida. Justifica também o projeto de pesquisa e desenvolvimento do sistema de monitoramento e identificação da segurança do veículo e da via.

2.1 Aspectos Cronológicos

A evolução cronológica das pesquisas sistemáticas metro-ferroviárias na Estado de São Paulo na visão deste autor, remonta a década de 1980 quando foi criado o Centro de Desenvolvimento Ferroviário – CDF no Instituto de Pesquisas do Estado de São Paulo – IPT. A malha ferroviária brasileira atingiu com investimentos públicos e privados, nacionais e internacionais (Ingleses e Americanos), cerca de 38.000 km de extensão em 1960, acompanhando a tendência dos paises continentais, apesar de ter apenas 10% do comprimento da malha americana. Durante o regime militar (1964-1985) a malha foi nacionalizada, reduzida para 30.000 km (1980) e focada em corredores de grande produtividade. Na época grande estimulo do governo federal foi aportado para a construção de novas linhas e para a expansão da industria nacional na produção de material rodante em grande escala (locomotivas e vagões). As antigas empresas de transporte urbano de passageiros (CBTU) e as ferrovias estaduais (FEPASA) e federais (RFFSA e Estrada de Ferro Vitória-Minas EFVM) se desprendiam de suas matrizes internacionais e iniciaram um processo de autonomia tecnológica com quadros próprios de engenheiros, demandando ensaios e estudos especializados. Como laboratório especializado em ferrovia, o Centro de Desenvolvimento Ferroviário – CDF, foi criado com a missão de atender a essa demanda. Foi dirigido inicialmente pelo engenheiro Fernando Bertin Gandara Mendes, onde este autor trabalhou, desde sua graduação como engenheiro mecânico, por cerca de 20 anos.

No início de suas atividades o CDF contou com a ampla estrutura laboratorial do IPT e um moderno sistema de atuadores eletro-hidráulico servo controlado (fabricado pela empresa *MTS*). Este sistema foi doado ao Estado de São Paulo por um convênio com o governo americano (*USAID*). Neste período os trabalhos tecnológicos foram voltados principalmente para ensaios estruturais e cíclicos de fadiga, brilhantemente orientados pelo Professor Otavio Gaspar Ricardo. Os ensaios estruturais consistem na aplicação de cargas estáticas sendo a estrutura monitorada por extensômetros elétricos (*strain-gages*). Este tipo de ensaio era aplicado a caixa do veículo (ensaio de carregamento vertical e compressão) e também ao truque. Então ensaios de fadiga eram realizados nos truques, com diversos atuadores aplicando cargas cíclicas em magnitudes e fases controladas. Eram ensaios longos atingindo

até três milhões de ciclos (*Barbosa*, 1988B). Serviam para qualificar a estrutura do truque para utilização em tráfego na via.

O sistema de atuação eletro-hidráulico da *MTS* possui enorme flexibilidade para ensaios dinâmicos onde pode-se destacar a técnica de ensaio por parâmetros remotos (*Remote Parameter Control - RPC*). A método consiste em amostrar a resposta do comportamento dinâmico do sistema mecânico para o qual se pretende realizar o ensaio e reconstituir sua resposta em frequência no laboratório para identificação do ciclo de carga de entrada ao sistema. Elementos da suspensão de veículos automotivos e metro-ferroviários foram testados com esta técnica. Desta experiência algumas ferramentas tecnológicas foram desenvolvidas. Entre elas podemos citar o algoritmo de contagem de ciclos de solicitação pelo método *Rain-Flow* (*Polese, Barbosa, 1985*) que permite identificar o histórico de solicitação de uma estrutura. Outro programa para quantificação da vida em fadiga da estrutura baseado no capítulo XI da norma americana (*American Association of Railroad - AAR Chapter* VII) foi desenvolvido. Neste caso as tensões e o número de ciclos contados sob a estrutura são aplicados ao critério de dano cumulativo linear de *Palmgren-Miner* para previsão de vida em função das propriedades de durabilidade (curva S-N) do material (*Barbosa*, 2000C).

Outros desenvolvimentos especializados na área metro-ferroviária como a máquina de chave hidráulica para aparelho de mudança de via ferroviária, realizado em conjunto com o Prof. Raul Gonzales Lima (*Barbosa*, *Lima*, et al, 1989) foram realizados. Este desenvolvimento deu origem a patente registrada no Instituto Nacional de Propriedade Intelectual - INPI (PI-89009061). Dois equipamentos especializados de medida de perfil de roda (*Barbosa*, *Mendes* 1989B) e de trilho (*Barbosa*, *Togni* 1992B) foram desenvolvidos. Um algoritmo numérico para a determinação das propriedades geométricas no contato roda-trilho foi elaborado (*Villani* e *Barbosa*, 1997 e *Montandon* e *Barbosa*, 1998). Este software foi objeto de patente no INPI (*Barbosa*, *Polese* e *Villani*, 1994 – Patente nº 94.009.292). Pode-se mencionar também que no IPT, desenvolveu-se um rodeiro ferroviário instrumentado com 120 extensômetros elétricos para a medição das forças de contato.

Durante a implantação dos sistemas de metro na cidade de São Paulo (1974), o IPT foi o palco para o início das atividades estruturadas de pesquisa metro-ferroviárias em São Paulo. Este autor teve a satisfação de pertencer ao corpo técnico da instituição e fazer parte deste período promissor. Apesar do grande número de ensaios de componentes e avaliação de sub-

sistemas metro-ferroviários desenvolvidos na instituição, provendo suporte as tradicionais companhias ferroviárias e dando apoio aos novos sistemas de transporte metropolitanos e metroviários, as expectativas eram sempre maiores que a experiência já existente. Este fato desafiador, mas estimulante, nos conduziu ao avanço.

2.2 Desafios a Vencer

Nos primórdios do sistema ferroviário, os problemas de falhas eram associados a defeitos de sinalização ou rupturas evidentes em trilho ou componentes mecânicos (eixo, roda, etc.). Os problemas de ruptura por fadiga em componentes mecânicos ferroviários remontam ao século XIX quando *August Wöhler* (1842) analisou fraturas de eixos ferroviários (falha por fadiga). Nos primórdios da metalurgia em São Paulo o engenheiro do IPT, *Hubertus Colpaert* (1957) escreveu um livro sobre o tema, com inúmeros exemplos ferroviários de estudos e análises de falhas metalúrgicas realizados pelo IPT.

Quando as eventuais falhas do sistema ferroviário não eram evidentes ou solucionáveis pelo quadro de engenheiros de manutenção das empresas, os eventos graves e às vezes catastróficos, eram quase sempre encaminhados para o IPT. Os descarrilamentos de veículos ferroviários não associados à falhas conhecidas ou fraturas visíveis de equipamentos mecânicos, foram objeto de vários projetos na instituição (*Barbosa*, 1988A). Nesta oportunidade a colaboração do Professor Paulo Sergio Carvalho Pereira da Silva e sua equipe da Divisão de Metalurgia do IPT, foi fundamental para análise metalúrgica de diversas falhas encaminhadas para o nosso departamento.

Cabe mencionar a importância do tema de "segurança operacional nas ferrovias", retratada pela preocupação da Agencia Nacional de Transportes Terrestres – ANTT, que instituiu um Indicador de Desempenho das ferrovias concessionadas. Neste indicador há o índice de segurança operacional da ferrovia, correspondente ao número de acidentes dividido por 1.000 km, que é utilizado para avaliar o desempenho das operadoras ferroviárias (valor típico de 12 ocorrências/1000km).

Inúmeras análises em falhas de componentes decorrente de acidentes foram desenvolvidas em conjunto com o Departamento de Metalurgia do IPT (*Barbosa*, 1989C, 1989D, 1990C). Ensaios preventivos normalizados sobre os componentes (ensaio de fadiga estrutural) foram sistematicamente realizados em testes no laboratório de ensaios dinâmicos do IPT (*Barbosa*, 1988B, 1992C).

A despeito de toda a competência dos diversos pesquisadores do Instituto, alguns eventos permaneciam sem solução comprovada. O desafio foi exatamente construir uma base de conhecimento para abordar e tratar problemas de falhas complexas com múltiplas causas não justificadas em sistema metro-ferroviários.

Portanto os acidentes ferroviários com mecanismo de atuação de difícil compreensão, especialmente os descarrilamentos com causa não evidente, constituíram a motivação da linha de pesquisa perseguida por este autor ao longo de sua carreira profissional e cujo contexto dos diversos aspectos tecnológicos e de segurança serão descritos a seguir.

2.3 Contexto da Dinâmica Longitudinal

Alguns acidentes envolvendo trens longos devido a problemas de freio ou fratura em componentes causaram enormes prejuízos. A magnitude e, portanto a preocupação com estes eventos reside no aspecto do armazenamento de enorme quantidade de energia cinética em trens longos. O controle de velocidade em descida de serra, decorrente da dissipação da energia potencial nos freio causa enorme solicitação térmica nas rodas. Falhas por ruptura de roda devido à reversão de tensão residual interna, quando submetidas à carga térmica cíclica, eram freqüentes. Um evento de ruptura de trilho, causando descarrilamento de apenas um vagão, é suficiente para envolver os demais veículos interconectados do trem, transformando a pequena falha num acidentes de proporções catastróficas.

O tema “Dinâmica Longitudinal de Trem” passou a ter significado importante neste país em função das grandes empresas mineradoras (VALE, MRS), que se utilizam de trens longos de alta produtividade, para transportar minério de ferro em larga escala com trens de até 330

vagões. Para viabilizar tal solução até seis locomotivas distribuídas podem ser empregadas. Desta tendência decorreram desafios na operação e condução do trem em relevo acidentado (serra) típicos deste país. Decorre dai problemas devido a esforços longitudinais elevados, comprometendo a vida útil dos elementos de ligação ente vagões (engates) e causando desgastes em componentes do veículo e da via férrea.

Investigações e medidas experimentais foram realizadas no IPT sobre o tema. Avaliação de desempenho de trens longos com medida dos esforços de tração com engates instrumentados com extensômetros elétricos e devidamente calibrados é um exemplo (*Barbosa*, 1999B). Testes de impacto em aparelho de choque e tração (elemento de dissipação de energia montado em serie com o engate) permitem medida experimental da energia dissipada pelo elemento durante um impacto. Infelizmente o equipamento utilizado para medida (martelo de queda para impacto - *drop hammer*) não é disponível no país. Portanto o modelo do aparelho de choque e tração se vale de dados de literatura ou fornecidos pelos fabricantes do dispositivo.

Em 1984 foi desenvolvido no IPT um programa numérico para a simulação de marcha de trens (*Mendes*, *Felício*, *Barbosa*, *Mechilini* 1984 e 1989A) com auxilio do Professor Luiz Carlos Felício. O programa tinha a finalidade de estudar o comportamento dinâmico de trens longos. Este programa deu origem a uma patente de programa de computador registrada no INPI (nº 90.000.936 - *Barbosa*, et al., 1990). Esta ferramenta permitiu o cálculo dos esforços de tração em trens longos extra-pesados. No laboratório do IPT foram projetados e implementados dispositivos para instrumentação e calibração de engates. Este equipamento era necessário para a realização de medidas experimentais em trens. Outros equipamentos como o dinamômetro para teste de sapata de freio ferroviário (*Barbosa*, 1990B) foram projetados e construídos para atender a demanda da industria nacional.

Em 1993 ainda no IPT, este autor, concluiu seu mestrado em dinâmica longitudinal de trem (*Barbosa*, 1993) orientado pelo Professor Hans Ingo Weber na Universidade Estadual de Campinas (UNICAMP) e produziu artigo publicado em revista indexada nacional da Associação Brasileira de Ciências Mecânicas - ABCM (*Barbosa*, *Weber*, 1996).

Na USP as pesquisas sobre a dinâmica de trem prosseguiram. Um dos projetos relevantes foi o desenvolvimento do Simulador de Trem para treinamento de maquinistas. Este foi um

projeto multi-departamental (LDSV, LAC, TPN) patrocinado pela VALE que resultou no simulador de trem para treinamento de maquinistas mais moderno existente.

Desenvolvido em plataforma *Linux* e códigos em linguagem *C* para rodar em equipamentos convencionais interconectados por rede de internet. Trata-se de um simulador com ambiente completo de imersão virtual (interface homem-máquina, imagem 3D, som, console de comandos, etc.) e modelo matemático incluindo todos os vagões do trem (simuladores antigos foram concebidos com corpos rígidos agrupados) inédito no cenário internacional. Na primeira fase do projeto (entre 2008 a 2010) foram modelados todos os sistemas associados ao trem (conjunto tração, sistema de freio pneumático, dinâmica longitudinal, geometria unifilar da via, sistema de sinalização, formação e despacho de composições) e utilizou-se de recursos modernos inéditos no cenário internacional como geo-posicionamento da via férrea editável, ambiente virtual renderizado topograficamente por foto de satélite e a visão estereoscópica 3D nas telas de projeção. Comporta até 24 estações de treinamento simultâneas, 6 unidades de instrução e conexão remota por internet (*Barbosa* et al, 2008, 2010).

Durante o desenvolvimento da primeira fase do projeto do simulador, o conceito de operação do trem e seus efeitos longitudinais requisitou a modelagem do esforço trativo da locomotiva (motor diesel e elétrico), modelo do sistema pneumático de freio (resposta exponencial e tempo de atraso) e modelo não linear do acoplamento (engate com folga).

Na segunda fase de desenvolvimento (2011 a 2013), incorporou o processamento e visualização em tempo real da dinâmica completa do veículo ferroviário (11 corpos com 66 graus de liberdade), inclusão da malha ferroviária (varias linhas e cruzamentos) interligação entre estações de treinamento (modulo *multiplayier*) permitindo troca de informações entre estações (adequada para treinamento com locomotiva de auxilio) e modulo de visualização de alta definição (*Barbosa* et al, 2011). Finalmente a nível acadêmico um artigo em congresso internacional (*Santos*, *Barbosa*, *Joy*, 2012) e dois trabalhos de conclusão de curso sobre controle da dinâmica longitudinal de trem foram orientados por este autor (*Todesco*, 2011 e *Gilz*, 2014).

Neste tema o conhecimento sobre a dinâmica longitudinal, identificação das solicitações nos engates entre vagões, sobre o conjunto trativo de motores de locomotiva diesel-elétrica, e

sistemas de freio pneumáticos foram consolidados durante a elaboração dos modelos matemáticos, análise de resultados de simulação e medidas experimentais realizadas em campo.

2.4 Contexto de Investigação Experimental Veicular

Diversos trabalhos de investigação e medidas experimentais foram realizados com diferentes objetivos focalizados no comportamento dinâmico de veículos metro-ferroviários.

A então Divisão de Transportes do IPT possuía um laboratório de instrumentação muito bem equipado. Sensores de diversas naturezas (acelerômetros, defletômetros, células de carga, extensiometria, etc.) e sistemas de amostragem de dados digitais (*Lynx*, *LabView*, etc.) compunha o recurso instrumental necessário para as mais diversas atividades de investigação experimental.

Dentre os projetos de investigação e medições realizados no IPT pode-se destacar os intrigantes e sistemáticos acidentes com vagões ferroviários no trecho São Paulo ao Distrito Federal (SR-2) da antiga Rede Ferroviária Federal (RFFSA). Na década de 1990 os recursos para manutenção das linhas foram muito reduzidos. Decorrente desta escassez os acidentes aumentaram significativamente. Devido aos acidentes sistemáticos de vagões tanque que foram associados à falta de manutenção da via, a velocidade operacional foi reduzida unilateralmente e inadvertidamente sintonizada com o modo de balanço lateral do vagão, aumentando o número de acidentes. Para manter a produtividade uma engenharia de sobrevivência era necessária. O trabalho de medição dinâmica realizada no vagão instrumentado permitiu identificar o movimento de balanço lateral do vagão tanque devido irregularidade da via. Este comportamento modal sabidamente alivia a carga vertical e permitiu comprovar este efeito (*Barbosa*, 1992A). A solução proposta foi simplesmente dessintonizar a frequência de excitação alterando a velocidade de operação do trem em via com irregularidades periódicas. Estudo similar foi realizado para SR-10 da região de Bauru no interior do Estado de São Paulo (*Barbosa*, 1995A). Estudo do desempenho dinâmico de vagão

HAD foi realizado na VALE em Vitória, em trecho de via preparada com irregularidades periódicas que permitiu a caracterização modal de seus movimentos (*Barbosa*, 2001A).

Outra investigação experimental desafiadora foi o projeto realizado para a SuperVia, operadora dos trens de subúrbio do Rio de Janeiro onde descarrilamentos sistemáticos ocorriam na saída do trem da estação D. Pedro (*Barbosa*, 2001C). Constatou-se após muitas medidas e análises que o sistema de nivelamento do carro de passageiros que operava em 4 pontos, produzia desequilíbrio de pressão nas bolsas de ar quando o carro permanecia estacionado em via empenada. Durante a partida, como a resposta do sistema pneumático é lenta, ocorria o alivio da carga vertical da roda. A primeira curva era suficiente para produzir carga lateral, aumentando a relação L/V, reduzindo a segurança e propiciando o acidente. Problema similar foi identificado na Companhia Paulista de Trens Metropolitanos - CPTM em São Paulo para carros de passageiros modernos. A suspensão deste veículo contém barras de torção mais rígidas. Esta característica ocasionou o alivio da carga vertical devido a empenamento excessivo na via na entrada da estação do Brás, propiciando o descarrilamento.

A identificação modal experimental também foi ferramenta utilizada para análise em diversas oportunidades (*Barbosa*, 1995B). Para a identificação modal dos veículos, modelos matemáticos e um programa de visualização numérica foi desenvolvido (*Hashimoto*, *Barbosa*, 1994).

Frutos destas competências, diversos trabalhos de avaliação e caracterização dinâmica de vagões foram realizados. Pode-se citar: Análise da Inscrição em Curvas do VLT de Campinas (*Barbosa*, 1995C); Estudo da segurança de carro de passageiro da Estrada de Ferro Carajás (*Barbosa*, 1997B); Avaliação de desempenho e segurança de vagão graneleiro da Ferro-norte (*Barbosa*, 1999C); Estudo de estabilidade do vagão graneleiro (*Barbosa*, 2000A) Avaliação de vagões do tipo gôndola (*HAD*) na Estrada de Ferro Vitória a Minas (*Barbosa*, 2001A); Avaliação do comportamento dinâmico de carro metro-ferroviário da Companhia Paulista de Trens Metropolitanos (*Barbosa*, 2001B); Avaliação de Desempenho e Segurança do Carro de Trem Metropolitano da Série 8000 do Rio de Janeiro (*Barbosa*, 2001C).

Na USP esta especialidade foi continuada. Implantou-se o laboratório de Dinâmica e Simulação Veicular - LDSV (www.usp.br/ldsv) com alunos de graduação e pós-graduação, recursos de software e instrumentos de medição. Neste laboratório foi implementada uma

estação de treinamento do simulador de trens. Desta equipe outras avaliações da dinâmica e segurança de vagão ferroviário foram realizadas (*Grando*, *Barbosa* et al., 2011, 2012).

Em função da experiência adquirida em diversos trabalhos experimentais realizados no IPT para as empresas de operação mero-ferroviária, desenvolveu-se a habilidade na elaboração de "Procedimento de Ensaios". Este tipo de documento se mostrou bastante eficiente na organização das atividades experimentais que envolvam várias áreas dentro de uma empresa. Como não existe pistas de testes no país, os ensaios experimentais só poderiam ser feitos dentro das empresas operadoras. São portanto um estorvo no ritmo operacional das empresas, e a aceitação e colaboração das áreas de engenharia, operação e manutenção são de fundamental importância. Daí a utilidade do procedimento de ensaio que planeja e esclarece com detalhes todas as atividades experimentais a serem realizadas com a colaboração de cada área envolvida da empresa.

Como decorrência da experiência em medidas experimentais e modelagem de vagão ferroviário propôs-se uma patente de suspensão de truque (PI-PI08027226, *Barbosa*, 2008) que permite a inscrição radial de truque em curva. Esta configuração reduz o desgaste das rodas e melhora a segurança do vagão na inscrição em curvas.

O desenvolvimento e sedimentação do conhecimento e experiência sobre instrumentação e medição experimental aplicada ao comportamento dinâmico de veículos foram consolidados devido às atividades intensas realizadas no IPT e na USP.

2.5 Contexto de Modelagem Veicular

A dinâmica de veículos é uma área apaixonante, embora razoavelmente complexa, dentre as diversas áreas da engenharia mecânica. A compreensão do comportamento dinâmico do veiculo é de fundamental importância para avaliação de seu desempenho. O domínio da técnica de concepção física representativa de sistemas mecânicos para elaboração de modelos matemáticos de veículos para a simulação do comportamento dinâmico é essencial para obter

resultados representativos e confiáveis, para a análise de seu desempenho e verificação da segurança.

A evolução da experiência deste autor na área de modelagem de veiculou passou por modelos simples de dois graus de liberdade com elementos lineares de ligação, que foi utilizado para análise de um rodeiro ferroviário e deu origem ao artigo com título: "Dinâmica do Rodeiro Ferroviário" publicado na Revista Brasileira de Ciências Mecânicas (*Barbosa* e *Costa,* 1996). Evoluiu para modelos com 4 graus de liberdade (*Barbosa*, 2012) até modelo completo do veículo ferroviário com sete corpos rígidos e elementos de ligação não lineares (*Barbosa*, 1999A e 2011).

Ainda no IPT este autor teve a oportunidade de participar de dois projetos de intercambio internacional no Japão (1983), período da implantação da Estrada de Ferro Carajás – EFC VALE e nos Estados Unidos (TTC, 1991) acompanhando a análise do carro do Metro-SP. Naquela época o Instituto Nacional de Propriedade Intelectual (INPI) designava compulsoriamente equipes técnicas para acompanhar e absorver tecnologia que permitiu trazer ao país experiência de ponta na área.

A elaboração de diversos estudos contendo modelos de veículo metro-ferroviários como vagões, carros de passageiros e locomotivos foram realizados por este autor. Destas atividades originou-se a motivação para o desenvolvimento do seu doutorado (*Barbosa*, 1999A) realizado na Escola de Engenharia de São Carlos – EESC-USP e orientado pelo Professor Álvaro Costa Neto. Nesta tese a modelagem completa do veículo metro-ferroviário foi realizada utilizando a técnica de sistemas multicorpos (*Multibody System* - MBS). O programa utilizado foi o *ADAMS*®, que emprega o método de *Lagrange* para geração das equações diferenciais de movimento O programa de doutorado teve parte das atividades experimentais sobre mecânica de contato, realizadas em Paris na França (*Institut National de Recherche sur le Trasnport et leur Sécurité* – INRETS, 1997A).

Com intuito de avaliar as condições de operação, conforto e segurança em trens, segundo exigências de normas internacionais (AAR - Chapter XI, UIC-518, EN-14363 e SAE-2631) vários projetos foram desenvolvidos (*Grando*, *Barbosa* et al., 2015, 2016A e 2016B). Dentre eles podemos destacar o modelo do veículo considerando a estrutura da caixa como corpo flexível. Neste caso a estrutura da caixa foi discretizada em elementos finitos (*MSC*-

Nastran®) e seus modos principais de movimentos foram importados para o programa de multicorpos (*MSC-Adams*®). Desta forma a simulação do comportamento dinâmico do sistema incluiu os efeitos de corpo flexível da caixa.

Outro exemplo foi o estudo de desempenho de carro de passageiros incluindo o modelo pneumático de bolsa de ar e o sistema de válvulas de nivelamento da suspensão. Neste estudo o modelo pneumático de *Krettek* foi utilizado (*Grando*, *Barbosa*, et al., 2008). Neste caso a simulação do comportamento dinâmico do sistema incluiu o efeito não linear elásto-pneumático da bolsa de ar com válvulas de nivelamento assimétricas (MSC-*Easy5*®).

No desenvolvimento do simulador de trem (*Barbosa* et al., 2011), projeto multi-departamental na USP realizado por equipes de três laboratórios associados, houve a oportunidade de desenvolver o modelo completo do vagão ferroviário utilizando os programas SD-Fast® e AutoLev®, que se utilizam do método de *Gibbs-Apell* (1900, 1925) para produzir códigos abertos a partir da descrição topológica do sistema de corpos rígidos vinculados sob ação de forçamentos externos. Este modelo é muito eficiente e pode ser processado em tempo real em uma máquina independente. Apresenta também em tela os movimentos do veículo em tempo real, que permite a visualização de causa-efeito entre o trem e um vagão, recurso inédito no cenário internacional.

Na área de veículos automotivos, tese de mestrado (*Marchesin*, 2012) e doutorado (*Vilela* 2010) foram orientadas e artigos produzidos em análise de dirigibilidade de veículos (*Vilela* e *Barbosa*, 2011A, 2011B, 2013) e modelagem de veículos esportivos (*Marchesin*, *Barbosa* et al. 2012, 2016 e 2017). Dois trabalhos de graduação sobre suspensão ativa foram orientados (*Maciel*, 2008, *Moretti* e *Baptista*, 2015) um sobre modelagem completa de veiculo tipo Baja (*Yamagata*, 2012) e outro sobre controle em sistema de freio ABS (*Oliveira*, 2015).

Para enfrentar a descrição de sistemas com muitos graus de liberdade, ou realizar processamento em tempo real, técnicas de redução de ordem de modelos foram exploradas. O artigo sobre "Técnicas para redução da ordem de sistemas dinâmicos na base modal" além da dissertação de mestrado orientada, relatam este método (*Maciel*, *Barbosa*, 2015A, 2015B, 2015C).

Durante a elaboração de modelo de veículo representado por corpos rígidos é de fundamental importância conhecer as propriedades inerciais das partes envolvidas. Para prover aos modelos as massas, sua localização e momentos de inerciais dos corpos, algumas técnicas e ensaios experimentais foram explorados. Entre elas pode-se mencionar a técnica de caracterização experimental modal de veículo, que consiste em excitar o veículo livre de seus amortecedores e medir a frequência de resposta de seu movimento do veículo instrumentado com acelerômetros ou defletômetros. Esta técnica foi empregada para obter as propriedades inerciais de veículos ferroviários (*Barbosa*, 2007).

A modelagem representativa do veículo requer também a correta e detalhada descrição física dos vínculos de ligação e em particular a descrição da mecânica de contato entre a roda e o trilho. É necessário conhecer o movimento relativo oriundo da dinâmica veicular entre as partes na superfície de contato. Este fato justifica a proposta de contextualização de vínculos e contato de rolamento que estão detalhadamente apresentados no item 2.6. Destes diversos trabalhos originou-se uma patente de suspensão de truques (PI-018090005545, *Barbosa*, 2009).

Pesquisas internacionais buscam identificar formas de prever a segurança de veículos. Esta tendência reafirma a atualidade e interesse sobre o tema. Modelo de dinâmica inversa do vagão foi utilizado para estimativa das excitações da via (*Xia* et al., 2007). Trabalhos realizados na Universidade de Tókio (*Hung*, et al., 2010) identificaram grandezas relacionadas com o movimento de parte do truque, que são associadas ao processo de identificação precoce de tendências ao descarrilamento.

O fato da segurança do veículo em tráfego, estar, portanto, intimamente ligada ao tipo e magnitude da excitação recebida da via, justifica a proposta de medição da qualidade da via em função da resposta dinâmica do veículo. Este aspecto está detalhadamente apresentado no item 2.7.

Finalmente o conhecimento sobre modelagem de veículos, seu comportamento modal e estabilidade, foram consolidado devido aos diversos estudos, modelos matemáticos elaboração e análise de resultados de simulação realizadas. Os intercâmbios internacionais colaboraram para o amadurecimento da experiência profissional. De posse destes conhecimentos e experiências a compreensão de alguns acidentes analisados passaram a ter

base fundamentada. Os artigos publicados sobre este tema encontram-se nos anexos deste documento.

2.6 Contexto de Vínculos e Contato de Rolamento

Durante a elaboração de modelos matemáticos de sistemas mecânicos de corpos rígidos é de fundamental importância conhecer as características e propriedades dos elementos de ligação entre os corpos (vínculos). Para fornecer aos modelos as características dos vínculos de ligação, algumas técnicas e ensaios experimentais foram explorados. Entre elas pode-se mencionar os inúmeros ensaios experimentais para a medida de curva de resposta estática e dinâmica de elementos de ligação (molas, amortecedores, coxins, buchas, etc) realizados com o equipamento servo-controlado de aplicação de força (*MTS*) nos laboratórios do IPT.

O contato entre a roda e o trilho numa seção de via produz na região uma elipse, que é função dos raios das superfícies e da carga vertical envolvida. Baseado na teoria de *Hertz* é possível calcular as dimensões da elipse de contato fundamentais para a determinação da rigidez no contato necessária para o cálculo das forças dinâmicas (*Kalker*, 1967, *Johnson*, 1985). Para incrementar a representatividade e qualidade dos modelos elaborados, o contato rodas-trilho numa seção da via foi minuciosamente descrito. Dois equipamentos especializados de medida de perfil de roda (*Barbosa*, *Mendes* 1989B) e trilho (*Barbosa*, *Togni* 1992B) foram desenvolvidos e fabricados. Adicionalmente um algoritmo numérico para a determinação das propriedades geométricas no contato roda-trilho em função do deslocamento lateral do rodeiro foi elaborado (*Barbosa* e *Fuzetti*, 1993) e aperfeiçoado com algoritmos otimizados (*Villani* e *Barbosa*, 1997 e *Montandon* e *Barbosa*, 1998 e *Barbosa*, 2000B). Este programa foi protegido no *INPI* sob nº 94.009.292 (Barbosa, Polese e Villani, 1993). Deste conjunto especializado é possível quantificar a rigidez local do par de rolamento, necessária para a simulação dinâmica (*Barbosa*, 1994A e 1994B). Conhecidos os escorregamentos determinados pelo modelo da dinâmica do veículo é possível calcular as forças instantâneas de contato em função da rigidez do par de contato naquela posição.

O vagão ferroviário de carga é um veículo muito simples. Entretanto alguns elementos de ligação utilizados, que são de baixo custo (prato e pião, cunha de fricção com atrito seco, palmilha de apoio de caixa de rolamento, guia de deslizamento com folga, etc), apresentam uma dificuldade extrema na modelagem e integração numérica. Para os elementos de contato entre superfícies não conformes, desenvolveu-se a utilização da discretização por elementos de ligação com forças tri-direcional e três momentos (vários elementos discretos 6D). Para atrito seco em superfícies inclinadas com pressão variável em função da posição, algoritmos de integração numérica para sistema não linear de alta frequência (*stiff*) foram empregados. Outro elemento de ligação é a palmilha elástica utilizada sobre o rolamento do truque. Em geral este elemento tem apenas a propriedade elástica em uma direção fornecida pelo fabricante. Em alguns casos a obtenção experimental em laboratório é dispendiosa. Para contornar esta limitação pode-se elaborar um modelo em elementos finitos (MSC-*Nastran*®) ou eventualmente modelos não lineares contínuos (MSC-*Mark*®) para obtenção da rigidez angular, torsional, de cisalhamento e deflexão em todas as direções, necessárias para a elaboração de modelagem detalhada.

O pneu automotivo também foi investigado e modelado para estudo de dinâmica de veículos automotivos e monotrilho. Modelos de representação (*Salvagni*, *Barbosa* e *Alves*, 2014) e técnicas de simulação em veículos (*Maciel*, *Barbosa*, 2016) foram desenvolvidas. O trabalho de conclusão de curso de Monteiro (2016), colaborou a acumular dados sobre pneus em função de consorcio internacional estimulado pela *SAE* (*Tire Test Consortium*) que realiza medidas experimentais de pneus em dinamômetro especializado para este fim (*Calspan Tire Test Facility*).

Para garantir a credibilidade no modelo matemático concebido é recomendado utilizar grandezas obtidas de medidas experimentais estáticas ou dinâmicas. Neste tema o conhecimento sobre a mecânica de contato roda-trilho, os elementos elásticos e dissipativos da suspensão de vagão, suspensão pneumática, elementos de ligação estrutural entre truque e caixa, foram consolidados devido as diversos estudos e resultados de ensaios experimentais realizados. Finalmente dispositivos de medida perfil de roda e de trilho associados com algoritmos de tratamento de superfícies foram elaborados, permitindo a determinação das propriedades de contato do par de rolamento roda/trilho essenciais para os modelos de veículos metro-ferroviários foram desenvolvidos.

2.7 Contexto da Via Férrea

A oscilação do veiculo em transito decorre da excitação atuante na sua base devido à geometria e irregularidade da superfície. Para a determinação do comportamento dinâmico do veículo é necessário portanto incluir no modelo físico a descrição da geometria da via férrea.

O projeto básico da uma linha férrea ao longo da topografia do terreno contém retas e curvas, que corresponde à geometria de grande comprimento de onda. As irregularidades são decorrentes de pequenos desvios naturais em torno do traçado geométrico nominal. As irregularidades são em geral quantificadas de forma estatística (desvios em torno de valores médios). As irregularidades têm variações aleatórias e também podem ser descritas pelo seu conteúdo de comprimento de onda no domínio espectral.

A quantificação da geometria da via é fundamental para sua descrição dentro do modelo matemático de simulação. Pode-se medir a geometria da via por topografia (*Barbosa*, 2006). Alternativamente pode-se utilizar espectros padronizados por normas internacionais (*FRA – Manual*, 2014; *EN* 13848-6, 2014) para a geração de geometria de forma aleatória.

A medida da geometria da via, contendo as irregularidades da superfície (trilho), pode ser feita tipicamente por três métodos: a) levantamento topográfico com base referenciada fixa (medida absoluta), É um processo de excelente precisão, trabalhoso e caro. b) medida com régua apoiada em dois pontos (medida da flecha numa corda determinada) que mede a curvatura do trilho. É muito utilizada em função da simplicidade e facilidade de medição. Entretanto é uma medida relativa. c) carro especializado de medida da geometria. Estudos sobre curvatura de linhas em particular a forma clotóide foram realizados por este autor (*Barbosa* e *Villani*, 1998B).

O método de dois pontos de base móvel de movimento continuo é utilizado em carro especializado de medida (carro controle). São veículos especiais de alto custo, mas grande produtividade. Tem a capacidade de medir vários parâmetros de interesse metro-ferroviário (bitola de uma seção, desvio lateral médio, desvio vertical médio, inclinação, torção

longitudinal em base definida, marca quilométrica, etc.) com o carro em movimento. Alguns fornecedores típicos destes equipamentos são: *Plasser & Theurer* (Áustria) ou *Matisa* (Suíça), *Voiture Mauzin* (França), *Ensco* (EUA), *Mermec* (Itália), etc.. Mais recentemente dispositivos de escaneamento a laser (sem contato) foram incorporados e estes carros de medida que foram avaliados por este autor (*Barbosa*, 2006). As medidas são, entretanto de curvatura local e, portanto, medidas relativas devido ao referencial ser móvel.

Muitos pesquisadores em diversas instituições internacionais investiram na identificação da geometria da via utilizando acelerômetros verticais instalados no rodeiro (*Xia*, 2008). Está técnica exige a integração dupla das medições realizadas para resgatar a geometria da via (processo sabidamente sensível devido à possibilidade de divergência).

Buscando contemplar as restrições dos métodos de medida foi desenvolvido um sistema de medição de irregularidades (Pavimetro, *Barbosa*, 2012) que corrige as distorções decorrentes do método de medida em dois pontos. Esta correção das coordenadas medidas de uma trilha é realizada utilizando a função de transferência do dispositivo. Este desenvolvimento foi amparado pela pesquisa realizada por *Aknin* (*Aknin*, 1995) do *Institut National de Recherch sur les Transports et ler Sécurité* (*INRETS*, Paris, França) onde este autor realizou parte experimental do seu doutorado orientado pelo Dr. Jean Pierre Pascal (*Barbosa*, 1997A). Também foi desenvolvida uma rotina de identificação espectral de conteúdo em comprimento de onda das irregularidades que facilita a qualificação do conteúdo de irregularidade em trecho de via. Deste desenvolvimento foram publicados alguns artigos sobre a interação entre o veículo e pavimento com irregularidade medida experimentalmente com excitação pela base (*Barbosa*, 2011A, 2011B) e excitação em dois pontos com atraso de fase (*Barbosa*, 2012). Sistemas de medição mais modernos (exemplo: *Plasser & Theurer*) incorporam sistemas inerciais e de geo-posicionamento, necessários para referenciar a medida feita no referencial relativo em movimento.

O trilho é apoiado sobre o dormente em uma placa rígida de fixação com grampos elásticos. Outro tipo de elemento de apoio é a palmilha elástica. Em geral o fabricante deste elemento fornece apenas a propriedade elástica na direção vertical. Para contornar esta restrição foi elaborado modelo em elementos finitos (MSC-*Nastran*®) para obtenção da rigidez angular, torsional e de cisalhamento em todas as direções. Estes valores são utilizados como propriedades de contato no modelo elástico da via férrea (MSC-*Adams*®-VI-Rail®)

Outro aspecto importante é a rigidez global da grade formada pelos trilhos, dormentes e sistema de fixação (super-estrutura) e o lastro (pedra britada que forma a infra-estrutura). Os modelos mais detalhados do sistema de suporte requerem o conhecimento da rigidez da grade em todas as direções e ângulos. Está técnica de medição foi utilizada em testes de componentes em laboratório e do conjunto na própria via (*Grando*, *Barbosa*, et al., 2015). Adicionalmente, como os componentes da grade são discretos, a elasticidade ou mesmo deformações permanentes, produzem irregularidades periódicas na via (espaçamento entre dormentes ou comprimento da barra do trilho). Especialmente em construção do tipo massa-mola (*floating slab track*), bloco rígidos suspensos em molas ou mantas elásticas, são pré-moldados para suportar os trilho formando espaçamento regulares. No sistema de apoio massa-mola há o agravante da vibração local. As deformações periódicas afetam o comportamento modal do veículo e tem velocidade definida de influência, também investigada por este autor (*Grando*, *Barbosa*, 2012).

Adicionalmente como a infra-estrutura da via se deforma e degrada durante o uso, as irregularidades se alteram ao longo do tempo. Portanto medidas realizadas têm representatividade em determinado período. Este aspecto justifica a necessidade de medição mais freqüente da qualidade da via. Entretanto apenas alguns comprimentos de onda das irregularidades afetam substancialmente o comportamento do veículo. Portanto incluir a resposta dinâmica do veículo no processo de medição das irregularidades qualifica melhor os trechos perniciosos da via.

Neste tema o conhecimento sobre a medição da via, modelagem e descrição dos elementos elásticos de ligação, a descrição geométrica, a caracterização espectral das irregularidades da via, os sistemas de medição experimental das irregularidades da superfície foram consolidados. Os artigos publicados sobre este tema encontram-se nos anexos deste documento.

2.8 Contexto da Interação Veículo/Via/Operação

Tendo consolidadas as técnicas de elaboração de modelos matemáticos a partir da descrição física representativa do veículo, da fonte de tração e frenagem e da geometria e irregularidade da via, agregam-se os três tópicos para obtenção de modelo completo para estudo da interação entre o veículo, a via e a operação. O modelo do conjunto retrata a condição real de operação de um veículo ferroviário trafegando sobre a via férrea irregular e permite o estudo de forma muito detalhada de seu comportamento dinâmico global.

O desenvolvimento de modelo completo do sistema inclui, além dos itens tradicionais, os seguintes tópicos aprimorados por este especialista:

- Elementos de contato discretizados e não lineares;
- Estrutura da caixa como corpo flexível como modos naturais de movimento;
- Sistema de suspensão pneumática com controle de nivelamento;
- Geométrica da via como irregularidades e elasticidade;
- Sistema de tração da locomotiva com controle;
- Sistema pneumático de freio dos vagões;
- Efeito da dinâmica longitudinal do trem.

Para ganhar confiança no modelo concebido é necessário verificar sua representatividade global, realizando validações experimentais. O mundo real é entretanto, bastante complexo dificultando o conhecimento detalhado de todos suas características. A tarefa de interpretar dados experimentais parte do pressuposto do conhecimento de todas as variações das entradas para as quais as respostas são medidas. Então técnicas de ensaios sob condições controladas são convenientes para quantificar a relação entrada × saída. Este técnica consiste em magnificar apenas uma entrada mantendo as demais constantes e verificar a amplitude da resposta da variável de interesse (*single input* × *single output* - *SISO*).

A validação do sistema metro-ferroviário é geralmente realizada pelos seguintes métodos:

- Validação dos Componentes do Veículo;
- Validação dos Componentes da Via Férrea;
- Validação Modal do Carro em Oficina;
- Validação Modal da Via Tipo Massa/Mola;
- Validação do Modelo na Via com Irregularidades;
- Validação das Forças de Contato roda/trilho;
- Validação da Dinâmica Longitudinal do Trem.

A validação dos componentes do veículo, em particular dos elementos de ligação, é usualmente realizada de forma estática em máquinas de ensaio laboratorial. Este aspecto foi apresentado no item 2.6. A validação dos componentes da via férrea, sua descrição geométrica com irregularidades e modos de vibrar, estão apresentados no item 2.7.

A validação modal do veículo consiste em teste experimental bastante útil para ajuste fino do modelo (realizado com o carro parado em oficina). O teste é realizado excitando o carro em seus modos principais e medindo as frequência de seus movimentos livres. O carro é instrumentado com acelerômetros ou defletômetros e flexionado em cada direção preferencial (vertical, lateral e angulares) e abandonado ao movimento. Os dados experimentais obtidos são confrontados com resultados de simulações similares no modelo matemático para efeito de validação modal. Para este teste todos os dissipadores (amortecedores, cunha de atrito, etc.) devem estar desconectados sendo necessário também conhecer o peso próprio do veículo (pesagem estática em balança).

Outra validação típica do modelo do veículo é o percurso em via com irregularidades definidas em condições controladas de tráfego. Neste caso dois trechos consecutivos de via são modificados com irregularidades periódicas normalizadas. As irregularidades são verticais em cada trilho no formato cúspide em fase (implementadas com calços de espessura variável, instalados entre o trilho e o dormente). Esta irregularidade excita os movimentos de galope (*bounce*) e arfagem (*pitch*) do veículo. No trecho seguinte as irregularidades são defasadas para excitar os movimento de rolagem lateral e guinada (*lower sway* e *yaw*). O trem é acelerado passando pelos trechos com velocidade constante e freado em seguida. O capitulo XI da norma AAR fornece indicações para a realização deste tipo de teste. A interação entre

veiculo automotor e rodovia pavimentada também foi explorada por este autor (*Barbosa*, 1998A).

A verificação experimental da dinâmica longitudinal global do trem é algo mais complexo de ser realizado. Exige a medição das forças em engates distribuídos ao longo do trem e forma de excitação impulsiva ou periódica conhecida de difícil produção. Alternativamente os testes de impacto em aparelho de choque e tração permitem a quantificação razoável do aspecto longitudinal para elaboração do modelo (conforme descrito no item 2.3).

A validação das forças no contato pode ser realizada com dados de medida experimental com o rodeiro instrumentado (ver item 2.1). Entretanto medir estas grandezas experimentalmente é muito complexo e de custo elevado. Outra possibilidade é a instrumentação das pernas da estrutura do truque que permite medir, com algumas restrições, as solicitações sobre o rodeiro (soma do L/V de um par de rodas). Alternativamente a técnica de instrumentação dos trilhos (com extensômetros elétricos) em seções consecutivas da via permite medir o L/V. Entretanto esta medida corresponde a apenas uma posição do veículo ao longo da via. Esta última técnica pode ser conveniente para monitorar uma frota de veículos desde que instalada num trecho de via que produza excitação definida no vagão. Entretanto é muito limitada para observar o comportamento dinâmico do veículo.

Testes de múltiplas entrada e múltiplas saídas (*MIMO*) são possíveis de realizar, mas com instrumentação extensa e análise de resultados complexa e trabalhosa. Neste caso análises de representatividade estatísticas, como por exemplo a análise espectral (*fast fourier transform - FFT*) podem ser empregadas.

Um exemplo de estudo completo de desempenho de carro de passageiros com validação dos diversos elementos foi o trabalho realizado em trens da CPTM de São Paulo que incluiu o sistema de controle de válvulas de nivelamento da suspensão com bolsa de ar (*Grando*, *Barbosa*, et al., 2008). Deste estudo resultou a elaboração do artigo sobre diferentes alternativas de sistemas de nivelamento (*Prado*, *Barbosa*, et al., 2011).

Outro exemplo relevante de estudo detalhado e modelagem do comportamento dinâmico do trem foi o trabalho desenvolvido para a empresa Rumo S/A. Neste estudo foi considerando o vagão com caixa flexível, forças nos engates devido ao efeito longitudinal, sistema

pneumático de freio, via elástica irregular sinuosa e locomotiva de grande porte com controle de tração em tráfego em trecho de serra (*Grando*, *Barbosa*, et al., 2016A). Ferramentas de controle para emulação de força de tração da locomotiva diesel-elétrica foram utilizadas no ambiente multicorpos (MSC-*Adams VI-Rail®)* e em co-simulação com o programa *Matlab*.

Cabe mencionar que o simulador de treinamento de maquinistas (ver item 2.3) contem o modelo completo de um vagão que é calculado em tempo real (simulação com processamento paralelo distribuído em máquinas distintas) e disponibiliza informações completas sobre o comportamento dinâmico do vagão. Uma ferramenta de pós-processamento de imagem apresenta todos os movimentos do vagão e indicação das forças, e permite ao treinando associar a relação entre causa-efeito de seus atos de condução do trem (*Barbosa* et al 2011). Finalmente o desenvolvimento das atividades de pesquisa do doutorado de Santos no programa de pós-graduação, resultou na publicação de segurança veicular sobre excitação periódica (*Santos* e *Barbosa*, 2017).

Com os modelos globais validados as simulações permitem obter resultados numéricos dos aspectos de relevância para o analista. Informações das acelerações e deflexões dos diversos corpos permitem a analise de desempenho segundo critérios normalizados (EN-14363). Resultados das variações da força vertical na roda e relação L/V no contato roda/trilho, permitem quantificar a possibilidade de elevação de roda e a segurança respectivamente (UIC-518). As acelerações também são utilizadas para avaliar o conforto (SAE-2631). Nestes projetos as normas internacionais de avaliação de desempenho de veículos (Chapter XI da AAR, UIC-518, EN-14363 e SAE-2631) foram amplamente utilizadas.

Neste tema o conhecimento sobre modelagem de veículos incluindo, seu comportamento dinâmico quando submetido à interação com a geometria e irregularidade da via férrea devidamente validado e influenciado pelos efeitos da operação do trem, foram consolidados devido aos diversos estudos, modelagens elaboradas, validações realizadas, análise de resultados de simulação. A prática analítica absorvida na USP contribuiu na qualidade da produção científica assim desenvolvida, decorrendo na publicação de artigos em revistas indexadas internacionais. A partir deste conhecimento a justificativa de inúmeros acidentes analisados passou a ter base fundamentada para compreensão. Deu também ensejo e contribuição à criação de novas alternativas para monitoramento da segurança operacional de veículos, que é a proposta deste autor.

3 FUNDAMENTOS DE SEGURANÇA

A segurança de um sistema de transporte é a capacidade de cumprir sua missão adequadamente, com eficácia e segurança. Para fundamentar esta proposta de pesquisa (desenvolvimento do sistema de monitoramento da via e segurança do veículo) é necessário conhecer a natureza dos acidentes (perda da segurança), qualificar as razões que os acarreta, quantificar sua incidência e magnitude e identificar formas de mitigar sua ação. Dentre os inúmeros tipos de acidentes como por exemplo: o choque frontal, decorrente da falha na sinalização ou perda de freio, fratura de componentes (trilho ou roda) que pode ter conseqüências vultuosas, apenas a segurança do veículo será abordada neste texto.

3.1 Tipos dos Acidentes

Dentre as ocorrências de acidentes observados com veículos, dois grandes grupos podem ser delineados:

- Acidentes fortuitos;
- Acidentes repetitivos.

Acidentes fortuitos são aqueles decorrentes, em geral, de mais de uma causa concomitante e inesperada. São fatos casuais não controlados e imprevisíveis. Já os acidentes repetitivos são típicos com causas determinísticas e, portanto previsíveis. Para os acidentes envolvendo o veículo e que ocorrem com características repetitivas, ações de engenharia planejada podem contribuir para minimizar a probabilidade de ocorrência e mitigação de efeitos colaterais. O primeiro caso listado não é objeto de análise desta pesquisa.

A segurança em veículos do tipo metro-ferroviário está associada com perda da capacidade de guiagem conhecida como descarrilamento. O descarrilamento é uma das mais graves

intercorrencias e consiste da passagem da roda do veículo por sobre o topo (boleto) do trilho. Para os veículos guiados o descarrilamento pode ser fatal. Este fenômeno pode ocorrer apenas em um eixo (rodeiro) ou em um truque completo (dois rodeiros). No caso mais severo um veículo completo pode ser acometido de descarrilamento (dois truques) que eventualmente pode produzir um tombamento associado. Cabe lembrar o aspecto catastrófico quando um vagão de um trem descarrila e arrasta outros vagões devido ao acoplamento entre eles (engates), podendo induzir ao colapso de parte do trem (em alguns casos pode haver até dezenas de vagões envolvidos).

O conceito de segurança contra o descarrilamento de veiculo ferroviário está associado com a capacidade de guiagem do rodeiro. Quando o rodeiro satura sua capacidade de direcionamento decorrente das rodas com pista cônica, a guiagem passa a ser forçada pelo flange. Nesta situação, a força lateral (*L*) de guiagem aumenta. Adicionalmente modos naturais de movimento do vagão podem ser excitados por irregularidades periódicas da via, produzindo o alívio da carga vertical na roda (*V*), pode favorecer a roda passar por sobre o boleto do trilho, causando o descarrilamento. Este é o tipo de falta de segurança que será tratado neste texto.

A tradicional formula de segurança proposta por *Nadal* (1908) é utilizada para quantificar a tendência ao descarrilamento. Esta fórmula identifica um limite para a razão entre as forças lateral e vertical (L/V) no contato roda/trilho além do qual há tendência da passagem do roda sobre o trilho. Para valores de forças de contato, com razão L/V acima deste limite, a segurança fica comprometida.

Pesquisa realizada por este autor propôs estender a aplicabilidade da formulação de *Nadal*, deduzida para uma seção transversal, incluindo os efeitos do ângulo de ataque do rodeiro e força longitudinal no contato. Os detalhes da dedução da formula de Nadal e da nova proposição, podem ser apreciados nos artigos deste autor (*Barbosa*, 2004 e 2005A). Diversas medidas experimentais (*Barbosa*, 1995A) e estudos sobre descarrilamento foram realizados (*Barbosa*, *Sisdelli*, 2005B) incluindo modelagem para cálculo do L/V (*Grando*, *Barbosa*, et al., 2014).

3.2 Mecanismo de Descarrilamento

O mecanismo de descarrilamento é influenciado por diversos fatores. Serão apresentados os principais efeitos buscando descrever cada contribuição no processo de descarrilamento. Conforme descrito anteriormente, a segurança veicular depende de três contribuições básicas:

- Características dinâmicas do veículo;
- Geometria e irregularidade da via férrea;
- Velocidade de operação do trem.

Da influencia da geometria da via e velocidade de operação, resulta o comportamento dinâmico do veículo que produz forças de contato roda/trilho que direcionam seu movimento e atitude. Quando o limite da razão entre as forças de direcionamento é violado as condições para um descarrilamento tornam-se suficientes e o estado de insegurança se estabelece.

A magnitude das forças de direcionamento e, portanto a segurança, é afetada pela intensidade da velocidade de tráfego. Assim, três faixas de velocidade são em geral adotadas para descrever esta influência:

- Descarrilamento em baixa velocidade;
- Descarrilamento em media e alta velocidade;
- Descarrilamento em alta velocidade.

Quando o veículo trafega em média e alta velocidade, os efeitos inerciais devido ao direcionamento são de grande magnitude. As forças centrípetas laterais nas rodas são elevadas e índice de segurança se reduz. Em alta velocidade também pode ocorrer o fenômeno de instabilidade lateral (*hunting* ou *lacet*) devido a conicidade das rodas apresentado em artigo deste autor (*Barbosa* e *Costa*, 1996). Quando a geometria da via tem variações severas (torção da via em curvas de pequeno raio) a distribuição da carga vertical é intensamente afetada. Este fato favorece o alívio da carga vertical na roda em função da rigidez torsional da

suspensão do truque e do veículo. Nestes trechos a velocidade operacional de tráfego em geral é reduzida (baixa velocidade).

Finalmente dois mecanismos típicos de passagem do roda sobre o trilho podem ocorrer:

- Escorregamento lateral;
- Escalada do boleto do trilho.

O escorregamento lateral da roda sobre o trilho ocorre em geral em média e alta velocidade e pequeno ângulo de ataque do rodeiro. Já a escalada do boleto do trilho ocorre com alto coeficiente de atrito, grande ângulo de ataque e baixa velocidade. O segundo caso é típico de curvas de pequeno raio ou aparelhos de mudança de via. Este aspecto foi detalhadamente apresentado no artigo em revista internacional sob título: "Safety of a railway wheelset – *derailment simulation with increasing lateral force*" (*Barbosa*, 2009).

Note então que o índice de segurança retrata a resposta do veículo devido à irregularidade da via. Portanto o processo de monitoramento de comportamento dinâmico do veículo em tráfego para determinação das condições de segurança deve ser baseado na identificação das forças de contato roda/trilho. Conclui-se também que um sistema de medição de segurança pode ser utilizado para localizar as regiões de pior qualidade da via.

3.3 Índice de Segurança

Na comunidade metro-ferroviário a segurança contra o descarrilamento é quantificada pela relação entre as forças de contato lateral e vertical no par roda/trilho, conhecida como a relação L/V. É uma formulação facilmente compreendida e internacionalmente aceita. Entretanto cada companhia ou instituição normalizadora estabelece um limite com a devida margem de segurança. Assim, por exemplo, na Europa o limite adotado é de 0.8 (*UIC*-518), ou seja, quando a força lateral de contato roda/trilho atinge 80% da força vertical, o limite de máxima insegurança é atingido. Normalizando o valor L/V medido pelo limite estabelecido pela norma e subtraindo da unidade, obtêm-se de fato o índice de segurança (*Safety Index* -

SI) que quantifica diretamente a segurança, conforme proposto por este autor (*Barbosa*, 2015):

$$SI = \left(1 - \frac{(L/V)_{medido}}{(L/V)_{norm}}\right) * 100$$

A medição das forças no contato não é uma tarefa simples. Pode ser realizada por rodeiros instrumentados instalados no truque, que medem diretamente as forças dinâmicas de contato roda/trilho durante o tráfego do veículo. Trata-se, entretanto de um equipamento caro, pois utiliza inúmeros extensômetros elétricos, tacômetro, sistema coletor de informações de partes girantes (*slip ring*) e algoritmo sofisticado para o tratamento de dados. São dispositivos aplicáveis exclusivamente a um determinado tipo de truque com instalação e utilização complexa (requer uma equipe técnica especializada).

Outras formas de identificação da tendência ao descarrilamento estão sendo pesquisadas:

O trabalho de *Sun* (*Sun*, et al., 2015) da Austrália, propõe a utilização de um modelo de dois graus de liberdade para estimar as solicitações verticais. Pode-se entretanto destacar o trabalho de *Hung* da Universidade de Tókio (*Hung*, et al., 2010) que propõe a identificação precoce de tendências ao descarrilamento monitorando a velocidade e posição angular de partes do truque. Durante um descarrilamento a velocidade de arfagem (*pitch*) da viga lateral do truque deve aumentar para que a passagem da roda por sobre o trilho seja possível. Associado a este fato a posição angular de rolagem do truque (*roll*) deve ser considerada. Este é o gatilho utilizado para a detecção de tendência ao descarrilamento.

Como alternativa, este autor, propõe recuperar as forças de contato roda/trilho a partir da medição global das acelerações de corpo rígido do veículo em tráfego na via irregular em uma determinada velocidade e identificar as solicitações associadas a níveis de segurança. Essa proposta está descrita no próximo item (4).

4 SISTEMA DE MEDIÇÃO DE SEGURANÇA

Um sistema de medição da segurança do veículo em tráfego pela via requer a estimativa de uma figura de mérito diretamente relacionada com a segurança. No caso de descarrilamento de veículos metro-ferroviários, a grandeza associada à segurança é o índice L/V. Este índice é obtido da relação entre as forças vertical e lateral no contato roda/trilho. A medida das forças de contato pode ser feita com rodeiro instrumentado. Este equipamento, entretanto, é caro e de difícil operação. Um método de monitoramento alternativo mais prático e barato é bem vindo.

Um sistema inercial de medição, que é a proposta em desenvolvimento, permite medir os movimentos do veículo e estimar as forças de contato que os produz, a partir de um algoritmo de dinâmica inversa. Sensores de aceleração e rotação instalados no veículo medem as acelerações translacionais e velocidade angular do veículo (ver Figura 1). Utilizando algoritmos de estimação identificam-se as acelerações angulares e atitude do veículo que são informações necessárias para estimar as forças.

Para estimar as forças que causam as acelerações, as equações da dinâmica são utilizadas. O teorema da resultante e o teorema da quantidade de movimento angular nos fornecem as seguintes equações vetoriais:

$$m\,\vec{a}_G = \sum \vec{F}_{rodas} - m\,\vec{g} \tag{1}$$

$$[J]_G\{\alpha\} + [\omega_B] \wedge [J]_G\{\omega_B\} = \{M_G^{ext}\} \tag{2}$$

A solução deste sistema de seis equações permite calcular as forças ativas sobre o veículo. Este é o fundamento utilizado para a recuperação das forças de contato a partir das acelerações medidas. Note que as medidas dos sensores ocorrem no referencial solidário ao corpo (índice *B* dos termos da equação) e que o pólo escolhido para as equações coincide com centro de massa do veículo (*G*).

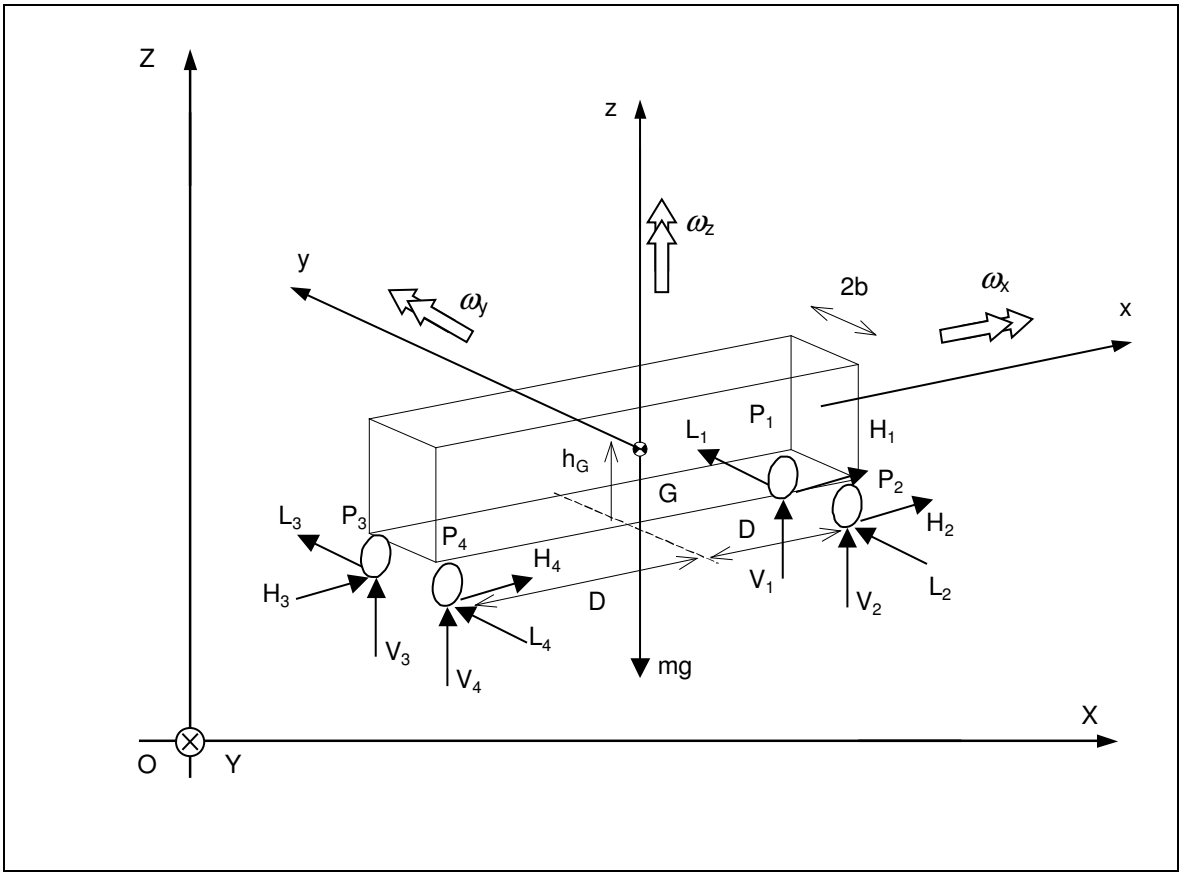

Figura 1 – Diagrama do Veículo e das Forças Ativas

A solução deste sistema de seis equações permite calcular as forças ativas sobre o veículo. Este é o fundamento utilizado para a recuperação das forças de contato a partir das acelerações medidas. Note que as medidas dos sensores ocorrem no referencial solidário ao corpo (índice *B* dos termos da equação) e que o pólo escolhido para as equações coincide com centro de massa do veículo (*G*).

A concepção do sistema de monitoramento de comportamento dinâmico do veículo requer, portanto pelo menos seis sensores para medição dinâmica completa da movimentação do veículo. Portanto conhecendo as acelerações (equação 1) e as variações de atitude do corpo

(equação 2) pode-se determinar as forças ativas das rodas nas direções lateral e vertical que permite calcular o índice L/V.

O artigo publicado na Revista Brasileira de Ciências Mecânicas sob título: "*New method for railway track quality identification through the safety dynamic performance of instrumented railway vehicle*" (*Barbosa*, 2015) descreve com detalhes esta implementação.

4.1 Descrição do Sistema

O sistema de medição foi concebido a partir de equipamentos de baixo custo utilizado sensores de medida do tipo *MEMS* (*micro eletromechanic measuring systems*) que já são digitais e tem custo muito reduzido para montagem inicial do sistema. Os sensores disponíveis no mercado são do tipo inercial (*IMU – inertial measuring unit*) e medem a aceleração translacional e a velocidade angular em três direções ortogonais. Um dispositivo controlador (ARM Cortex M4F CPU de 168 MHz) foi utilizado para gerenciar as atividades dos diversos dispositivos eletrônicos. Os dados digitais são armazenas em cartão de memória (*SD-Card*) para análise posterior. O sistema foi complementado com o dispositivo de *GPS* para a identificação da velocidade e posição geo-referenciada do veículo. Trabalhos realizados na POLI-USP são referencias para esta implementação (*Trigo*, 2005; *Santana*, 2011; *Mori*, 2013; *Mendes*, 2014; *Zanoni* e *Barros*, 2014; *Koga*, 2015).

Para a estimativa da aceleração angular, algoritmos de pós-processamento específicos foram desenvolvidos. Com o conjunto de medições, as equações (1, 2) permitem a determinação das forças ativas de contato e, portanto do índice de segurança (***SI***). O relatório de andamento de pesquisa descreve com detalhes os requisitos do sistema (*Barbosa*, 2017).

4.2 Prova de Conceito

Para a prova de conceito do sistema de medição, foram propostos testes de campo em condições reais de operação. Como balizador para avaliação de desempenho, figuras de mérito da geometria da via (medida com carro controle) e medidas das forças de contato roda/trilho (medição com rodeiro instrumentado) foram utilizadas para efeito comparativo.

Dois testes foram realizados:

- Medida em carro de passageiro em tráfego em linha urbana;
- Medida em vagão de carga em tráfego em ferrovia.

a) Na primeira prova o sistema de medição foi instalado em um carro de passageiros metro-ferroviário da CPTM em São Paulo para um programa de medições em tráfego na região leste da cidade. O trem foi conduzido de forma tradicional em linha 12 (Safira) e os movimentos do carro em tráfego pelas irregularidades da via férrea. Sua posição e velocidade foram registradas por *GPS*. Os dados medidos foram tratados e combinados para estimar o índice de Segurança (*Safety Index* - SI) conforme procedimento descrito no item 3.2. Para avaliação do sistema de medição os resultados foram comparados com valores medidos de geometria da via obtidos com o carro controle *EM*-100 da CPTM, conforme descrito no item 2.7.

As estimativas obtidas de ***SI*** guardaram boa correlação com a geometria da via medida, ou seja, em locais onde a geometria medida estava acima dos limites, o ***SI*** confirmou esta tendência. Os locais com menor segurança foram identificados pelo *GPS*. Para maiores detalhes da avaliação veja a publicação na Revista Brasileira de Ciências Mecânicas (*Barbosa*, 2015 em anexo).

b) Uma segunda prova de desempenho foi realizada na Estrada de Ferro Carajás da VALE, próximo a São Luis no Maranhão. Neste teste o sistema de medição foi instalado em um vagão de minério carregado (120 toneladas) do tipo GDT. Um trem especial formado por

quatro vagões percorreu um trecho com retas e curvas com cerca de 25 quilômetros nos dois sentidos em diversas velocidades.

Nesta oportunidade obteve-se a vantagem de ter dois rodeiros instrumentados instalados no vagão, além das medidas de geometria da via com carro controle (modelo *EM*-100 da *Plasser*). Os valores das forças de contato roda/trilho foram medidos diretamente com os rodeiros instrumentados. Os resultados obtidos mostraram boa correlação entre as irregularidades da via e o índice de segurança medido. Quando comparado com os valores das forças medidas com os rodeiros instrumentados a correlação fica mais nítida nos transitórios mais acentuados.

A ferrovia de Carajás tem excelente padrão de qualidade e um traçado com curvas de grande raio (típico de 800 metros). Desta forma, apesar da velocidade ser de 70 km/h, as irregularidades produzem pequenas oscilações e, portanto elevada segurança.

Para maiores detalhes desta avaliação veja a publicação no *International Journal of American Society of Civil Engineers*: "*Evaluation of Railway Track Safety with a New Method for Track Quality Identification*" (*Barbosa*, 2016A em anexo).

4.3 Benefícios constatados

Ficou comprovada a viabilidade de estimar a segurança no tráfego medindo as acelerações no veículo. A comprovação foi realizada pela comparação da segurança estimada (***SI***) com os valores medidos de irregularidade da via com carro controle. Na segunda medição, a validação foi realizada também pela comparação com as força de contato medidos com os rodeiros instrumentados.

A utilização do *GPS* para localização geo-referenciada instantânea do veículo permitiu a associação adequada com a marca quilométrica da linha. A identificação da velocidade por *GPS* (sem tacômetro e cabos) resultou também em facilidade de montagem. Durante a prova de conceito ficou comprovada a facilidade de montagem do sistema de medição que requereu

nada além de 10 minutos para sua instalação. Os dados armazenados em *SD card* forneceram fácil acesso as medições. Foi testado o aplicativo de transferência de dados por conexão *USB* e verificada a alta velocidade de transferência de dados do *SD card* quando acoplado como um driver de computador. O tempo de teste a ser realizado dita a capacidade de armazenagem do *SD card* a ser utilizado.

4.4 Restrições encontradas

A avaliação mais representativa consiste na comparação direta das medidas das forças de contato roda/trilho (forças laterais e verticais) com a estimativa do índice de segurança (***SI***). Nesta comparação os valores obtidos para pequenas acelerações ficaram aquém do esperado. Analisando com mais detalhes os resultados medidos, observa-se ruídos das acelerações da ordem de 0,05 m/s^2. Entretanto para curvas de grande raio (600 metros) e baixa velocidade (30 km/h) níveis típicos mínimos de aceleração não compensada são da ordem de 0,033 m/s^2 (conforme relatório Fapesp, *Barbosa*, 2017). Adicionalmente foram determinados ruídos da ordem de ± 4,0 °/s^2 para as acelerações angulares estimadas. É desejado medir a acelerações angulares com erro na casa de ± 0,02 °/s^2, correspondente a curva com transição de 300 metros para velocidades em torno de 30 km/h (*Barbosa*, 2017). Resulta, portanto a necessidade de melhorar a qualidade dos sensores de medida e a eficácia dos algoritmos de tratamento dos dados.

Além do ruído *Gaussiano* típico do sinal dos sensores há contaminação com interferência sinusoidal de uma única freqüência e seus harmônicos, eventualmente devido à blindagem inadequada da eletrônica do sensor ou vibrações e dinâmica secundária do sistema. As estratégias de filtragem utilizadas devem ser aprimoradas para melhorar a qualidade do tratamento numérico.

A observação serial dos sensores devido ao protocolo de comunicação utilizado (I^2C) resulta em atraso de leitura dos dados prejudicando a simultaneidade e deve ser mitigada. A quantificação exata das grandezas inerciais (massa e momento de inércia) fica incerta, uma

vez que não está disponível a quantidade de passageiros no carro nem sua distribuição. Portanto alguma forma complementar de identificação é bem vinda.

Verificou-se adicionalmente que a torção longitudinal da suspensão contribui bastante no alivio da carga vertical, fato este não contemplado adequadamente no projeto inicial. Interfaces de programação e controle e limitações de memória do controlador foram restrições detectadas e devem ser adequadamente contempladas.

Mais detalhes sobre o funcionamento do sistema e resultados de medidas pode ser apreciado também no artigo publicado sob título: "*Quantification of Railway Track Safety with an Inertial Vehicle Response Identification*" (*Barbosa*, 2016B) em anexo.

5 PROJETO FASE II

Em função dos bons resultados obtidos pelos primeiros testes de campo, foram implementas alterações em equipamentos no sistema de medição e aprimorados os algoritmos de pós-processamento. Nesta etapa foram consideradas as restrições identificadas nas funcionalidades do sistema. O segundo projeto concebido implementou as seguintes modificações básicas:

- Utilização de um micro-computador em placa única;
- Utilização de múltiplos sensores distribuídos ao longo do veículo;
- Utilização de acelerômetros de melhor qualidade;
- Identificação direta da torção longitudinal da suspensão;
- Processo de calibração;
- Novos algoritmos de tratamento de dados;
- Análise Modal.

5.1 Micro-Computador

Em função das restrições apontadas no item 4.4 o micro-controlador inicialmente utilizado foi substituído na Fase II por um micro-computador em placa única que tem as seguintes vantagens:

- Maior quantidade de memória;
- Diversas interfaces homem-máquina (*HMI*);
- Maior rapidez de processamento;
- Habilidade de controlar e armazenar dados;
- Linguagem de programação universal (*Linux*).

O micro-controlador é utilizado em controle de processo digital dedicado a equipamento específico e tem a vantagem do reduzido consumo de energia e baixo custo. Possui em geral um *chipset*, tem recurso de entrada e saída (input/output) e interrupções e uma pequena memória de acesso aleatório (randon-access memory – *RAM)*. No segundo projeto utilizou-se um micro-computador em placa única (*single board computer – Raspberry*) com maior quantidade de memória *RAM*, mais interfaces homem-máquina (teclado, monitor e mouse); maior rapidez de processamento, mais habilidade para controlar e armazenar dados e sistema operacional na plataforma *Linux*.

5.2 Múltiplos Sensores

No projeto Fase II foram empregados quatro acelerômetros de melhor qualidade (*Kistler*), em função das restrições observadas na primeira fase (item 4.4). Os sensores utilizados serão instalados aos pares nas extremidades do veículo sobre os truques (ortogonais nas direções y e z). Conversor A/D com resolução de 16 bits de resolução por canal foram utilizados. Desta forma as medições de aceleração terão mais precisão e a estimação da aceleração angular será também beneficiada. O uso de múltiplos sensores tomou como referencia o artigo de *Park* (*Park* et al., 2011). Será utilizado filtro de *Kalman* no pós-processamento para junção das informações dos vários sensores.

Para a medição da velocidade do veiculo e identificação da sua localização ao longo da via, foi utilizado um *GPS* com capacidade de visualização de até 72 satélites simultâneos nos quatro sistemas disponíveis (*GNSS, Glonass, BeiDou e Galileo*) e taxa de amostragem de 10 Hz (*uBlox-M8N*). O micro-computador, sistema de alimentação com baterias, o *GPS* e uma *IMU* serão instalados no centro do veículo.

5.3 Torção da Suspensão

A torção longitudinal da suspensão do veículo decorre da geometria da via por onde o veiculo está trafegando. Em uma curva de transição onde a variação da superelevação nominal da curva pode variar linearmente, o truque frontal do veículo apresentará inclinação angular distinta do truque traseiro. Esta torção longitudinal da suspensão do veículo acarreta variação na distribuição da carga vertical em cada roda, influenciando o índice L/V. Este efeito é significativo, mas não é detectado pelo sistema de medição inercial original.

Introduziram-se então duas novas *IMU* instaladas solidariamente a cada truque para identificação da inclinação relativa. A diferença das medições corresponde ao ângulo de torção longitudinal da suspensão. Nova rotina de pós-processamento incluirá a identificação da torção longitudinal da suspensão do veículo. De posse da rigidez torsional da suspensão é possível estimar o momento M_{xx} e, portanto a variação entre as cargas verticais entre as roda externas e internas do veículo.

Note que esta técnica pode ser expandida para cada um dos eixos do mesmo truque, melhorando a estimativa de segurança para veículos de quatro eixos.

5.4 Algoritmos

Em função das restrições apontadas no item 4.4 novos algoritmos de pré e pós processamento foram desenvolvidos e implementados no sistema. Uma estrutura de gerenciamento dos múltiplos sensores considerando a inicialização, calibração, coleta e armazenamento de dados foi desenvolvida na plataforma *Linux* que também controla as atividades do micro-computador.

Algoritmos mais robustos de derivação (*Savitzky* e *Golay*, 1964) e filtro de *Kalman* devem melhorar a estimativa das acelerações angulares. Para a identificação da torção da suspensão será utilizado o algoritmo de orientação (*attitude and heading reference system* - *AHRS*, *Titterton*, 2004) das *IMUs* que possuem processamento embarcado no sistema de medida (*digital motion processor* - DMP) e estima a atitude do corpo. Portanto espera-se significativo avanço em *software*.

Devido à simplicidade dos equipamentos e forma de comunicação e capacidade de processamento, a taxa de amostragem do sistema para os diversos sensores não é muito elevada. O protocolo de comunicação utilizado é o I^2C. Para melhorar a simultaneidade na observação dos sensores, os algoritmos devem ser otimizados para atingir uma taxa de amostragem de 100 *Hz*. Desta forma a mídia de armazenamento deve ter sua capacidade incrementada devido o aumento na quantidade de dados.

5.5 Calibração

A calibração dos sensores da *IMU* é de fundamental importância para garantir o funcionamento adequado do sistema. Especialmente para a identificação do plano de instalação dos sensores como o zero dos valores digitais dos sensores. O processo de calibração tomou como referencia a publicação de *Kozlov* (*Kozlov* et al., 2014) que se utiliza simplesmente da plataforma girante de um torno para calibração. O processo consiste em girar lentamente o sensor em cada face e amostrar as variações dos sinais que permitem obter a matriz de erros. Espera-se com este novo método obter melhores resultados de calibração dos sensores.

5.6 Analise Modal

Para identificar as forças associadas ao comportamento dinâmico do veículo é necessário o conhecimento das propriedades inerciais do corpo rígido (massa e momento de inércia) e da rigidez da suspensão. Os valores nominais de projeto são facilmente obtidos. Entretanto o valor exato fica incerto, uma vez que não se conhece a quantidade exata de passageiros no carro nem sua distribuição.

A partir de valores conhecidos do projeto da rigidez da suspensão, uma análise modal das oscilações do veículo em tráfego pela via, pode-se estimar com mais qualidade o peso adicional e sua distribuição. De posse das frequências de vibração obtidas por análise em frequência (*FFT*) dos modos de movimento vertical e arfagem do veículo, é possível corrigir os valores das propriedades inerciais e sua distribuição (massa e momento de inércia) a serem utilizados nos algoritmos de estimação. Este é um processo prévio a ser realizada antes do processamento das medidas para a estimativa do índice de segurança (***SI***).

A mesma inferência pode ser aplicada para a determinação prévia das propriedades elásticas globais, conhecendo-se o peso próprio por pesagem estática em balança. Em função do comportamento modal do veículo é possível também identificar que tipo de excitação das irregularidades da via foi mais contributivo para reduzir o índice de segurança. Assim por exemplo no caso do índice de segurança ser reduzido devido à aceleração angular no eixo y, o movimento de arfagem (*pitch*) do vagão foi magnificado. Portanto as irregularidades verticais em fase dos trilhos existente na via no comprimento de onda duas vezes a maior que à distância entre os truques, deve ser objeto de atenção e correção (manutenção).

5.7 Conclusões

A estimação indireta das forças ativas sobre o veículo foi realizada com uma instrumentação especializada simples que mede a resposta e atitude do veículo frente às solicitações externas. As acelerações translacionais e velocidades angulares de corpo rígido foram medidas utilizando sensores inercial instalados o centro do veículo. O tratamento dos dados amostrados permite obter das acelerações angulares e ângulos de atitude. Finalmente baseado nas equações da dinâmica de corpo rígido (item 3.3), determina-se as forças ativas e o índice de segurança (***SI***).

Os testes de campo foram realizados com êxito e seus resultados validados por comparação com medidas de geometria da via e medidas de *L*/*V* com rodeiros instrumentados. Os resultados indicam o nível de segurança contra o descarrilamento do veículo em cada ponto da via para uma determinada velocidade de tráfego.

Na Fase II do projeto de pesquisa serão utilizados um novo micro-computador (item 5.1), sensores de aceleração de melhor resolução distribuídos nas extremidades do veículo (item 5.2). Serão empregados também sensores complementares instalados nos truques para monitorar o ângulo de torção longitudinal da suspensão do veículo (item 5.3). Algoritmos de pré processamento (item 5.4) otimizados, melhor combinados e mais eficazes devem melhorar a qualidade das estimações realizadas. Isto representa em avanços nos algoritmos utilizados (*software*). As rotinas de calibração (item 5.5) e pós processamento modal (item 5.6) devem melhorar a identificação dos parâmetros do veículo. Isto resulta em avanços na instrumentação utilizada (*hardware*). Desta forma espera-se obter melhores e mais confiáveis resultados do sistema de medição para a estimativa do índice de segurança (***SI***). Esta etapa da pesquisa do projeto FAPESP nº 2015/25955-9, teve a colaboração do Prof. Flávio Celso Trigo e dos alunos de pós-graduação Renan Mendes e Marlon Koga que recebem agradecimentos (*Barbosa*, 2017). Os artigos publicados sobre este desenvolvimento encontram-se nos anexos deste documento.

6 COMENTÁRIOS FINAIS E TRABALHOS FUTUROS

Esta investigação tornou possível o monitoramento especializado de veículos metro-ferroviários com objetivo de identificar índices de segurança operacional. Comprovou-se durante este trabalho de pesquisa e desenvolvimento de uma instrumentação especializada para o monitoramento do comportamento dinâmico do veículo metro-ferroviário que:

- É possível detectar, a partir da combinação dos vários modos de vibração do veículo, índice associado à segurança durante o tráfego na via irregular.
- É possível identificar os locais da via férrea onde o comportamento do veículo tem desempenho prejudicado em termos de segurança.
- É possível identificar o tipo de geometria perniciosa da via férrea nos locais que produzem pior desempenho do veículo (item 5.6).
- Desta figura de mérito pode-se orientar as intervenções de manutenção da via férrea, de forma otimizada.
- Pode-se ainda identificar tendência ao comportamento oscilatório do veículo.

O desenvolvimento desta metodologia deve se aprimorar no futuro, em função da melhoria da precisão e qualidade dos sensores de medição, capacidade dos micro-computadores, aumento da velocidade de amostragem, otimização dos algoritmos de processamento embarcados, desenvolvimento de novos algoritmos de tratamento de dados, novos recursos de comunicação. Esta metodologia tem potencial também para incrementar a capacidade dos equipamentos embarcados em veículos incluindo métodos de detecção que possam atuar no controle do veículo em tempo real, permitindo um tráfego rápido e seguro, mesmo em condições adversas.

Cabe lembrar que o presente desenvolvimento deu origem a três artigos em revistas indexadas internacionais (*Barbosa*, 2015, 2016A, 2016B) e uma patente de privilégio de invenção (PI nº BR1020130190721, *Barbosa*, 2013). Este sistema pode ser disseminado como instrumento de

monitoramento em larga escala, para todos os veículos de transporte coletivos (VLT, ônibus, Vans, etc.).

6.1 Trabalhos Futuros

Como atividades futuras pode-se indicar a implementação de comunicação padrão via rede *Ethernet* de 100 Mbit/s em PTP (*precision time protocol*). Utilizar conversor A/D com maior resolução (24 bits de resolução por canal). Comunicação via *WiFi* para trocar dados e enviar para estações fixas.

Em breve tecnologias como girômetro a laser (*laser ring rate gyros*) serão mais acessíveis ou girômetro MEMS de anel oscilatório (http://www.siliconsensing.com/technology/mems-gyroscopes/) que é mais imune ao efeito cruzado de aceleração podem produzir melhores resultados. São novas tecnologias que devem ser perseguidas.

A evolução dos MEMS tem velocidade vertiginosa. A utilização de múltiplos sensores em cada veiculo já é uma realidade (exemplo: Trem Velaro da Siemens com 24 sensores MEMs Colibrys VS1000). Oportunidades de monitoramento de veículos para controle e diagnósticos são o futuro das pesquisas.

Pesquisar sobre uso de tratamento de dados alternativos como *wavelet multiresolution analysis* (*WMRA*) (*Abdel-Hamid*, 2004).

Na medição da irregularidade de pavimentos a complementação da medição de uma trilha com a medida acoplada da elevação da segunda pista, ou seja, medida da inclinação da seção é um recurso que permitirá gerar superfície de forma aleatória a partir de espectros.

7 REFERENCIAS BIBLIOGRÁFICAS

7.1 Trabalhos Publicados

Appell, P. (1900) **Sur une forme générale des équations de la dynamique**. Journal für die reine und angewandte Mathematik. Zeitschriftenband (1900), Artikel, pp. 310 – 319.

Appell, P. (1925) **Sur une forme générale des équations de la dynamique**. Mémorial des Science Mathématiques de L'Académie des Sciences de Paris, pp. 1-48.

Aknin, P. (1995) **Outils de description de la géométrie des voies et déconvolution des relevés expérimentaux – Application aux tracés ferroviaires**. *Institut National de Recherch sur les Transports et ler Sécurité* , Rapport INRETS nº 204, pp. 76, Paris, France.

Abdel-Hamid, W.; Osman, A.; El-Sheimy, N.; Noureldin, A. (2004) **Improving the Performance of MEMS-Based Inertial Sensors by Removing Short-Term Errors Utilizing Wavelet Multi-Resolution Analysis**. Proceeding of the ION National Technical Meeting, pp. 260 – 266, USA.

Barbosa, R. S.; Mendes, F. B. G.; Felício L. C., Michellini, A.; (1984) **Modelagem e Simulação do Comportamento Dinâmico de uma Composição Ferroviária.** Relatório Técnico IPT n° 20.311.

Barbosa, R. S. (1987) **Fatigue Life Prediction on a Specimen of Structural Steel**. Relatório de especialização em fadiga na British Railway Research, Derby, England. pp. 48.

Barbosa, R. S. (1988A) **Análise em Corpo de Prova de Trilho**. Relatório Técnico - IPT-CDF, nº 26.870.

Barbosa, R. S. (1988B) **Ensaio Estático e de Fadiga em Travessa e Lateral de Truque**. Relatório Técnico IPT nº 26.968.

Barbosa, R. S.; Felício L. C.; Michellini, A.; Mendes, M. A. G.; Cordeiro, J. C. S. (1989A) **Programa de Simulação de Marcha de Trens**. Relatório técnico - IPT-CDF, nº 27.742.

Barbosa, R. S.; Mendes, F. B. G. (1989B) **Medidor de perfil de roda ferroviária**. Produto Tecnológico, Desenvolvimento IPT.

Barbosa, R. S.; Sisdelli, A. (1989C) **Análise do Problema de Formação de Trincas em Rodas**. Relatório técnico - IPT-CDF, nº 27.459.

Barbosa, R. S. (1989D) **Análise de Eixo Fraturado**. Relatório Técnico - IPT-CDF, nº 27.356.

Barbosa, R. S.; Michelini, A.; Mendes, M. A. B. G. (1990A) **Programa de Simulação de Marcha de Trens**. Desenvolvimento IPT. Patente: Programa de Computador. Número do registro: 90.000.936.

Barbosa, R. S. (1990B) **Desenvolvimento de Dinamômetro de Freio**. Trabalho Técnico apresentado no 4º Encontro Pan-americano de Ferrovias, Rio de Janeiro.

Barbosa, R. S. (1990C) **Análise do Problema de Formação de Trincas em Rodas - Ensaios de Campo**. Relatório técnico - IPT-CDF, nº 28.668.

Barbosa, R. S.; Ferreira, S. I. (1992A) **Análise para Determinação de Causas de Descarrilamento.** Rede Ferroviária Federal – RFFSA – SR 2. Relatório Técnico - IPT-DITT/ADF, nº 30.298.

Barbosa, R. S.; Togni, J. L. (1992B) **Medidor de perfil de trilho ferroviário**. Produto Tecnológico, Desenvolvimento IPT.

Barbosa, R. S. (1992C) **Ensaio de Fadiga em Lateral de Truque Ferroviário**. Relatório Técnico IPT-CDF nº 30.591.

Barbosa, R. S. (1993A) **Dinâmica Longitudinal do Trem**. Dissertação de Mestrado em Engenharia Mecânica sob orientação de Weber, H. I.: Universidade Estadual de Campinas, UNICAMP, pp. 120, Brasil.

Barbosa, R. S.; Fuzetti, E. (1993B) **Manual de Utilização do Programa de Caracterização Geométrica do Contato Roda/Trilho** (CCRT). Relatório Técnico IPT - DITT/ADF, nº 31.576.

Barbosa, R. S. (1994A) **Análise do Contato Roda/Trilho: Caso da Estrada de Ferro Vitória a Minas**. Relatório Técnico IPT - DITT/ADF, nº 32.491.

Barbosa, R. S. (1994B) **Análise do Contato Roda/Trilho: Caso da Estrada de Ferro Carajás**. Relatório técnico IPT - DITT/ADF, nº 32.554.

Barbosa, R. S. (1995A) **Estudo para Determinação de Causas de Descarrilamento: Avaliação da Resposta Dinâmica dos Vagões na Via**. Rede Ferroviária Federal - RFFSA SR-10. Relatório Técnico IPT - DITT/ADF, n. 33.802.

Barbosa, R. S. (1995B) **Identificação de Modos Naturais de Movimento de Vagões**. RFFSA SR-10 Bauru. Relatório Técnico IPT - DITT/ADF, n. 33.262.

Barbosa, R. S. (1995C) **Análise da Inscrição em Curvas do VLT de Campinas**. FEPASA. Relatório Técnico IPT - DITT/ADF, n. 33.070.

Barbosa, R. S.; Weber, H. I. (1996A) **Dinâmica Longitudinal do Trem**. Revista Brasileira de Ciências Mecânicas, SP, Vol. 18, nº 2, pp. 107-116.

Barbosa, R. S.; Costa Neto, A. (1996B) **Dinâmica do Rodeiro Ferroviário**. Revista Brasileira de Ciências Mecânicas, SP, v. 18, n.4, p. 318-329.

Barbosa, R. S. (1997A) **Verification Experimentale de Coeficients de Raideur au Contact**. Especialização em Mecânica de Contato no Programa de Doutorado. Institut National de Recherche sur le Transport et leur Sécurité, INRETS, Orientador: Jean Pierre Pascal. França.

Barbosa, R. S. (1997B) **Estudo de Segurança de Carro de Passageiro**. EFC – CVRD. Relatório Técnico IPT-DITT-ADFR nº, 35.617.

Barbosa, R. S. (1998A) **Interação veículo/pavimento, conforto e segurança veicular**. Anais da 31ª Reunião Anual de Pavimentação, Associação Brasileira de Pavimentação (ABPv), Vol. 2, pp. 1164–1182, Rio de Janeiro, Brasil.

Barbosa, R. S.; Villani, E. (1998B) **Reconstrução Cartesiana da Trajetória definida pela Curvatura**. Relatório Técnico IPT-DITT-ADFR, nº 36.271.

Barbosa, R. S. (1999A) **Aplicação de sistemas multicorpos na dinâmica de veículos guiados**. Tese de Doutorado, Universidade de São Paulo (USP), São Paulo, Brazil, pp. 273.

Barbosa, R. S. (1999B) **Medida do Esforço de Tração em Trem de Minério. Estrada de Ferro Vitória-Minas** (EFVM), Companhia Vale do Rio Doce (CVRD). Relatório Técnico IPT-DITT-ADFR, nº 39.399.

Barbosa, R. S. (1999C) **Avaliação de Desempenho e Segurança de Vagão Graneleiro**. Ferronorte. Relatório Técnico IPT-DITT-ADFR, nº 42.226.

Barbosa, R. S. (2000A) **Avaliação de Estabilidade Lateral de Vagão Graneleiro**. Ferronorte. Relatório Técnico IPT-DITT-ADFR, nº 45.879.

Barbosa, R. S. (2000B) **Programa de Caracterização Geométrica do Contato Roda/Trilho e Aplicativos** (Versão 3.0 - Matlab) Relatório Técnico IPT-DITT-ADFR, nº 46.754.

Barbosa, R. S. (2000C) **Desenvolvimento de Programa de Análise de Fadiga**. Relatório Técnico IPT-DITT-ADFR, nº 46.657.

Barbosa, R. S. (2001A) **Avaliação do Comportamento de Vagão Ferroviário Tipo HAD**. Estrada de Ferro Vitória-Minas – EFVM. Relatório Técnico IPT-DITT-ADFR, nº 53.165.

Barbosa, R. S. (2001B) **Avaliação do Comportamento Dinâmico de Carro Metro-ferroviário**. Companhia Paulista de Trens Metropolitanos – CPTM. Relatório Técnico IPT-DITT-ADFR, nº 55.760.

Barbosa, R. S. (2001C) **Avaliação de Desempenho e Segurança do Carro de Trem Metropolitano** (Série 8000). SuperVia, Rio de Janeiro, Relatório Técnico IPT-DITT-ADFR, nº 51.391.

Barbosa, R. S.; Costa, A. (2001D) **Safety vehicle traffic speed limit**. Proceedings of IX International Symposium on Dynamic Problems of Mechanics (IX-DINAME), Brazilian Society of Mechanical Science (ABCM), Rio de Janeiro, Brazil, pp. 435–443.

Barbosa, R. S. (2004A) **A 3D Contact Force Safety Criterion for Flange Climb Derailment of a Railway Wheel**. International Journal of Vehicle System Dynamics, ISSN 0042-3114, Taylor & Francis, Vol. 42, nº 5, pp. 289-300.

Barbosa, R. S.; Dias, C. A. N. (2004B) **Avaliação de Desempenho Dinâmico e Estrutural de Carro de Passageiros da Estrada de Ferro Carajás** – CVRD. Projeto FUSP nº 1039.

Barbosa, R. S. (2005A) **Safety Criterion for Wheel Climb Derailment**. Proceedings of the 8th International Heavy Haul Conference - International Heavy Haul Association - IHHA, pp. 477-484, Rio de Janeiro, Brasil.

Barbosa, R. S.; Sisdelli, A. (2005B) **Derailment Investigation on a HFT wagon**. Proceedings of the 8th International Heavy Haul Conference - International Heavy Haul Association - IHHA, pp. 485-490, Rio de Janeiro, Brasil.

Barbosa, R. S. (2005C) **Avaliação do Desempenho Dinâmico do Vagão de Minério GDT da Estrada de Ferro Carajás** – CVRD. Projeto FUSP nº 1301. Relatório Técnico final nº 040/2005, pp. 136.

Barbosa, R. S. (2006) **Avaliação do sistema não referenciado de medição da geometria da via**. Modernização do carro controle da Estrada de Ferro Carajás – CVRD. Projeto FUSP nº 1563. Relatório Técnico final nº 011/2006, Volume I, pp. 144.

Barbosa, R. S. (2007) **Investigação Experimental do Comportamento Dinâmico de Vagão de Minério em Tráfego na Via com Travessão**. EFVM-CVRD, Projeto FUSP nº 1569. Relatório Técnico final nº 010/2007, Volume I, pp. 109.

Barbosa, R. S. (2008A) **Investigação experimental do comportamento dinâmico de vagão de minério tipo GFD** (EFVM – VALE). Projeto FUSP nº 1571.

Barbosa, R. S.; Padovesse, L. R.; Kassab F.; Nishimoto K.; Marques R. P.; Taniguchi, D. (2008B) **Simulador de Realidade Virtual para Treinamento de Maquinistas**. In: Encontro de Ferrovias, 2008, Vitória. Encontro de Ferrovias. São Paulo: OTM Editora, 2008.

Barbosa, R. S. (2009A) **Safety of a railway wheelset - derailment simulation with increasing lateral force.** International Journal of Vehicle System Dynamics, pp. 1-18.

Barbosa, R. S.; Batista, M. V. M. (2009B) **Conforto ao Rolamento Devido Interação do Veículo com Pavimento Irregular Descrito pelo Espectro Em Comprimento de Onda**. In: Congresso Brasileiro de Rodovias e Concessões, Florianópolis. Vol. 1. pp. 1-38.

Barbosa, R. S. (2010A) **Simulador de Realidade Virtual para a Operação de Trens ferroviários e Treinamento de Maquinistas** (VALE S/A). Projeto FUSP nº 1747.

Barbosa, R. S.; Kassab F.; Nishimoto K.; Padovesse, L. R.; Marques R. P.; Taniguchi, D. (2010B) **Sistemas de Realidade Virtual para Simulação de Equipamentos de Movimentação e Treinamento de Operadores**. In: II Encontro de Ferrovias, Vitória. Anais do II Encontro de Ferrovias. OTM Editora, 2010. Vol. 1. p. 1-2.

Barbosa, R. S. (2011A) **Vehicle Dynamic Response Due to Pavement Roughness**. Journal of the Brazilian Society of Mechenical Science & Engineering – ABCM. Vol. XXXIII, nº 3, pp. 302-307.

Barbosa, R. S. (2011B) **Vehicle Dynamic Safety in Measured Rough Pavement**. Journal of Transportation Engineering, 10.1061/(ASCE)TE.1943-5436.0000216, Vol. 137, Issue 5, pp. 305-310.

Barbosa, R. S.; Kassab F.; Marques R. P.; Nishimoto K.; Makiyama, H. S. (2011C) **Sistema de Realidade Virtual de Simulação Multiusuários de Trens em Malha Ferroviária para Treinamento de Operadores**. III Encontro de Ferrovias, 2011, Juiz de Fora. São Paulo: OTM Editora.

Barbosa, R. S. (2012) **Vehicle Vibration Response Subjected to Longwave Measured Pavement Irregularity**. Journal of Mechanical Engineering and Automation, DOI: 10.5923/j.jmea.20120202.04, Vol.: 2, nº 2, pp. 17-24.

Barbosa, R. S. (2015) **New method for railway track quality identification through the safety dynamic performance of instrumented railway vehicle**. Journal of Brazilian Society of Mechanical and Science Engineering. DOI: 10.1007/s40430-015-0471-9, Vol.: 38, Issue: 8, pp 2265–2275.

Barbosa, R. S. (2016A) **Evaluation of Railway Track Safety with a New Method for Track Quality Identification**. American Society of Civil Engineers - ASCE, DOI: 10.1061/(ASCE)TE.1943-5436.0000855. Volume 142, Issue 11, pp. 1-11.

Barbosa, R. S. (2016B) **Quantification of Railway Track Safety with an Inertial Vehicle Response Identification**. International Journal of Railway Technology, Saxe-Coburg Publication, DOI: 10.4203/ijrt.5.2.3, Vol. 5, Issue 2, pp. 47-63.

Baruh, H. (1999) **Analytical dynamics**. Publisher McGraw-Hill, New York, p 718.

Benini, C.; Gadola, M.; Chindamo, D.; Uberti, S.; Marchesin, F. P. Barbosa, R. S. (2017) **The influence of suspension components friction on race car vertical dynamics**. International Journal of Vehicle Mechanics and Mobility, DOI: 10.1080/00423114.2016.1267370, Vol.: 55, Issue 3, pp. 338-350.

Grando, D.; Barbosa, R. S. (2008). **Análise do Comportamento Dinâmico de Carro de Passageiros da Série 2000 da CPTM**. Companhia Paulista de Trens Metropolitanos - Consorcio Cobrasman. Projeto MC., nº 1-2008.

Grando, D.; Barbosa, R. S. (2011) **Avaliação da dinâmica do vagão ferroviário tipo GFD.** Estrada de Ferro Vitória a Minas - EFVM - VALE. Projeto MC., nº 7.710.

Grando, D.; Barbosa, R. S. (2012) **Avaliação da dinâmica e segurança de vagão ferroviário tipo HAS.** MRS. Projeto MC., nº 5.511

Grando, D.; Barbosa, R. S. (2014) **Avaliação da dinâmica do vagão ferroviário tipo GDE. Estrada de Ferro Vitória a Minas** - EFVM - VALE. Projeto MC., nº 14.016.

Grando, D.; Barbosa, R. S.; Costa Neto, A. (2015A) **Relatório de análises de carro passageiros série 9000 da CPTM**. Projeto MC., nº 3.111.

Grando, D.; Costa Neto, A.; Barbosa, R. S.; Santos G. F. M. (2015B) **Análise Paramétrica de Segurança de Vagão GDE**. Encontro de Ferrovias: Novas Idéias para Novos Desafios, Vitória, Espirito Santo, OTM Editora,Brasil.

Grando, D.; Barbosa, R. S.; Costa Neto, A.; Santos G. F. M. (2015C) **An analysis and solution of a railway vehicle speed restriction**. In: International Heavy Haul Conference - IHHA 2015, Australia.

Grando, D.; Barbosa, R. S.; Croce, R.; Costa Neto, A. (2016A) **Relatório de modelagem dos vagões HPE e madrinha e locomotiva**. Projeto MC., Relatório Final de Análises, nº 15.049. pp. 107, Curitiba

Grando, D.; Barbosa, R. S.; Costa Neto, A. (2016B) **Avaliação de Características de Veículos Ferroviários de Transporte Urbano Através de Ensaios Normalizados**. Projeto MC., nº 14.052.

Hung, C.; Suda Y.; Aki, M.; Tsuji, T.; Morikawa, M.; Yamashita, T.; Kawanabe, T. Kunimi T. (2010) **Study on detection of the early signs of derailment for railway vehicles**. Vehicle System Dynamics, Vol. 48, Supplement, pp. 451–466.

Johnson, K. L. (1985) **Contact Mechanics**. Cambridge University Press, pp. 452.

Kalker, J. J. (1967) **On the rolling contact of two elastic bodies in the presence of dry friction**. Doctoral Theses, University of Delft.

Kozlov, A.; Sazonov, I.; Vavilova N. (2014) **IMU Calibration on a Low Grade Turntable: Embedded Estimation of the Instrument Displacement from the Axis of Rotation**. 2014 International Symposium on Inertial Sensors and Systems (ISISS), Publisher IEEE, pp. 1-4.

Maciel, G. P. R.; Barbosa, R. S. (2015A) **Técnicas para redução da ordem de sistemas dinâmicos na base modal**. Anais do XXIII Simpósio Internacional de Engenharia Automotiva - SIMEA 2015, São Paulo, DOI: 10.5151/engpro-simea2015-PAP189, Vol.: 2 nº 1, pp. 514-530.

Maciel, G. P. R.; Barbosa, R. S. (2015B) **Error bound for low order approximation of dynamic systems subjected to initial conditions**. In: 23 ABCM International Congress of Mechanical Engineering - COBEM 2015, Rio de Janeiro.

Maciel, G. P. R.; Barbosa, R. S. (2016) **Monorail vehicle model to study influence of tyre modelling on overall dynamics**. International Journal of Heavy Vehicle Systems, DOI: 10.1504/IJHVS.2016.079270, Vol. 23, nº 4, pp. 317–332.

Marchesin, F. P.; Barbosa, R. S. (2012) **Análise do desempenho de veículos de competição**. VII Congresso Nacional de Engenharia Mecânica. ABCM, pp. 1-10.

Marchesin, F. P.; Barbosa, R. S. Alves, M. A. L. Gadola, M. Chindamo, D. Benini, C. (2016) **Upright mounted pushrod: the effects on racecar handling dynamics**. The Dynamics of Vehicles on Roads and Tracks, Taylor & Francis Group, London, ISBN: 978-1-138-02885-2, Vol. 57, pp. 543-552.

Mendes, R. J. (2014) **Development of a Test Bench for a Kistler Navigation Sensor**. Cologne University of Applied Sciences, Internship Report, pp. 1-18.

Mori, A. M. (2013) **O uso de sistema inercial para apoiar a navegação autônoma**. Dissertação de Mestrado, Engenharia de Transportes, EP-USP, pp. 180

Nadal, M. J. (1908) **Locomotives à vapeur**. Bibliotéque de Mecanique Appliquée et Genie. Collection encyclopédie scientifique, Vol. 186, Paris, France.

Park, S.; Hong, S. K. (2011) **Angular Rate Estimation Using a Distributed Set of Accelerometer**. Sensors, Publisher MDPI, Vol. 11, pp. 1044-10457.

Prado, M.; Costa Neto, A.; Barbosa, R. S.; Grando, D. (2011) **A stability study of a three-point and a four-point secondary suspension configuration for a rail passenger car**. International Journal of Vehicle System Dynamics, XIV IAVSD Symposium. DOI: 10.13140/2.1.2595.7126, Vol. 1, pp. 6.

Salvagni, R. B.; Barbosa, R. S.; Alves, M. A. L. (2013) **A geometrical model for tires under vertical loading**. Anais do XXI Simpósio Internacional de Engenharia Automotiva — SIMEA 2013. São Paulo, DOI: 10.5151/engpro-simea-PAP2, Vol. 1, nº 1, pp. 1-15.

Santana, D. D. S. (2011) **Navegação terrestre usando unidade de medição inercial de baixo desempenho e fusão sensorial com filtro de kalman adaptativo suavizado**. Teses de Doutorado em Engenharia de Controle Automação. EP-USP.

Santos G. F. M.; Barbosa, R. S.; Joy R (2012) **Analysis of longitudinal forces in heavy and long train.** In: The First International Conference on Railway Technology: Research, Development and Maintenance, 2012, Las Palmas Gran Canaria, Spain, Civil-Comp Press. Vol. 1. pp. 5-12.

Santos G. F. M.; Barbosa, R. S.; Urban, C ; Shu, X.; Joy, R. (2014) **Characterization and Modelling of a New Heavy Axle Load Freight Wagon for Wheel Rail Wear Prediction**. Journal of Mechanical Engineering and Technology, DOI: 10.18005/JMET0203001, pp. 17-28.

Santos, G. F. M.; Barbosa, R. S. (2016) **Modeling of a railway vehicle travelling through a turnout**. SAGE Publishing, Proceedings of the Institution of Mechanical Engineers, Part F: Journal of Rail and Rapid Transit, DOI: 10.1177/0954409715595256, Vol. 230, Issue 4, pp. 1397–1404.

Santos, G. F. M.; Barbosa, R. S. (2017) **Safety Analysis of a Railway Car under the Periodic Excitation from the Track**. Journal: Cogent Engineering, DOI: 10.1080/23311916.2016.1263027. Volume 3, Number 1, pp. 1-12.

Savitzky, A.; Golay, M. J. E. (1964) **Smoothing and differentiation of data by simplified least squares procedures**. Analytical Chemestry, Vol. 36, Issue nº 8, pp 1627–1639.

Sun, Y. Q. Cole, C. Spiryagin, M. (2015) **Monitoring vertical wheel–rail contact forces based on freight wagon inverse modelling**. Centre for Railway Engineering, Central Queensland University, Australia. Advances in Mechanical Engineering, Vol.: 7, nº 5, pp. 1–11.

Terra, R. T.; Barbosa, R. S. (2015) **Inclusion of the displacement variable on the damper modeling in multibody environment**. In: Congresso SAE BRASIL 2015, Vol. 2015. pp. 1-8.

Titterton, D. H.; Weston, J. L. (2004) **Strapdown Inertial Navigation Technology**. Publisher Peregrinus, 2nd edition, pp. 581, U. K.

Trigo, F. C. (2005) **Estimação Não Linear de Parâmetros através dos Filtros de Kalman na Tomografia por Impedância Elétrica**. Tese de Doutorado, Escola Politécnica da Universidade de São Paulo, EP-USP, São Paulo, Brasil.

Vilela, D.; Barbosa, R. S. (2011A) **Analytical models correlation for vehicle dynamic handling properties**. Journal of the Brazilian Society of Mechanical Sciences and Engineering, DOI: 10.1590/S1678-58782011000400007, Vol. 33, nº 4, pp. 437-444.

Vilela, D.; Barbosa, R. S.; (2011B) **Analytical solution proposal to vehicle dynamic handling properties**. International Journal of Vehicle Systems Modelling and Testing - IJVSMT, DOI: 10.1504/IJVSMT.2011.039831, Vol. 6, nº 1, pp. 56-71.

Vilela, D.; Barbosa, R. S. (2012) **Vehicle Dynamics Handling Determination with Enhanced Analytical Models**. SAE Technical Paper nº 2012-36-0165, DOI: 10.4271/2012-36-0165. pp. 10.

Vilela, D.; Barbosa, R. S. (2013) **Numerical optimisation methods applied to the concurrent problem of vehicle ride and handling**. International Journal of Vehicle Systems Modelling and Testing - IJVSMT, DOI: 10.1504/IJVSMT.2013.057526, Vol. 8, nº 4, pp. 316-334.

Villani, E.; Barbosa, R. S. (1998) **Programa de Caracterização Geométrica do Contato Roda/Trilho**. Relatório Técnico IPT-DITT-ADFR, nº 36.315.

Xia, F. J.; Cole, C.; Wolfs, P. (2007) **An inverse railway wagon model and its applications**. Vehicle System Dynamics, Vol. 45 Issue 6, pp. 583-605.

Xia, F.; Cole, C.; Wolfs, P. (2008) **Grey box-based inverse wagon model to predict wheel–rail contact forces from measured wagon body responses**. Vehicle System Dynamics, Vol. 46, pp. 469–479.

Zanoni, F. D.; de Barros, E. A. (2014) **A real-time navigation system for autonomous underwater vehicle**. Journal of the Brazilian Society of Mechanical Sciences and Engineering, DOI: 10.1007/s40430-014-0231-2. Volume 37, Issue 4, pp 1111–1127.

7.2 Teses de Mestrado e Doutorado

Luciano Ribeiro Pinto Consoli. (2007) **Análise do Comportamento Dinâmico Lateral de um Veiculo Ferroviário**. Dissertação de Mestrado em Engenharia Mecânica - Universidade de São Paulo. Orientador: Roberto Spinola Barbosa.

Daniel Vilela (2010) **Aplicação de Métodos Numéricos de Otimização ao Problema Conjunto da Dirigibilidade e Conforto Veicular**. Tese de Doutorado em Engenharia Mecânica - Universidade de São Paulo. Orientador: Roberto Spinola Barbosa.

Felipe Marchesin (2012) **Análise de Desempenho de Veiculo do Tipo Formula**. Dissertação de Mestrado em Engenharia Mecânica - Universidade de São Paulo. Orientador: Roberto Spinola Barbosa.

Gabriel P. R. Maciel (2015) **Métodos para a redução de graus de liberdade em sistemas dinâmicos lineares**. Dissertação de Mestrado em Engenharia Mecânica - Universidade de São Paulo, Orientador: Roberto Spinola Barbosa.

Guilherme Fabiano Mendonsa dos Santos. (2015) **Análise Dinâmica de Segurança em Veiculo Ferroviário de Carga em Tangente considerando a excitação periódica da via permanente**. Tese de Doutorado em Engenharia Mecânica - Universidade de São Paulo, Orientador: Roberto Spinola Barbosa.

7.3 Normas Nacionais e Internacionais

EN 14363 (2016) **Railway applications - Testing and Simulation for the acceptance of running characteristics of railway vehicles - Running Behaviour and stationary tests**. Comité Européen de Normalisation (CEN), pp. 118.

UIC-518 (2009) **Testing and approval of railway vehicle from the point of view of their dynamic behaviour**. Union Internationale des Chemins de Fer - UIC Code, 4th edition, pp. 119.

EN 13848-6 (2014) **Railway applications - Track geometry quality - Part 6: Characterisation of track geometry quality**. Comité Européen de Normalisation (CEN).

FRA Manual (2014) **Track and Rail and Infrastructure Integrity Compliance Manual. Volume II - Chapter 1 - Track Safety Standards - Classes 1 through 5**. Federal Railroad Administration.

AAR M-1001 Chapter 7 (1993) **Fatigue Design of New Freight Cars**. Association of American Railroads – AAR. pp. CII-95-CI-336.

AAR M-1001 Chapter 11 Service (1993) **Service Worthiness Test and Analyses for New Freight Cars**. Association of American Railroads – AAR. pp. 397-415.

ISO 2631-1 (1997) **Mechanical Vibration and Shock – Evaluation of Human Exposure to Whole Body Vibration. Part 1: General Requirements**. ISO (International Organization for Standardization), pp. 31.

CPTM (2007) **Projeto Geométrico do Traçado de Via Permanente. Especificação Técnica da Companhia Paulista de Trens Metropolitanos** – CPTM, documento AK7803.

7.4 Iniciações Científicas e Trabalho de Conclusão de Curso

A seguir são apresentados as Iniciações Científicas IC e Trabalhos de Conclusão de curso (TCC) relevantes:

Roberto Polese (1985) Sistema de contagem de ciclos. Iniciação Científica do Graduando em Engenharia Mecânica - Universidade de São Paulo. Orientador: Prof. Dr. Roberto Spinola Barbosa.

Flávio Makoto Hashimoto. (1994) Desenvolvimento de programa para apresentação de movimento modal. Iniciação Científica. Curso de Graduando em Engenharia Mecânica - Universidade de São Paulo. Orientador: Prof. Dr. Roberto Spinola Barbosa, pp. 37.

Emilia Villani (1997) Desenvolvimento de programa de cálculo de propriedades de contato. Iniciação Científica. Curso de Graduando em Engenharia Mecânica - Universidade de São Paulo. Orientador: Prof. Dr. Roberto Spinola Barbosa.

Marcelo Montandon (1998) Desenvolvimento de programa de calculo de propriedades de contato. Iniciação Científica de Graduando em Engenharia Mecânica - Universidade de São Paulo. Orientador: Prof. Dr. Roberto Spinola Barbosa

Renan Destéfani Monteiro. (2006) Estudo Básico de uma Suspensão do tipo Duplo A com ênfase para o veiculo Mini-Baja. Orientador: Prof. Dr. Roberto Spinola Barbosa.

Vinicius Lopes dos Santos (2007) Estudo e Otimização da Dinâmica Vertical de um Veículo através da Teoria de Sistemas Multicorpos.. Trabalho de Conclusão de Curso de Graduação em Engenharia Mecânica - Universidade de São Paulo. Orientador: Prof. Dr. Roberto Spinola Barbosa.

Vinícius Lopes dos Santos (2007) Estudo da dinâmica vertical de um veículo através da teoria de sistemas multicorpos. Trabalho de Conclusão de Curso de Graduação em Engª Mecânica - Escola Politécnica de São Paulo. Orientador: Prof. Dr. Roberto Spinola Barbosa.

Gabriel Pedro Ramos Maciel (2008) Estudo de Suspensão Veicular Ativa e Semiativa Utilizando a Técnica de Multicorpos. Trabalho de Conclusão de Curso de Graduação em Engenharia Mecânica - Universidade de São Paulo. Orientador: Prof. Dr. Roberto Spinola Barbosa.

Vinicius Alves Fernandes (2008) Modelagem de Sistemas Multicorpos Utilizando Programa AUTOLEV. Orientador: Prof. Dr. Roberto Spinola Barbosa.

Erik Ohara (2009) Análise dinâmica de um veículo de passeio equipado com sistema de esterçamento nas quatro rodas. Trabalho de Conclusão de Curso de Graduação em Engenharia Mecânica - Universidade de São Paulo. Orientador: Prof. Dr. Roberto Spinola Barbosa.

Joao Ribeiro de Oliveira Gomes. (2009) Modelagem e Simulação da Dinâmica de um Veículo Ferroviário. Trabalho de Conclusão de Curso de Graduação em Engenharia Mecânica - Universidade de São Paulo. Orientador: Prof. Dr. Roberto Spinola Barbosa.

Juliano Todesco (2011) Otimização do controle da dinâmica longitudinal do trem de carga equipado com sistema de frenagem eletro-pneumático (ECP). Trabalho de Conclusão de

Curso. de Graduação em Engª Mecânica - Escola Politécnica de São Paulo. Orientador: Prof. Dr. Roberto Spinola Barbosa.

Paulo Yamagata (2012). Modelagem de Sistema de Suspensão e Veiculo tipo BAJA SAE com Software de Dinâmica Multicorpos. Trabalho de Conclusão de Curso de Graduação em Engenharia Mecânica - Universidade de São Paulo. Orientador: Prof. Dr. Roberto Spinola Barbosa.

Paulo Ricardo Arantes Gilz (2014) Método de planificação e otimização de trajetórias não oscilantes para o movimento longitudinal de trens. Trabalho de Conclusão de Curso de Graduação em Engenharia Mecânica - Universidade de São Paulo. Orientador: Prof. Dr. Roberto Spinola Barbosa.

Prandy Lôvo de Oliveira (2015) Controle de Sistema de Freio ABS. Trabalho de Conclusão de Curso de Graduação em Engenharia Mecânica - Universidade de São Paulo. Orientador: Prof. Dr. Roberto Spinola Barbosa.

Leonardo Novak Rossi e Diego Delgado Colombo de Oliveira (2015) Modelagem, controle e prototipação de veículo baseado em pêndulo invertido. Trabalho de Conclusão de Curso de Graduação em Engenharia Mecânica - Universidade de São Paulo. Orientador: Prof. Dr. Roberto Spinola Barbosa.

Marlon Dio Fukuda Koga (2015) Modelagem e controle de veículo aéreo não tripulado do tipo quadricóptero com melhoria de resposta em frequência. Trabalho de Conclusão de Curso de Graduação em Engenharia Mecânica - Universidade de São Paulo. Orientador: Prof. Dr. Roberto Spinola Barbosa.

Raphael Vian Montani (2016) Análise e controle da dinâmica de um caminhão. Trabalho de Conclusão de Curso de Graduação em Engenharia Mecânica - Universidade de São Paulo. Orientador: Prof. Dr. Roberto Spinola Barbosa.

Moretti, E.; Baptista, G. F.; (2015) Modelagem e Projeto de um Sistema de Controle Ótimo da Suspensão Semi-ativa de um Automóvel. Trabalho de Conclusão de Curso de Graduação

em Engenharia Mecânica - Universidade de São Paulo, Orientador: Prof. Dr. Roberto Spinola Barbosa.

Daniel Augusto de Souza Mello Monteiro (2016) Modelagem dinâmica de veículo. Trabalho de Conclusão de Curso de Graduação em Engenharia Mecânica da EP-USP. Orientador: Prof. Dr. Roberto Spinola Barbosa, pp. 69.

7.5 Patentes Obtidas

Barbosa, R. S.; Michelin, A.; Kamigushi, M. A.; Rogero, M. T.; Mendes, F. G.; Lima, R. G. (1989). Máquina de Chave Ferroviária com Acionamento Hidráulico. Patente: Privilégio de Inovação. Número do registro: PI89009061, Instituição de registro: INPI - Instituto Nacional da Propriedade Industrial. Instituição financiadora: FINEP. Brasil.

Barbosa, R. S.; Polese, R; Villani, E. (1994) Programa para Calculo das Propriedades de Contato Roda/Trilho. 1993. Patente: Programa de Computador. Número do registro: 94.009.292.

Barbosa, R. S. (2008) Truque de Inscrição Radial. Pedido de Patente de Invenção. INPI - Instituto Nacional da Propriedade Industrial - PI08027226.

Barbosa, R. S. (2009) Sistema de amortecimento de rolagem e torção de suspensão de veículo. Patente: Privilégio de Inovação. Número do registro: 018090005545.

Barbosa, R. S. (2013) Sistema de identificação da qualidade de vias férreas e de veículos metroferroviários e método de identificação do índice de segurança por estimativa direta das forças de contato entre as rodas do veículo metroferroviário e a via férrea. Pedido de Patente de Invencão de Processo. INPI - Instituto Nacional da Propriedade Industrial - BR1020130190721.

7.6 Programas Registrados

Barbosa, R. S.; Michelini, A.; Mendes, M. A. P. G. (1990) Programa de Simulação de Marcha de Trens. Patente: Programa de Computador. Número do registro: 90.000.936.

Barbosa, R. S.; Polese, R.; Villani, E. (1993) Programa para Calculo das Propriedades de Contato Roda/Trilho. Patente: Programa de Computador. Número do registro: 94.009.292.

8 ANEXOS - TRABALHO RELAVANTES PUBLICADOS EM REVISTAS INDEXADAS

TRABALHOS RELEVANTES PUBLICADOS EM REVISTAS INDEXADAS

8.1 ANEXO A

EVALUATION OF RAILWAY TRACK SAFETY WITH A NEW METHOD FOR TRACK QUALITY IDENTIFICATION

Barbosa, R. S. (2016A). Evaluation of Railway Track Safety with a New Method for Track Quality Identification. International Journal of Transportation Engineering, Publisher: American Society of Civil Engineers - ASCE, DOI: 10.1061/(ASCE)TE.1943-5436.0000855, Vol.: 142, Issue 11, pp. 1-11.

Evaluation of Railway Track Safety with a New Method for Track Quality Identification

Roberto Spinola Barbosa, Ph.D.[1]

Abstract: A new method for track inspection is developed to complement traditional geometric methods. An inertial measuring system and a specialized data treatment method is proposed to evaluate railway track safety, observed from the vehicle dynamic performance point of view. System equations for the inverse vehicle dynamic problem, augmented with the suspension torsion equation, are solved to estimate the wheels driving forces that are directly correlated with the vehicle safety traveling over an irregular track. Results of a measuring campaign on a railway wagon are used to evaluate the present system by direct positional comparison with lateral and vertical contact forces (L/V) safety ratio measured with two instrumented wheelsets (IWS) installed on the leading bogie of the wagon. Also, data collected and treated are compared with track geometry measurements. The results of quantified track safety present good agreement with those found using traditional measuring methods. This confirms the ability of the new method to detect the location of the highest potential hazard region, for optimized track maintenance purposes. The new system proves to be a promising method for track safety evaluation. **DOI: 10.1061/(ASCE)TE.1943-5436.0000855.**

Author keywords: Railway; Track; Quality; Safety.

Introduction

Railway companies always seek to operate transport systems with greater confidence and productivity. To meet this expectation, tracks should be reliable, available for use, and easy to maintain. Therefore, track quality must satisfy a set of desirable convenient properties to guarantee availability.

Different track quality indexes (TQI) have been proposed by several agencies [European Railway Agency 2011; Union Internationale des Chamins de Fer (UIC) (Nederlof and Dings 2010); Federal Railway Administration (FRA) (Stuart 2012)], but almost all are only related to geometric track issues. In fact, no safety aspect has been objectively considered. According to the Det Norske veritas (DNV) Report (European Railway Agency 2011), railway interruptions can be produced from: infrastructure failure, operational failure, and train/vehicle failure. All problems described are well quantified and mainly related to component or subsystem failure. Component failure is an event easily observable, the correlation of which is well posed. Therefore, the mentioned technique is only corrective, and some mitigation measures can be proposed.

Traditionally, railway track quality is quantified by a specialized car that measures the track's basic geometric parameters, short wavelength irregularities, and absence of complete track settlement. Usually, the inspection measures and records the variation of the track gauge, vertical and lateral alignments, and cross-level (angular variation on a track section—cant or superelevation). The values measured are compared to standardized limits. Additionally, the cross-level variation per meter (track twist) can be calculated depending on the data sample rate. Others deleterious aspects can be mentioned: lateral instability, poor wheel load equalization, vehicle overturning, longitudinal train forces, passengers' comfort (or ride quality) tailored by the vertical and lateral acceleration of the vehicle car-body, mutual vehicle/track aggression, etc. (Suarez et al. 2013).

Nevertheless, poor vehicle dynamic performance frequently occurs at a track location that does not exceed track geometry limits such as curve entry or exit or lacks track misalignments that promote vehicle yaw instability or hunting. Conversely, track geometry locations that exceed track geometry standard limits do not often cause poor vehicle performance. Poor vehicle performance may point to an area of track that needs maintenance to prevent further degradation (Ketchum and Wilson 2012).

A safety diagnosis is the ability to identify the particular region of the line where vehicle dynamic performance is poor or dangerous. To meet a security aspect, the evaluation must also consider the outcome of a lack of safety: a vehicle that effectively derails. As the track and the vehicle form a naturally mutual dependent system, the vehicle's behavior reflects its own properties and its forced movements, which are directly affected by the track geometry input, track stiffness, and train speed. This is the goal of this methodology: to include the vehicle's response in the track safety quantification.

State of the Art

Several track inspection systems or methods are still being developed. The American Federal Railway Administration has a project (Stuart 2012) to develop a system to carry out autonomous track inspections. Gullers et al. (2011) proposed a track condition analyzer (TCA) based on high-frequency vertical wheel load measurements (up to 2 kHz) performed with an instrumented wheelset (IWS) to detect mainly rail corrugations and stiff rail support. Also, the vertical wheelset acceleration (Tsunashima et al. 2014) with proper data treatment is still being researched. The European project dynamic of train (DYNOTRAIN) (Haigermoser et al. 2014) uses a multiple regression model of the vehicle dynamic behavior, within the wavelength range of 3 and 25 m, to assess track quantity. New IWS techniques are still being developed (Matsumoto et al.

[1]Professor, Dept. of Mechanical Engineering, Polytechnic School of Sao Paulo Univ. (EP-USP), Av. Prof Mello Moraes 2231, CEP 05508-970, Sao Paulo, Brazil. E-mail: spinola@usp.br

Note. This manuscript was submitted on December 19, 2014; approved on January 28, 2016; published online on June 27, 2016. Discussion period open until November 27, 2016; separate discussions must be submitted for individual papers. This paper is part of the ***Journal of Transportation Engineering***, © ASCE, ISSN 0733-947X.

2014), and others methods to estimate vehicle properties have been proposed (Pence et al. 2013). Luber et al. (2010) proposed a method for track geometry evaluation, based on a representative vehicle vertical and lateral transfer functions, to predict the vehicle response due to track geometry input.

As an acceptance process described by Wilson et al. (2011) in the state-of-the-art assessment method, a new vehicle has to demonstrate safety traveling over the track in the following conditions: low-speed flange-climbing derailment (wheel unload or body rotation resistance), vehicle dynamic response, and overturning due to overspeeding in curves. As the track's safety performance is closely affected by the track design, maintenance conditions, and effects of the local environment, it was recommended to improve measurement techniques and analysis methods. Wei et al. (2013) proposed vehicle-suspension fault detection based on acceleration sensors in the four corners of the car-body.

Calçada and Vale (2014) presents a vehicle–track dynamic-interaction one-dimension model for predicting the evolution of the vertical track profile degradation process and the attained results reveal the importance of track irregularities, vehicle speed, and vehicle characteristics on the evolution of the track profile (Hung et al. 2010). The numerical simulations demonstrate the potential of the proposed methodology to serve as a tool to forecast track settlement and estimate the dynamic response of the track along the degradation process.

Safety Fundaments

The concept of safety associated with track quality is not well described and is usually misunderstood. The track safety is the ability to promote nondangerous traffic of vehicles and trains. A vehicle transporting goods obviously depends on the track's structural integrity, efficient train operation, and the vehicle's performance to reach a minimal probability of derailment. The only way to guarantee effective track quality by focusing on safety is to objectively contemplate all these aspects including vehicle behavior.

A track's properties are mainly described by its geometric parameters such as curvature, transition curve form and length, and superelevation. Track deformation also affects the passing vehicle due its stiffness. The track usually has to be shared between passenger and freight and partial compensated (or speed-ideal) superelevations are employed. This produces a nonsymmetric wheel load distribution. Transition curve length and cant value produce a twisting variation rate, usually limited due to its influence on the vehicle suspension torsion. Finally, curve radius inhibits speed and is usually limited due to wheelset and bogie restrictions. The track irregularities are variations around the nominal geometry and may be a random or a periodic variation. As can be observed in the previous description, no safety consideration is perceived regarding the track geometry properties or roughness issue.

Regardless of the type of irregularity, the fact is that a track shape with varying geometry imposes a range of load distributions on the wheels, and their sum imposes a variation on the vehicle's kinematics. Therefore, the wheel's acting forces produce the bogie directioning and vehicle accelerations to negotiate the curves. The objective safety of the system is associated with vehicle derailment, traditionally quantified with the lateral and vertical contact forces (L/V) factor, which is well-known and widely accepted. This means that the vehicle reacts according to its transfer function to the track irregularities input. Therefore, the vehicle must be included in the evaluation process to objectively quantify the track quality from the point of view of safety.

Unsafe Types

Generally speaking, there are three types of relevant unsafe vehicle conditions. The first type is the wheel-climb derailment (Barbosa 2009). This may occur at low speed in sharp curves and is particularly related to vehicle suspension stiffness and the wheel's load-distribution condition. The second type is mainly related to large movements of a vehicle's main body. This condition can be associated with the vehicle's unsprung mass dynamic movements and directioning bogie/wheelset properties. The latter type is relative to a syntonized train speed and a particular type of track irregularities. This last one is associated the evenness of the track's wavelength, the vehicle's natural frequencies, and the specific train speed (Barbosa 2011). Although there are other types of unsafe conditions, including vehicle instability, accidents, and component failures the second type here described is mainly related to the vehicle body's low-frequency movements and small energy dissipation.

The methodology proposed here to quantify track safety is based on detecting signs of unsafe railway vehicle performance, mainly associated with the second and third types unsafe conditions when considering track evenness when traveling (Barbosa 2015). These signs are used to identify the exact location along the track and to prioritize the pertinent track geometry corrections for the most harmful irregularity to vehicle safety.

The metric adopted to identify the potential harmful location associated with the vehicle safety is the traditional L/V ratio between the wheel lateral (L) and vertical (V) contact force. The wheel forces are quantified from the measurement of the vehicle attitude and its overall dynamic behavior. This task is performed with an inverse vehicle dynamic model, fed with data acquired from the instrumented vehicle during its transit journey. The vehicle instrumentation is composed of an inertial measuring device (IMU) with nine high-resolution transducers and an inertial navigation algorithm (INS) for attitude recognition and a global positioning system (GPS) signal.

Track–Vehicle Interaction

The track irregularities are the input to the vehicle dynamics on a moving train. Track geometry variations are generally described by their circular radius, cant, and transition length. Some types of irregularities do affect the modal vehicle behavior (e.g., bounce vibration due to longwave track level or lower sway mode due to track alignment). Other track irregularities are absorbed by vehicle's suspension (e.g., short wavelength track twist). In addition, the track stiffness does affect the geometry during the vehicle passage.

The wheel–rail contact force, due to the vehicle's dynamic behavior, is a function of the roughness of the track on which the vehicle is traveling. To identify the acting contact forces that produce the vehicle's directioning movements, it is necessary to solve an inverse dynamic problem. Vehicle dynamics are described by a set of differential equations obtained from the Newton-Euler theorems applied to a model of the vehicle considered as a rigid body. This equation is valid for a fixed reference frame **N** (OXYZ) as presented in Fig. 1. For the translational movements, the following differential equations relate accelerations and external forces in an earth fixed-reference frame:

$$m^N \vec{a}_G = \sum \vec{F}^{\text{ext}} \tag{1}$$

This equation does not consider the drag and Coriolis effects from the earth rotations due to the irrelevant magnitude faced by the vehicle accelerations. The external forces are mainly due to wheel contact forces and gravitational effects as shown in Fig. 1.

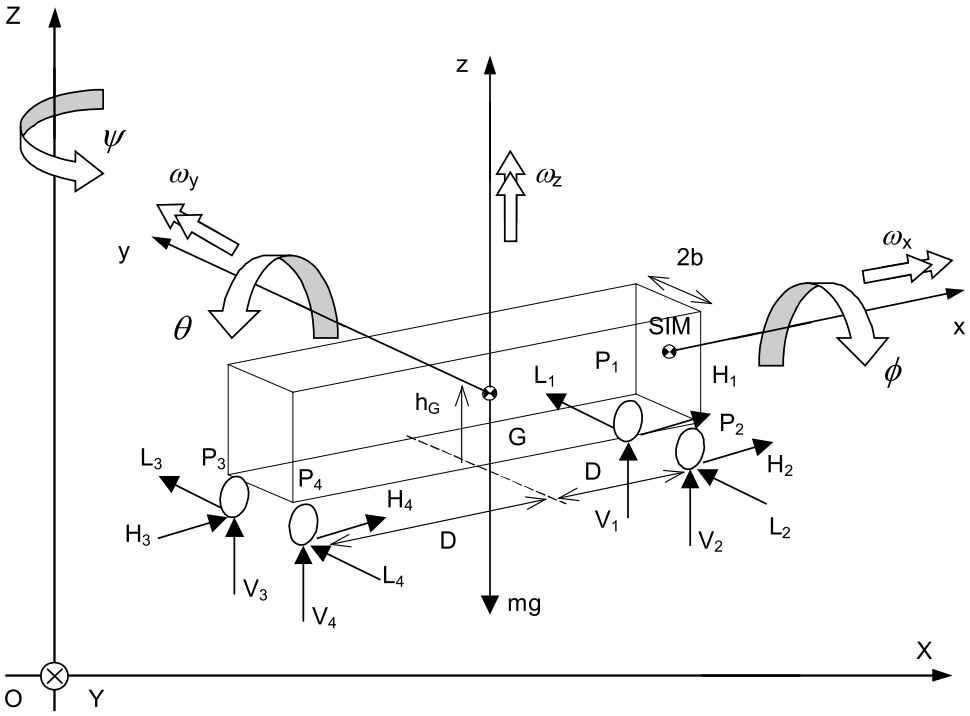

Fig. 1. Body attitude and forces distribution on the vehicle

$$m^N\vec{a}_G = \sum \vec{F}_{\text{wheels}} - m^N\vec{g} \tag{2}$$

The equation can also be expressed in the body reference frame (Gxyz) using a rotational transformation matrix $\boldsymbol{T}$, composed of the three Euler angles (roll ϕ, pitch θ, and yaw ψ) as identified in Fig. 1, from which the accelerations are to be measured and the forces computed

$$mT_N^B({}^N\vec{a}_G + {}^N\vec{g}) = T_N^B \sum \vec{F}_{\text{wheels}} \tag{3}$$

When the measuring system is fixed at a particular point P, not coincident with the vehicle center of gravity $\boldsymbol{G}$, the measured acceleration must be projected according to the field acceleration equation, to be used by the Newton equation

$$\vec{a}_G = \vec{a}_P + \dot{\vec{\omega}} \wedge (G-P) + \vec{\omega} \wedge [\vec{\omega} \wedge (G-P)] \tag{4}$$

where the angular velocity $\vec{\Omega} = \dot{\phi}\,\vec{i} + \dot{\theta}\,\vec{j}' + \dot{\psi}\,\vec{K}$, composed of roll rate $\dot{\phi}$, pitch rate $\dot{\theta}$, and yaw rate $\dot{\psi}$. For the rotational movements described in a moving reference frame attached to the vehicle, the following differential equations relate angular accelerations $\dot{\omega}$ and body angular velocity $\omega_B = [\,\omega_x \quad \omega_y \quad \omega_z\,]^T$ and external moments with respect to the same pole:

$$[J]_G\{\dot{\omega}\} + [\omega_B] \wedge [J]_G\{\omega_B\} = \{M_G^{\text{ext}}\} \tag{5}$$

The body external contact forces due to each wheel (H_i, L_i, and V_i) are shown in Fig. 1. The body external moments (M_G) due to the wheel forces are obtained from the car-body dimensions as shown in Fig. 1. To work out the contact forces by solving the system equation, it is necessary to know the vehicle body's accelerations, as stated in Eq. (1). Additionally, it is also necessary to measure the angular velocity and estimate the angular acceleration, which are needed to solve Eq. (2). Finally, the body's angular attitude must be identified to solve torsion Eq. (6).

The system has six equations and 12 contact-force unknowns. Disregarding the longitudinal effects, one equation is removed and four longitudinal contact forces are ignored (no acceleration or breaking effects). Due to the system being hyperstatic, the contact lateral forces in each wheelset are summed. To solve the system with five equations and six unknowns, an additional suspension torsion equation is disclosed to access each vertical force relationship, completing the system.

The vehicle longitudinal torsion due to track twist affects mainly the vertical wheel load distribution. Considering the car structure as a rigid body, the track twist deflects the suspension unloading the diagonal wheels. This effect depends on the vehicle suspension stiffness, length and width of the vehicle, and magnitude and wavelength of track twist.

Namely, the expression for the vertical load variation as a function of the track's angular twist per meter (δ) is related to body geometry proportion ($D/2b$) and suspension torsional stiffness (k_ϕ) stated as

$$\Delta V = -k_\phi \frac{D}{2b}\delta \tag{6}$$

To estimate the track twist from the overall vehicle inclination, a special filter is used to recover the local track superelevation (α). However, the IMU coupled to the body measures the absolute vehicle roll angle in reference to the earth plane (ϕ). The total or earth referenced body angle, as shown in Fig. 2, is composed by the track cant angle (α) added to the relative vehicle roll angle (β) due to suspension movements and inertial mass center height (h_G)

$$\phi = \alpha + \beta \tag{7}$$

The track cant angle (α) can be measured with an additional IMU installed on the wheelset. If this value is not available, another identification method is necessary. Disregarding any small vehicle suspension roll, the twist variation can be obtained from

J. Transp. Eng., 2016, 142(11): 04016053

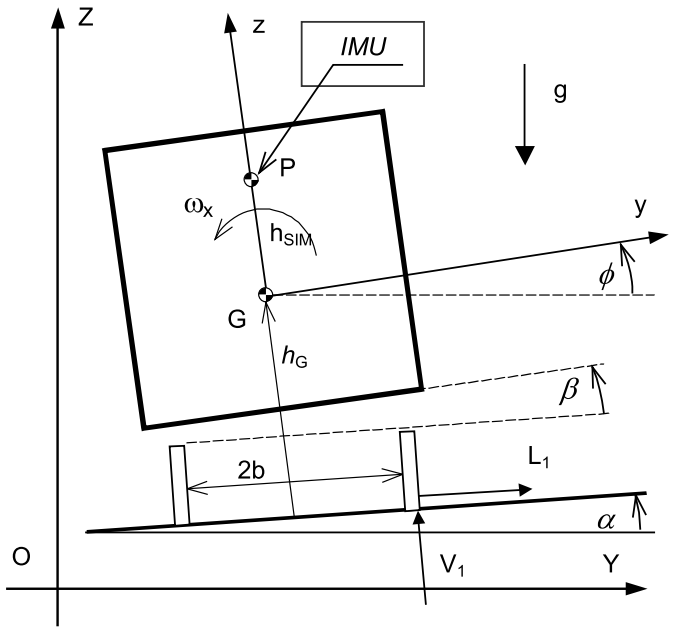

Fig. 2. Track and vehicle roll angles

$$\delta = \frac{d\alpha}{dS} \tag{8}$$

To identify the angles and attitude, the inertial navigation algorithm (INS) based on an extended Kalman filter is used as a multivariable estimator. With all this information, it is possible to solve the vehicle inverse dynamic equations to evaluate the driving contact forces and calculate the traditional safety ratio force L/V. Only for facility, a safety index (SI) for track safety quantification, calculated as the difference between the maximum L/V limit and the module of the measured L/V value for each wheel (Barbosa 2004), is used

$$SI = \left|\frac{L}{V}\right|_{\text{Limit}} - \left|\frac{L_i}{V_i}\right|_{\text{measured}} \tag{9}$$

To solve the inverse identification problem, the model of the system has to be known, have a unique existing solution, and continuously have data on the system available. Therefore, the requirements for the solution of the inverse problem are available using a complete measuring system, continuously monitoring vehicle body movement, and its attitude's dynamic behavior.

Measuring System and Data Treatment

The measuring system consists of an inertial measurement unit fixed on the vehicle, a GPS (uBlox, Switzerland) and a computer (Dell, Texas) for command actions, data acquisition and storage media. The inertial measurement unit (Honeywell, Morristown, New Jersey) is a micro-electro-mechanical system (MEMS) that measures the body movement. It utilizes a set of triorthogonal accelerometers to measure the vehicle accelerations ${}^{B}\vec{a}_G$ and an angular speed device to measure attitude variation ${}^{B}\vec{\omega}$. Additionally, a triorthogonal magnetometer set and a precision barometer measures the orientation ${}^{B}\vec{m}$ based on the earth's magnetic field and the relative level. A GPS identifies the vehicle speed and position expressed in the geographic-referenced latitude and longitude coordinate system. All this information is antialiasing filtered, digitalized, and recorded in the on-board control computer to identify the vehicle's three-dimensional movements.

To recover the complete vehicle attitude to calculate the SI index, an algorithm based on attitude heading reference system (AHRS) is used to treat rough data from the sensor and identify vehicle attitude. Vehicle accelerations and angular attitude are the main information to recover from the accelerometers, rate-gyros, and magnetometers information. To this end, a local-level frame identification algorithm must be involved for the vehicle's angular attitude recognition. An integrated navigation system on terrestrial movement methodology should combine the measured state data, with independent redundant data in a Kalman filter algorithm to provide a long-term stable solution. The strapdown inertial recovery (SIR) system identifies the external loads by solving the vehicle's dynamic equations.

The vehicle attitude relative to an inertial reference frame $\boldsymbol{N}$, is described by three Euler angles denoting vehicle roll angle ϕ, elevation angle θ, and heading angle ψ as shown in Fig. 1. The absolute position of a point in the vehicle is described by the vector ${}^{N}\vec{r}$ expressed in the inertial reference frame $\boldsymbol{N}$ and its time rate of change as

$${}^{N}\vec{r} = T_B^{NB}\vec{r} \quad \text{and} \quad {}^{N}\dot{\vec{r}} = T_B^{NB}\dot{\vec{r}} + \dot{T}_B^{NB}\vec{r} \tag{10}$$

where the superscript N over the vector = the fixed reference frame and the superscript B = the body fix moving reference frame; T_B^N = direction cosine matrix (DCM) formed with the three Euler rotation angles, which leads to the transformation matrix in terms of the three successive sequential body rotations [Sequence 3-2-1, according to NASA Standard (Baruh 1999)]

$$T_B^N = \begin{bmatrix} c\theta\, c\psi & c\theta\, s\psi & -s\theta \\ -c\theta\, s\psi + s\phi\, s\theta\, c\psi & c\theta\, c\psi + s\phi\, s\theta\, s\psi & s\phi\, c\theta \\ s\phi\, s\psi + c\phi\, s\theta\, c\psi & -s\phi\, c\psi + c\phi\, s\theta\, s\psi & c\phi\, c\theta \end{bmatrix} \tag{11}$$

where prefixes s and c = for sine and cosine for the respective angle.

The velocity vector ${}^{N}\vec{V}$ expressed in the inertial fixed frame $\boldsymbol{N}$ is defined in terms of position ${}^{B}\vec{r}$ expressed in rotating body fix reference $\boldsymbol{B}$, as

$${}^{N}\vec{V} = T_B^N\ {}^{B}\dot{\vec{r}} \text{ and its time derivative as } {}^{N}\vec{a} = \dot{T}_B^N\ {}^{B}\dot{\vec{r}} + T_B^N\ {}^{B}\ddot{\vec{r}} \tag{12}$$

The relation between the body angular velocities ω_B (roll rate, pitch rate, and yaw rate) and the vehicle attitude rate Ω_N (rate in bank, attitude, and heading) is described by Baruh (1999)

$$\begin{Bmatrix} \omega_x \\ \omega_y \\ \omega_z \end{Bmatrix} = \begin{bmatrix} 1 & 0 & -s\theta \\ 0 & c\phi & s\phi\, c\theta \\ 0 & -s\phi & c\phi\, c\theta \end{bmatrix} \begin{Bmatrix} \dot{\phi} \\ \dot{\theta} \\ \dot{\psi} \end{Bmatrix} \tag{13}$$

and the time rate of change of the transformation matrix $\dot{T}_N^B$ is

$$\dot{T}_B^N = T_B^N\, \omega_B \quad \text{where } \omega_B = \begin{bmatrix} 0 & -\omega_z & \omega_y \\ \omega_z & 0 & -\omega_x \\ -\omega_y & \omega_x & 0 \end{bmatrix} \tag{14}$$

where ω_i = the three angular speeds components described in the skew symmetric rotating matrix expressed on the body reference frame.

The problem of attitude determination involves determining the transformation matrix that maps the information sensed on-board with model transformation to the geographic frame magnetic and

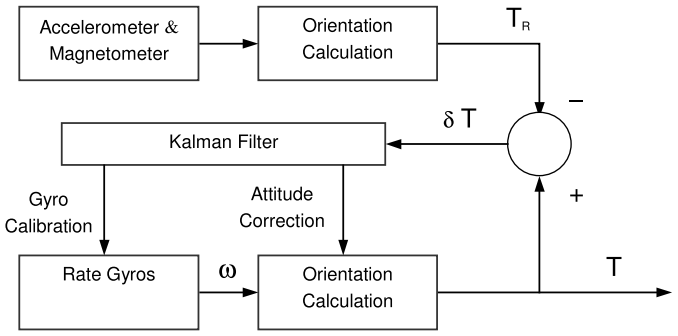

Fig. 3. Block diagram

gravity field components (Kuga and Carrara 2013). For the body-referenced magnetic sensor to match the local geographic-referenced magnetic field, and for the body-referenced accelerometer sensor to match the local geographic-referenced acceleration, then

$$^{N}\vec{m} = T_B^{NB}\vec{m} \quad \text{and} \quad ^{N}\vec{a}_G = T_B^{NB}\vec{a}_G \tag{15}$$

Assuming these two vectors are not parallel, a third orthogonal vector can be produced by the cross product. The matrix formed using these three vectors as columns (superscript T over the vector = transposed vector) can be associated with

$$[^{N}\vec{m}^T \quad ^{N}\vec{a}^T \quad (^{N}\vec{m} \wedge ^{N}\vec{a})^T] = T_B^N\,[^{B}\vec{m}^T \quad ^{B}\vec{a}^T \quad (^{B}\vec{m} \wedge ^{B}\vec{a})^T] \tag{16}$$

The matrix on the left-hand side is composed by known geographic-referenced information. The matrix on the right-hand side is composed of sensed information. Therefore, the unknown DCM orthogonal matrix can be obtained from

$$T_B^N = [^{B}\vec{m}^T \quad ^{B}\vec{a}^T \quad (^{B}\vec{m} \wedge ^{B}\vec{a})^T]^T[^{N}\vec{m}^T \quad ^{N}\vec{a}^T \quad (^{N}\vec{m} \wedge ^{N}\vec{a})^T]$$
$$\text{and} \quad T_N^B = (T_B^N)^T \tag{17}$$

A more-refined estimation for the DCM matrix to identify body attitude is obtained using a Kalman filter technique (Marins et al. 2001). Typical integration accumulated drift errors, such as heading vehicle attitude, are to be corrected with multiple cross-sensor information. With the accelerometers and the magnetometer, a level frame is to be determined. Based on this error difference, an extended Kalman filter algorithm corrects and stabilizes the rate-gyros' orientation calculations as shown in Fig. 3. Complementary GPS data allows estimating the vehicle speed, alignment, and curvature of the trajectory (Anderson and Bevly 2010).

The angular description can be in the Euler angles or Quaternion form, depending on the need to solve the singular problems due to angular quantification. With the accelerations, angular rate, and attitude angles, the vehicle's guiding force is calculated with the aid of a strapdown inertial recovery (SIR) algorithm that allows determination of the vehicle's L/V safety index. Data were previously filtered with a low-pass 15 Hz FIR filter.

Validation Process

The validation process of the proposed system was based on the comparison of the safety index (SI) calculated with the SIR algorithm, with measured bogie L/V wheel forces ratio acquired with two IWS.

The L/V wheel force ratio was measured with two Swedish instrumented wheel sets (IWS) (Interfleet, Sweden) installed on the leading bogie of the wagon. For compatible direct comparison with SIR results, the bogie L/V values were calculated from the sum of the lateral load of each wheel divided by the sum of the vertical measured loads. Speed and position of the train along the track were acquired with a GPS.

The track geometry and irregularities, measured with a specialized measuring car, are employed to complement the evaluation. Track geometry has an indirect correlation with safety but contributes to it and is also used in the comparison process. The measuring car (Plasser EM-100, Plasser & Theurer, Austria) was used to measure the variation of the track gauge, vertical and lateral rail alignments (left and right), and track section cant. Additionally, it identifies track curvature and track twist.

Test Campaign

A special test train was prepared to travel along a selected track section (Fig. 4). The train was formed with two locomotives (one at each end), four iron-ore 120-t loaded wagons (Fig. 5),

Fig. 4. Train formation (image by the author)

Fig. 5. 120-t iron ore wagon (image by the author)

Fig. 6. Instrumented wheelsets and measuring system (image by the author)

and two laboratory cars. The SIR system was installed underneath the first wagon as can be observed in Fig. 6. The two IWS are installed in the leading bogie of this wagon. The selected 25-km track section goes from 35 to 10 km (in the east sense) of the Carajas railway located in the northern region of Brazil. There are some curves and a bridge over a sea firth. This railway is 1.6-m gauge with almost 900 km connecting the Carajas Mine to the Sao Luiz port. The typical iron-ore wagon is a 120-t gondola *GDT*, with 0.1778×0.2794 m (7×11 in.) ride-control bogies.

Several tests were performed in this track section in the eastbound direction (traveling from mine to port, which is typical for the loaded wagon) at a constant speed and returning in the westbound direction at maximum authorized speed.

General Results

Several tests were conducted at controlled speeds (30, 50, 60, 70, and 75 km/h) in the eastbound direction (mine to port). The test

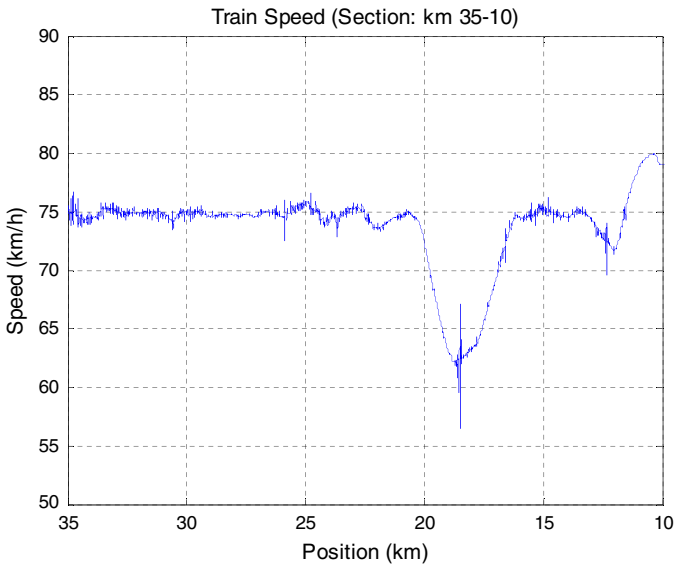

Fig. 7. Train speed

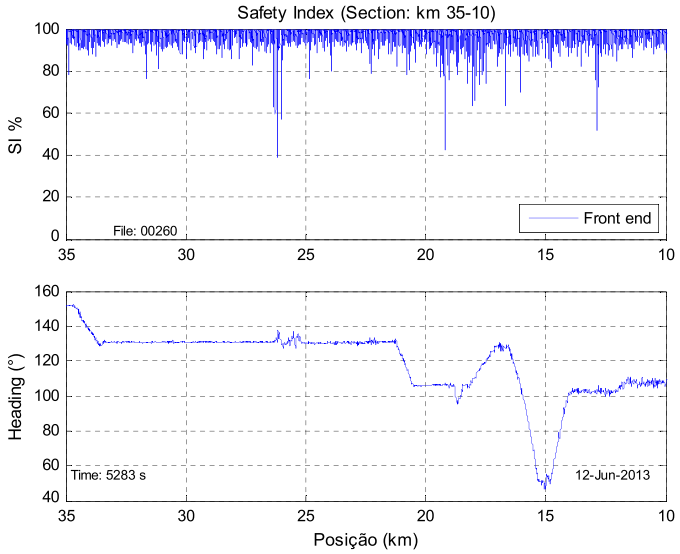

Fig. 8. Safety index ($35 + 000$ until $10 + 000$ km)

at 75 km/h was selected for a closer analysis. The train speed was expected to be constant but due to restrictions near a bridge, the real speed varied around programmed values and its time history is presented in Fig. 7. The track SI values determined in function of kilometric position are presented in the upper graph of Fig. 8. The lower graph in this figure shows the heading of the wagon.

The track geometry of this section, as measured with the EM-100 measuring car, is presented in Fig. 9. The upper graph shows the track cant along the kilometric position and the lower graph the track curvature. The wagon heading (lower graph in Fig. 8) is compatible and synchronized with the track curvature (lower graph in Fig. 9) measured with EM-100 car.

The L/V for the leading bogie, calculated from measured values of the two wheelsets, is presented in Fig. 10.

Particularly three track subsections are analyzed in detail. Results are presented as follow.

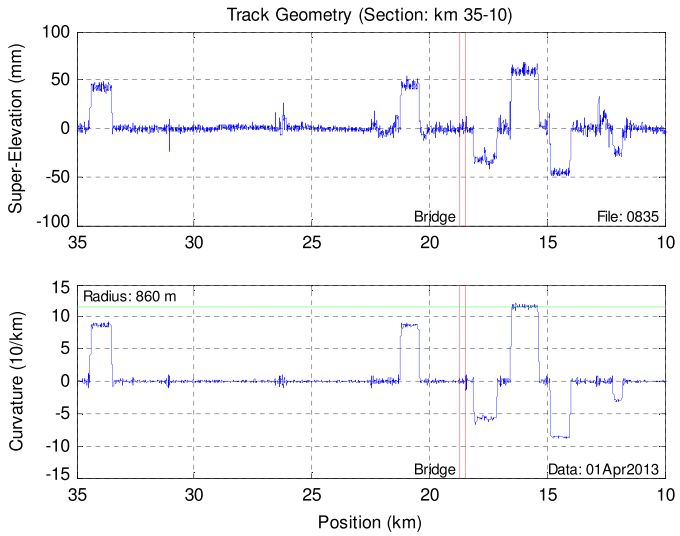

Fig. 9. Track-measured geometry (EM-100 measuring car)

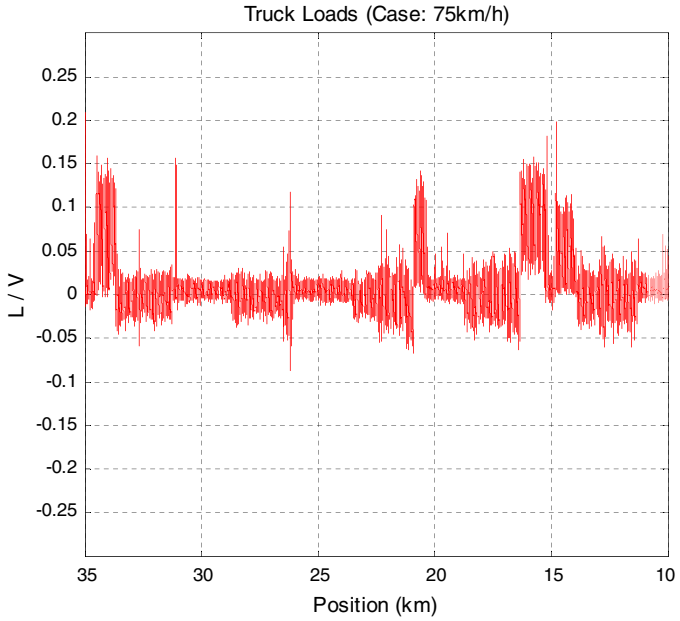

Fig. 10. Leading bogie L/V results

Subsection between 13.5 and 12 km

The subsection between kilometers $13+500$ and $12+000$ is a tangent segment of track as described by the wagon heading presented in the lower graph of Fig. 11. A SI of at least 50% is identified at $12+800$ km, as shown in the upper graph of Fig. 11.

The track geometry measurements detect a superelevation point of 30 mm at $12+800$ km, as shown in Fig. 12. In this region, the measured track twist variation is approximately -25 mm (Fig. 13). The leveling reaches -28 mm maximum, as shown in Fig. 14. The track alignment deviation of ± 8 mm can also be verified. The track gauge-widening reaches 10 mm, as shown in Fig. 13. Therefore the poor track geometry is correspondently identified with the SIR system. The safety in this track subsection is confirmed with the L/V measured with the instrumented wheelsets of ± 0.06, as shown in Fig. 15.

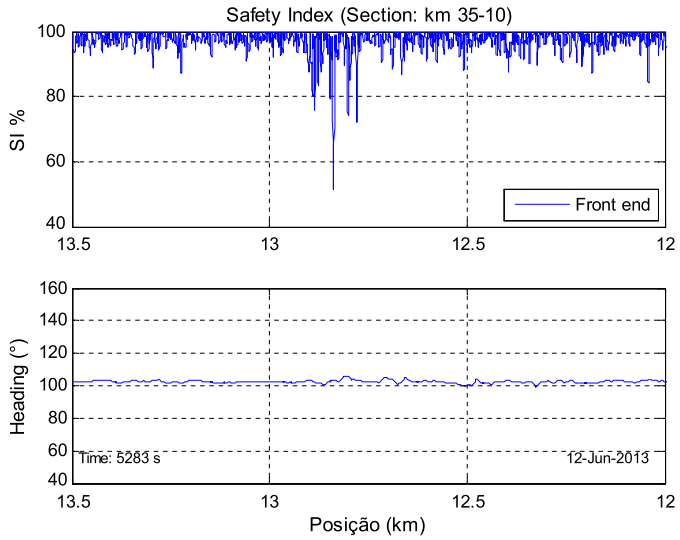

Fig. 11. Safety index and heading (13.5–12 km)

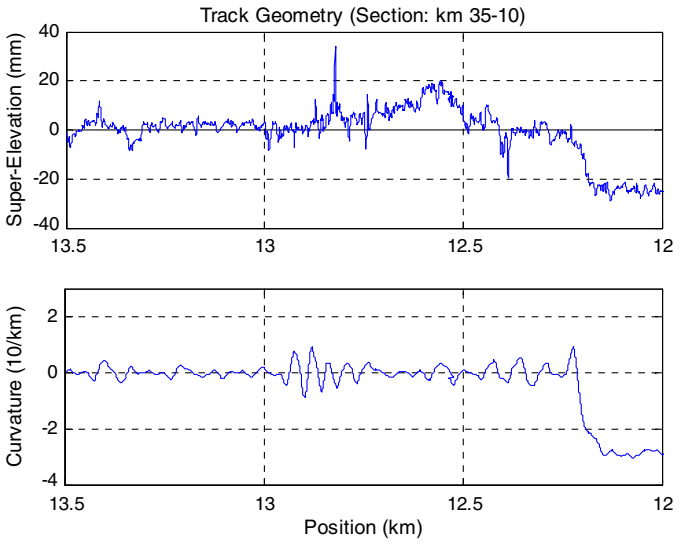

Fig. 12. Track superelevation and curvature (13.5–12 km)

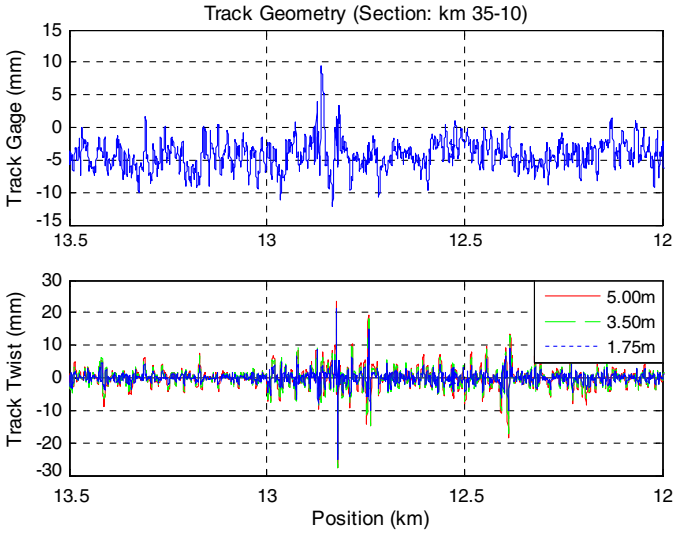

Fig. 13. Track gauge and twist (13.5–12 km)

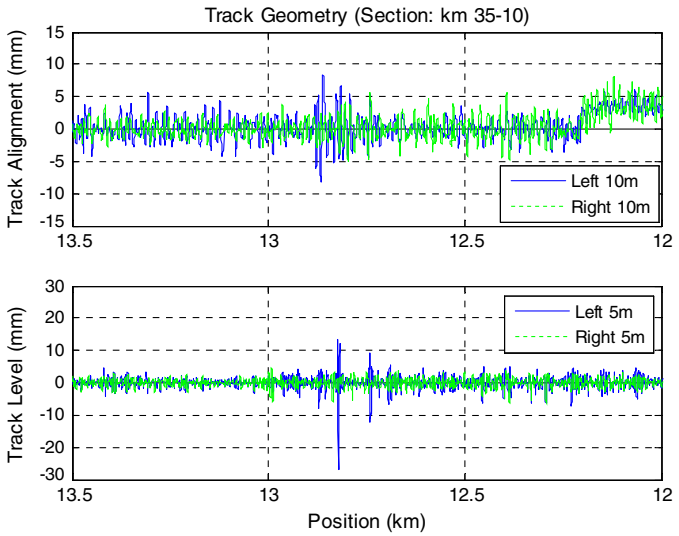

Fig. 14. Track alignment and level (13.5–12 km)

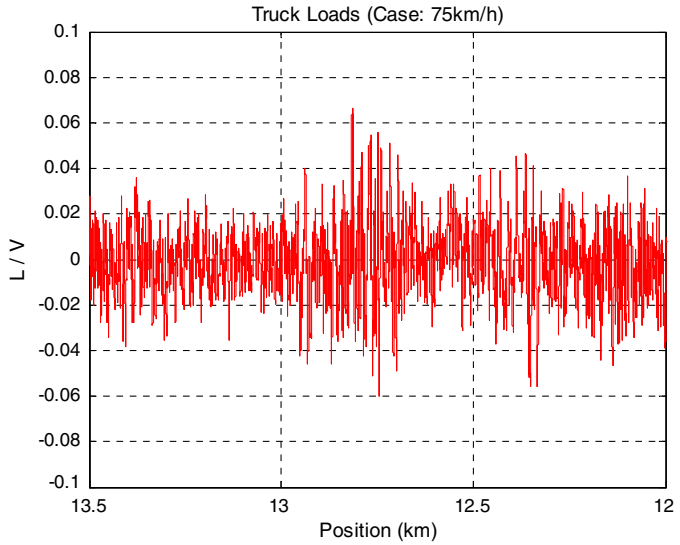

Fig. 15. Measured L/V for the front bogie (IWS) (13.5–12 km)

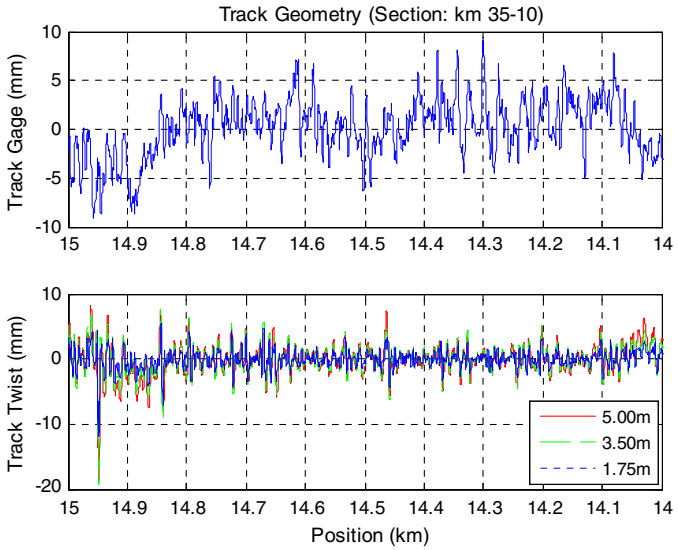

Fig. 17. Track gauge and twist (from 15 to 14 km)

Subsection between 15 and 14 km

The subsection between 15 + 000 and 14 + 000 km has been also analyzed in detail. In this section, there is a curve with a 1,150 m radius that starts at 14 + 900 km, considering the eastbound traffic. It is observed that the SI had a value of at least 80% just after the transition curve, as shown in Fig. 16.

Although the track geometry does not present any significant variations (Figs. 17 and 18) in this region, the L/V measured with instrumented wheelsets for the leading bogie shows a relevant peak of 0.2, as shown in Fig. 19, confirming the correct SIR identification.

Subsection from 31 + 500 *to* 30 + 500 km

The subsection between 31 + 500 and 30 + 500 km is a tangent segment of the track. At 31 + 100 km, an SI of at least 80% was identified, as shown in Fig. 20. A sudden change is noticed in the superelevation value, to 23 mm at 31 + 080 km, as shown

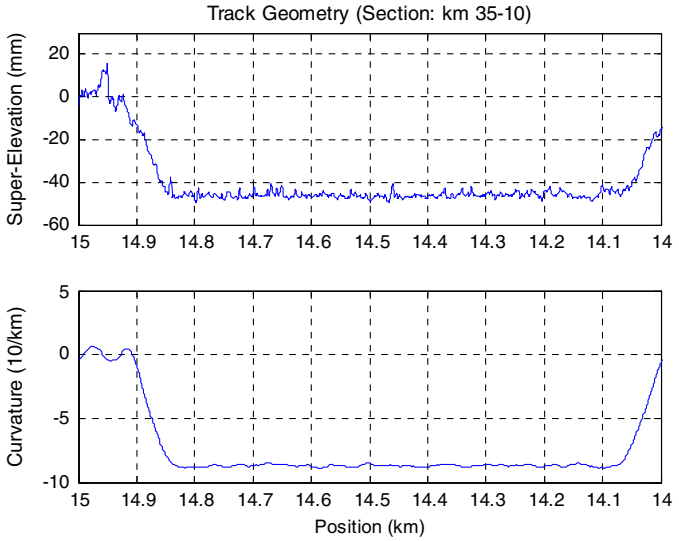

Fig. 18. Track superelevation and curvature (from 15 to 14 km)

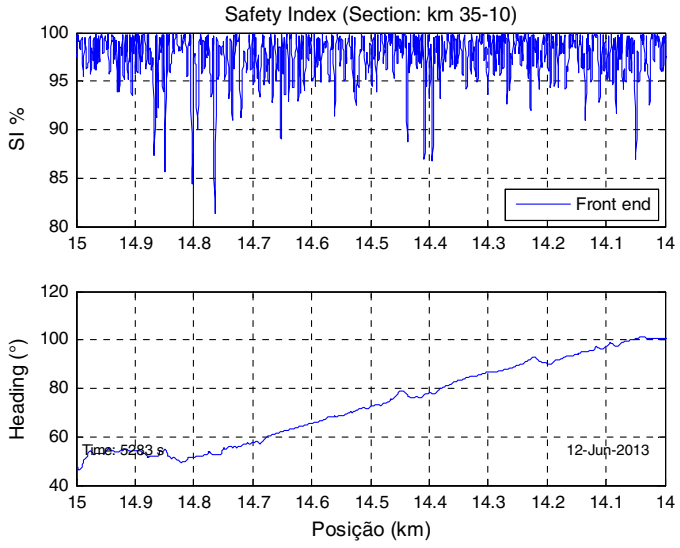

Fig. 16. Safety index (from 15 to 14 km)

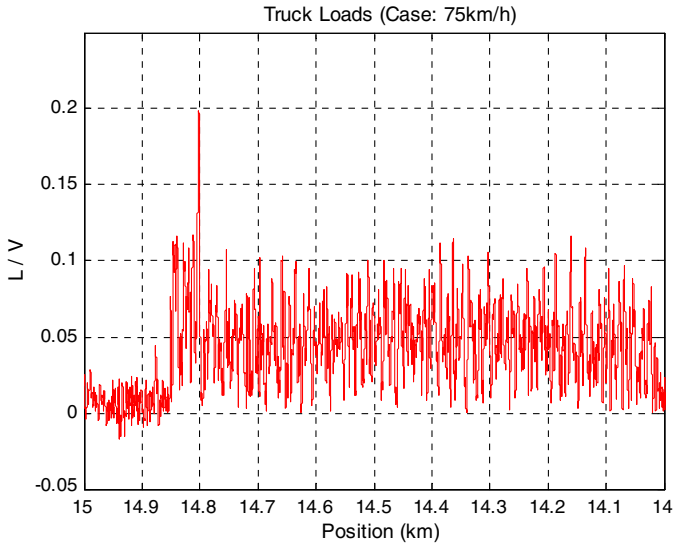

Fig. 19. Leading bogie L/V (from 15 to 14 km)

Fig. 20. Safety index (31 + 500 to 30 + 500 km)

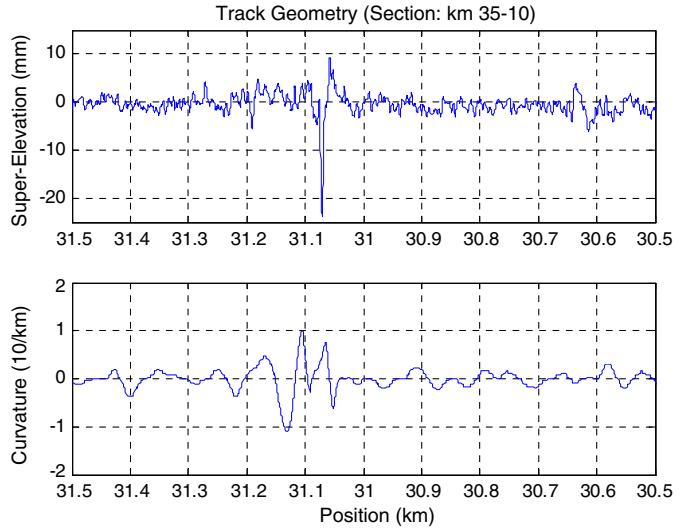

Fig. 21. Track superelevation and curvature (31.5–30.5 km)

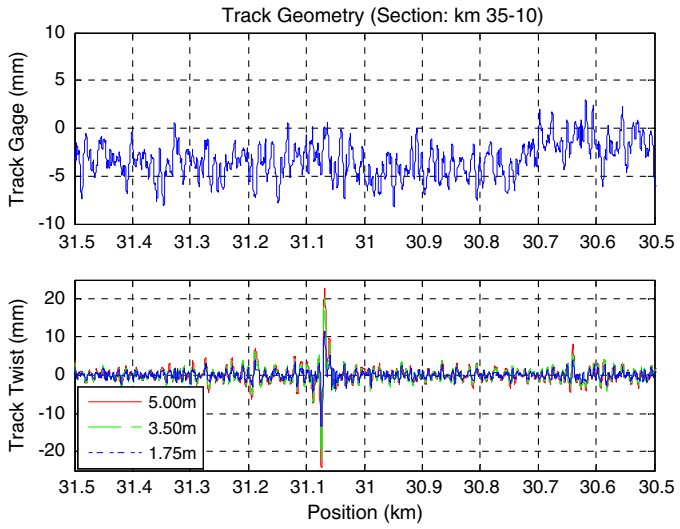

Fig. 22. Track gauge and twist (31.5–30.5 km)

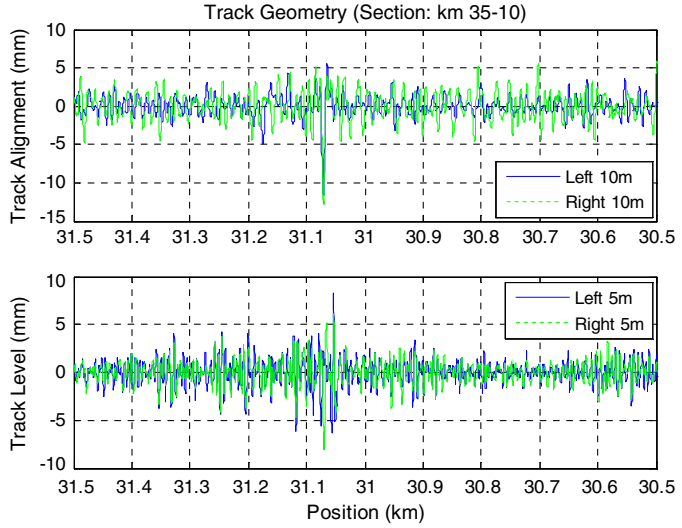

Fig. 23. Track alignment and level (31.5–30.5 km)

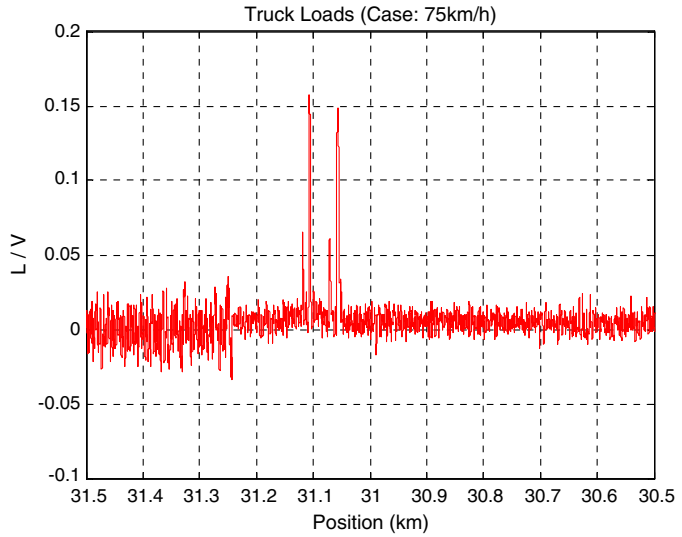

Fig. 24. Leading bogie L/V (31.5–30.5 km)

in Fig. 21. At this point, the track twist reached ±23 mm (Fig. 22). There is also a sudden change in the track alignment, shown in Fig. 23. Therefore, the poor geometry is correspondently identified using the SIR system. Safety at this point is confirmed with the L/V measured with the instrumented wheelsets of 0.15, as shown in Fig. 24.

Discussion

Obviously, the magnitudes of the results are related to the speed of the train during the journey. The operating speed varied depending on the driver style, train load, weather conditions, and any speed restrictions existing on the track. However, at different speeds, the magnitude of forced movements will change, altering the magnitude of the identified L/V values but keeping the position of the harmful location. Even the natural movements, induced by periodic irregularities, change due to the suspension's damping factor, but the position remains. The process is deterministic and depends on the initial conditions and speed. Therefore, system

repeatability may be spread due to initial conditions and speed variability.

Even a wagon with chronic lateral instability will correctly identify the undesirable type of track irregularity, according to its own point of view. A spectral analysis can easily identify this wagon feature due to its periodic characteristic behavior.

This method also takes into account the effects of nonstationary train longitudinal coupler forces, albeit unnecessarily from the point of view of track quality. This action does affect the wheel load distribution and safety as a consequence, particularly in curves where its projection affects the lateral acceleration and the angular yaw body acceleration. Therefore, this *jerk* phenomenon is characterized by the body angular accelerations accordingly recovered.

This quantification method complements other existing geometric tools. The possibility of evaluating similar vehicles across various load conditions or distinct vehicle fleets is easily performed simply by changing the installation of the measuring device. The data measured can also be used to evaluate passenger comfort using the vertical and lateral accelerometers' signals in accordance with the comfort standard [ISO 2631 (ISO 2001)] or even the vehicle modal quantification. Differently from other systems that use only statistical information from a few sensors, the system presented herein is MISO, which takes into account the vehicle's complete multisignal input and delivers a single output index directly correlated to the track's safety condition.

Conclusion

An inertial measuring system and a specialized data treatment method to perform the railway track quality and safety quantification as observed from the vehicle performance point of view is presented. Using a strapdown inertial recovery (SIR) method, the system measures the vehicle's dynamic movements and attitude during its transit along an irregular track. The values measured are used in an attitude heading reference system (AHRS) algorithm with an extended Kalman filter to identify the full vehicle attitude, including angular positions and accelerations. The vehicle system equations for the inverse dynamic problem, augmented by suspension torsion equation, are solved to directly calculate the wheels' driving forces. The safety L/V contact force ratio at low frequency is identified. A safety index (SI), which is directly correlated with vehicle safety, is determined based on the railway's L/V safety limits. Values obtained are used to qualify the most harmful track locations.

A field test program was conducted in a special train traveling at controlled speed. The system was installed on a loaded iron ore wagon and the train ran on a selected track section at various speeds. The track SI quantification was directly compared with measures of the IWS. Results show good agreement between both systems. Additionally, the results are also compared with the measured geometry of the local track and variations are confirmed with the new system results. The GPS signal simultaneously captures the train speed and the exact georeferenced location of the highest potential hazard region for track maintenance purposes.

Due to its simplicity and low cost, the new system can be easily installed in any vehicle and operate with any load condition and at variable traveling speeds, without the traditional traffic disturbance. The system can be applied to any specific vehicle fleet, traveling on any track section, at the usual operational speed, and detect the most harmful track location to complement geometric measuring methods. The analyses can also be focused to compute different priority criteria (passenger comfort, minimal dynamic vertical load applied to the track, instantaneous safety indicator, etc.) according to user interests. Better classification of the most harmful track locations allows prioritizing the track intervention strategy. The complementary combination of new and traditional monitoring track-inspection techniques can help to better understand asset behavior and produce effective investment efficiency in railway track maintenance, and is thus a promising technique.

Acknowledgments

The author would like to thank the Mechanical Department of the Engineering School of the University of Sao Paulo (EP-USP) for the support to this research, engineer Guilherme Fabiano dos Santos and VALE S.A., which organized and made available the railway resources for the validation tests.

References

Anderson, R., and Bevly, D. M. (2010). "Using GPS with a model-based estimator to estimate critical vehicle state." *Veh. Syst. Dyn.*, 48(12), 1413–1438.

Barbosa, R. S. (2004). "A 3D contact force safety criterion for flange climb derailment of a railway wheel." *J. Veh. Syst. Dyn.*, 42(5), 289–300.

Barbosa, R. S. (2009). "Safety of a railway wheelset-derailment simulation with increasing lateral force." *Veh. Syst. Dyn.*, 47(12), 1493–1510.

Barbosa, R. S. (2011). "Vehicle dynamic response due to pavement roughness." *J. Braz. Soc. Mech. Sci. Eng.*, 33(3), 302–307.

Barbosa, R. S. (2015). "New method for railway track quality identification through the safety dynamic performance of instrumented railway vehicle." *J. Braz. Soc. Mech. Sci. Eng.*, 10.1007/s40430-015-0471-9, 1–11.

Baruh, H. (1999). *Analytical dynamics*, McGraw-Hill, 419.

Calçada, R., and Vale, C. (2014). "A dynamic vehicle-track interaction model for predicting the track degradation process." *J. Infrastruct. Syst.*, 10.1061/(ASCE)IS.1943-555X.0000190, 04014016.

European Railway Agency. (2011). "Assessment of freight train derailment risk reduction measures: B1–Derailment risk models. Det Norske Veritas–DNV: Report for European Railway Agency." *Rep. No. BA000777/06(2)*, Valenciennes, France.

Gullers, P., Dreik, P., Nielsen, J. C. O., Ekberg, A., and Andersson, L. (2011). "Track condition analyser: Identification of rail rolling surface defects, likely to generate fatigue damage in wheels, using instrumented wheelset measurements." *Proc. Inst. Mech. Eng. F J. Rail Rapid Transit.*, 225(F1), 1–13.

Haigermoser, A., et al. (2014). "Describing and assessing track geometry quality." *Veh. Syst. Dyn.*, 52(Suppl. 1), 189–206.

Hung, C., et al. (2010). "Study on detection of the early signs of derailment for railway vehicles." *Veh. Syst. Dyn.: Int. J. Veh. Mech. Mobility*, 48(Suppl. 1), 451–466.

ISO. (2001). "Mechanical vibration and shock—Evaluation of human exposure to whole-body vibration. Part 4: Guidelines for the evaluation of the effects of vibration and rotational motion on passenger and crew comfort in fixed-guideway transport systems." *ISO 2631*, Geneva.

Ketchum, C. D., and Wilson, N. (2012). "Performance-based track geometry—PBTG. Phase: 1. Transit cooperative research program." *Document 52*, Transportation Technology Center, 89.

Kuga, H. K., and Carrara, V. (2013). "Attitude determination with magnetometers and accelerometers to use in satellite simulator." Hindawi Publishing Corporation, Cairo, Egypt, 1–6.

Luber, B., Haigermoser, A., and Grabner, G. (2010). "Track geometry evaluation method based on vehicle response prediction." *Veh. Syst. Dyn.: Int. J. Veh. Mech. Mobility*, 48(Suppl. 1), 157–173.

Marins, J. L., Yun, X., Bachmann, E. R., McGhee, R. B., and Zyda, M. J. (2001). "An extended Kalman filter for quaternion-based orientation estimation using MARG sensors." *Proc., 2001 Int. Conf. on Intelligent Robots and Systems*, IEEE, 2003–2011.

Matsumoto, A., et al. (2014). "Actual states of wheel/rail contact forces and friction on sharp curves—Continuous monitoring from in-service trains and numerical simulations." *Wear*, 314(1–2), 189–197.
Nederlof, C., and Dings, P. (2010). "Monitoring track condition to improve asset management." Union International Chamin de Fer–UIC, Paris.
Pence, B., et al. (2013). "Vehicle sprung mass estimation for rough terrain." *Int. J. Veh. Des.*, 61(1/2/3/4), 3–26.
Stuart, C. (2012). "Autonomous track geometry measurement system (ATGMS). Reseach and development review." Federal Railway Administration (FRA), Dept. of Transportation (DOT), Washington, DC, 22.
Suarez, B., Felez, J., Lozano, J. A., and Rodriguez, P. (2013). "Influence of the track quality and of the properties of the wheel—Rail rolling contact on vehicle dynamics." *Veh. Syst. Dyn.*, 51(2), 301–320.
Tsunashima, H., Naganuma, Y., and Kobayashi, T. (2014). "Track geometry estimation from car-body vibration." *Veh. Syst. Dyn.*, 52(1), 207–219.
Wei, X., Jia, L., and Liu, H. (2013). "A comparative study on fault detection methods of rail vehicle suspension systems based on acceleration measurements." *Veh. Syst. Dyn.*, 51(5), 700–720.
Wilson, N., et al. (2011). "Assessment of safety against derailment using simulations and vehicle acceptance tests: A worldwide comparison of state-of-the-art assessment methods." *Veh. Syst. Dyn.*, 49(7), 1113–1157.

8.2 ***ANEXO B***

QUANTIFICATION OF RAILWAY TRACK SAFETY WITH AN INERTIAL VEHICLE RESPONSE IDENTIFICATION.

Barbosa, R. S. (2016B) Quantification of Railway Track Safety with an Inertial Vehicle Response Identification. International Journal of Railway Technology, DOI: 10.4203/ijrt.5.2.3 Vol.: 5, Issue 2, pp. 47-63.

8.2 ***ANEXO B***

QUANTIFICATION OF RAILWAY TRACK SAFETY WITH AN INERTIAL VEHICLE RESPONSE IDENTIFICATION.

Barbosa, R. S. (2016B) Quantification of Railway Track Safety with an Inertial Vehicle Response Identification. International Journal of Railway Technology, DOI: 10.4203/ijrt.5.2.3 Vol.: 5, Issue 2, pp. 47-63.

International Journal of Railway Technology
Volume 5, Issue 2, Pages 47-63, 2016.
doi:10.4203/ijrt.5.2.3

SAXE-COBURG
PUBLICATIONS

Quantification of Railway Track Safety with an Inertial Vehicle Response Identification

R. Spinola Barbosa
Department of Engineering Mechanics
University of São Paulo
Brazil

Abstract

A new method for track inspection was developed to complement the traditional geometric methods. An inertial measuring system installed on the vehicle is used to acquire the vehicle's response to irregular track input. A specialized data treatment method is used to evaluate railway track safety, observed from the vehicle dynamic performance point of view. System equations for the inverse vehicle dynamic problem are solved to estimate the wheels driving forces which are directly correlated with the vehicle's safety when travelling over track unevenness. Results of a measuring campaign on a railway wagon are used to evaluate the present system, by direct positional comparison with track geometry measurements. Also, data collected and treated are compared with the lateral to vertical dynamic loading safety (L/V) ratio measured with instrumented wheelsets installed on the wagon. The results of the quantified track safety present good agreement with the traditional measuring methods. This confirms the ability of the method to detect the location of the potentially most hazardous regions, for optimised railway track maintenance purposes.

Keywords: safety, railway, track, quality, inertial, dynamic, vehicle.

1 Introduction

The quality of a railway track is quantified by its structural strength and geometric parameters deviation. The inspection is performed with a specialized vehicle which measures and records the variations of the track gage, vertical and lateral alignments, and cross-level. Measured values are compared to standardized limits. Usually, only short to medium wavelength irregularities are detected. Additionally, the cross-level variation per meter (track twist) can be calculated depending on the data sample rate.

A poor vehicle dynamic performance frequently occurs in locations such as curve entries or exits, severe track irregularities, or misalignments which promote yaw instability or hunting. Therefore, a bad vehicle performance may point out areas of track which need maintenance. Conversely, there are some track locations which exceed track geometry standard limits but do not cause poor vehicle performance.

Safety diagnosis is the ability to identify on which region of the line the vehicle dynamic performance is poor or dangerous. To meet security aspects, the evaluation must also consider the victim of the lack of safety: the vehicle which effectively derails. As the track and the vehicle form a naturally mutual dependent system, the vehicle's behaviour reflects its own properties and forced movements, which are directly affected by the track geometry input, track stiffness, and train speed [2].

The track safety concept is the ability to promote the non-dangerous traffic of vehicles and trains. A vehicle transporting goods obviously depends on the track's structural integrity, an efficient train operation, and the vehicle's performance to reach a minimal probability of derailment. The only way to guarantee effective track quality, focusing on safety, is to objectively contemplate all these aspects, including vehicle behaviour.

Track properties are mainly described by their geometric parameters as curvature, transition curve form and length, and super-elevation. Track deformation also affects the passing vehicle as a result of its stiffness. The track irregularities are the variations around the nominal geometry, which may be a randomic or a periodic variation [6]. Regardless of the type of irregularities, the fact is that the track shape, with varying geometry, imposes a range of load distribution to the wheels and their sum imposes a variation on the vehicle's kinematics. Therefore, the wheel acting forces produce the bogie directioning and the vehicle accelerations to negotiate the curves. The objective safety of the system is associated with the vehicle's derailment, traditionally quantified with the L/V factor. This well-known and widely accepted factor derives from the wheel/rail system characteristics. This means the vehicle's response is as a result of the track irregularities input. Therefore, the whole system must be evaluated simultaneously to objectively quantify the track quality, from the point of view of safety [1].

An instrumented iron-ore wagon was proposed by Darby [9] to measure the suspension spring deflection, lateral side frame acceleration, brake pipe pressure, inter-car separation, longitudinal wagon acceleration; coupler force, and structural stress. Despite using various sensors, it is essentially a simple captive system, based only on measurements of deflection and some particular accelerations of a wagon to indirectly evaluate the track quality.

The use of an instrumented wheel-set is another method to evaluate the effect caused by the track's irregularity over the vehicle's behaviour in traffic. In spite of being an expensive and laborious instrument, the quantification of the wheel/rail contact force ratio is an indication of track quality [11] and, therefore, the vehicle's safety. Also, the use of portable accelerometers is employed for passenger comfort measurements [11] based on the ISO-2631 and UIC-513 Standards.

Inertial measurement devices (IMU) are new technologies developed in the aerospace industry with widespread application in military equipment. These devices are now available in the automotive industry and are used, in particular, in automotive control systems. Examples of use of this new technology can be found in Feldmann [12] who proposes to detect the vertical track settlement and deterioration by using frequency domain transformation from the inertial measurements of the vehicle's behaviour. Weston [13] uses rate gyros and lateral acceleration for track curvature and alignment monitoring. Xia [14] used an inverse vehicle model to estimate high-frequency wheel/rail contact forces from the measurements of sensors installed in a track-recording car. One can observe in the temporal results, the difficulty of vehicle dynamics correlation with the wheel forces as a result of high frequency movements of the body with reduced weight (ex. wheelset, side frame, *etc.*). However, at low frequencies, vehicle mass has predominance over the system's movements and can be used for a particular application, which is the object of this work. Hung [15] reports that peak threshold of the pitch angular rate and the integral threshold of the roll angular rate of the vehicle truck frame are closely related to unsafe vehicle conditions. Heirich [16] uses an inertial device in the vehicle to infer the track features, such as bank, bank change, slope, slope change, relative heading, curvature, and basic track elements. Luber [17] proposes a method for track geometry assessment taking into account the vehicle/track interaction. The method is supported with vehicle vertical and lateral transfer function used for the prediction of the vehicle reaction forces. The results show a significant enhancement of the correlation between the track assessment quantities and the vehicle reaction forces. However, the use of the transfer function related to the parameters of the track (Track Geometry Assessment TGA, EN 14363) [18] is restricted to only two translational directions (vertical and lateral) and a wavelength range of 3-25 m, and does not include rotational aspects. These aspects reinforce the need to broaden the spectrum of evaluation that is the proposal here presented.

Track geometry should be designed to meet the requirements of the fleet of cars or wagons which use it. During its service life, a perfect track develops irregularities which cause vehicle oscillation. In an extreme case, the vehicle can lose its guidance. Defects and failure of the track superstructure and vehicle dynamic performance may be mixed and cause these undesirable derailment events (DNV Report [19]). Focusing on the track geometry defects, structural elasticity, vehicle suspension characteristics, and train speed, all of these are potential, possible contribution causes and should, therefore, be evaluated together to minimize hazard risk, improving the safety of traffic. As can be observed, all the systems described are mainly based on only geometric aspects of the track.

Generally speaking, there are three types of relevant, unsafe vehicle conditions. The first type is the wheel-climb derailment. It may occur at low speed in sharp curves and is particularly related to vehicle suspension stiffness and wheel load distribution conditions. The second type is mainly related to large movements of the vehicle's main body. This condition can be associated with the vehicle's unsprung mass dynamic movements and directioning bogie/wheelset properties. The third type is relative to a syntonized train speed and a particular type of track irregularity. This

last one is associated with the dominant track evenness wavelength, the vehicle's natural frequencies, and specific train speed. Although there are other types of unsafe conditions, including vehicle instability, accidental, and component failure, the second type here described, is mainly related to the vehicle body low frequency movements and small energy dissipation.

Our proposed methodology to quantify track safety through inspection is based on the detection of signs of unsafe railway vehicle performance, mainly associated with the second and third types of unsafe conditions, when travelling along the track unevenness. These signs are used to identify the exact location along the track and to prioritise the pertinent track geometry correction to the most harmful irregularities for the vehicle's safety.

The metric adopted to identify the potential harmful location on the track associated with the vehicle's safety is the traditional L/V ratio between the wheel lateral (L) and vertical (V) contact force. The wheel forces are quantified from the measurement of the vehicle's attitude and its overall dynamic behaviour. This task is performed with an inverse vehicle dynamic model, fed with data acquired from the instrumented vehicle during the transit journey. The vehicle's instrumentation is composed of an inertial measuring unit (IMU) with nine high-resolution transducers and an inertial navigation system (INS) for attitude recognition, and a GPS positioning signal [3].

2 Track vehicle interaction

The track geometry is the input to the vehicle's dynamics on a moving train. Its curve circular radius, cant, and transition length generally describes track variation. In addition to the long geometry profile, a small wavelength irregularity is usually present. The maximum irregularity over the nominal geometry are usually limited to the track class (*e.g.* gage, level, alignment, cant, twist, *etc.)* as described by normative standards (*e.g.* FRA, UIC, *etc.*). Some types of irregularity do affect the modal vehicle's behaviour (*e.g.* bounce vibration as a result of long-wave track level or lower sway mode as a result of track alignment). Other track irregularities are absorbed by the vehicle's suspension (*e.g.* short wave-length track twist).

The wheel/rail contact force (L and V), as a result of the vehicle's dynamic behaviour, is a function of the roughness of the track which the vehicle is travelling on. To identify the acting contact forces which produce the vehicle's directioning movements, it is necessary to solve an inverse dynamic problem. The vehicle's dynamics are described by a set of differential equations obtained from the Newton-Euler theorems applied to a model of the vehicle considered as a rigid body. This equation is valid for a fixed reference frame N (OXYZ) as presented in Figure 1. For the translational movements, the following differential equations relate to accelerations and external forces in an earth fixed reference frame [3]:

$$m\,{}^{N}\vec{a}_{G} = \sum \vec{F}^{ext} \tag{1}$$

This equation does not consider the drag and Coriolis effects from the earth rotations as a result of the irrelevant magnitude faced by the vehicle's acceleration. The external forces are mainly as a result of wheel contact forces and gravitational effects, as shown in Figure 1.

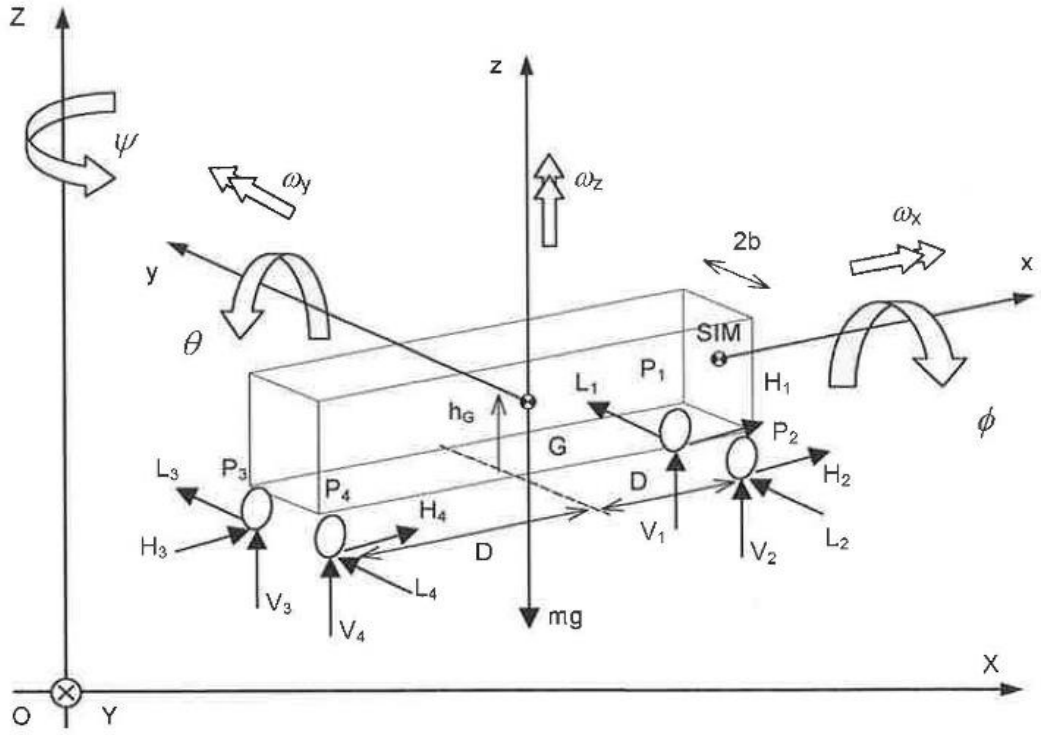

Figure 1: Body attitude and forces distribution on the vehicle

$$m\,{}^{N}\vec{a}_{G} = \sum \vec{F}_{wheels} - m\,{}^{N}\vec{g} \tag{2}$$

The equation can also be expressed in the body reference frame (Gxyz) using a rotational transformation matrix T, composed of the three Euler angles (roll ϕ, pitch θ, yaw ψ) as identified in Figure 1, from which the accelerations are to be measured and the forces computed:

$$m T_{N}^{B}\left({}^{N}\vec{a}_{G} + {}^{N}\vec{g}\right) = T_{N}^{B} \sum \vec{F}_{wheels} \tag{3}$$

When the measuring system is fixed at a particular point P, not coincident with the vehicle centre of gravity G, the measured acceleration must be projected according to the field acceleration equation, to be used by the Newton equation:

$$\vec{a}_{G} = \dot{a}_{P} + \dot{\vec{\omega}} \wedge (G - P) + \vec{\omega} \wedge [\vec{\omega} \wedge (G - P)] \tag{4}$$

where the angular velocity is $\vec{\Omega} = \dot{\phi}\vec{i} + \dot{\theta}\,\vec{j} + \dot{\psi}\,\vec{K}$ composed by the body roll rate $\dot{\phi}$, the pitch rate $\dot{\theta}$ and the yaw rate $\dot{\psi}$.

For the rotational movements described in a moving reference frame attached to the vehicle, the following differential equations relate angular accelerations α and body angular velocity $\omega_B = [\omega_x \quad \omega_y \quad \omega_z]^T$ and external moments with respect to the same pole:

$$[J]_G\{\alpha\} + [\omega_B] \wedge [J]_G\{\omega_B\} = \{M_G^{ext}\} \tag{5}$$

The body external contact forces arising from each wheel (Hi, Li, Vi) are shown in Figure 1. The body external moments (MG) as a result of the wheel forces are obtained from the carbody dimensions as shown in Figure 1. To work out the contact forces solving the system equation, it is necessary to know the vehicle's body accelerations, as stated in Equation 1. Additionally, it is also necessary to measure the angular velocity and to estimate the angular acceleration, needed to solve Equation 2. Finally, the bodies angular attitude must be identified to solve torsion Equation 6.

The system has six equations and twelve contact force unknowns. Disregarding the longitudinal effects, one equation is removed and four longitudinal contact forces are ignored (no acceleration or breaking effects are evaluated). As a result of the system being hyperstatic, the contact lateral forces in each wheelset are summed. To solve the system with five equations and six unknown forces, an additional suspension torsion equation is disclosed to access each vertical force relationship, completing the system compatibility.

The vehicle longitudinal torsion, as a result of track twist, mainly affects the vertical wheel load distribution. Considering the car structure as a rigid body, the track twist deflects the suspension, unloading the diagonal wheels. This effect depends on the vehicle's suspension stiffness, length and width of the vehicle, and magnitude and wavelength of track twist.

Namely, the expression for the vertical load variation as a function of the track angular twist per meter (δ) is related to a body geometry proportion (D/2b) and suspension torsional stiffness ($k\varphi$) stated as:

$$\Delta V = -k_{\varphi} \frac{D}{2b} \delta \tag{6}$$

To estimate the track twist from the overall vehicle inclination, a special filter is used to recover the local track superelevation (α). However, the IMU coupled to the body measures the absolute vehicle roll angle referred to the earth plane (ϕ). The total or earth referred body angle, as shown in Figure 2, is composed by the track cant angle (α) added to the relative vehicle roll angle (β) as a result of suspension movements and inertial mass center height (hG):

$$\phi = \alpha + \beta \tag{7}$$

The track cant angle (α) can be measured with an additional IMU installed on the wheelset. If this value is not available, another identification method is necessary.

Disregarding any small vehicle suspension roll, the twist variation can be obtained along the length (S) from:

$$\delta = \frac{d\alpha}{dS} \tag{8}$$

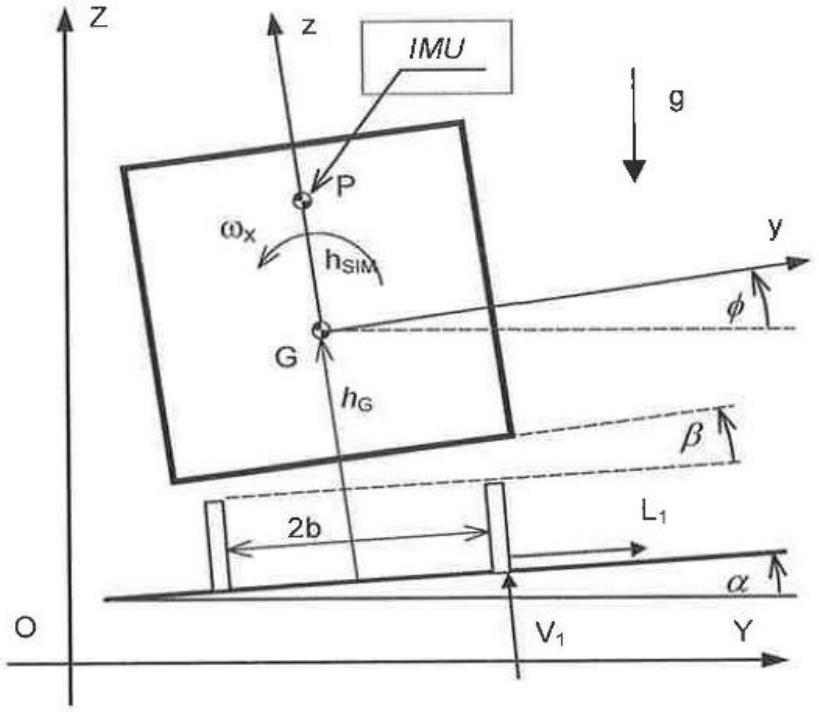

Figure 2: Track and vehicle roll angles

To identify the angular accelerations, the vehicle's angles and attitude, a specialized data treatment method based on an inertial navigation algorithm (INS) aided with extended Kalman filter is used as a multivariable estimator [3]. With all this information, it is possible to solve the vehicle's inverse dynamic equations to evaluate the driving contact forces and calculate the traditional safety ratio force L/V.

To solve the inverse identification problem, the vehicle model has to be known, have a unique existing solution, and have continuous data of the measuring system available. Therefore, the requirements for the solution of the inverse problem are available using a complete measuring system, continuously monitoring vehicle body movement and its attitude dynamic behaviour (INS). A safety index (SI) is used to quantify track quality ($SI = 1 - L/V$) [3].

3 Measuring results and comparison

The safety index (SI) calculated with the system strapdown inertial recovery (SIR) algorithm, were compared with: a) the measured track geometry and b) the measured

bogie L/V wheel forces ratio (instrumented wheelsets (IWS)). A test campaign performing track inspection measuring track safety was carried out on a selected 25 kilometres track section with 1.6 metre gage located in the north region of Brazil. The typical iron-ore wagon was a 120 ton gondola GDT, with "7×11" and ride-control bogies.

The track geometry and irregularities were measured with a specialized measuring car (Plasser EM-100) in the same track location. The measurements were the variation of the track gage, vertical and lateral rail alignments (left and right), and track section cant. Additionally, it identifies track curvature and track twist.

The L/V wheel force ratio was also measured during the test campaign with two instrumented wheelsets (IWS) installed on the leading bogie of the wagon. For compatible comparison with SIR results, the bogie L/V value is calculated from the sum of the lateral load of each wheel divided by the sum of the vertical measured loads.

A special test train was prepared to travel on a selected track section. The train was formed with two locomotives (one at each end), four iron-ore loaded wagons and two laboratory cars. The instrumentation SIR system was installed underneath the first wagon, as can be observed in Figure 3. The two instrumented wheelsets (IWS) are installed in the leading bogie of this wagon. Additionally, a GPS is used to identify the speed of the train and position of the instrumented wagon.

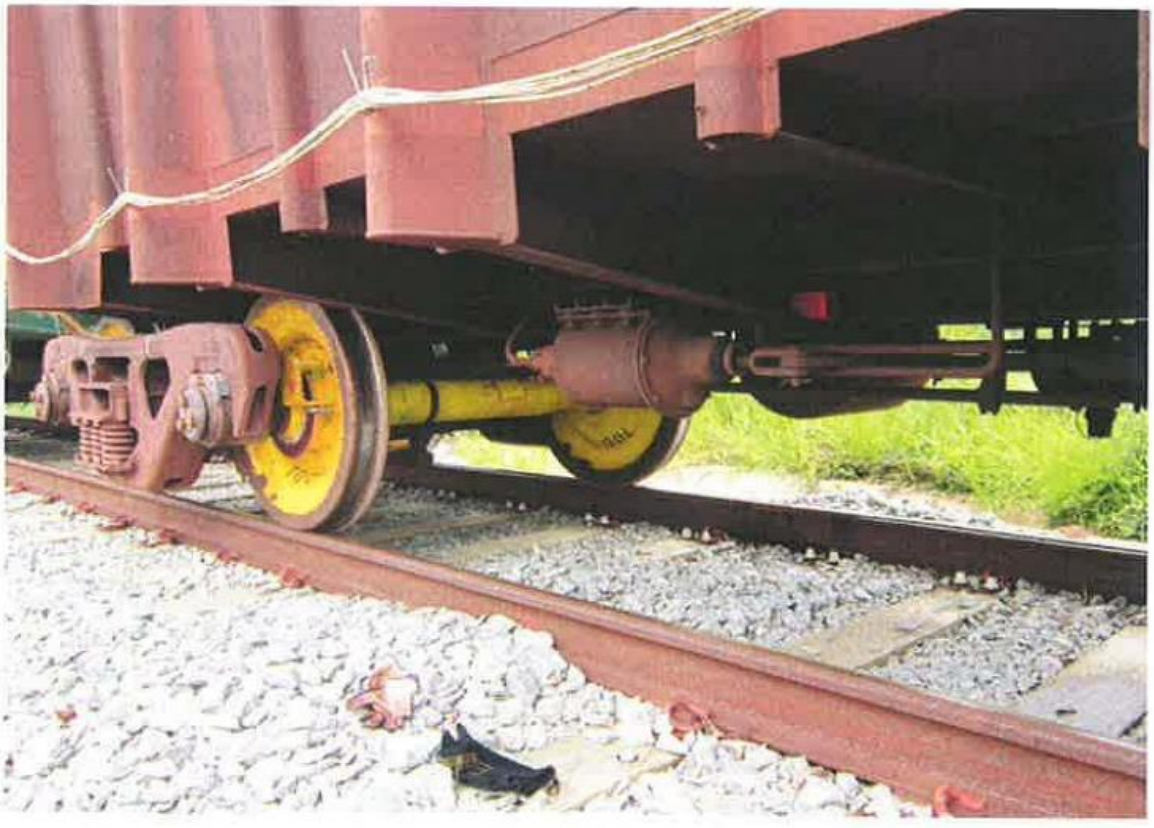

Figure 3: Instrumented Wheelsets (yellow) and Measuring System (red)

Several tests were conducted at controlled speed (30, 50, 60, 70 and 75 km/h) in the eastbound direction (mine to port). The test at 75 km/h was selected for a closer analysis. The train speed was expected to be constant but as a result of a restriction near a bridge, the real speed varies around programmed values and its time history is presented in Figure 7. The track Safety Index (SI) values determined in function of kilometric position are presented in the upper graph of Figure 4. The lower graph in this figure shows the measured heading of the wagon.

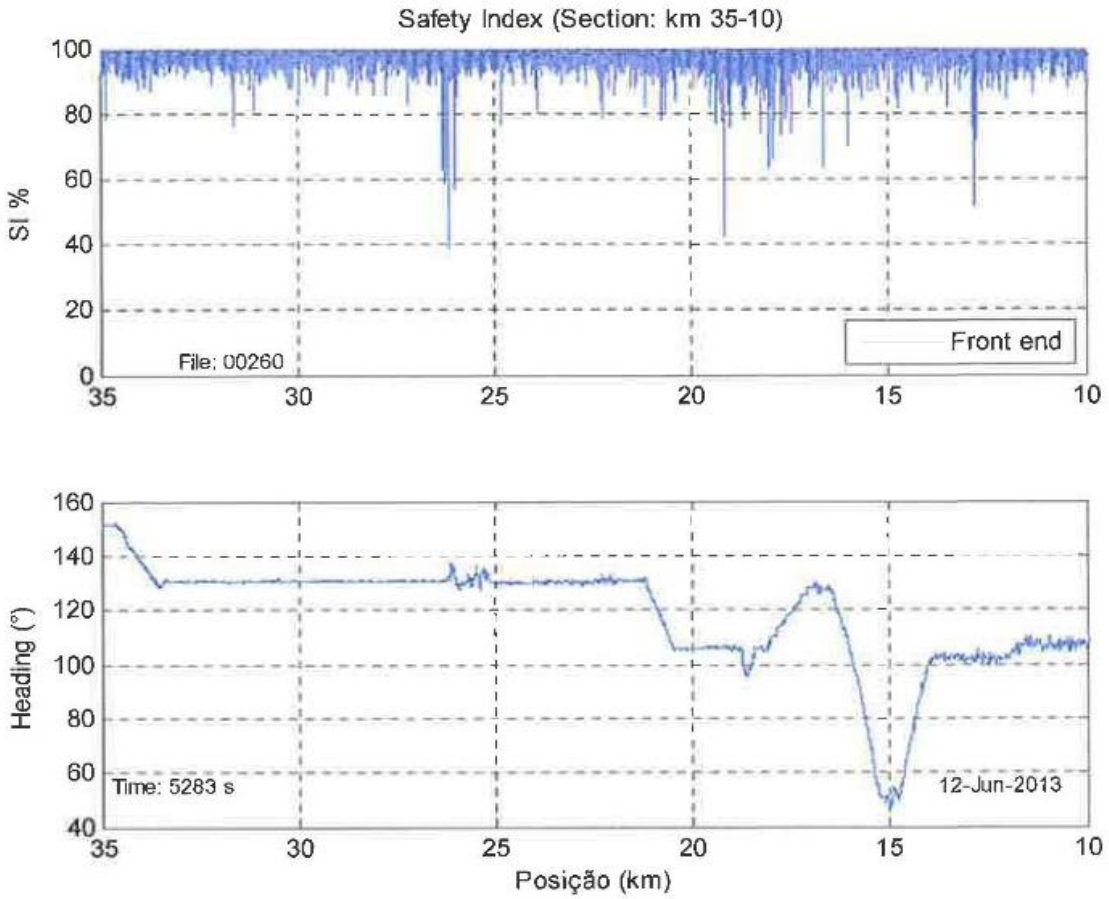

Figure 4: Safety Index (km 35+000 until km 10+000)

The track geometry of this section, as measured with the EM-100 measuring car, is presented in Figure 5.

The upper graph (of Figure 5) shows the track super elevation along the kilometric position and the lower graph the track curvature. It can be observed in this section that there is a left curve of 860 meters of radius between km 16+800 and km 15+150. The bridge is identified at around 18 km (red vertical lines at Figure 5). The bogie L/V for the leading bogie, calculated from measured values of the two wheelsets, is presented in Figure 6.

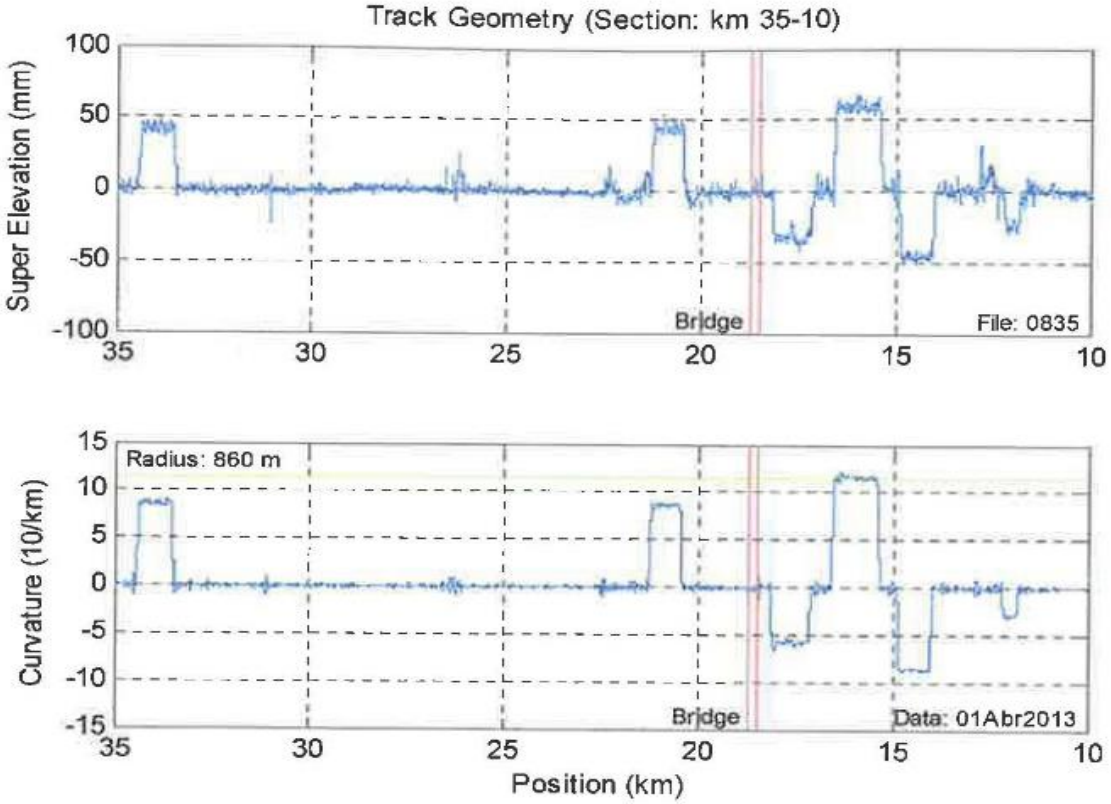

Figure 5: Track Measured Geometry (EM-100 Measuring Car)

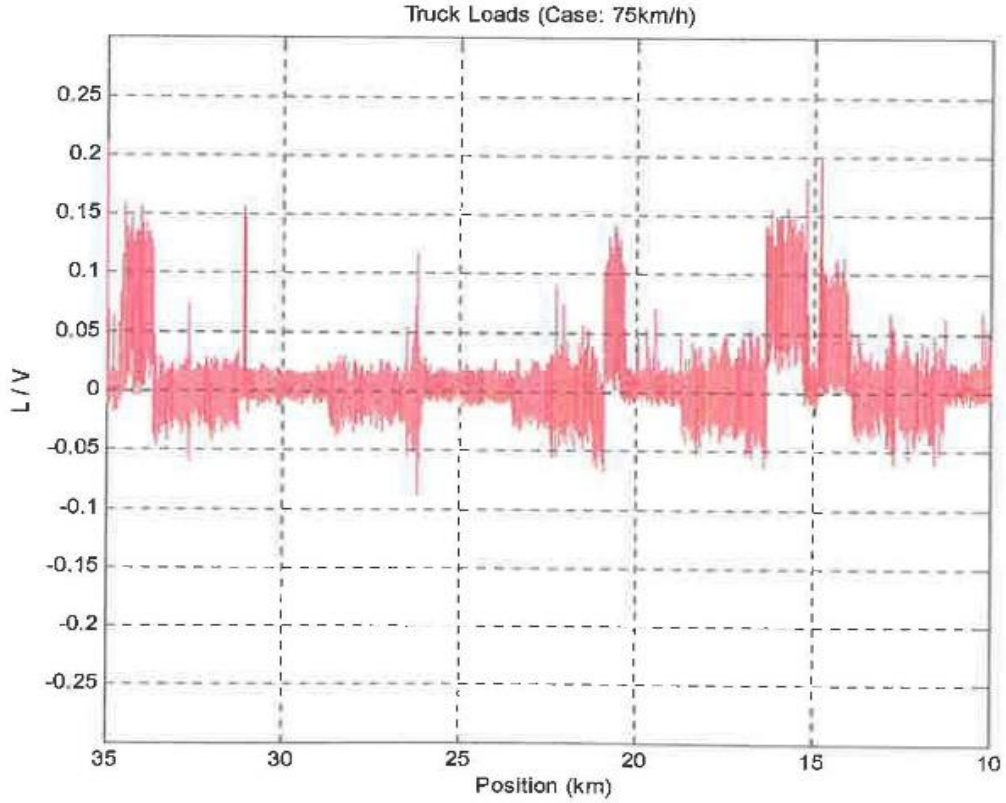

Figure 6: Leading Bogie L/V Results

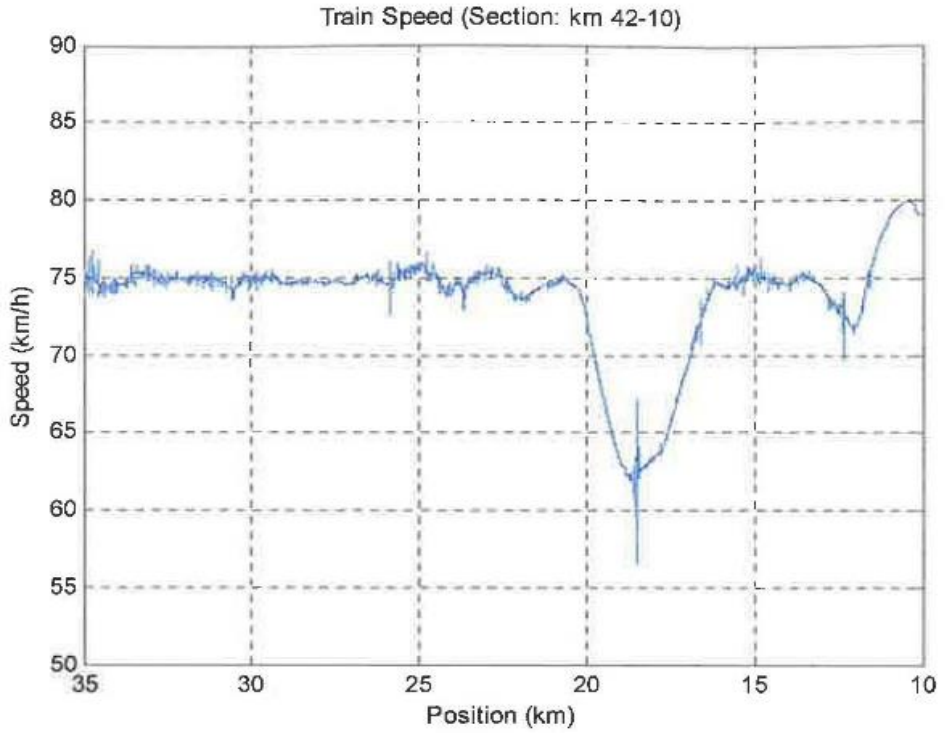

Figure 7: Train Speed

The subsection between 27+000 km to 25+500 km was analysed in detail. This is a tangent track region as can be observed on the wagon absolute heading on Figure 8b measured with the SIR system installed on the vehicle.

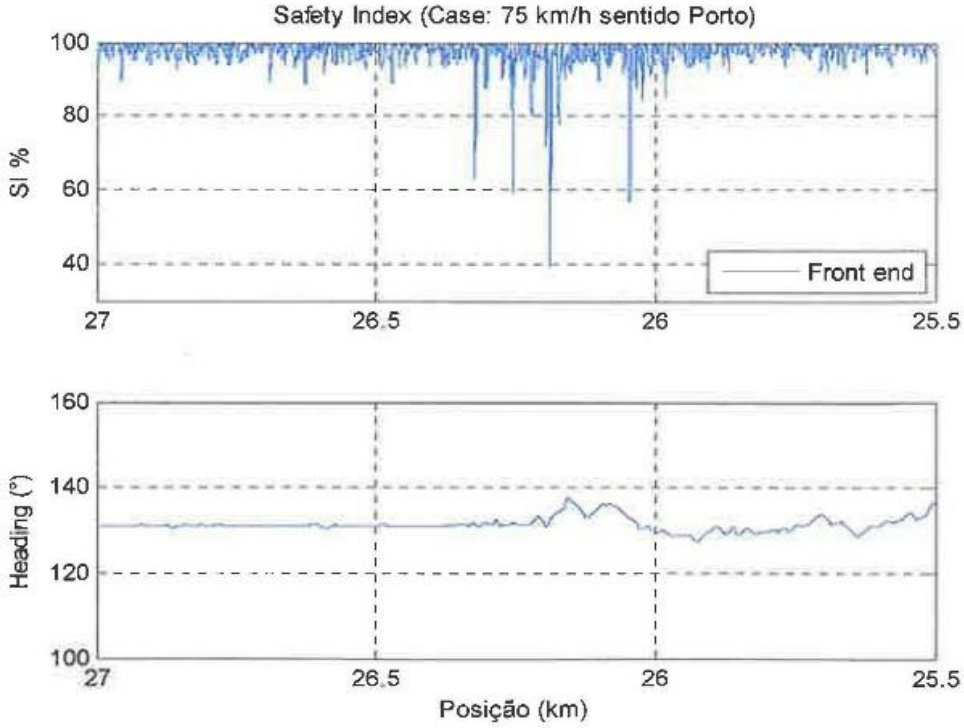

Figure 8: Safety Index (leading bogie) and wagon heading

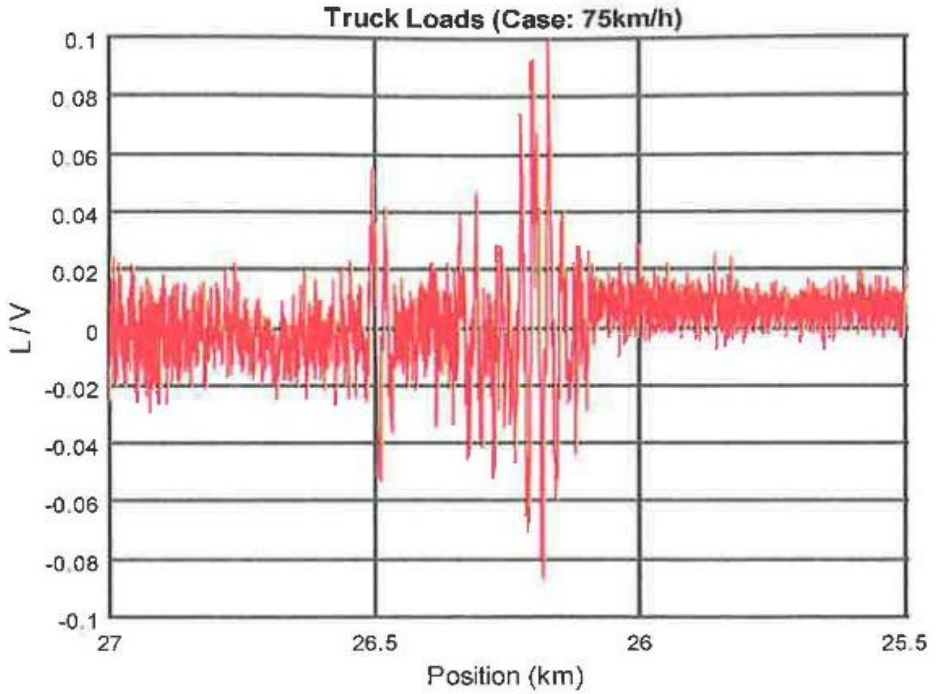

Figure 9: Measured L/V (leading bogie)

Figure 10 to Figure 12 show the track geometry measured with the Passer car. One can observe that there is a localized super elevation of 28 mm on 26+200 km, almost linearly rising and suddenly lowered as measured with the EM-100 car shown in Figure 10.

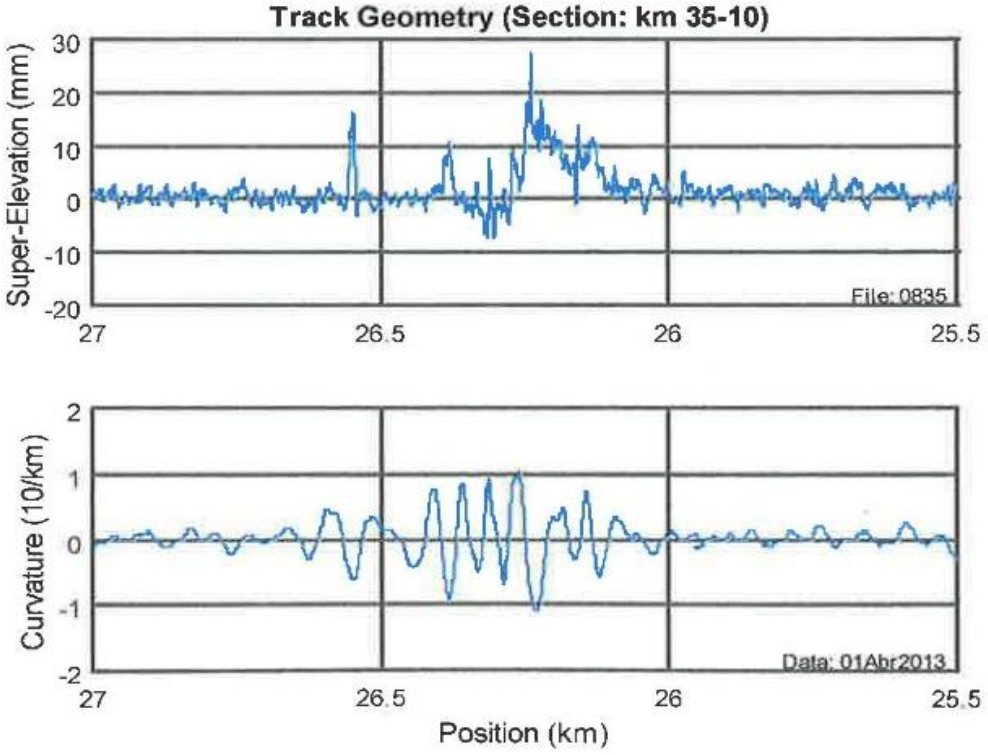

Figure 10: Track super elevation and curvature (EM-100)

In the same region, the track twist (5,0 metre chord) varies around ± 15 mm (Figure 11). Additionally, the rail levelling goes up to –15 mm as shown in Figure 12.

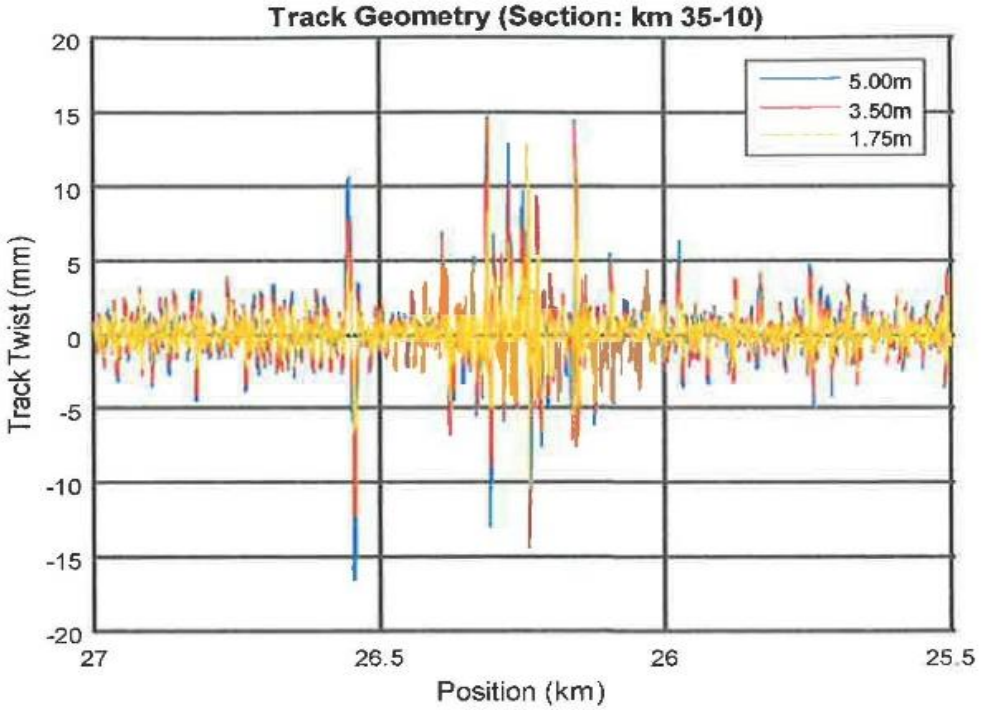

Figure 11: Track Twist (chord length 5m 3.5 m and 1.75 meters)

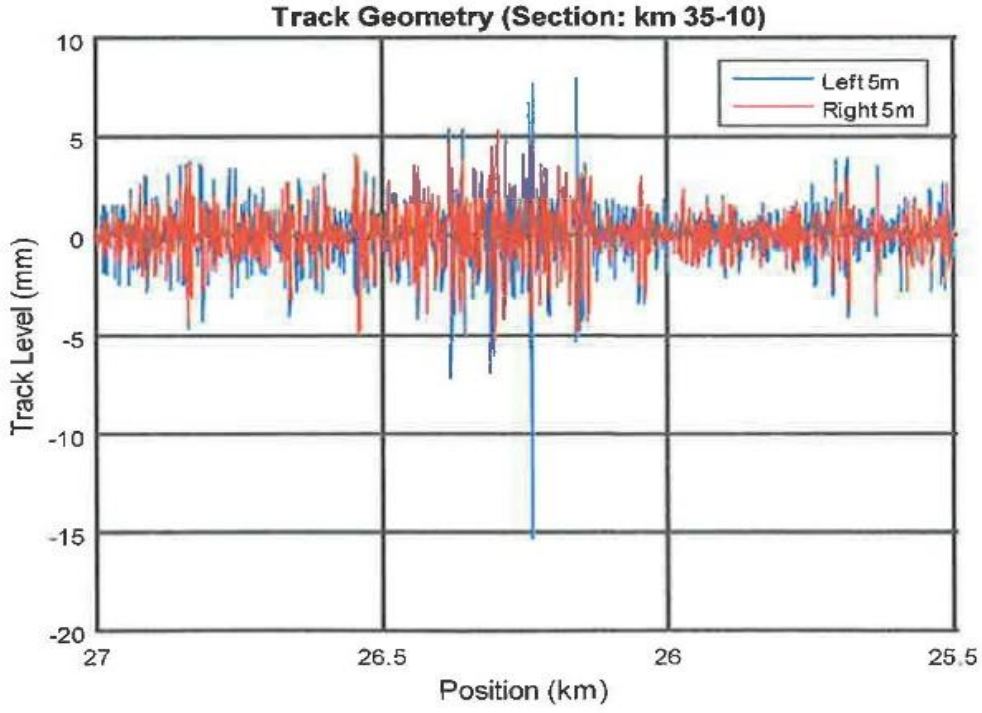

Figure 12: Track Levelling (left and right rail on 5 metre chord)

The safety index (SI) reached a lower value of 40%, as shown in Figure 8. In the same region, the L/V measured with the instrumented wheelsets was distinguishable from others with severe variation (Figure 9).

4 Comments

Albeit unnecessary from the point of view of track quality, this method takes into account the non-stationary longitudinal coupler forces effects. This action does affect the wheel load distribution, particularly in curves where its projection affects the lateral acceleration and the angular yaw body acceleration. Therefore, this jerk phenomenon is characterized with the body angular accelerations covered accordingly with this approach.

The results are related to the speed of the train during the journey. The operating speed is variable depending on the style of the driver, train load, climatic variations, and any speed restrictions existing on the track. However, at different speeds, forced movements will change its magnitude, modifying the values measured, but keeping the location identified. Even the natural movements induced by periodic irregularities change, but location remains as a result of the damping factor of the suspension. The vehicle's response to track excitation is magnified by the vehicle frequency response function - FRF [2]. Therefore, cause and effect are related to this function.

Inspecting the sensor values, it is possible to identify which vehicle-moving mode contributes more to the SI values. Therefore, the type and magnitude of track wavelength roughness which is more harmful is identified and may be eliminated with maintenance intervention. Location without a GPS signal (*e.g.* long tunnels) can be complemented with a tachometer installed on the vehicle or an extrapolation performed from the INS algorithm. One limitation of the system is the precision and noise of the sensors which degrade the quality of the estimative.

This method is based on a simplified vehicle model which is complex enough to characterise the vehicle's low frequency behaviour, associated with the track long wavelength events and, therefore, can quantify safety between medium to high operation speeds (type 2 and 3 unsafety mode). Although a more sophisticated model, including suspension travel, can be realized [4, 8] to include medium to high frequency related to short wavelength roughness (first unsafety mode), the instrumentation, which must include the bogie and its inertial properties, will be much more complex.

The possibility of evaluating other types of wagon in different load conditions, or even passenger's car fleets, is possible providing that the model describes adequately the vehicle (inertial properties). This option is easily performed by only changing the installation of the measuring device. The data measured can also be used to evaluate passenger comfort using the vertical and lateral accelerometer signals in accordance with the comfort standard (*e.g.* ISO 2631), or even the vehicle modal quantification.

Differing from other systems which use only a few sensors or statistical information from them [5], the present new system is MISO which takes into account the complete vehicle multisignal input (tridirectional acceleration and angular rate) and delivers a single output index directly correlated to the objective safety condition (L/V value) revealing the novelty of this system.

5 Conclusions

An inertial measuring system and a specialized data treatment method to perform the railway track quality and safety quantification observed from the vehicle performance point of view is presented. With a strapdown inertial recovery (SIR) method, the system measures the vehicle's dynamic movements and attitude during its transit along the irregular track using nine high-resolution transducers. The values measured are used to identify the full vehicle attitude, including angular positions and accelerations. The vehicle system equations for the inverse dynamic problem, augmented by the suspension torsion equation, is solved to directly calculate the wheels driving forces. The safety L/V contact force ratio at low frequency is identified. A safety index (SI) directly correlated with the vehicle safety, is determined based on the railway L/V safety limits. Values obtained are used to qualify the most harmful track locations for maintenance purposes.

A field test program inspecting the track was conducted on a special train travelling at controlled speed. The SIR was installed on a loaded iron ore wagon and the train ran on a selected track section at various speeds. The track safety index (SI) quantification was directly compared with local track measured geometry. Additionally, the results are also compared with measurements of the instrumented wheelset (IWS). Results show good agreement between both systems. The GPS signal simultaneously captures the train speed and the exact georeferenced location of the most potentially hazardous regions for track maintenance purposes.

The better classifying of the most harmful track locations allows prioritising of the track intervention strategy. The complementary combination of new and traditional monitoring track inspection techniques [7] can help to better understand asset behaviour and produce effective investment efficiency in railway track maintenance, being a promising technique.

Acknowledgements

The author would like to thank the Mechanical Department of the Engineering School of the University of Sao Paulo (EP-USP) for the support to this research, engineer Guilherme Fabiano dos Santos and VALE S.A. who organized and made available the railway resources for the on track tests.

References

[1] R.S. Barbosa, "Safety of a railway wheelset derailment simulation with increasing lateral force". Vehicle System Dynamics, Vol. 47, n° 12, 1493-1510, 2009.

[2] R.S. Barbosa, "Vehicle dynamic response due to pavement roughness". Journal of the Brazilian Society of Mechanical Sciences and Engineering. Vol. 33 n°. 3, 302-307, Brazil, 2011.

[3] R.S. Barbosa, "New Method for Railway Track Quality Identification Through the Safety Dynamic Performance of Instrumented Railway Vehicle". Journal of the Brazilian Society of Mechanical Sciences and Engineering, Brazil, 2015. Doi: 10.1007/s40430-015-0471-9

[4] H.R. Daiha, O. Garcia, J.V. Ferreira "Modelos e observadores de estados para dinâmica vertical de veículos terrestres", in XII Simpósio Brasileiro de Automação Inteligente - SBAI, Rio Grande do Norte, Brazil, 289-294, 2015.

[5] H. Tsunashima, A. Matsumoto, H. Mori, A. Asano, "Track Condition Monitoring System using On-board Sensing Device", in J. Pombo, (Editor), Proceedings of the Second International Conference on Railway Technology: Research, Development and Maintenance, Civil-Comp Press, Stirlingshire, UK, Paper 84, 2014. doi:10.4203/ccp.104.84

[6] H. Tsunashima, Y. Naganumab, T. Kobayashic, "Track geometry estimation from car-body vibration", in Vehicle System Dynamics, Volume 52, Supplement 1, Special Issue: IAVSD Proceeding Supplement, 207-219, 2014.

[7] P. Weston, C. Roberts, G. Yeo, E. Stewart, "Perspectives on railway track geometry condition monitoring from in-service railway vehicles", in Vehicle System Dynamics, Vol. 53, n° 7, 1063-1091, 2015.

[8] F. Xia, C. Cole, P. Wolfs, "An inverse railway wagon model and its applications" Vehicle System Dynamics, Vol. 45, 6, 583–605, 2007.

[9] M. Darby, E. Alvarez, J. McLeod, G. Tew, G. Crew, "The Development of an Instrumented Wagon for Continuously Monitoring Track Condition", International Heavy Haul Association, Conference IHHA-2003, 2003.

[10] P. Gullers, P. Dreik, J.C.O. Nielsen, A. Ekberg, L. Andersson, "Track condition analyser: identification of rail rolling surface defects, likely to generate fatigue damage in wheels, using instrumented wheelset measurements", Proceedings of The Institution of Mechanical Engineers – Part: F - Journal of Rail and Rapid Transit. Vol.: 225, Ed. F1, pp. 1-13, 2011.

[11] R.J. Borgovini, "Development of an Ultra- Portable Ride Quality Meter". Federal Railraod Administration (FRA), U.S. Department of Transportation (DOT), Research Results Report RR 12-19, pp. 4, 2012.

[12] U. Feldmann, E. Kreuzer, F. Pinto, "Dynamic Diagnosis of Railway Tracks by Means of the Karhunen-Loève Transformation", Nonlinear Dynamics, Editor Kluwer Academic Publishers, Vol 22, n° 2, pp. 183-193, 2000.

[13] P.F. Weston, C.S. Ling, C.J. Goodman, C. Roberts, P. Li, R.M. Goodall, "Monitoring Lateral Track Irregularity from in-Service Railway Vehicle",

Institution of Mechanical Engineers, Part F: Journal of Rail Rapid Transit. IMechE, Vol. 221, Special Issue, pp 89-99, 2007.

[14] F. Xia, C. Cole, P. Wolfs, "Grey box-based inverse wagon model to predict wheel–rail contact forces from measured wagon body responses", Vehicle System Dynamics, Vol. 46, Supplement, pp. 469–479, 2008.

[15] H.C. Suda, Y.M. Aki, T. Tsuji, M. Morikawa, T. Yamashita, T. Kawanabe, T. Kunimi, "Study on detection of the early signs of derailment for railway vehicles", Vehicle System Dynamics, Vol. 48, Supplement, pp. 451-466, 2010.

[16] O. Heirich, A. Lehner, P. Robertson, T. Strang, "Measurement and Analysis of Train Motion and Railway Track Characteristics with Inertial Sensors", IEEE 14TH International IEEE Conference on Intelligent Transportation Systems (ITSC), pp. 1995-2000, 2011.

[17] B. Luber, A. Haigermoser G. Grabner, "Track geometry evaluation method based on vehicle response prediction", Vehicle System Dynamics, International Journal of Vehicle Mechanics and Mobility IAVSD: Special Issue, Volume 48, Supplement 1, pp. 157-173, 2010.

[18] EN 14363 Railway applications - Testing for the acceptance of running characteristics of railway vehicles - Testing of running behaviour and stationary tests, The European Standard EN 14363-2005, pp. 113, 2005.

[19] European Railway Agency "Assessment of freight train derailment risk reduction measures: B1 – Derailment Risk Models", Report for European Railway Agency, Report No: BA000777/06, Det Norske Veritas (DNV), 36 pp., 2011.

8.3 ANEXO C

NEW METHOD FOR RAILWAY TRACK QUALITY IDENTIFICATION THROUGH THE SAFETY DYNAMIC PERFORMANCE OF INSTRUMENTED RAILWAY VEHICLE

Barbosa, R. S. (2015) New method for railway track quality identification through the safety dynamic performance of instrumented railway vehicle. Journal of the Brazilian Society of Mechanical Sciences and Engineering, DOI:10.1007/s40430-015-0471-9, Vol.: 38, Issue 8, pp 2265–2275.

J Braz. Soc. Mech. Sci. Eng. (2016) 38:2265–2275
DOI 10.1007/s40430-015-0471-9

REVIEW

New method for railway track quality identification through the safety dynamic performance of instrumented railway vehicle

Roberto Spinola Barbosa[1]

Received: 30 January 2014 / Accepted: 9 December 2015 / Published online: 22 December 2015

Abstract Track geometry locations that exceed geometry-standardized limits do not necessarily cause poor vehicle performance. However, there are locations under geometric limits that promote unsafe dynamic vehicle performance. To handle this dichotomy, a new method for track inspection is proposed to complement the traditional ones. An inertial measuring system and a specialized data treatment method is presented to evaluate the railway track quality, observed from the vehicle dynamic performance point of view. With inertial devices the system measures the vehicle dynamic movements during transit along an irregular track. Values measured are used in an inertial navigation algorithm with a Kalman filter, to identify the full vehicle attitude, including angular positions and accelerations. System equations for the inverse vehicle dynamic problem, augmented with the suspension torsion equation, is solved to directly estimate the wheels driving forces that are directly correlated with the vehicle safety. An adimensional Safety Index (SI) is proposed to evaluate track quality. Values obtained are used to quantify track harmful locations. Results of two test campaign travelling on the irregular track in a conventional train identify the full vehicle attitude and movement. The SI and the location of the most potential hazard region for track maintenance purposes were identified. Good correlation between SI and measured track geometry is observed being a promising technique.

✉ Roberto Spinola Barbosa
spinola@usp.br

[1] Depto. Eng. Mecânica, POLI - USP, Escola Politécnica da Universidade de São Paulo, São Paulo, SP 05508-900, Brazil

Keywords Railway · Track · Quality · Safety · Vehicle · Dynamic

1 Introduction

Railway companies seek to operate transport systems with greater confidence. Tracks should be reliable, available for use and easy to maintain (reliability–availability–maintainability and safety—RAMS as defined by the European Union—UIC). To guarantee safe traffic conditions, the operator should keep track geometry standards at the highest quality possible, for an inspection time interval. This maintenance process is expensive due to tamping, ballast cleaning or renewal, sleeper replacement, joint repair, rail grinding or replacement and substructure treatment and other maintenance interventions. Railways also seek to establish explicit processes for decision-making regarding various activities to be undertaken to keep the track infrastructure in satisfactory condition or within desirable (required) condition/operational limits. Jovanovic [19] proposed a track maintenance management system where the Track Quality Index (TQI) is one of the conditions to be met, to apply maintenance resource more effectively. The Track Expert Group of UIC reveals in the report "Future of railway monitoring in Europe" [27] an increasing vehicle-based measuring systems rather than trackside or manual that will enable comparison and trend identification, leading to deeper understanding of asset behaviour: "This can help optimise maintenance strategy".

Track quality is traditionally quantified with a specialized-on-moving measuring car that measures track geometric basic parameters. Usually, the inspection car measures and records the variation of the track gage, vertical and lateral alignments and cross-level (angular variation on a track

section—cant or super elevation). Additionally, the cross-level variation per meter (track twist) can be calculated depending on the data sample rate. Some systems also use the three-point middle-chord technique as a device for particular measurement [14]. Values recorded are confronted with standard recommended limits and harmful regions are identified for maintenance planning. These measuring techniques are focused on measuring the track geometry and local irregularities and compare values to normalize limits. The average geometric variation associated with track quality is also used for track classification purposes (e.g. [13] or [9]). To assess track geometry quality, Li et al. [23] use the dynamic track–vehicle simulations on the spectra wave-length irregularity spectral domain to access the track–vehicle dynamic and indicate the use of second-order derivatives of track vertical irregularity for assessing track geometry quality [24].

Most of the track measuring systems identify only the track geometry variation within short wavelength identification (3–25 m, [16]). Also these systems do not deform the track during the measuring process. Therefore, the real deformed track geometry with the vehicle fully loaded is not recovered. An initiative to overcome these restrictions is the Track Machine Guidance project (TMG) developed by the UIC committee. For this purpose, requirements for a real-time machine guiding system were established based on absolute references and co-ordinate-based definition of the track geometry, using satellite positioning. The primary benefit is cost reduction for measurements absolute positioning, levelling, lining and tamping of the tracks [11]. Another complementary technique employed is the Ground Penetrating Radar (GPR) to evaluate the track substructure.

In addition to the well-known geometric measuring methods, researches related to the vehicle response characterization, when travelling over the track irregularities, are observed. Correlation metrics between the track roughness characteristic and the dynamic vehicle behaviour is the key for these methods. Several researchers [22, 28] discuss the detection of rail track irregularities, based on the measurements of the bearing box vertical acceleration during the operation of rail vehicles. Wilson and Ketchum [32] develop a performance-based track geometry (PBTG), an inspection method based on an accelerometer installed on a conventional track geometry inspection vehicle. The method calculates the vehicle behaviour in real-time based on the measured track geometry input. Kawazaki and Youcef-Toumi [20], Czop et al. [6], Sun et al. [29] and Tsunashima et al. [30] proposed a procedure-based system identification technique that solves an inverse dynamic problem, estimating track irregularities from the measured acceleration applied to the vehicle model of the frequency domain. English and Moynihan [8] also used a real-time processing inverse wagon linear model excited with measured track frequency content to predict wheel–rail contact forces.

An instrumented iron-ore wagon was proposed by Darby et al. [7] to measure the suspension spring deflection, lateral side frame acceleration, brake pipe pressure, inter-car separation, longitudinal wagon acceleration; coupler force and structural stress. Despite using various sensors, it is essentially a simple captive system, based only on measurements of deflection and some particular accelerations of a wagon to indirectly evaluate the track quality.

The use of instrumented wheel-set is another method to evaluate the effect caused by the track irregularity over the vehicle behaviour in traffic. In spite of being an expensive and laborious instrument, the quantification of the wheel-rail contact force ratio is an indication of track quality [15] and, therefore, the vehicle safety. Also portable accelerometers are employed for passenger comfort measurements [2] based on the ISO-2631 and UIC-513 Standards.

Inertial measurement devices (IMU) are new technologies developed in the aerospace industry with widespread application in military equipment. These devices are now available in the automotive industry and are particularly used in automotive control systems. Examples of use of this new technology can be found in Feldmann et al. [12] who propose to detect the vertical track settlement and deterioration using frequency domain transformation from the inertial measurements of the vehicle behaviour. Weston et al. [31] uses rate gyros and lateral acceleration for track curvature and alignment monitoring. Xia et al. [33] used an inverse vehicle model to estimate high-frequency wheel–rail contact forces from measurements of sensors installed in a track-recording car. One can observe in the temporal results, the difficulty of vehicle dynamics correlation with the wheel forces due to high-frequency movements of the body with reduced weight (e.g. wheelset, side frame, etc.). However. at low frequencies vehicle mass has predominance over the system movements and can be used for a particular application, which is the object of this work. Hung et al. [18] report that peak threshold of the pitch angular rate and the integral threshold of the roll angular rate of the vehicle truck frame are closely related to vehicle unsafe conditions. Heirich et al. [17] use an inertial device in the vehicle to infer the track features such as bank, bank change, slope, slope change, relative heading, curvature and basic track elements. Luber et al. [25] propose a method for track geometry assessment taking into account the vehicle/track interaction. The method is supported with vehicle vertical and lateral transfer function used for the prediction of the vehicle reaction forces. The results show a significant enhancement of the correlation between the track assessment quantities and the vehicle reaction forces. Although use of transfer function related to the parameters of the track (Track Geometry Assessment TGA [10, 16]) is

restricted to only two translational directions (vertical and lateral) and a wavelength range of 3–25 m, and not include rotational aspects. These aspects reinforce the need to broaden the spectrum of evaluation that is the proposal here presented.

Track geometry should be designed to meet the requirements of the fleet of car or wagons that uses it. During its service life, a perfect track develops irregularities that cause vehicle oscillation. In the extreme case, the vehicle can lose its guidance. Defects and failure of the track superstructure and vehicle dynamic performance may be mixed and cause these undesirable derailment events [11]. Focusing on the track geometry defects, structural elasticity, vehicle suspension characteristics and train speed, all these are potential possible contribution causes and should therefore be evaluated together to minimize hazard risk improving safe traffic.

Conversely, track geometry locations that exceed the standardized limits often do not cause obligatory poor vehicle performance. On the contrary there are good track locations under geometric limits that promote unsafe dynamic vehicle performance [21]. Additionally track stiffness does affect the passing vehicle dynamic. The larger the irregularities, the stronger the dynamic interaction effects. This process is auto propelled and increases the track defects at each passing vehicle. Additionally, depending on the train speed, a particular track roughness wavelength excites the vehicle modal resonance that substantially magnifies the dynamic effect. Safety is a complex phenomenon and depends simultaneously on the vehicle dynamic characteristics and on the track system response and geometry. To optimise track maintenance, would be of interest to include vehicle performance on the track evaluation method. It would be of interest to also identify the problems as they arise rather than waiting for the scheduled inspection campaign.

To handle this subject a new method for track inspection is proposed to complement the traditional ones. Track irregularities excite vehicle vibrations main modes and produce translational and angular movements. Wheel/rail contact forces that support the vehicle vertical load and produce the lateral directioning guiding forces cause these movements. The guiding forces are directly related to the vehicle accelerations. Hence, the results of the vehicle dynamic behaviour can be employed to evaluate the track geometry adequacy. Complementarily to the traditional measuring method, the vehicle dynamic performance can be used to identify the potential place of low safety on the track. The evaluation of these results can be used as metrics to prioritise location of maintenance on the already measured track geometry. This methodology can even more optimise maintenance intervention and improve the vehicle traffic safety.

2 Methodology

The methodology adopted to quantify track quality is to identify where it is more aggressive to vehicle safety. The specific circumstance for this scenario is three general types of vehicle unsafe conditions. The first condition is the wheel-climb derailment at a low speed on sharp curves. Another such condition is related to vehicle main body large movements. The latter condition is relative to a specific speed and a particular type of track irregularities.

The first condition is mainly related with vehicle suspension stiffness and load distribution. The second is related with the vehicle unsprung mass dynamic movements and directioning bogie/wheelset properties. The third is related to the track evenness wavelength, the vehicle natural frequencies and train speed [4]. Although there are other types of unsafe conditions, including the accidental and component failure ones, those described here are only related to the vehicle body low frequency movements and small energy dissipation.

The new methodology proposed and presented here is based on detection of signs of unsafe railway vehicle performance, mainly related to the second and third described types, when travelling on the track evenness. These signs are used to identify the location along the track and prioritise the pertinent track geometry correction in the most harmful irregularity to the vehicle safety.

For this purpose, the metric adopted to identify the potential harmful location is associated with the vehicle safety. This adimensional index is directly correlated to the traditional ratio between the wheel lateral (L) and vertical (V) contact force. The wheel forces are quantified from the measurement of the vehicle attitude and its overall dynamic behaviour. Using an inertial measuring device (IMU) with ten high-resolution transducers and a GPS signal, the Safety Index (SI) can be directly estimated from the wheel driving forces. This task is performed with an inverse vehicle dynamic model, fed with data acquired from complete vehicle instrumentation, during the transit journey and an inertial navigation algorithm (INS) for attitude recognition.

3 Vehicle dynamics

The wheel-rail contact force, due to the vehicle dynamic behaviour, is a function of the track roughness where the vehicle is travelling above. To identify the acting contact forces that produce the vehicle directioning movements, it is necessary to solve an inverse dynamic problem. The vehicle dynamics is governed by a set of differential equations obtained from the Newton–Euler theorems applied to the car body (considered as a rigid body) valid for a fixed reference

frame ***N*** (*OXYZ*) presented in Fig. 1. For the translational movements, the following differential equations relate accelerations and external forces in an earth fixed reference frame (left upper index, mean the reference frame used):

$$m\,{}^{N}\vec{a}_G = \sum \vec{F}^{\text{ext}} \tag{1}$$

This equation does not consider the drag and coriolis effects from the earth rotations due the irrelevant magnitude faced to the vehicle accelerations. The external forces are mainly due to wheel contact forces and gravitational effects as shown in Fig. 1.

$$m\,{}^{N}\vec{a}_G = \sum \vec{F}_{\text{wheels}} - m\,{}^{N}\vec{g} \tag{2}$$

The equation also can be expressed in the body reference frame $B(G_{xyz})$ using a rotational transformation matrix $\boldsymbol{T}$ (where the right underscript N states for the fixed reference frame and the right superscript B states for the body fix moving reference frame), composed with the three Euler angles (roll ϕ, pitch θ, yaw ψ) as identified in Fig. 1, where the accelerations are to be measured and the forces computed:

$$m\,T_N^B\left({}^{N}\vec{a}_G + {}^{N}\vec{g}\right) = T_N^B \sum \vec{F}_{\text{wheels}} \tag{3}$$

When the measuring system is fixed at particular point P, not coincident with the vehicle center of gravity $\boldsymbol{G}$, the measured acceleration must be projected according to the field acceleration equation, to be used by the Newton equation:

$$\vec{a}_G = \vec{a}_P + \vec{\alpha} \wedge (G - P) + \vec{\Omega} \wedge \left[\vec{\Omega} \wedge (G - P)\right] \tag{4}$$

where the angular velocity is $\vec{\Omega} = \dot{\phi}\,\vec{I} + \dot{\theta}\,\vec{J} + \dot{\psi}\,\vec{K}$ compose by the roll rate $\dot{\phi}$, the pitch rate $\dot{\theta}$ and the yaw rate $\dot{\psi}$. For the rotational movements described in a moving reference frame attached to the vehicle, the following differential equations relates angular accelerations α and body angular velocity $\omega_B = [\,\omega_x\ \omega_y\ \omega_z\,]^{\mathrm{T}}$ and external moments with respect to the same pole:

$$[J]_G\{\alpha\} + [\omega_B] \wedge [J]_G\{\omega_B\} = \left\{M_G^{\text{ext}}\right\} \tag{5}$$

The body external contact forces due to each wheel (H_i, L_i, V_i) are shown in Fig. 1. The body external moments (M_G) due to the wheel forces binary are obtained from the carbody dimensions as shown in Fig. 1. To work out the contact forces solving the system equation, it is necessary to know the vehicle body accelerations, as stated in Eq. 1. Additionally, it is also required to measure the angular velocity and to estimate the angular acceleration, needed to solve Eq. 5. Finally, the body angular attitude must be identified to solve the torsion Eq. 6.

The system has six equations and twelve contact forces unknowns. Disregarding the longitudinal effects, one equation is removed and four longitudinal contact forces are ignored (no acceleration or breaking effects). Due to the system being hyperstatic, the contact lateral forces in each wheelset are summed. To solve the system with five equations and six unknowns, an additional suspension torsion equation is disclosed to access each vertical force relationship, completing the system.

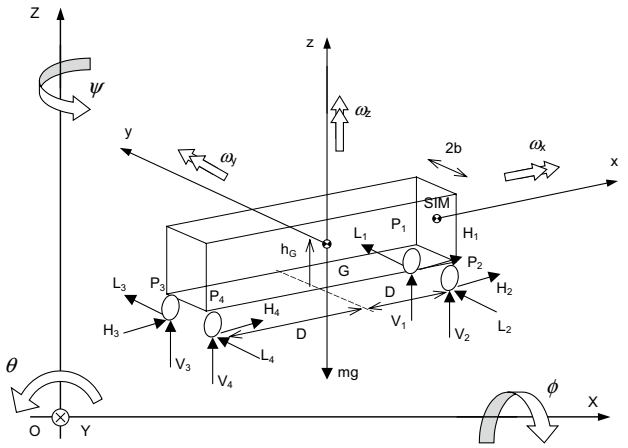

Fig. 1 Body attitude and forces distribution on the vehicle

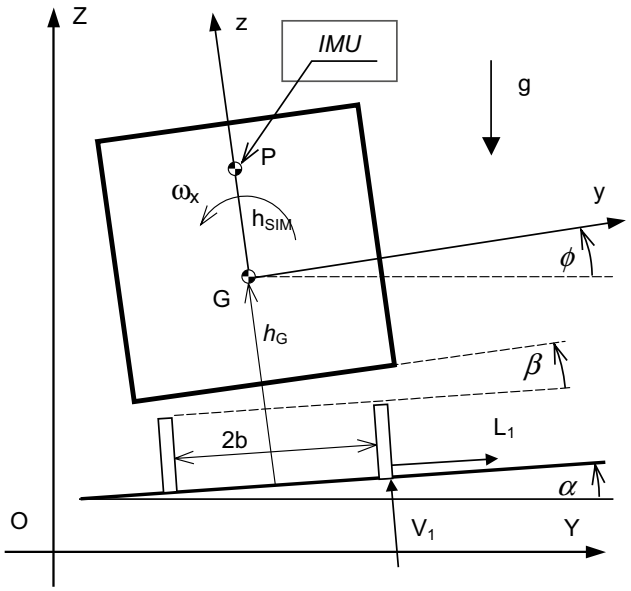

Fig. 2 Track and vehicle roll angles

The vehicle longitudinal torsion due to track twist affects mainly the vertical wheel load distribution. Considering the car structure as a rigid body, the track twist deflects the suspension unloading the diagonal wheels. This effect depends upon the vehicle suspension stiffness, length and width of the vehicle and magnitude and wavelength of track twist.

Namely, the expression for the vertical load variation as a function of the track angular twist per meter (δ) is related to a body geometry proportion ($D/2b$) and suspension torsional stiffness (k_φ) stated as:

$$\Delta V = -k_\phi \frac{D}{2b}\delta \tag{6}$$

To estimate the track twist from the overall vehicle inclination, a special filter is used to recover the local track superelevation (α). However, the IMU coupled to the body measures the absolute vehicle roll angle referred to the earth plane (ϕ). The total or earth referred body angle, as shown in Fig. 2, is composed by the track cant angle (α) added to the relative vehicle roll angle (β) due to suspension movements and inertial mass center height (h_G):

$$\phi = \alpha + \beta \tag{7}$$

The track cant angle (α) can be measured with an additional IMU installed on the wheelset. If this value is not available, another identification method is necessary. Disregarding any small vehicle suspension roll, the twist variation can be obtained from:

$$\delta = \frac{\mathrm{d}\alpha}{\mathrm{d}S} \tag{8}$$

Finally to identify the angles and attitude, the inertial navigation algorithm (INS) based on extended Kalman filter is used for multivariable estimator.

With all this information, it is possible to solve the vehicle inverse dynamic equations to evaluate the driving contact forces and calculate the SI on each wheel. The SI is the difference between the L/V adopted limit and the module worked out L/V value for each wheel [3].

$$\mathrm{SI} = \left|\frac{L}{V}\right|_{\mathrm{Limit}} - \left|\frac{L_i}{V_i}\right|_{\mathrm{measured}} \tag{9}$$

4 Measuring system and data treatment

The measuring system consists of an inertial measurement unit fixed on the vehicle, a GPS and a computer for command actions, data acquisition and storage media. The inertial measurement unit, or simply IMU, is a micro-electro-mechanical system (MEMS) that measures and reports the body movement. It utilizes a set of tri-orthogonal accelerometers to measures the vehicle accelerations ${}^B\vec{a}_G$ and angular speed device to measure the attitude variation ${}^B\vec{\omega}$. Additionally a tri-orthogonal magnetometer set and a precision barometer measures the orientation ${}^B\vec{m}$ based on the earth magnetic filed and the relative level. All the sensors are mounted in the vehicle and measurement the three-dimensional movements. A GPS identifies the vehicle speed and position expressed in the geographic-referenced latitude and longitude. All this information is anti-aliasing filtered, digitalized and recorded in the on-board control computer.

To recover the complete vehicle attitude to calculate the SI index a process based on inertial navigation algorithm (INS) is used to treat rough data from the sensor and identify vehicle external loads. Vehicle accelerations and angular attitude are the main information to recover from the accelerometers, rate-gyros and magnetometers information. To this end, a strapdown inertial recovery (SIR) algorithm and a local level frame identification must be involved for vehicle angular attitude recognition. An integrated navigation system on terrestrian movement's methodology should combine state data, generated by the dynamic equations, with independent redundant data in a Kalman filter algorithm.

The vehicle translational motion expressed in a fixed reference frame $\boldsymbol{N}$ is described by:

$$m\,{}^N\vec{a}_G = \sum {}^N\vec{F}_i^{\mathrm{ext}} \tag{10}$$

The vehicle attitude relative to an inertial reference frame $\boldsymbol{N}$, is described by three Euler angles denoting vehicle roll angle ϕ, elevation angle θ and heading angle ψ as shown in Fig. 1. The absolute position of a point in the vehicle is described by the vector ${}^N\vec{r}$ expressed in the inertial reference frame $\boldsymbol{N}$ and its time rate of change are:

$${}^N\vec{r} = T_B^{NB}\vec{r} \quad \text{and} \quad {}^N\dot{\vec{r}} = T_B^{NB}\dot{\vec{r}} + \dot{T}_B^{NB}\vec{r} \tag{11}$$

where the left superscript N over the vector states for the fixed reference frame and the left superscript B states for the body fix moving reference frame. T_B^N is the direction cosine matrix (DCM) formed with the three Euler rotation angles, which leads to the transformation matrix in terms of the three successive sequential body rotations (sequence 3–2–1, according to NASA Standard, Baruh):

$$T_B^N = \begin{bmatrix} c\theta\, c\psi & c\theta\, s\psi & -s\theta \\ -c\theta\, s\psi + s\phi\, s\theta\, c\psi & c\theta\, c\psi + s\phi\, s\theta\, s\psi & s\phi\, c\theta \\ s\phi\, s\psi + c\phi\, s\theta\, c\psi & -s\phi\, c\psi + c\phi\, s\theta\, s\psi & c\phi\, c\theta \end{bmatrix} \tag{12}$$

the prefix "s" and "c" stands for sine and co-sine for the respective angle.

The velocity vector ${}^N\vec{V}$ expressed in the inertial fixed frame $\boldsymbol{N}$ is defined in terms of position ${}^B\vec{r}$ expressed in rotating body fix reference $\boldsymbol{B}$, as:

$${}^N\vec{V} = T_B^{NB}\dot{\vec{r}} \quad \text{and its time derivative as } {}^N\vec{a} = \dot{T}_B^{NB}\dot{\vec{r}} + T_B^{NB}\ddot{\vec{r}} \tag{13}$$

The relation between the body angular velocities ω_B (roll rate, pitch ate and yaw rate) and the vehicle attitude rate Ω_N (rate in bank, attitude and heading) is described by [5]:

$$\begin{Bmatrix} \omega_x \\ \omega_y \\ \omega_z \end{Bmatrix} = \begin{bmatrix} 1 & 0 & -s\theta \\ 0 & c\phi & s\phi\, c\theta \\ 0 & -s\phi & c\phi\, c\theta \end{bmatrix} \begin{Bmatrix} \dot{\phi} \\ \dot{\theta} \\ \dot{\psi} \end{Bmatrix} \tag{14}$$

and the time rate of change of the transformation matrix $\dot{T}_N^B$ is:

$$\dot{T}_B^N = T_B^N\ \omega_B \quad \text{where} \quad \omega_B = \begin{bmatrix} 0 & -\omega_z & \omega_y \\ \omega_z & 0 & -\omega_x \\ -\omega_y & \omega_x & 0 \end{bmatrix} \tag{15}$$

where ω_i are the three angular speeds components described in the skew symmetric rotating matrix expressed on the body reference frame.

The problem of attitude determination involves determining the transformation matrix that maps the on-board sensed information with model transformation to the geographic frame magnetic and gravity field components. For the body-referenced magnetic sensor to match the local geographic-referenced magnetic field, and for the body-referenced accelerometer sensor to match the local geographic-referenced acceleration then:

$${}^N\vec{m} = T_B^{NB}\vec{m} \quad \text{and} \quad {}^N\vec{a}_G = T_B^{NB}\vec{a}_G \tag{16}$$

Assuming these two vectors are not parallel, a third orthogonal vector can be produced by the cross product. The matrix formed using these three vectors as columns (superscript T over the vector states for transposed vector) can be associated to:

$$\left[{}^N\vec{m}^{\mathrm{T}}\ {}^N\vec{a}^{\mathrm{T}}\ \left({}^N\vec{m} \wedge {}^N\vec{a}\right)^{\mathrm{T}} \right] = T_B^N \left[{}^B\vec{m}^{\mathrm{T}}\ {}^B\vec{a}^{\mathrm{T}}\ \left({}^B\vec{m} \wedge {}^B\vec{a}\right)^{\mathrm{T}} \right] \tag{17}$$

The matrix on the left-hand side is composed by known geographic-referenced information. The matrix on the right-hand side is composed by sensed information. Therefore, the unknown DCM orthogonal matrix can be obtained from:

$$T_B^N = \left[{}^B\vec{m}^{\mathrm{T}}\ {}^B\vec{a}^{\mathrm{T}}\ \left({}^B\vec{m} \wedge {}^B\vec{a}\right)^{\mathrm{T}} \right]^{\mathrm{T}} \left[{}^N\vec{m}^{\mathrm{T}}\ {}^N\vec{a}^{\mathrm{T}}\ \left({}^N\vec{m} \wedge {}^N\vec{a}\right)^{\mathrm{T}} \right]$$
$$\text{and} \quad T_N^B = \left(T_B^N\right)^{\mathrm{T}} \tag{18}$$

A better refined estimative for the DCM matrix to identify body attitude is obtained using a Kalman filter technique [26]. Typical integration accumulated drifts errors, such as heading vehicle attitude, are to be corrected with multiple cross sensor information. With the accelerometers and the magnetometer a level frame is to be determined. Based on this error difference, an extended Kalman filter algorithm, merge multi sensor data, to correct and stabilize the rate-gyros orientation calculations as shown in Fig. 3. Complementary GPS data allows estimating the vehicle speed, alignment and the curvature of the trajectory [1].

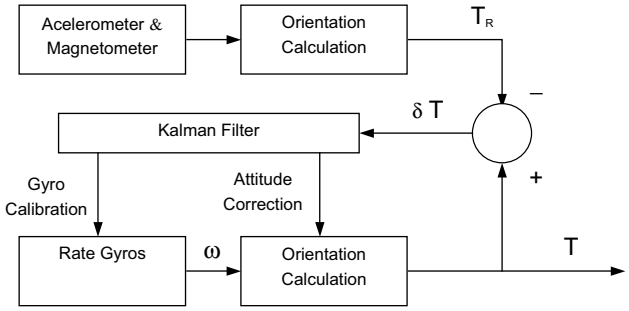

Fig. 3 Block diagram

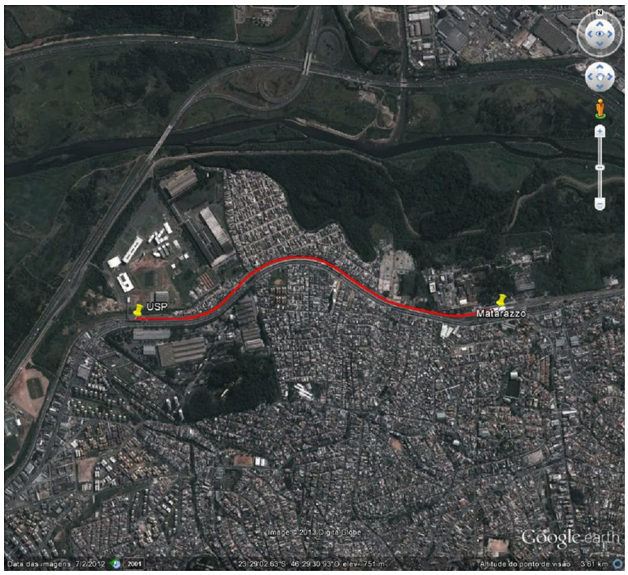

Fig. 4 Path travelled (satellite photo)

The angular description can be on the Euler form or Quaternion form, depending on the need to solve the singular problems due to angular quantification. With the accelerations, angular rate and attitude angles, the vehicle guiding force is calculated with aid of a strapdown inertial recovery (SIR) algorithm that allows to determine the SI. Data is filtered with a low-pass 15 Hz FIR filter.

5 Field measurements

Two field tests were performed with a passenger car equipped with the measuring system installed in the middle of the first passenger car. The first on-traffic-performance-concept proof was performed on the train on line 12 of the Companhia Paulista de Trens Metropolitanos (CPTM) from Bras Station to Calmon Viana Station in the east of Sao Paulo city, Brazil.

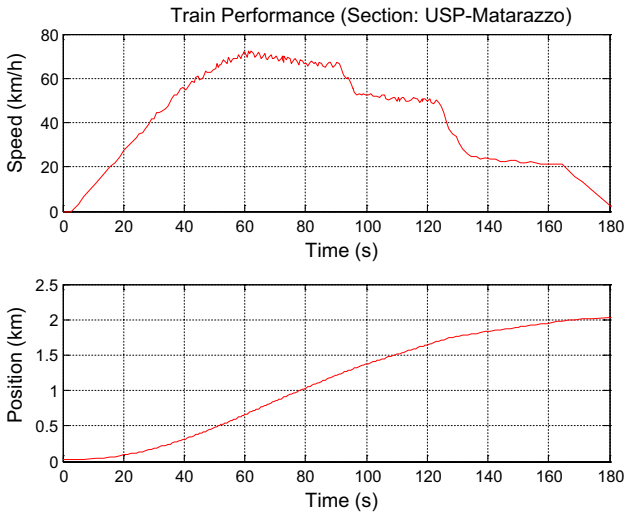

Fig. 5 GPS information

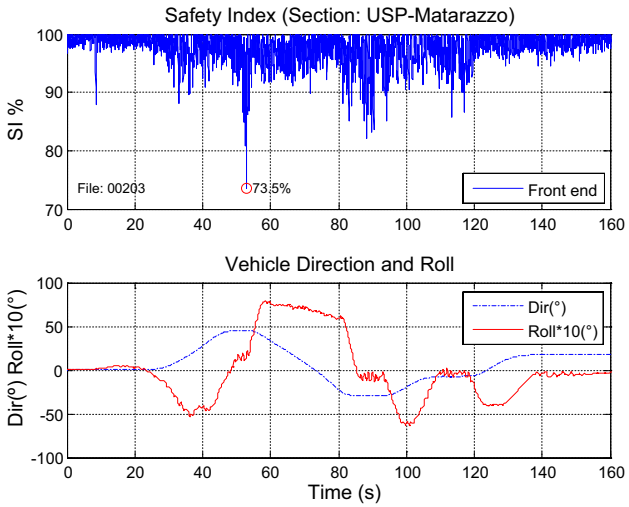

Fig. 7 Safety Index for the car front end—SI

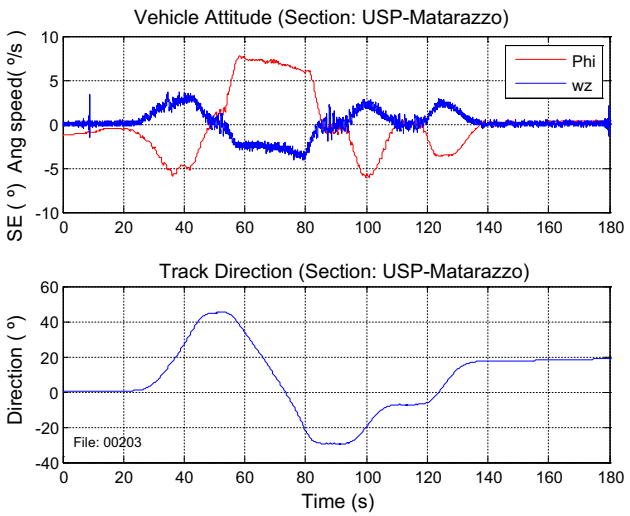

Fig. 6 Vehicle attitude

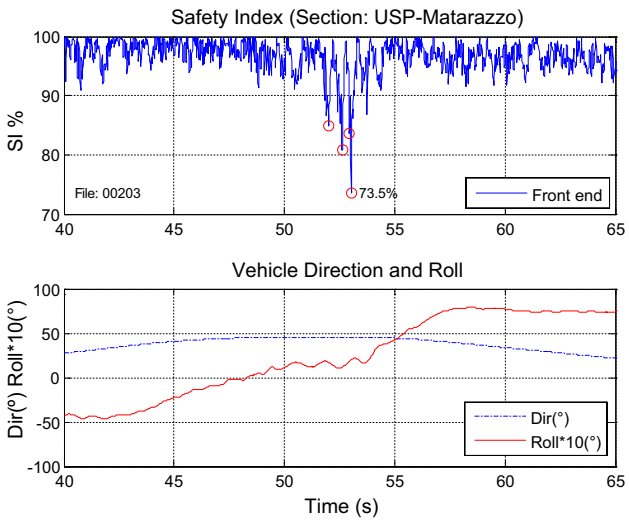

Fig. 8 Detail of the smallest values of the SI

A slice of path travelled, with a reversed curve, is selected for visualization and analysis. This section is between two stations (USP and Matarazzo) as can be observed in Fig. 4, which presents the satellite photo of the region (path travelled in red). After the USP station, the first short left curve can be observed (train moves to east), then the long right curve and two short left curves before the Matarazzo station. The train was conducted at the normal operational speed along this line, which is almost 50 km long. Particularly, the section between the two stations is around 2 km long and the train performance can be observed in Fig. 5 (speed and position).

The results of the rough measurements are presented in Fig. 6. The upper graph shows the vehicle angular yaw speed (ω_z) and the roll angle (Phi angle). The lower graph of Fig. 6 presents the car body or track direction (Psi angle). The long right curve of the section, between 50 and 55 s, can be clearly observed, when the train speed is around 67–69 km/h.

6 Analysis of data

To compute the wheel loads, it is necessary to measure the translational acceleration and angular velocity, to identify the angular accelerations and the car body Euler angles as described in item 3. Values for the SI can be determined at any vehicle extremity. Adopting an *L*/*V* limit of 1.0, the resulting values for the SI of the vehicle front end are presented in Fig. 7. The upper graph presents the SI values and the

Fig. 9 Photo from satellite

lower graph, the vehicle movements. Reduced SI values are observed in the first reversed curves before the long right turn.

Figure 8 presents a closed look of the most critical region. The upper graph presents the SI and the extreme values are identified (red circles). As can be seen, the smallest SI value is 73.47 % at time 53.03 s, probably due to track twist in the straight track between the first reversed curves that promote roll movement oscillations of the car body. Other large values are observed next to 52.95; 52.63 and 52.00 s (SI values of 83, 7, 80.9 and 84.9 % respectively). This method point out exactly the place of reduced safety of the track, from the vehicle point of view and reinforces the recommendation for track maintenance on the geometric and irregularity properties in this location.

The exact location of the critical region is: Latitude: −23.484347° (23°29′3.65″S); Longitude: −46.496272° (46°29′46.58″O); Altitude: 737.949 m; Speed: 68.0 km/h; Heading: 43.45°; Time: 2013-02-20 T12:20:30Z (minus 3 h in this country).

The second test was performed at line 11 from Luz Station at Sao Paulo center to Guaianazes Station also on the east bound of the city. On this evaluation results measured were compared to the real track geometry measurements performed with a specialized car (EM-100 from Plasser).

In the section from km 10+800 to km 11+200 near Station Vila Matilde which exact geo-referenced location is shown in the satellite photo presented in Fig. 9, it is identified a reduced SI. The quantified value was 79 %, as

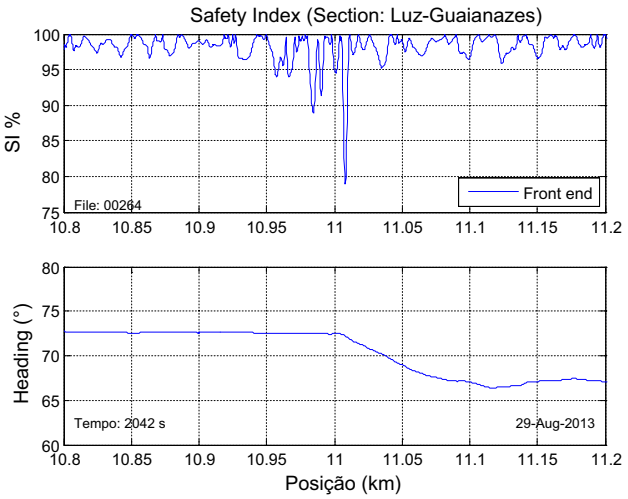

Fig. 10 Safety Index (km 11+000)

shown in Fig. 10. At the bottom of the same figure is shown the direction of the passenger car in this region. Immediately after the critical point, there is a curve with a transition until km 11+100 after a circular curve with radius of approximately 650 m.

The track geometry and irregularities measured with the EM-100 vehicle are presented in the following figures. The track alignment shows a local variation before the transition curve as can be observed in Fig. 11. Also the track

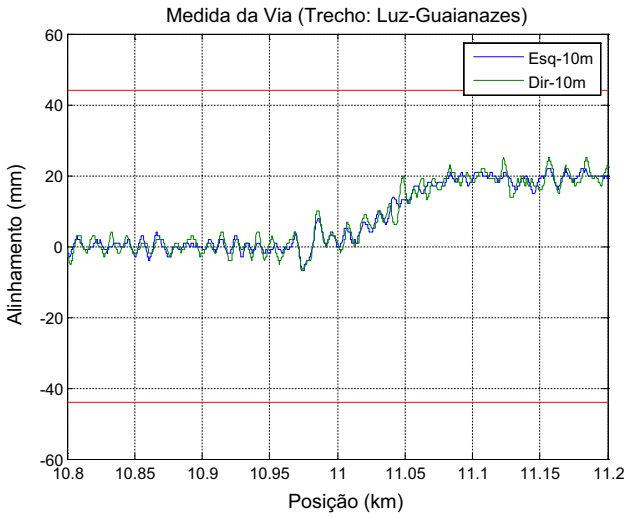

Fig. 11 Track alignment

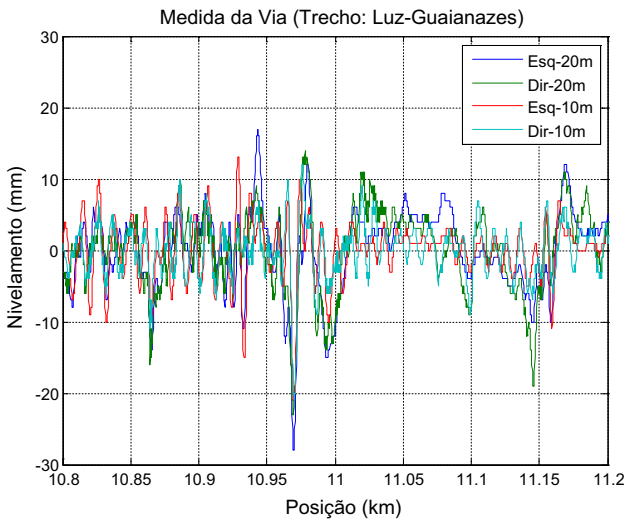

Fig. 12 Track leveling

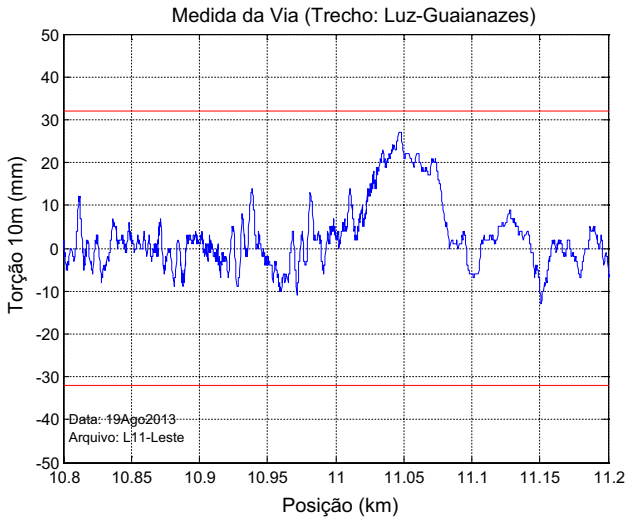

Fig. 13 Track twist (chord length 10 m)

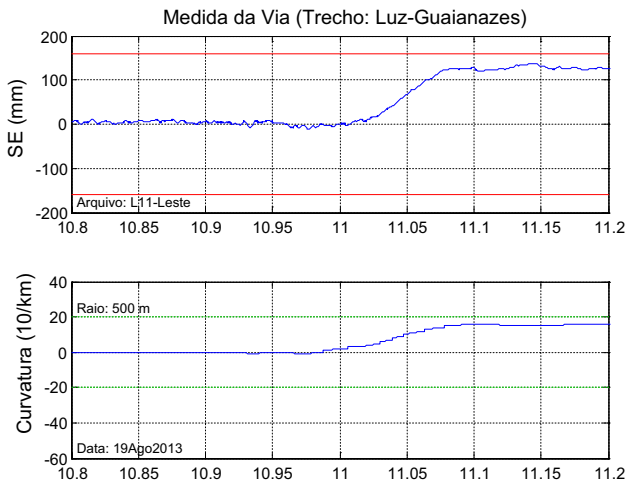

Fig. 14 Track cant and curvature

levelling presented in Fig. 12 shows abrupt variations. The track twist and track can and curvature are presented in Figs. 13 and 14 respectively.

It can be observed that all the track geometry measurements are below the FRA Class 3 level (red line on the graphs). At position km 11+010 inside the transition curve segment, there is small levelling deviation (Fig. 12) but not the highest value, and a twist in the transitions curve entrance (Fig. 13). Exactly on this position a reduced SI of 79 % was identified.

7 Comments

Albeit unnecessary from the point of view of track quality, this method takes into account the non-stationary longitudinal coupler forces effects. This action does affect the wheel load distribution, particularly in curves where its projection affects the lateral acceleration and the angular yaw body acceleration. Therefore, this jerk phenomenon is characterized with the body angular accelerations covered accordingly with this approach.

The results are related to the speed of the train during the journey. The operating speed is variable depending on the style of the driver, train load, climatic variations and any speed restrictions existing on the track. However, in different speeds, forced movements will change its magnitude, modifying the values measured, but keeping the location identified. Even the natural movements induced by periodic irregularities changes, but location remains due to the damping factor of the suspension.

The repeatability of the system is confirmed with different passenger cars of the same fleet. The possibility of evaluating similar vehicles in various load conditions or distinct passengers car fleets is easily performed, only by changing the installation of the measuring device. The data measured can also be used to evaluate passenger comfort using the vertical and lateral accelerometers signals in accordance with the comfort standard (ISO 2631) or even the vehicle modal quantification.

Differently from the other systems that use only statistics information from few sensors, the present new system is MISO that takes into account the complete vehicle multisignal input and deliver a single output index directly correlated to the safety condition.

8 Conclusions

A new inertial measuring system and a specialized data treatment method are presented to perform the railway track quality quantification, observed from the vehicle performance point of view. With an inertial device, the system measures the vehicle dynamic movements and attitude during its transit along the irregular track. The values measured are used in the strapdown inertial recovery (SIR) algorithm with an extended Kalman filter, to identify the full vehicle attitude, including angular positions and accelerations. The vehicle system equations for the inverse dynamic problem, augmented by suspension torsion equation, is solved to directly calculate the wheels driving forces Also the safety *L*/*V* contact force ratio in the low frequency region is identified. The SI directly correlated with the vehicle safety is determined based on the traditional railway *L*/*V* ratio. Values obtained are used to qualify track harmful locations.

The results of a preliminary test campaign travelling on the irregular track in a conventional train are presented. The full vehicle attitude and movement identification as far as the calculations of the SI is performed. Values obtained for the SI drop down to almost 75 % probably due to track twist in the straight track between the reversed curves that promote roll movement oscillations of the vehicle. The GPS signal simultaneously captures the exact georeferenced location and train speed of the most potential hazard region for track maintenance purposes. The second test results were compared to the measured track geometry and a good correlation was observed and the most harmful location was identified. The new method developed is direct and objectively identifies the location of undesirable track geometry and irregularities, through the unsafe dynamic vehicle behaviour.

This quantification is not unique but may complement the other existing geometric tools. Due to its simplicity and low cost, the new system can be easily installed in any vehicle and operate with any load condition and variable travelling speed, without the traditional traffic disturbance. The system can be applied to any specific vehicle fleet, travelling in any track section, in the usual operational speed and detect the most harmful location for this specific track to complement the geometric measuring methods. The analyses can also be focused to compute different priority criteria (passenger comfort, minimal dynamic vertical load applied to the track, instantaneous safety indicator, etc.) according to user interests. The better classification of the most harmful track locations, allows prioritising the track intervention strategy. The complementary combination of new and traditional monitoring track inspection techniques can help to better understand asset behaviour and produce effective investment efficiency in railway track maintenance, being a promising technique. Future development aims to extend this concept to a system with a full sensor in each rigid body, all of them time synchronized, and with the correspondent set of equations of motions.

Acknowledgments The author would like to thank the Mechanical Department of the Polytechnic School of São Paulo University (EP-USP) for the support to this research and Companhia Paulista de Trens Metropolitanos—CPTM, in São Paulo, Brazil that made available the resources for the railway measurements.

References

1. Anderson R, Bevly DM (2010) Using GPS with a model-based estimator to estimate critical vehicle state. Veh Syst Dyn 48(12):1413–1438
2. Borgovini RJ (2012) Development of an ultra-portable ride quality meter. Federal Railraod Administration (FRA), U. S. Department of Transportation (DOT), Research Results Report RR 12-19, p 4
3. Barbosa RS (2004) A 3D contact force safety criterion for flange climb derailment of a railway wheel. Veh Syst Dyn 42(5):289–300
4. Barbosa RS (2011) Vehicle dynamic response due to pavement roughness. J Braz Soc Mech Sci Eng 33(3):302–307
5. Baruh H (1999) Analytical dynamics. McGraw-Hill, New York, p 718
6. Czop P, Mendrok K, Uhl T (2011) Application of inverse linear parametric models in the identification of rail track irregularities. Arch Appl Mech 81:1541–1554
7. Darby M, Alvarez E, McLeod J, Tew G, Crew G (2003) The development of an instrumented wagon for continuously monitoring track condition. In: International Heavy Haul Association, Conference IHHA-2003
8. English GW, Moynihan TW (2005) Realizing performance-based track geometry standards. In: Proceedings of The 8th International Heavy Haul Conference, IHHA, Rio de Janeiro, Brazil, pp 539–546
9. EN 13848-1 (2003) Railway applications—track geometry quality—characterisation of track geometry, 2003. In: Measuring systems: track recording vehicles, EN 13848-2, 2006. Geometric quality levels. Plain line, EN 13848-5, 2008. European Standard
10. EN 14363 (2005) Railway applications—testing for the acceptance of running characteristics of railway vehicles testing of

running behaviour and stationary tests. The European Standard EN 14363-2005, p 113
11. European Railway Agency (2011) Assessment of freight train derailment risk reduction measures: B1—derailment risk models. Report for European Railway Agency. Report No. BA000777/06, Det Norske Veritas (DNV)
12. Feldmann U, Kreuzer E, Pinto F (2000) Dynamic diagnosis of railway tracks by means of the Karhunen–Loève transformation. Nonlinear Dyn 22(2):183–193
13. FRA-Standard (2012) Track Safety Standards. In: Track and rail and infrastructure integrity compliance manual, vol II, chapter 1. Federal Railroad Administration, p 171
14. Glaus R (2006) Kinematic track surveying by means of a multi-sensor platform. Swiss Federal Institute of Technology Zurich—ETH, Doc. Diss. ETH No. 16547, p 185
15. Gullers P, Dreik P, Nielsen JCO, Ekberg A, Andersson L (2011) Track condition analyser: identification of rail rolling surface defects, likely to generate fatigue damage in wheels, using instrumented wheelset measurements. Proc Inst Mech Eng F: J Rail Rapid Transit 225(F1):1–13
16. Haigermoser A et al (2014) Describing and assessing track geometry quality. Veh Syst Dyn 52(Supplement 1):189–206
17. Heirich O, Lehner A, Robertson P, Strang T (2011) Measurement and analysis of train motion and railway track characteristics with inertial sensors. In: IEEE 14TH International IEEE Conference on Intelligent Transportation Systems (ITSC), pp 1995–2000
18. Hung C, Suda Y, Aki M, Tsuji T, Morikawa M, Yamashita T, Kawanabe T, Kunimi T (2010) Study on detection of the early signs of derailment for railway vehicles. Veh Syst Dyn 48:451–466
19. Jovanovic S (2004) Railway track quality assessment and related decision making. In: 2004 IEEE International Conference on Systems, Man and Cybernetics, vol 1–7, pp 5038–5043
20. Kawazaki J, Youcef-Toumi K (2002) Estimation of rail irregularities. In: Proceedings of the American Control Conference, vol 1–6 Book Series, pp 3650–3660
21. Ketchum CD, Wilson N (2012) Performance-based track geometry—PBTG. Phase: 1. Transit Cooperative Research Program, Document 52. Transportation Technology Center, Inc., p 89
22. Lee JS, Choi S, Kim S, Park C, Kim YG (2012) A mixed filtering approach for track condition monitoring using accelerometers on the Axle Box and Bogie. IEEE Trans Instrum Meas 61(3):749–758
23. Li M, Berggren EG, Berg M, Persson I (2008) Assessing track geometry quality based on wavelength spectra and track—vehicle dynamic interaction. Veh Syst Dyn 46:261–276
24. Li M, Persson I, Spannar J, Berg M (2012) On the use of second-order derivatives of track irregularity for assessing vertical track geometry quality. Veh Syst Dyn 50(Supplement 1):389–401
25. Luber B, Haigermoser A, Grabner G (2010) Track geometry evaluation method based on vehicle response prediction. Veh Syst Dyn 48(Supplement 1):157–173 **(special issue)**
26. Marins JL, Yun X, Bachmann ER, McGhee RB, Zyda MJ (2001) An extended Kalman filter for quaternion-based orientation estimation using MARG sensors. In:Proceedings of the 2001 International Conference on Intelligent Robots and Systems. IEEE, pp 2003–2011
27. Nederlof C, Dings P (2010) Monitoring track condition to improve asset management. In: UIC WG track condition monitoring synthesis report, International Union of Railways, Paris
28. Real JI, Montalban L, Real T, Puig V (2012) Development of a system to obtain vertical track geometry measuring axle-box accelerations from in-service trains. J VibroEng 14(2):813–826 **(special issue)**
29. Sun YQ, Cole C, Spiryan M (2013) Evaluation of heavy Haul Wagon dynamic behaviours based on acceleration measuring systems. In: Proceedings of the 10th International Heavy Haul Association Conference, IHHA. New Delhi, India, pp 546–553
30. Tsunashima H, Naganuma Y, Kobayashi T (2014) Track geometry estimation from car-body vibration. Veh Syst Dyn 52(Supplement 1):207–219
31. Weston PF, Goodall RM et al (2007) Monitoring lateral track irregularity from in-service railway vehicle. Inst Mech Eng F: J Rail Rapid Transit (ImechE) 221:89–99 **(special issue)**
32. Wilson N, Ketchum CD (2012) Performance-based track geometry (PBTG). Transit Cooperative Research Program, Transportation Research Board, Report D-7, Task 18, p 89
33. Xia F, Cole C, Wolfs P (2008) Grey box-based inverse wagon model to predict wheel–rail contact forces from measured wagon body responses. Veh Syst Dyn 46:469–479

8.4 ANEXO D

VEHICLE VIBRATION RESPONSE SUBJECTED TO LONGWAVE MEASURED PAVEMENT IRREGULARITY

Barbosa, R. S. (2012) Vehicle Vibration Response Subjected to Longwave Measured Pavement Irregularity. Journal of Mechanical Engineering and Automation, DOI: 10.5923/j.jmea.20120202.04, Vol.: 2, Issue 2, pp. 17-24.

Journal of Mechanical Engineering and Automation 2012, 2(2): 17-24
DOI: 10.5923/j.jmea.20120202.04

Vehicle Vibration Response Subjected to Longwave Measured Pavement Irregularity

Roberto Spinola Barbosa

Department of Mechanical Engineering of the Engineering School of the University of Sao Paulo

Abstract The motivation of this work is to develop a spectral method to deal with the vehicle vibration response when subjected to a longwave measured pavement irregularity. For this purpose, the vehicle model vibration is correlated in the frequency domain with the spectral density function of the pavement irregularity, to achieve the system spectral transfer function. Vehicle transfer function and spectral pavement irregularity results are treated in the frequency domain to obtain the vehicle frequency response due to a longwave road evenness input. The results show that, at 120 km/h in an asphalt pavement with ondulation, the first vehicle vibration mode has a significant movement enlargement, due to the pavement irregularity signature, causing passenger vibrational discomfort and identifying location for maintenance.

Keywords vehicle, dynamic, vibration, pavement, irregularity, roughness, road, confort

1. Introduction

During the vehicle project and design development, the automotive industry in general uses the vehicle modal response and numerical simulation (*Costa*, 1992), optimisation methods for suspension settle (*Vilela*, 2010), laboratory shaker test rig (*Boggs*, 2009) and the results of experimental field road test to fine-tune vehicle suspension (*Vilela*, *Tamai*, 2005). New techniques as magnetic active suspension is being developed to minimize road evenness effects improving vehicle ride comfort (*Gysen*, 2010). Another important aspect in the suspension design is the variability of the vehicle load and road evenness. The quarter-car model is usually employed to study vehicle vibration response (*Kropac*, 2009). State space half-vehicle model is used to identify pavement load but only in the time domain (*Sun*, 2007).

The main contribution of this work consists in the devel-opment of a half-vehicle with two point delayed base exci-tation model and correlate with the spectral density function of a measured pavement irregularity in the frequency domain to obtain the vertical and angular vehicle frequency response due to a road evenness input. For this purpose, a two-wheels vehicle model is derived using the Lagrange method and its frequency response function considering the time delay of the out of phase input to each wheel, is obtained. The pavement vertical surface profile has been measured along two road sections with a special broadband wavelength measuring system. The spectral density function of thepavement irregularity with longwave content is determined and surface signature has been identified. The product of the two spectral functions in the frequency domain is performed in order to attain the system spectral transfer function.

Notwithstanding the efficiency of the numerical methods, the laboratory and experimental works are still performed, despite costly and time-consuming. This approach contributes and extending the power of the design analytical tools due to the possibility to analyse vehicle dynamic response in a wide range of road evenness (*Barbosa*, 2001, 2011), reducing of the number of tuning experimental works. Also allows identifying vehicle dynamic response due to normalized irregularity density distribution or a measured pavement irregularity. The method addresses the passenger comfort due to vehicle vibration in rough pavement, vehicle safety through pavement/tyre contact force and complement the portfolio of the analytical design tools.

2. Vehicle Modelling

The description of the dynamic vehicle behaviour is performed with the half-car representation. Four degrees of freedom lumped parameter model describing relevant movements is adopted to describe the vehicle in this research, as shown in **Figure 1**. The vehicle model associated with mass m_3 and inertia moment J_G, allows the vertical translation z_3 and angular movement θ for the body. The front and rear suspensions have only vertical displacement. The lumped masses are connected with parallel spring-damper system. Vehicle suspension is associated to masses m_1 and m_2 and has correspondent elastic and dissipative properties (k_f, c_f, k_r and c_r). The tyre stiffness and damping values are k_1,

* Corresponding author:
spinola@usp.br (Roberto Spinola Barbosa)
Published online at http://journal.sapub.org/jmea

c_1, k_2 and c_2. The model is excited by the same road evenness $u_1(t)$ and $u_2(t)$ with a time delay, which induces front and rear suspension movements, respectively.

The equations of motion are obtained using the *Lagrange* method applied to the lumped rigid bodies. The kinetic and potential energy function and generalized dissipation function are:

$$T = \frac{1}{2} m_3 \dot{z}_3^2 + \frac{1}{2} J_G \dot{\theta}^2 + \frac{1}{2} m_1 \dot{z}_1^2 + \frac{1}{2} m_2 \dot{z}_2^2 \quad (1)$$

$$V = \frac{1}{2} k_f (z_3 + b\theta - z_f - l_{f0})^2 + \frac{1}{2} k_r (z_3 - b\theta - z_r - l_{r0})^2 + \frac{1}{2} k_1 (z_1 - u_1 - l_{10})^2 + \frac{1}{2} k_2 (z_2 - u_2 - l_{20})^2 \quad (2)$$

$$R = \frac{1}{2} c_f (\dot{z}_3 + b\dot{\theta} - \dot{z}_f)^2 + \frac{1}{2} c_r (\dot{z}_3 - \dot{b}\theta - \dot{z}_r)^2 + \frac{1}{2} c_1 (\dot{z}_1 - \dot{u}_1)^2 + \frac{1}{2} c_2 (\dot{z}_2 - \dot{u}_2)^2 \quad (3)$$

Performing the partial derivative and applying the *Lagrange* expression described as:

$$\frac{d}{dt}\left(\frac{\partial T}{\partial \dot{q}_i}\right) - \frac{\partial T}{\partial q_i} + \frac{\partial V}{\partial q_i} + \frac{\partial R}{\partial \dot{q}_i} = Q_i \quad (4)$$

Detailed equations are presented in the appendix A. The adopted inertia vehicle properties, the suspension elasticity and dissipation values are presented in **Table 1**. These values are typical of a medium-sized passenger car.

Table 1. Half-car properties

Element/Charac.	Vehicle Body	Suspension	Hub/Tyre[A]
Mass	750 kg	-----	30 kg
Inertia moment	360 kg m^2	----	----
Rigidity	-----	18.25 kN/m	150[B] kN/m
Damping	-----	912.5 Ns/m	0.0[C] Ns/m

Obs.: [A] individual properties; [B] rigidity depends on tyre pressure; [C] not considered

The modal system properties characterize four coupled vibration modes due to the non-diagonal constitution of the system matrix. The vehicle body modal response has two natural damped frequencies around 1.0~2.0 and the suspension has two more around 12 Hz. For the body modes (front and rear end bounce), as shown in **Figure 3**, damping factors are 1.4 and 2.6, respectively. For the suspension modes, associated with the unsprung mass of the hub and the tyre elasticity, damping factors are around 0.2, as presented in **Table 3**.

Note that the suspension vehicle frequency is around one decade above those from the vehicle body modes. The normalised modal eigen-vectors obtained from the dynamic matrix are presented on **Table 3**.

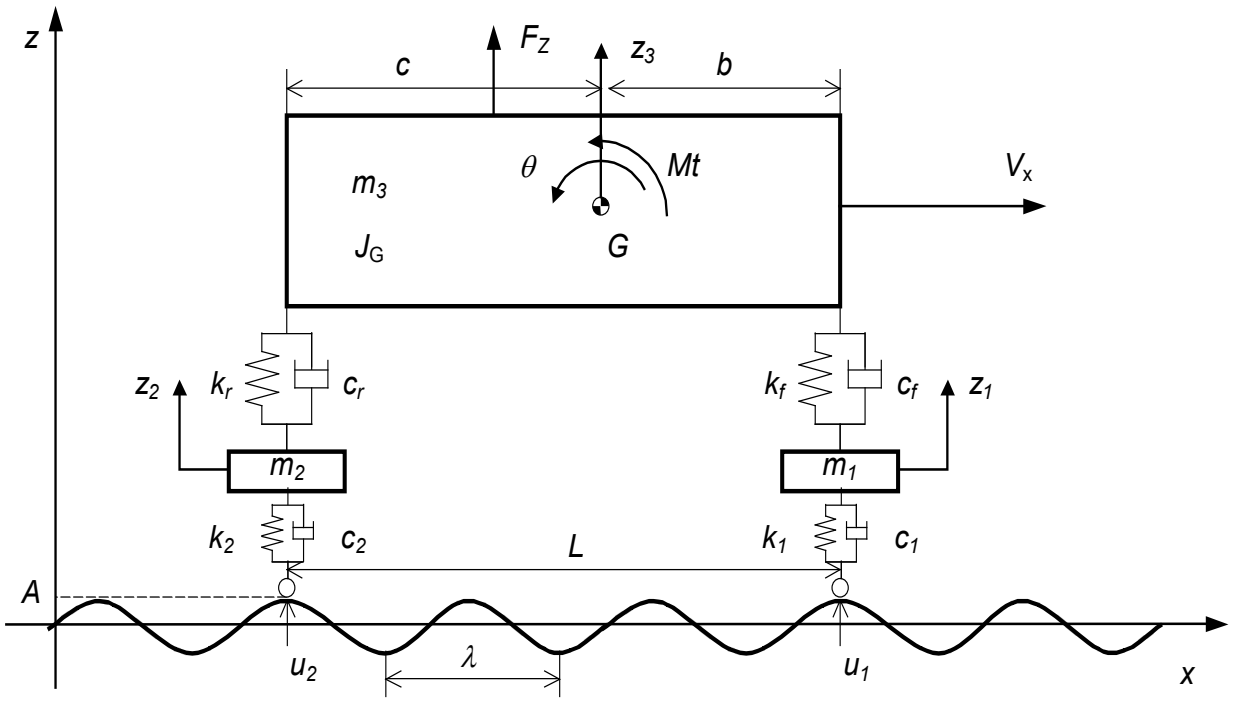

Figure 1. Half-car model

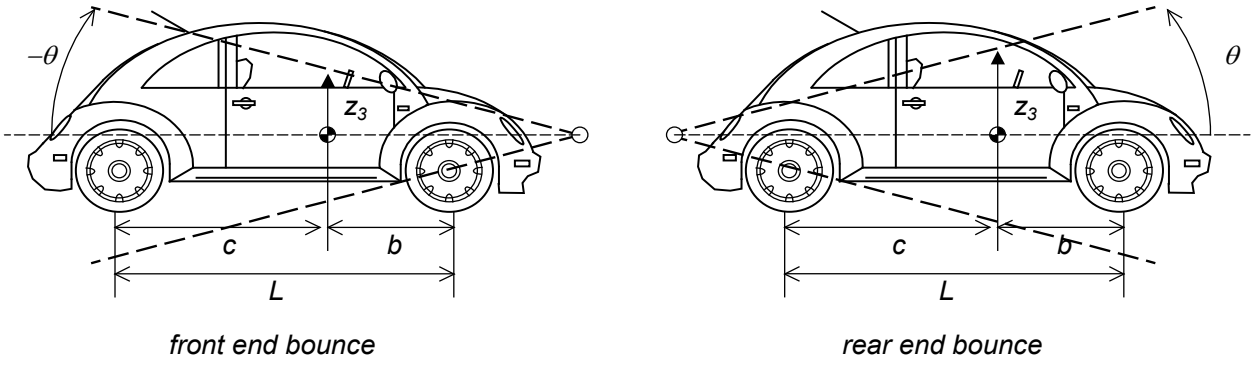

Figure 3. Vehicle coupled modes (front and rear end bounce)

Table 3. Modal properties

Mode Number	Mode 1 – vehicle front end bounce		Mode 2 – vehicle rear end bounce		Mode 3 – in phase wheel/hub		Mode 4 – out of phase wheel/hub	
Damped Natural Freq	1.03 Hz		1.88 Hz		11.72 Hz		11.86 Hz	
Damping Factor	0.144		0.261		0.216		0.207	
D. Freedom	Mag.	Phase	Mag.	Phase	Mag.	Phase	Mag.	Phase
z_1	0.0000	-305.87°	0.0000	-307.44°	0.0842	-105.13°	0.9880	180.00°
z_2	0.0002	-203.91°	0.0002	-204.96°	0.9964	0.00°	0.1523	81.712°
z_3	0.0134	-101.95°	1.0000	0.00°	0.0006	-315.41°	0.0235	-16.576°
θ	1.0000	0.00°	0.0136	-102.48°	0.0842	-201.27°	0.0036	-114.86°

By taking the *Laplace* transform of the system equations and assuming zero initial conditions (*Felício*, 2007), one obtains:

$$[Z_n(s), \theta(s)] = f[U_n(s), F_z, Mt] \tag{9}$$

Considering that the rear wheel runs on the same track as the front wheel, the surface elevation that produces the vertical displacement in each wheel is the same function with a time delay. Taking a periodic function $u(t)$ as the imposed input, the rear wheel input is expressed as:

$$u_1(t) = u(t) = A\,\mathrm{sen}(\omega t) \;\rightarrow\; u_2(t) = u(t-T) \tag{11}$$

where the periodic excitation frequency is $\omega = 2\pi V_x / \lambda$ and the time delay $T = L / V_x$, being L the inter-axis distance and V_x the vehicle speed and λ the wavelength, as shown in **Figure 1**.

The *Laplace* transformation of the front and rear wheel input function, considering the transformation of the delay function, is:

$$U_1(s) = \mathcal{L}[u_1(t)] \text{ and } U_2(s) = \mathcal{L}[u_2(t)] \;\rightarrow\; U_1(s) = U(s)$$
$$\text{and } U_2(s) = U(s)e^{-Ts} \tag{12}$$

By replacing $U_1(s)$, $U_2(s)$ and eliminating Z_1 and Z_2 from these equations and after some algebraic manipulation to sort the vertical and angular movements of the vehicle body over displacement excitation *U(s)* relationship, the following transfer function is obtained:

$$\frac{Z_3(s)}{U(s)} = H_z(s) \text{ and } \frac{\Theta(s)}{U(s)} = H_\Theta(s) \tag{13}$$

The displacement frequency response function (FRF) is known as *receptance H(s)*. However, considering a periodic input, there is a simple relationship between acceleration and displacement, since $\ddot{u}(t) = -A\omega^2\,\mathrm{sen}(\omega t)$. The acceleration frequency response function known as *inertance I(s)* can be obtained. Analysing the system vertical and angular forced movements in the frequency domain response, replacing *s* with $(i\omega)$ and assuming vehicle properties presented in **Table 1**, the frequency response inertance functions are expressed as:

$$I_{z_3}(i\omega) = \omega^2 H_{z_3}(i\omega) \text{ and } I_\Theta(i\omega) = \omega^2 H_\Theta(i\omega) \tag{14}$$

The vertical (I_{z_3}) and angular (I_θ) vehicle modal transfer function depends on *T* that is a speed function ($T = L / V_x$). Therefore, the vehicle FRF shape will be speed-dependent as can be observed in **Figure 5** for 7.1 m/s (25.6 km/h) and **Figure 7** for 33.3 m/s (120 km/h). In this case, *L* = 2.4 meters.

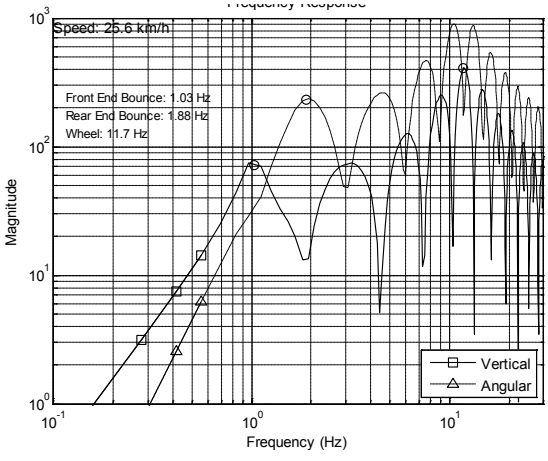

Figure 5. Vehicle inertance frequency response at 7.1 m/s (25.6 km/h)

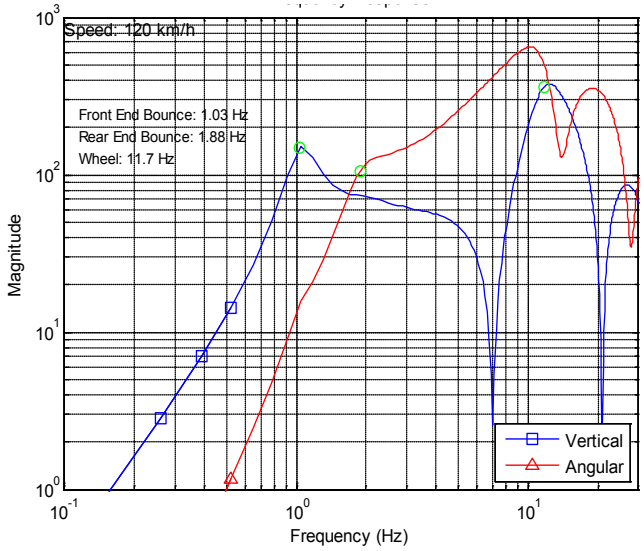

Figure 7. Vehicle inertance frequency response at 33.3 m/s (120 km/h)

Note that the hump in the PSD curve is due to the inter-axle distance L (2.4 meters) and vehicle speed (7.1 m/s). For the vertical mode, they occur at every integer, resulting in peaks around 1, 3, 6, 9 *Hz* as shown in **Figure 5** (square marked line) for a travelling speed of 25.6 km/h. For the vehicle speed at 120 km/h (33.3 m/s), the peaks occur at 13.9 and 27.8 *Hz* (see the square marked line in **Figure 7**).

Note that for a vehicle with an inter-axle distance of 2.4 meters, travelling at 86 km/h (24 m/s), T will be 0.1 and, therefore, the next vertical hump is one decade above first mode.

Figure 9. Measuring device

3. Pavement Irregularity Measurement

The road pavement irregularity can be measured by different methods. On this study the surface irregularity was measured with the 3-point-middle-chord broadband wavelength system as presented in **Figure 9**. This system is composed of three aligned wheels supported on a frame dragged by a conventional car. The two external wheels are steered and the central wheel is articulated referring to the others constituting a moving reference frame. A conventional car pulls the measuring system along the road measuring the track evenness. The central wheel vertical movement was measured with a high precision linear variable differential transformer (LVDT) at every centimetre. The values are sampled with an analogue to digital sample board installed in a portable computer (*Pavimetro*, 2010). The data acquired are stored in magnetic media for post processing purposes.

Elevation of two sections of asphalt highway with 2000 and 500 meters long, were measured. The measured data is treated with the measuring system transfer function to obtain the topographic vertical elevation of the surface irregularity specially including longwave contents, due to the data integration process. The vertical displacement of the center wheel system transfer function $Hy(p)$ (*Aknin*, 1995) is defined by:

$$H_y(p) = \sum \lambda_i \, e^{a_i \, p} \tag{15}$$

The measuring system transfer function is presented in **Figure 11** .

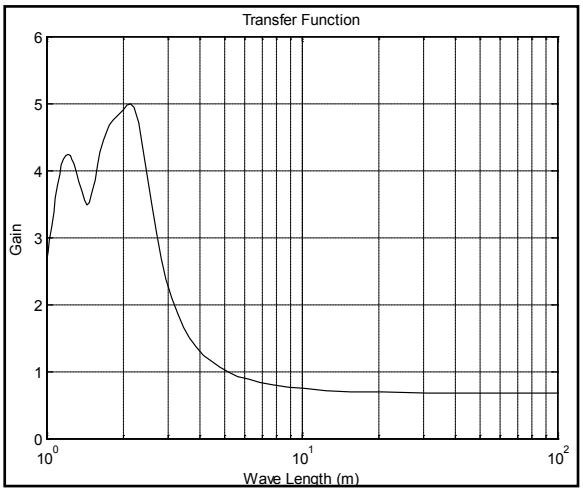

Figure 11. Measuring system transfer function

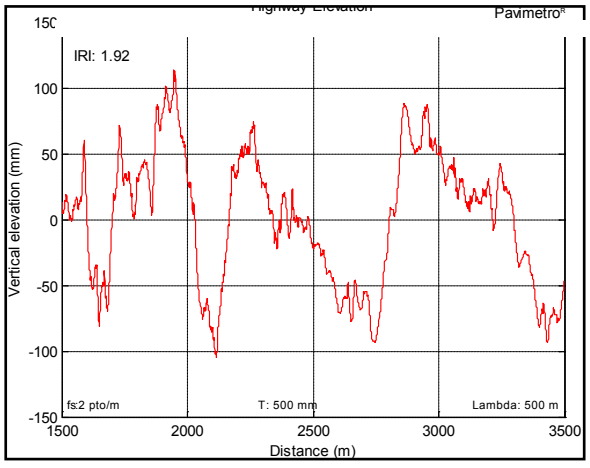

Figure 13. Highway vertical elevation (asphalt)

The vertical elevation of the road is obtained from the function integral. Wavelength up to 100 meters is recovered. This aspect is unique and not usual on conventional irregularity measuring systems. Results of the treated data are presented in **Figure 13** and **Figure 15**, for each section respectively.

The vertical elevation of the surface is presented in **Figure 13**. In this case, two points per meter were sampled (or one sample at each 0.5 meter). Up to 500 meters wavelength were considered in the data reconstruction processes. The result of the asphalt road evenness is statistically represented in irregularity index units (International Roughness Index – IRI, ASTM E1926-08). The mean IRI value for this section with 2000 meters is 1.92.

The second road section of 500 meters has an elevation presented in **Figure 15** where a periodic undulation around 10 mm high (between abscissa 100 and 300 meters) is observed.

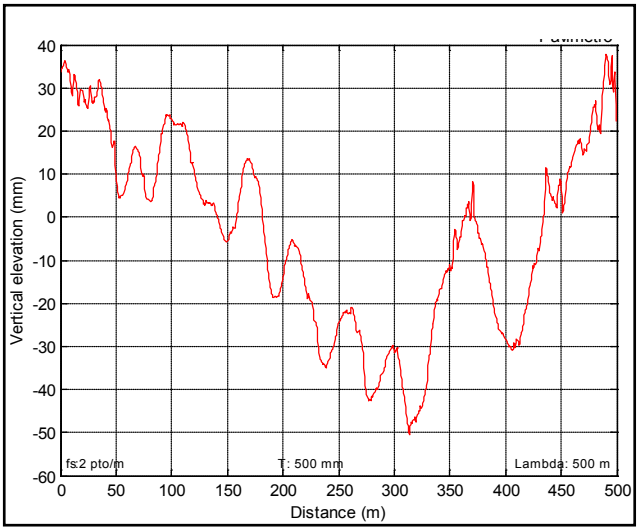

Figure 15. Road elevation with undulation (0.5 km long)

Although other process have been used to measure the pavement irregularity, such as vehicle acceleration (*Gonzalez*, 2008, *Kropac*, 2008, *Kropac*, 2009, *Farias*, 2009, *Harris*, 2010, Yousefzadeh, 2010), this particular method has a broadband and long wavelength evenness identification, which allows the vehicle interaction low frequency response analysis.

4. Pavement Irregularity Density Function

The pavement irregularity can be expressed through its spatial frequency density function. The surface vertical elevation measured on a track, along the road distance $z(x)$, can be transformed to the frequency domain to identify its contend of elevation wave length $S(n)$. The transformation is based on the *Fast Fourier Transformer* (FFT) technique. The data treatment can be performed up to 2048 points of a sample rate down to 10^{-2} meters. This range allows analysing wavelength as long as 100 meters and below 0.2 meters. This wide range values are not usual in the pavement measurement systems.

The asphalt track elevation measurements were manipulated to obtain the distribution in terms of wavelength of periodic irregularities. The power spectral density function (PSD) between 1 to 100 meters wavelength of the asphalt road vertical elevation is presented in **Figure 17**. The intensity of the measured pavement irregularity is classified, according to the magnitude of the power spectral pattern of the irregularities in an exponential fashion with a particular slope. The long road section measured spectrum has its particular signature and is compatible to A - level ISO Class (ISO 8606, 1995).

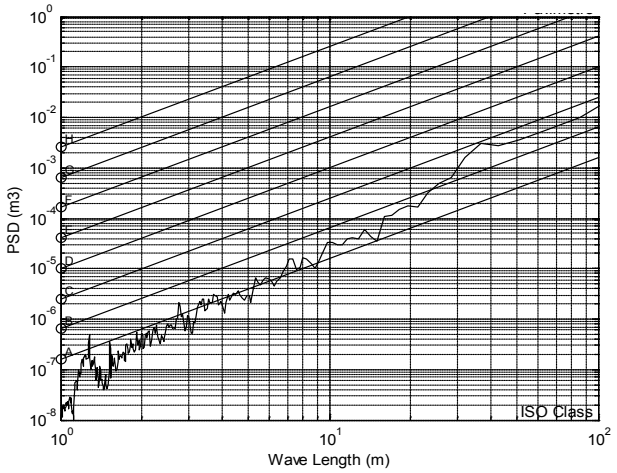

Figure 17. Elevation PSD of the long section of highway (2000 meters)

The short road section spectrum, presented in **Figure 19**, also has its particular signature being a little better than A - level ISO Class, but presents a clear high power content around 40 meters. Comparing the two sections, one can observe the overall reduction on the PSD elevation content present in **Figure 19**, the short wave content (0.85 meters) presented in **Figure 17** and the longwave content (34 meters) present in **Figure 19**.

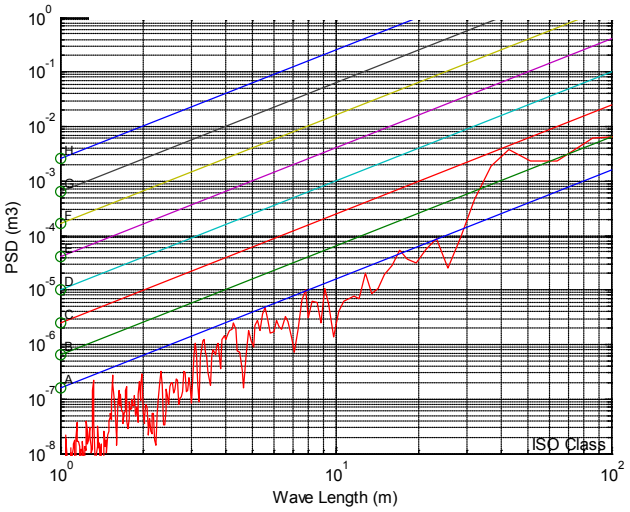

Figure 19. Road with ondulation (500 meters)

Although in this work the longwave evenness is focused for low-frequency vehicle vertical movements, other aspects, such as noise generation, rolling resistance, traction, wear, are all attributes to consider in the optimisation of the interaction between automotive tyres and road. This can be addressed with short-wave length irregularity (*Silva*, 1999, *Andrén*, 2006, *Andersson*, 2008).

5. Vehicle/Road Interaction

The vehicle natural behaviour is expressed through its frequency domain response function. The pavement irregularity considered as a rigid surface, is expressed through its spatial frequency (1/space). The relationship between time frequency ω and spatial frequency n is the vehicle speed V, expressed simply by $\omega = V \cdot n$

where ω is frequency in *Hertz* , $n = 1/\lambda$ is the inverse of the surface wavelength in meter and V is the vehicle speed in meter per second. Transforming $S(n)$ into the frequency domain, $S(\omega)$ is obtained from:

$$S(\omega) = S(n_o) \cdot (\omega / \omega_o)^{\theta} \tag{18}$$

According to the stochastic process theory, the output of a linear time-invariable system is a stationary random process if the input is also a stationary random process. In most cases, pavement irregularity could be described as a zero mean *Gaussian ergodic* random process (*Newland*, 1984). Hence, the response of the half-car system is also a zero mean *Gaussian* stationary random process. The relationship between the PSD of the system response $GH_i(\omega)$ and the PSD of the system excitation $S(\omega)$ is expressed by the product of the receptance functions:

$$GH_z(\omega) = |H_z(\omega)|^2 S(\omega) \quad \text{and} \quad GH_\theta(\omega) = |H_\theta(\omega)|^2 S(\omega) \tag{19}$$

Applying this method to the vehicle inertance function $I_{z3}(\omega)$ and $I_\theta(\omega)$ as shown in the block diagram of **Figure 21**, the following expression are obtained:

$$GI_{z3}(\omega) = |I_{z3}(\omega)|^2 S(\omega) \quad \text{and} \quad GI_\theta(\omega) = |I_\theta(\omega)|^2 S(\omega) \tag{20}$$

where $GI_{z3}(\omega)$ and $GI_\theta(\omega)$ are the PSDs of the vehicle vertical acceleration response and the pitch angular acceleration response of the sprung mass, respectively.

The acceleration density function of the vertical and angular vehicle mass centre is shown in **Figure 23**. It can be observed that at 33.3 m/s (120 km/h), the severe long wavelength content around 34 meters matches the first vehicle natural frequency (front end bounce). This effect magnifies the expected acceleration proneness around 1.0 *Hz* and therefore the passenger's discomfort in this situation.

When the ratio between the body and suspension frequency coincides with the ratio between the longitudinal speed V_x and the inter-axle distance (L), the largest magnification of the vertical translational interference occurs due to the track wavelength and the resonance of the suspension mode. This critical speed can be determined with the following relationship:

$$V_x = L \frac{\omega_{wheel}}{\omega_{body}} \tag{21}$$

A vehicle will be very susceptive to pavement irregularity with wavelength content around 2.85 an 34 meters ($\lambda = V / \omega$) when travelling at 120 km/h. This resonance causes discomfort, annoying the passenger during the trip. Therefore, a specialized maintenance intervention on the pavement surface can produce the best cost/benefit ratio between comfort and amount of work (*Namur*, 2009, *Martin*, 2010). Any other standard pavement irregularity description, such as the ISO 8606, may be used with this technique, increasing the power of this method. A complete vehicle may be analysed providing the axle dynamic behaviour coherence function between road irregularity in left and right wheel-path (*Bogsjo*, 2008), including the analysis of human vibration comfort as recommended by the international human standard for comfort (*ISO* 2631, 1978).

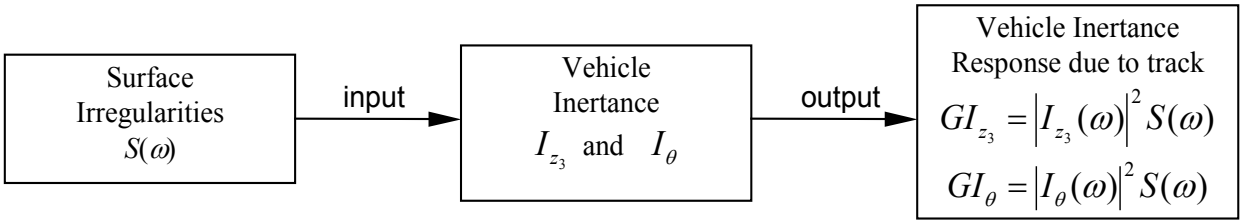

Figure 21. Inertance response block diagram

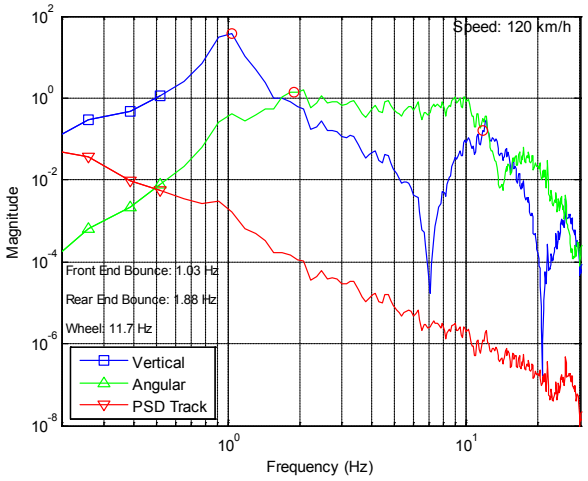

Figure 23. Vehicle inertance function in asphalt road at 120 km/h

6. Conclusions

A methodology was presented to evaluate vehicle/ pavement dynamic interaction. This methodology is based on the modal vehicle frequency response function and the statistical description of a rough pavement. For this purpose, a half-vehicle with two point delayed base excitation model is derived and the vertical and angular vehicle body transfer functions are calculated considering the time delay of the out of phase input. Two road section surface elevations were measured with a special referenced measuring system keeping the longwave evenness. This aspect is unique and not usual to conventional measuring systems. The data measured were treated to obtain the distribution in terms of periodic irregularity wavelength and surface signature has been identified. The vehicle body inertance vertical and angular transfer functions are weighed up by the surface irregularities distribution function, both in the frequency domain. The resulting system functions are related to the passenger comfort and can be used for suspension design purposes.

The vertical inertance function obtained for the translation and angular body movements were excited with the track irregularity density function of the measured road surface elevation in the frequency domain. For a vehicle speed of 120 km/h, the first vertical body vibration mode coincides with the surface longwave magnification (34 meters), increasing the vehicle vertical movement and causing passenger discomfort.. This methodology extends the efficiency of the numerical simulation with the power of the frequency response analysis.

The advantage of this approach is the possibility to analyse vehicle dynamic response subjected to any statistic description of pavement irregularity. Results allow quantifying passenger comfort and tune suspension parameters. After identified a particular harmful wavelength content on the pavement surface, a specialized maintenance intervention program to remove the longwave content can produce the best cost/benefit ratio between user comfort and amount of maintenance work.

A simple four degrees of freedom vertical vehicle model was used in this study. However, based on this methodology, a complete vehicle model can be used including the axle dynamic behaviour coherence function between road irregularity in left and right wheel-path to assess detailed vehicle-pavement relationship. Trucks, lorries and other complex suspension types may also be investigated. Human body behaviour may be included in the comfort analysis for the complete cycle of vibration propagation.

ACKNOWLEDGEMENTS

The author would like to thank the valuable contribution of Professor Edilson Tamai. Thanks also to the Mechanical Engineering Department of the Escola Politécnica da Universidade de São Paulo (EP-USP), for the support to this research.

Appendix A

Differential motion equations obtained are:

$$m_1\ddot{z}_1 + c_1(\dot{z}_1 - \dot{u}_1) + k_1(z_1 - u_1) - c_f(\dot{z}_3 - b\dot{\theta} - \dot{z}_1) - k_f(z_3 - b\theta - z_1) = 0 \quad (22)$$

$$m_2\ddot{z}_2 + c_2(\dot{z}_2 - \dot{u}_2) + k_2(z_2 - u_2) - c_r(\dot{z}_3 - c\dot{\theta} - \dot{z}_2) - k_r(z_3 - c\theta - z_2) = 0 \quad (23)$$

$$m_3\ddot{z}_3 + c_f(\dot{z}_3 + b\dot{\theta} - \dot{z}_1) + k_f(z_3 + b\theta - z_1) + c_r(\dot{z}_3 - c\dot{\theta} - \dot{z}_2) + k_r(z_3 - c\theta - z_2) = F_Z \quad (24)$$

$$J_z\ddot{\theta} + bc_f(\dot{z}_3 + b\dot{\theta} - \dot{z}_1) + bk_f(z_3 + b\theta - z_1) + cc_r(\dot{z}_3 - c\dot{\theta} - \dot{z}_2) + ck_r(z_3 - c\theta - z_2) = Mt \quad (25)$$

The *Laplace* transform of the system equations assuming zero initial conditions are:

$$\begin{aligned}
&[m_1s^2 + (c_1 + c_f)s + (k_1 + k_f)]\, Z_1(s) - (c_fs + k_f)\, Z_3(s) \\
&+(bc_fs + bk_f)\, \Theta(s) = (c_1s + k_1)U_1(s) \\
&[m_2s^2 + (c_2 + c_r)s + (k_2 + k_r)]\, Z_1(s) - (c_rs + k_r)\, Z_3(s) \\
&+(cc_rs + ck_r)\, \Theta(s) = (c_2s + k_2)U_2(s) \\
&[m_3s^2 + (c_f + c_r)s + (k_f + k_r)]\, Z_3(s) - (c_fs + k_f)\, Z_1(s) \\
&-(c_rs + k_r)\, Z_2(s) + [(bc_f - cc_r)s + (bk_f - ck_r)]\, \Theta(s) = F_z \\
&[J_Gs^2 + (b^2c_f - c^2c_r)s + (b^2k_f - c^2k_r)]\, \Theta(s) - b(c_fs + k_f)\, Z_1(s) \\
&-c(c_rs + k_r)\, Z_2(s) + c(c_rs + k_r)\, Z_3(s) = Mt
\end{aligned} \quad (26)$$

The vertical displacement of the center wheel system transfer function $Hy(p)$ is defined by:

$$H_y(p) = \sum \lambda_i\, e^{a_i\, p} \quad (15)$$

where the values for λ_i for the wavelength p and inter-wheel distances a_1 and a_2 are:

$$\lambda_i = \left[\frac{a_2}{a_2 - a_1}, \frac{-a_1}{a_2 - a_1}\right] \quad (16)$$

REFERENCES

[1] ASTM Standard E 1926-08 - Standard Practice for Computing International Roughness Index of Roads from Longitudinal Profile Measurements, DOI: 10.1520/E1926-08, 16 p., 2003.

[2] Costa, A. Application of Multibody Systems (MBS) Modelling Techniques to Automotive Vehicle Chassis Simulation for Motion Control Studies, Doctor Of Philosophy In Engineering, University of Warwick, England, 1992.

[3] Vilela, D. Aplicação de Métodos Numéricos de Otimização ao Problema Conjunto da Dirigibilidade e Conforto Veicular (Optimisation numerical methods application to the vehicular ride and comfort joint problem). PhD. These at University of Sao Paul,. 315 p., Sao Paulo, Brazil, 2010.

[4] Boggs, C., Southward, S. Ahmadian, M. Application of System Identification for Efficient Suspension Tuning in High-Performance Vehicles: Full-Car Model Study". SAE Document Number: 2009-01-0433 in the Book Tire and Wheel Technology and Vehicle Dynamics and Simulation, Product Code: SP-2221, 434 p. 2009.

[5] Vilela, D., Tamai, E. H. Optimisation of Vehicle Suspension Using Robust Engineering Method and Response Surface Methodology. Proceedings of The International Symposium on Dynamic Problems of Mechanics - DINAME. São Paulo, Brazil, 2005.

[6] Gysen, B.L.J., Paulides, J.H. Janssen, J.L.G., Lomonova, E.A. Active Electromagnetic Suspension System for Improved Vehicle Dynamics, IEEE Transactions on Vehicular Technology, Vol. 59, no. 3, pp. 1156-1163, 2010.

[7] Kropac, O. Mucka, P. Effects of longitudinal road waviness on vehicle vibration response. International Journal of Vehicle System Dynamics, Vol. 47, nº 2, pp. 135-153, 2009.

[8] Sun, L., Luo, F. Nonstationary Dynamic Pavement Loads Generated by Vehicles Travelling at Varying Speed". Journal of Transportation Engineering © ASCE. Vol. 133, pp. 252-263, 2007.

[9] Barbosa, R.S., Costa, A. Safety Vehicle Traffic Speed Limit. IX International Symposium on Dynamic Problems of Mechanics, IX DINAME. Associação Brasileira de Ciências Mecânicas – ABCM, Brazil, 2001.

[10] Barbosa, R .S., Vehicle Dynamic Safety in Measured Rough Pavement. Journal of Transportation Engineering © ASCE, Vol. 137, nº. 5, pp. 305-310, 2011.

[11] Barbosa, R. S., Vehicle Dynamic Response Due to Pavement Roughness. Journal of the Brazilian Society of Mechanical Sciences and Engineering - ABCM, Vol. 33, p. 302-307, Brazil, 2011.

[12] Felicio, L.C. Modelagem da Dinâmica de Sistemas e Estudo da Resposta (System Dynamic modelling and response study), Published by Editora Rima, São Carlos, São Paulo, Brazil, pp. 551, 2007.

[13] http://www.pavimetro.com.br. Pavimetro - The Pavement Roughness Measuring System. Accessed January 2012.

[14] Gonzalez, A.; O'Brien, E.J;. Li. Y.Y.; Cashell, K. The use of vehicle acceleration measurements to estimate road roughness. Vehicle System Dynamics, Vol. 46, Issue 6, pp. 485-501, 2008.

[15] Kropac, O. Mucka, P. Indicators of longitudinal unevenness of roads in the USA. International Journal of Vehicle Design, Vol. 46, nº 4, pp. 393-415, 2008.

[16] Kropac, O.; Mucha, P. Alternative single-number indicator of longitudinal road unevenness. Published by NRC Research Press, Canadian Journal of Civil Engineering, Vol. 36 pp. 389-401, 2009.

[17] Farias M.M.; Souza, R.O. Correlations and Analyses of Longitudinal Roughness Indices. Road Materials and Pavement Design, Vol. 10, Issue: 2, pp. 399-415, 2009.

[18] Harris, N.K., Gonzalez, A., OBrien, E.J. McGetrick, P. Characterisation of pavement profile heights using accelerometer readings and a combinatorial optimisation technique. Journal of Sound and Vibration, Vol. 329, pp. 497 –508, 2010.

[19] ISO 8606 - International Organisation for Standardisation. Mechanical Vibration Road Surface Profiles - Reporting of Measured Data. International Standard ISO-8608:1995, 30 p, 1995.

[20] Silva, J.G.S., Roehl, J.L.P. Probabilistic Formulation for the Analysis of Highway Bridge Decks with Irregular pavement Surface, Journal of the Brazilian Society of Mechanical Sciences (ABCM), Vol. XXI, nº 3, Brazil, pp. 433-445, 1999.

[21] Andrén, P. Power spectral density approximations of longitudinal road profiles Journal: International Journal of Vehicle Design, Vol. 40, nº.1/2/3, pp. 2-14, 2006.

[22] Andersson, P.B.U. Time domain contact model for tyre/road interaction including non-linear contact stiffness due to small-scale roughness. Journal of Sound and Vibration, Vol. 318, Issue 1-2, pp. 296-312, 2008.

[23] Newland, D. E. An introduction to random vibrations and spectral analysis. 2nd Edition, Longman Scientific & Technical, New York, 377 p, 1984.

[24] Namur, E.; de Solminihac, H. Roughness of Unpaved Roads Estimation and Use as an Intervention Threshold. Transportation Research Record, Issue 2101, pp. 10-16, 2009.

[25] Martin, T.C. Experimental Estimation of the Relative Deterioration of Surface Maintenance Treatments. Journal of Transportation Engineering. Vol. 136, nº 1, pp. 1-10, 2010.

[26] Bogsjo, K. Coherence of road roughness in left and right wheel-path". Vehicle System Dynamics, Vol. 46, Supplement S, pp. 599-609, 2008.

[27] ISO 2631 - International Organisation for Standardisation. Guide for evaluation of human exposure to whole-body vibration. International Standard ISO-2631:1978, 40 p., 1978.

[28] Yousefzadeh M., Azadi S., Soltani, A. (2010) Road profile estimation using neural network algorithm, Journal of Mechanical Science and Technology, Vol. 24 (3) pp. 743~754.

[29] Aknin, P. (1995) Outils de description de la géométrie des voies et déconvolution des relevés expérimentaux, Rapport nº 204 LTN-INRETS, 76 p., France.

8.5 ANEXO E

VEHICLE DYNAMIC RESPONSE DUE TO PAVEMENT ROUGHNESS

Barbosa, R. S. (2011A) Vehicle Dynamic Response Due to Pavement Roughness. Journal of the Brazilian Society of Mechenical Science & Engineering – ABCM. Vol. XXXIII, nº 3, pp. 302-307.

Roberto Spinola Barbosa
Member, ABCM
spinola@usp.br
University of São Paulo
Polytechnic School
Mechanical Engineering Department
São Paulo, SP, Brazil

Vehicle Dynamic Response Due to Pavement Roughness

The goal of the present study is the development of a spectral method to obtain the frequency response of the half-vehicle subjected to a measured pavement roughness in the frequency domain. For this purpose, a half-vehicle dynamic model with a two-point delayed base excitation was developed to correlate with the spectral density function of the pavement roughness, to obtain the system spectral transfer function, in the frequency domain. The vertical pavement profile was measured along two roads sections. The surface roughness was here expressed in terms of the spectral density function of the measured vertical pavement profile with respect to the evenness wave number of the pavement roughness. A frequency response analysis was applied to obtain the vertical and angular modal vehicle dynamic response with the excitation of the power spectral density (PSD) of the pavement roughness. The results show that at low speed, the vehicle suspension mode is magnified due to the unpaved track signature. At 120 km/h in an undulated asphalted road, the first vehicle vibration mode has a significant motion amplification, which may cause passenger discomfort.
Keywords: *vehicle, dynamic, pavement, roughness, random*

Introduction

In general, during the vehicle project and design development phase, the automotive industry utilizes a combination of design tools such as vehicle modal response from numerical simulation (Costa, 1992), laboratory tests with shaker rigs (Boggs, 2009) and the results of experimental field road tests, to fine tune vehicle suspension (Vilela and Tamai, 2005). Despite the efficiency of the numerical simulations, laboratory and experimental tests are still in use, even though being time-consuming, expensive and limited to the specific road conditions of the test track. Quarter car vehicle model with single random input is traditionally used for spectral studies (Barbosa, 2001; Sun, 1998; Cebon, 1999; Silva, 1999). The complete vehicle model is employed for modal and control purpose (Vilela, 2010; Costa 1992). The motivation of the present work is to extend the power of the analytic tools for the design of vehicle suspension with the application of the frequency domain response technique to deal with random input of the pavement roughness. One of the contributions of the present study is the development of a half-vehicle model with delayed two-point base excitation correlated with the spectral density function of a measured pavement roughness, in order to generate the system spectral transfer function in the frequency domain. The vertical pavement profile was measured along two roads sections. The surface roughness is expressed with the spectral density function of the measured vertical pavement profile with respect to the evenness wave number of the pavement roughness. This method allows the identification of the vehicle dynamic response due to the normalized roughness density distribution (or a measured pavement roughness) to address the passenger comfort and vehicle safety due to the pavement/tyre contact load.

Vehicle Modeling

The dynamic vehicle behaviour was accomplished with the traditional half-car vehicle representation (Sun, 2007). The four-degree of freedom lumped parameter model describing relevant motion was adopted as shown at Fig. 1. The vehicle body is free to move vertically in the z_3 direction and to acquire an angular motion θ associated with mass m_3 and moment of inertia J_G, respectively. The front and rear suspension connections are described by spring-damper properties (k_f, c_f, k_r and c_r). Here m_1 and m_2 are the vehicle unsprung mass with the correspondent tyre stiffness and damping are described by k_1, c_1, k_2 and c_2 values. The model is excited by the road evenness $u_1(t)$ and $u_2(t)$, which induces out-of-phase front and rear suspension movements, respectively, with a time delay.

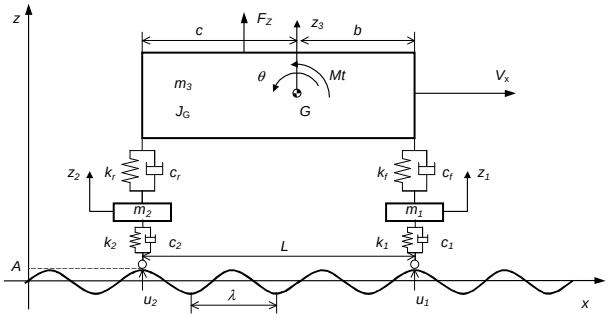

Figure 1. Half-car model.

The equations of motion are obtained using the *Lagrange* method applied to the lumped rigid bodies. The kinetic, potential and the generalized energy dissipation functions are respectively given by the following equations:

$$T = \frac{1}{2} m_3 \dot{z}_3^2 + \frac{1}{2} J_G \dot{\theta}^2 + \frac{1}{2} m_1 \dot{z}_1^2 + \frac{1}{2} m_2 \dot{z}_2^2 , \tag{1}$$

$$V = \frac{1}{2} k_{\mathrm{f}} (z_3 + b\theta - z_{\mathrm{f}} - l_{\mathrm{f}0})^2 + \frac{1}{2} k_{\mathrm{r}} (z_3 - b\theta - z_{\mathrm{r}} - l_{\mathrm{r}0})^2 + \frac{1}{2} k_1 (z_1 - u_1 - l_{10})^2 + \frac{1}{2} k_2 (z_2 - u_2 - l_{20})^2 , \tag{2}$$

$$R = \frac{1}{2} c_{\mathrm{f}} (\dot{z}_3 + b\dot{\theta} - \dot{z}_{\mathrm{f}})^2 + \frac{1}{2} c_{\mathrm{r}} (\dot{z}_3 - \dot{b}\theta - \dot{z}_{\mathrm{r}})^2 + \frac{1}{2} c_1 (\dot{z}_1 - \dot{u}_1)^2 + \frac{1}{2} c_2 (\dot{z}_2 - \dot{u}_2)^2 \tag{3}$$

Substituting the partial derivatives of the above equations to the *Lagrange* expression given by

Paper received 6 August 2009. Paper accepted 29 January 2011.
Technical Editor: Domingos Rade

$$\frac{d}{dt}\left(\frac{\partial T}{\partial \dot{q}_i}\right)-\frac{\partial T}{\partial q_i}+\frac{\partial V}{\partial q_i}+\frac{\partial R}{\partial \dot{q}_i}=Q_i \tag{4}$$

one obtains the following four differential equations:

$$m_1\ddot{z}_1+c_1(\dot{z}_1-\dot{u}_1)+k_1(z_1-u_1)- c_f(\dot{z}_3-b\dot{\theta}-\dot{z}_1)-k_f(z_3-b\theta-z_1)=0 \tag{5}$$

$$m_2\ddot{z}_2+c_2(\dot{z}_2-\dot{u}_2)+k_2(z_2-u_2)- c_r(\dot{z}_3-c\dot{\theta}-\dot{z}_2)-k_r(z_3-c\theta-z_2)=0 \tag{6}$$

$$m_3\ddot{z}_3+c_f(\dot{z}_3+b\dot{\theta}-\dot{z}_1)+k_f(z_3+b\theta-z_1)+ c_r(\dot{z}_3-c\dot{\theta}-\dot{z}_2)+k_r(z_3-c\theta-z_2)=F_Z \tag{7}$$

$$J_z\ddot{\theta}+bc_f(\dot{z}_3+b\dot{\theta}-\dot{z}_1)+bk_f(z_3+b\theta-z_1)+ cc_r(\dot{z}_3-c\dot{\theta}-\dot{z}_2)+ck_r(z_3-c\theta-z_2)=Mt \tag{8}$$

Table 1 shows the adopted values for the vehicle inertia, suspension elasticity and dissipation. These values are typical of a medium sized passenger car (Barbosa, 2001).

Table 1. Half-car properties.

Element/Charac.	Vehicle Body	Suspension	Hub/Tyre[A]
Mass	750 kg	-----	30 kg
Inertia moment	360 kg m^2	----	----
Rigidity[B]	-----	18.25 kN/m	150 kN/m
Damping	-----	912.5 Ns/m	----

Obs.: [A] individual properties; [B] rigidity depends on the tyre pressure.

The modal system properties are described by four coupled vibration modes due to the non-diagonal constitution of the system matrix. The vehicle modal response has four natural damped frequencies around 1.0~2.0 and 12 Hz, respectively. For the body modes (front and rear end bounce), as shown in Fig. 2, damping factors are 0.14 and 0.26, respectively, as presented in Table 2. For the suspension modes, associated with the unsprung mass of hub and tyre elasticity, damping factors are around 0.21 as presented in Table 3.

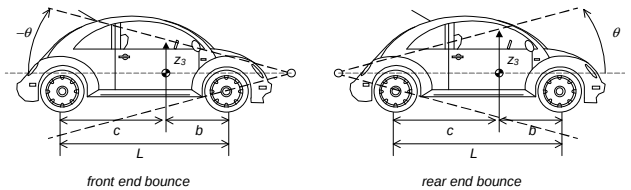

Figure 2. Vehicle coupled modes (front and rear end bounce).

It should be noted that the suspension frequency is about one decade above those from the vehicle modes.

The normalized modal Eigen-vectors obtained from the dynamic matrix are shown in the following tables.

Table 2. Vehicle modal properties.

Mode Number	Mode 1 – vehicle front end bounce		Mode 2 – vehicle rear end bounce	
Damped Natural Freq	1.03 Hz		1.88 Hz	
Damping Factor	0.144		0.261	
D. Freedom	Mag.	Phase	Mag.	Phase
z_1	0.0000	-305.87°	0.0000	-307.44°
z_2	0.0002	-203.91°	0.0002	-204.96°
z_3	0.0134	-101.95°	1.0000	0.00°
θ	1.0000	0.00°	0.0136	-102.48°

Table 3. Suspension modal properties.

Mode Number	Mode 3 – in phase wheel/hub		Mode 4 – out of phase wheel/hub	
Damped Natural Freq	11.72 Hz		11.86 Hz	
Damping Factor	0.216		0.207	
D. Freedom	Mag.	Phase	Mag.	Phase
z_1	0.0842	-105.13°	0.9880	180.00°
z_2	0.9964	0.00°	0.1523	81.712°
z_3	0.0006	-315.41°	0.0235	-16.576°
θ	0.0842	-201.27°	0.0036	-114.86°

By taking the *Laplace* transform of the system equations and assuming zero initial conditions (Felício, 2007), one obtains the four following equations:

$$\begin{aligned}
&[m_1s^2+(c_1+c_f)s+(k_1+k_f)]Z_1(s)-(c_fs+k_f)Z_3(s)+(bc_fs+bk_f)\Theta(s)=(c_1s+k_1)U_1(s),\\
&[m_2s^2+(c_2+c_r)s+(k_2+k_r)]Z_1(s)-(c_rs+k_r)Z_3(s)+(cc_rs+ck_r)\Theta(s)=(c_2s+k_2)U_2(s),\\
&[m_3s^2+(c_f+c_r)s+(k_f+k_r)]Z_3(s)-(c_fs+k_f)Z_1(s)-(c_rs+k_r)Z_2(s)+[(bc_f-cc_r)s+(bk_f-ck_r)]\Theta(s)=F_z,\\
&[J_Gs^2+(b^2c_f-c^2c_r)s+(b^2k_f-c^2k_r)]\Theta(s)-b(c_fs+k_f)Z_1(s)-c(c_rs+k_r)Z_2(s)+c(c_rs+k_r)Z_3(s)=Mt
\end{aligned} \tag{9}$$

One of the contributions of the present work is the introduction of the delayed out-of-phase inputs into the vehicle front and rear wheels. Considering that the rear wheel runs on the same track right after the front wheel, the surface elevation that produces the vehicle vertical suspension displacement is given by the same function which describes the excitation of the front wheel delayed in time. Taking a harmonic function $u_1(t)$ as the imposed vertical displacement of the front wheel, then the rear wheel delayed input $u_2(t)$ can be expressed as:

$$u_2(t)=u(t-T), \quad \text{where} \quad u_1(t)=u(t)=A\sin(\omega t) \tag{10}$$

In the above equation ω is the angular frequency given by $\omega=2\pi V_x/\lambda$ and T is the time delay given by $T=L/V_x$, where L the inter-axis distance, V_x is the vehicle speed and λ is the wavelength, (see Fig. 1).

The Laplace transformation of the front wheel and the rear wheel input functions, considering the transformation of the delayed function are respectively given by:

$$U_1(s) = \mathcal{L}[u_1(t)] \quad \text{and} \quad U_2(s) = \mathcal{L}[u_2(t)]$$
$$\text{where} \quad U_1(s) = U(s) \quad \text{and} \quad U_2(s) = U(s)e^{-Ts} \tag{11}$$

Upon the substitution of U(s) into Eq. (11) and the elimination of Z_1 and Z_2 from these two equations, and after some algebraic manipulation to get the vertical and angular motions of the vehicle body over displacement excitation U(s) relationship, the following transfer functions for the vertical and angular displacements can be obtained:

$$\frac{Z_3(s)}{U(s)} = H_z(s) \qquad \text{and} \qquad \frac{\Theta(s)}{U(s)} = H_\Theta(s) \tag{12}$$

The displacement frequency response function (*FRF*) is known as receptance $H(s)$. However, considering a periodic input, there is a simple relationship between acceleration and displacement, since $\ddot{u}(t) = -A\omega^2 sin(\omega t)$. The acceleration frequency response function known as inertance $I(s)$ can be obtained. Analyzing the system vertical and angular forced movements in the frequency domain response, replacing s with (iω) and assuming the vehicle properties presented in Table 1, the frequency response inertance function I(iω) can be obtained as:

$$I_{\ddot{z}_3}(i\omega) = \omega^2 H_{z_3}(i\omega) \quad \text{and} \quad I_{\ddot{\Theta}}(i\omega) = \omega^2 H_\Theta(i\omega) \tag{13}$$

The vertical (I_{z_3}) and angular (I_θ) vehicle modal transfer function depends on T that is a speed function ($T = L/V_x$). The inertance function for the coupled vertical and angular vehicle body motions is shown in Fig. 3. Therefore, the *FRF* shape will be speed-dependent as can be observed in Fig. 3 for 25.6 km/h (7.1 m/s) and Fig. 4 for 120 km/h (33.3 m/s). In both cases, L = 2.4 *m*.

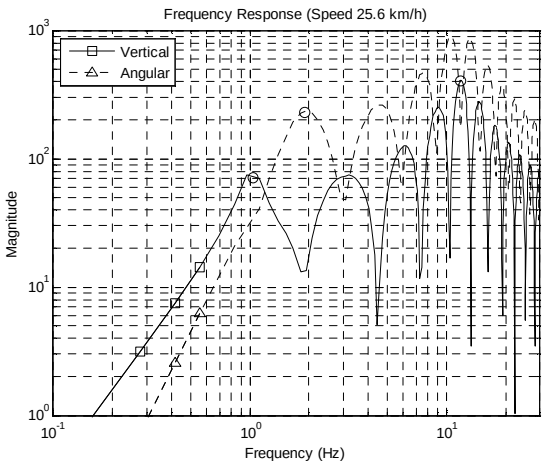

Figure 3. Vehicle inertance frequency response at 25.6 km/h (m³).

Humps can be noticed in the *PSD* curve shown in Fig. 3 due to the inter-axle distance L (2.4 meters) at a vehicle speed of 25.6 km/h (7.1 m/s). For the vertical mode, these humps occur at every integer, resulting in peaks at around 1, 3, 6, 9 Hz. The modal frequencies are identified with a circle in the figure (front end bounce at 1.03 Hz, rear end bounce at 1.88 Hz, wheel at 11.7 Hz). For the angular mode, the peaks occur at 13.9, 27.8 Hz etc. (see Fig. 4).

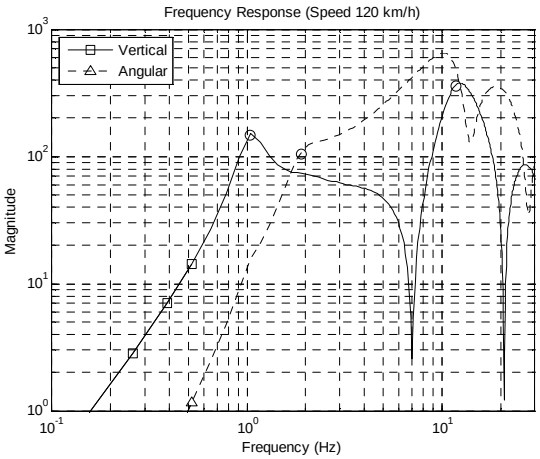

Figure 4. Vehicle inertance frequency response at 120 km/h (m³).

It should be pointed out that for a speed of 86 km/h (24 m/s) and an inter-axle distance of 2.4 m, T is equal to 0.1 and, therefore, the next vertical hump is one decade above the frequency of the first mode.

Pavement Roughness Measurement

Two sections of road surface irregularities were actually measured in the present work. The first section was a 1.4 km long road of rustic soil covered with gravel (unpaved road). The second section was a 2.0 km long of asphalted road of high quality. The pavement roughness was measured with the 3-point-middle-chord measuring device. This system is composed of three wheels and a displacement sensor. The two external wheels are steered and the central one is articulated with regard to the others. A conventional car pulls the measuring system along the road measuring the track evenness. The central wheel vertical motion is sampled every centimeter by an analogic to digital sample board installed in a portable computer. The data acquired are stored in magnetic media for post processing purposes (Pavimetro, 2009).

The measured data are treated with the device system transfer function, to obtain the topographic vertical elevation of the road surface roughness, as shown in Fig. 5 for the unpaved road. In this case, ten points per meter were sampled (one sample at every 0.1 meter). Wavelengths up to 200 m were considered.

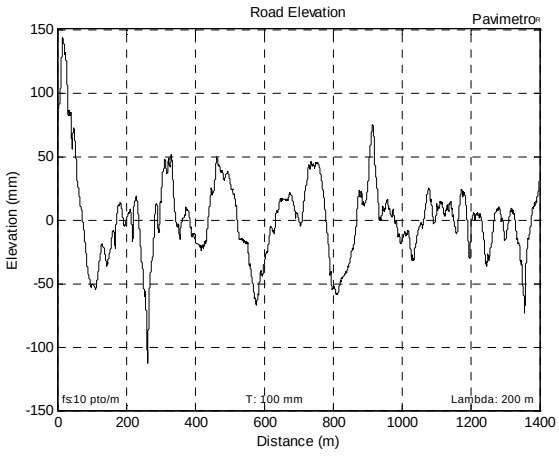

Figure 5. Road elevation (unpaved).

The results for the vertical elevation of the road surface roughness for the asphalted road are shown in Fig. 6. In this case, two points per meter were sampled. Wavelengths up to 500 m were considered in the anti-aliasing processes. The result for the asphalted road evenness is statistically represented by the roughness index unit (International Roughness Index – *IRI*). The mean *IRI* value for this road section is 1.92, classified as level A by the *ISO* criteria.

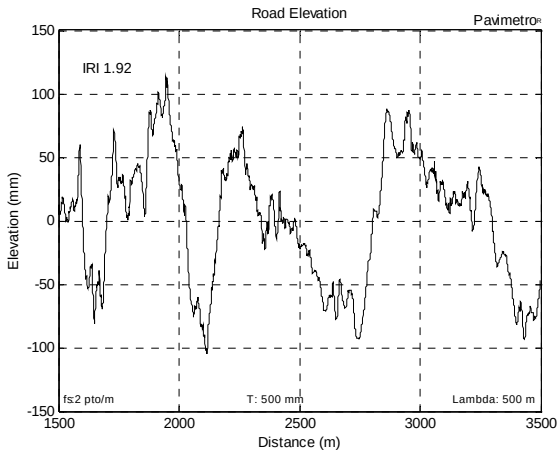

Figure 6. Highway elevation (asphalt).

The data treatment was performed up to 2048 points at a sample rate down to 10-2 m. This range allows analyzing wavelengths as long as 100 m and down to 0.2 m. This wide range is unprecedented in this area considering that traditional measuring devices have a restricted observable band.

The unpaved and the asphalted track elevation measurements were further treated to generate distributions wavelengths of the periodic irregularities. The spectral density function (*PSD*) in the range of wavelength between 0.1 to 10 m of the unpaved road vertical elevations is presented in Fig. 7. This measured road section spectrum has its particular signature with intensified wavelength content between 0.4 and 0.9 m.

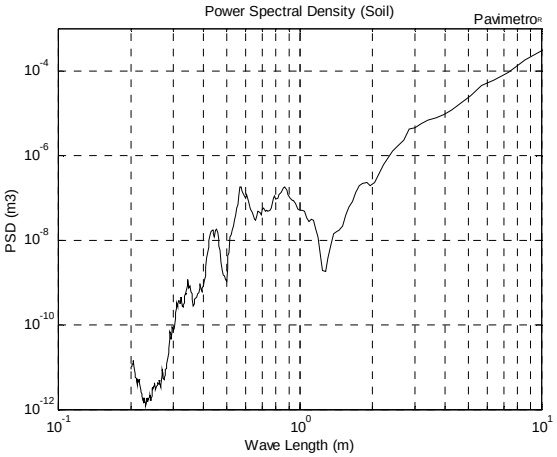

Figure 7. PSD of the unpaved track.

The spectral density function of wavelength between 1 and 100 meters of the asphalted vertical elevation road is presented in Fig. 8, where the levels of road roughness intensity are also presented. The spectrum of this road section has its intensified wavelength content between 30 and 40 meters.

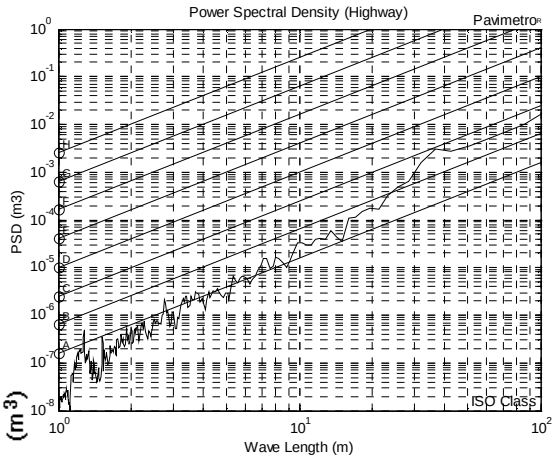

Figure 8. PSD of the asphalt pavement.

These measured spectra of vertical elevation of road surface roughness will be used to calculate the vehicle vertical and angular spectral responses. The intensity of the measured pavement roughness is classified, according to the magnitude of the power spectral pattern of the irregularities in an exponential fashion with a particular slope (*ISO* international standard, 1995). Displacement power spectral density (*PSD*) for a road roughness class is obtained by a logarithm expression in units of m^3:

$$Sd(n) = Sd(n_o) \cdot (n / n_o)^{\varpi} \tag{14}$$

where the slope in the log-log curve ϖ is fixed at –2 (40 dB per decade). The spatial frequency dependence term *Sd* at n_o is obtained from:

$$Sd(n_o) = 4^{cn+1.0} \tag{15}$$

where *cn* is the class number varying from 1 to 8 (from *A* to *H* for different classes of roads, according to *ISO*). The +1.0 exponent in Eq. (15) applies for the mean geometric roughness for n_o at 0.1 cycle/m, as shown in Table 4. It should be pointed out that the high quality of the asphalted road section measured is classified as *ISO* class *A*, with a $Sd_{(n)}$ wave-length value of 1 meter, given a 16×10^{-8} m^3 for the geometric mean and a *IRI* (International Roughness Index) of 1.92. These values were used as vehicle excitation in the frequency domain.

Table 4. Road Class Roughness.

Class number (cn)	Road Class	$Sd_{(n=1)}$ [A] ($\times 10^{-6}$ m^3)	$S_{RMS(n=1)}$ [B] ($\times 10^{-3}$ m)	$S_{RMS(n=1)}$ (mm)
1	A	0.16	0.4	0.4
2	B	0.64	0.8	0.8
3	C	2.56	1.6	1.6
4	D	10.24	3.2	3.2
5	E	40.96	6.4	6.4
6	F	163.84	12.8	12.8
7	G	655.36	25.6	25.6
8	H	2621.44	51.2	51.2

Ob.: [A]: Geometric Mean; [B]: rms value; n = 1 meter, from *ISO* 8608.

Considering the pavement irregularities as an ergodic stationary random process, described by the normal distribution, the evenness density can be expressed by the roughness root mean

square value (rms-value). According to the Perseval's theorem (Oppenheim, 1975), the rms-value of a normally distributed random vertical displacement roughness is equal to the square root of the power spectral density. Therefore, by taking the square root of the previous expression, one gets:

$$S_{RMS}(n) = \sqrt{Sd(n)} = Sd(n_o)^{1/2} \cdot (n/n_o)^{\theta} \tag{16}$$

where the logarithm slope θ changes to –1, which is half of the inclination of *Sd* (ϖ) (20 dB per decade).

Vehicle/Road Interaction

The vehicle natural behavior is expressed by its frequency domain response function (Barbosa, 1998). The pavement irregularities are expressed by its spatial frequency (1/space). In the present analysis, the road pavement is considered a rigid surface. The relationship between time frequency ω and the spatial frequency *n* is the vehicle speed *V*, simply given by:

$$\omega = V \cdot n \tag{17}$$

where ω is frequency in Hertz, $n = 1/\lambda$ is the inverse of the wavelength in meter and *V* vehicle speed in meters per second. By transforming *S*(*n*) into the frequency domain, one gets:

$$S(\omega) = S(n_o) \cdot (\omega/\omega_o)^{\theta} \tag{18}$$

According to the theory of stochastic process, the output of a linear time-invariant system is a stationary random process if the input is also a stationary random process. In most cases, the pavement roughness could be described as a zero mean Gaussian ergodic random process (Newland, 1984). Hence, the response of the half-car system is also a zero mean Gaussian stationary random process. The relationship between the *PSD* of the system response *H*(ω) and the *PSD* of the system excitation *S*(ω) is expressed by:

$$G_{z_3}(\omega) = \left|H_{z_3}(\omega)\right|^2 S(\omega) \quad \text{and} \quad G_{\theta}(\omega) = \left|H_{\theta}(\omega)\right|^2 S(\omega) \tag{19}$$

where $Gz_3(\omega)$ and $G_\theta(\omega)$ are the power spectral densities of the vehicle vertical displacement responses and the angular response of the sprung mass, respectively.

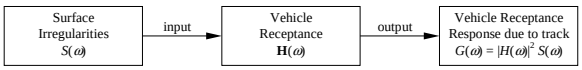

Figure 9. Block diagram function.

Applying this transformation to the vehicle inertance function $I_{z_3}(\omega)$ and $I_{\theta}(\omega)$, the following expressions can be obtained:

$$GI_{\ddot{z}_3}(\omega) = \left|\omega^2 I_{\ddot{z}_3}(\omega)\right|^2 S(\omega) \text{ and } GI_{\theta}(\omega) = \left|\omega^2 I_{\theta}(\omega)\right|^2 S(\omega) \tag{20}$$

The magnitude of the density function of the vertical and angular accelerations of the vehicle riding on the unpaved track at 25 km/h (7 m/s), is shown in Figure 10. It can observed in this figure that the most severe wavelength content of the unpaved track section, which is between 0.4 and 0.9 meters, coincides with the suspension natural frequency range. This effect magnifies the expected acceleration proneness around 12 Hz, which may cause discomfort to passenger.

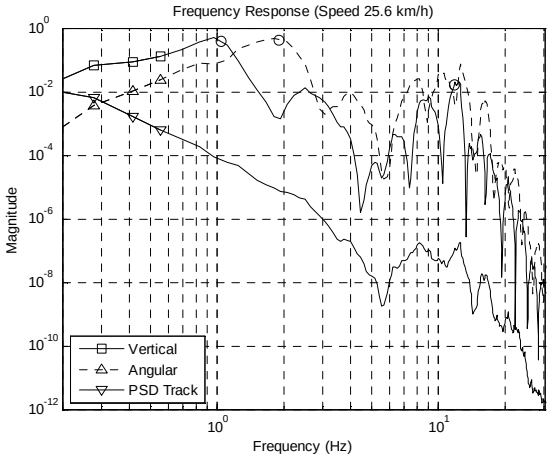

Figure 10. Vehicle inertance function to unpaved track (m³).

Figure 11 shows the magnitude of the density function of the vertical and angular acceleration of the vehicle riding at 120 km/h on the asphalted road.

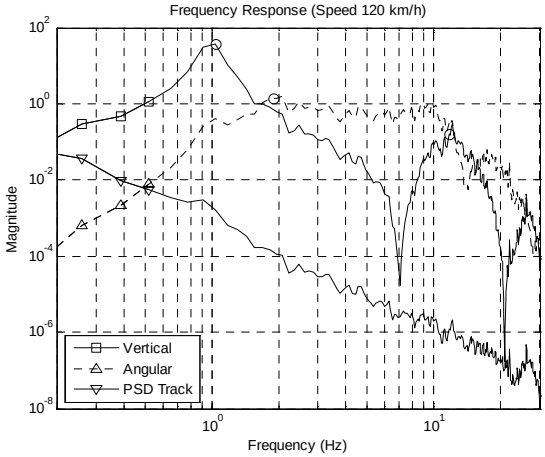

Figure 11. Vehicle inertance function in asphalt road at 120 km/h (m³).

A vehicle will be very susceptive to pavement roughness with wavelength content in the range about 2.85 and 34 m ($\lambda = V/\omega$) whenever traveling at 120 km/h, which will be detrimental to the vehicle performance. Therefore, vehicle suspension tuning process can be optimized against vibrations and a specialized maintenance intervention can produce the best cost/benefit ratio between comfort and the amount of work.

Summary and Conclusions

A methodology was presented to evaluate vehicle/rough-road dynamic interaction. This methodology is based on the modal vehicle frequency response function and the statistical description of the geometry of the rough. Firstly, a half-vehicle dynamic model with a two-point delayed base excitation was derived. Secondly, two-road sections surface elevations were measured with a special referenced measuring device. The vehicle inertance function was then obtained.

The inertance function is related to the passenger comfort and can be used for design purposes. The vertical and angular vehicle body transfer functions were calculated with the surface frequency irregularities function in the frequency domain as input.

The first measured road was a 1.4 km long section of an unpaved track and the second was a 2.0 km long section of good quality asphalted road. The geometrical data collected was then processed to obtain a special broadband distribution (with wavelengths between 100 m and 0.2 m) in terms of periodic roughness wavelengths. The wide range of wavelengths thus obtained is unprecedented, considering that the traditional measuring devices have a restricted observable band. The measured asphalted road section has an IRI of 1.92 and can be classified according to ISO criteria as level A. The measured unpaved road section has a spectral signature distribution with concentration between 0.4 and 0.9 m.

A two out-of-phase delayed vehicle inputs was considered corresponding to the front and rear wheel positions, by applying the measured track roughness density functions. The inertance function was obtained for the vertical and angular vehicle body motions. Considering the low speed (25.6 km/h), the vehicle suspension mode is magnified due to the unpaved track signature. In the asphalted track, at high speed (120 km/h), the first vehicle vibration mode has a significant motion amplification, which may cause discomfort to passenger.

The developed methodologies extend the efficiency of vehicle numerical simulation tools, with the power of providing vehicle frequency response analysis due to the pavement roughness statistically described. Results allow the evaluation of passenger discomfort.

A more complex model to address vehicle-pavement interaction can be derived based on a simple four degree of freedom system considered by the present study. Bus, trucks, lorries, complete vehicles and other complex suspension types will be investigated in future researches. For these cases, a two-dimensional pavement auto-correlation roughness function will be necessary. Also, the human comfort behavior according to ISO 2631 may be included in this analysis for the complete cycle of vibration propagation.

Acknowledgements

The author would like to thank the valuable contribution of Professor Edilson Tamai and Marcelo Batista. The author wishes to acknowledge the support to this research provided by the Mechanical Engineering Department of the Polytechnic School – University of São Paulo.

References

Barbosa, R.S., 1998, "Interação Veículo/Pavimento, Conforto e Segurança Veicular", 31ª Reunião Anual de Pavimentação, Associação Brasileira de Pavimentos – ABPv. Vol. 2, São Paulo, Brazil, pp. 1164-1182.

Barbosa, R.S., 1999, "Aplicação de Sistemas Multicorpos na Dinâmica de Veículos Guiados". PhD. Theses. Universidade de São Paulo (USP), São Paulo, Brazil, 273 p.

Barbosa, R.S. and Costa, A., 2001, "Safety Vehicle Traffic Speed Limit", IX International Symposium on Dynamic Problems of Mechanics, IX DINAME, Associação Brasileira de Ciências Mecânicas – ABCM, Florianópolis, Santa Catarina, Brazil.

Boggs, C., Southward, S. and Ahmadian, M., 2009, "Application of System Identification for Efficient Suspension Tuning in High-Performance Vehicles: Full-Car Model Study", SAE Document Number: 2009-01-0433 in the Book Tire and Wheel Technology and Vehicle Dynamics and Simulation, Product Code: SP-2221, 434 p.

Cebon, D., 1999, "Hand Book of Vehicle-Road Interaction", Swets & Zeitlinger Publishers, Netherlands, 589 p.

Costa, A. 1992, "Application of Multibody Systems (MBS) Modeling Techniques to Automotive Vehicle Chassis Simulation for Motion Control Studies", Doctor of Philosophy in Engineering, University of Warwick, England.

Felício, L.C., 2007 "Modelagem da Dinâmica de Sistemas e Estudo da Resposta", Editora Rima, São Carlos, São Paulo, Brazil, 551 p.

ISO 8606 – International Organization for Standardization, 1995, "Mechanical Vibration Road Surface Profiles - Reporting of Measured Data", International Standard ISO-8608:1995, 30 p.

Newland, D.E., 1984, "An introduction to random vibrations and spectral analysis", 2nd Edition, Longman Scientific & Technical, New York, 377 p.

Oppenheim, A.V., Schafer, R.W., 1975, "Digital Signal Processing", Prentice-Hall Publishers, 556 p.

Pavimetro, 2009, "The Pavement Roughness Measuring System", site: www.pavimetro.com.br, internet inquiry on may 2009.

Sun, L., Deng, X., 1998, "Predicting Vertical Dynamic Loads Caused by Vehicle-Pavement Interactions", *Journal of Transportation Engineering*, Vol. 124, No. 5, pp. 470-478.

Sun, L., Luo, F., 2007, "Nonstationary Dynamic Pavement Loads Generated by Vehicles Traveling at Varying Speed", *Journal of Transportation Engineering © ASCE*, Vol. 133, pp. 252-263.

Silva, J.G.S., Roehl, J.L.P., 1999, "Probabilistic Formulation for the Analysis of Highway Bridge Decks with Irregular pavement Surface", *Journal of the Brasilian Society of Mechanical Sciences and Engineering* (ABCM), Vol. XXI, No. 3, Brazil, pp. 433-445.

Vilela, D., Tamai, E.H., 2005, "Optimization of Vehicle Suspension Using Robust Engineering Method and Response Surface Methodology", Proceedings of The International Symposium on Dynamic Problems of Mechanics – DINAME. São Paulo, Brazil.

Vilela, D., 2010, "Aplicação de Métodos Numéricos de Otimização ao Problema Conjunto da Dirigibilidade e Conforto Veicular", Tese de Doutorado na Universidade de São Paulo, Brazil, 315 p.

8.6 ANEXO F

VEHICLE DYNAMIC SAFETY IN MEASURED ROUGH PAVEMENT

Barbosa, R. S. (2011B) Vehicle Dynamic Safety in Measured Rough Pavement. Journal of Transportation Engineering, DOI: 10.1061/(ASCE)TE.1943-5436.0000216, Vol.: 137, pp. 305-310.

Vehicle Dynamic Safety in Measured Rough Pavement

Roberto Spinola Barbosa[1]

Abstract: Dynamic vehicle behavior is used to identify safe traffic speed limits. The proposed methodology is based on the vehicle vertical wheel contact force response excited by measured pavement irregularities on the frequency domain. A quarter-car model is used to identify vehicle dynamic behavior. The vertical elevation of an unpaved road surface has been measured. The roughness spectral density is quantified as ISO Level C. Calculations for the vehicle inertance function were derived by using the vertical contact force transfer function weighed by the pavement spectral density roughness function in the frequency domain. The statistical contact load variation is obtained from the vehicle inertance density function integration. The vehicle safety behavior concept is based on its handling ability properties. The ability to generate tangential forces on the wheel/road contact interface is the key to vehicle handling. This ability is related to tire/pavement contact forces. A contribution to establish a traffic safety speed limit is obtained from the likelihood of the loss of driveability. The results show that at speeds faster than 25 km/h the likelihood of tire contact loss is possible when traveling on the measured road type. **DOI: 10.1061/(ASCE)TE.1943-5436.0000216.**

CE Database subject headings: Vehicles; Traffic safety; Pavements; Surface roughness.

Author keywords: Vehicle; Dynamic; Safety; Pavement; Roughness.

Introduction

It is clear for the vehicle driver that faster traveling speeds result in less travel time. It is also proven that safety is inversely related to speed. The road speed limits are established by Traffic Nation Rules. The current criteria for establishing the speed limit is controlled by a wide range of aspects including

- Driver aspects (e.g., handling skill, body response time, attention, concentration, vision acuity, forward visibility, light reflection, danger perception, comfort, fatigue, age, and trip expenditure);
- Vehicle properties (e.g., handling, suspension response, brake performance, window visibility, tire grip, maintenance conditions, and cost);
- Road aspects (e.g., road class, road quality, line number, track segregation, asphalt adhesion, surface condition and contamination, roughness, stagnant water, roadway geometry, sinuosity, signaling structure, horizontal visibility, maintenance conditions, sight distance, crossings, pedestrians, cyclists, and obstructions);
- Weather condition (e.g., lighting, visibility, reflection, clouded, temperature, wind, mist, rain, snow, ice, and leaves);
- Environmental affect (e.g., traffic density, traffic mixture, other moving bodies closeness, fuel consumption, pollution, noise, and road neighbors); and
- Other aspects (e.g., social, cultural, historical, political, heuristic, actual experimental observed speed, road tax, insurance value coverages and bonuses, driver risk acceptance, guesses, and intuitive judgments).

Some of the aspects mentioned in this list can be related to a specific social segment. Vehicle performance is associated with the competence of the automotive industry, the road quality is a public administration responsibility, and driver handling skill is controlled by the federal authority for driver's licenses. Others aspects have a common sense merit and are quantitatively imponderable or uncontrollable (e.g., the weather). Therefore, whatever the methodology used to study this subject, the result will likely produce something diffuse and prolix, poorly reliable nor creditable, rather then a universal, believed rational, scientifically-based recommendation.

According to Hauer,

> ...the evolution of speed over time is poorly documented, and the understanding of what drives the evolution is largely missing. It is known that speeds evolve over time, but not why. Although the prevalent and strongly held belief that the greater the speed, the higher is the probability that accidents will occur is, at present, not well supported by research... (Hauer 2009).According to Mannering,

> ...it has become more common for speed limits to be set for political reasons rather than for safety reasons. As a consequence, the motoring public seems to have increasingly begun questioning the rationality or speed limits. This is evident in observed speed data that show that the majority of drivers routinely exceed posted speed limits. A key motivating factor in drivers' tendency to exceed the speed limit is that they believe that the excess speed does not threaten safety... (Mannering 2009).It can be observed from different writers' opinions that a credible deterministic technical rule, with scientifically proven reliability, is necessary to stake public authority to deal with the subject. Also, according to Elvik, in Norway and Sweden, an optimal speed limit is set to minimize the total costs of transport to society. Travel time, vehicle operating costs, road accidents, traffic noise, and air pollution were considered in the determination of optimal speed limits (Elvik 2002).

[1]Professor and Doctor, Escola Politécnica, Univ. of São Paulo USP, Dynamic & Control Group, Brazil. E-mail: spinola@usp.br

Note. This manuscript was submitted on September 28, 2009; approved on August 30, 2010; published online on September 4, 2010. Discussion period open until October 1, 2011; separate discussions must be submitted for individual papers. This paper is part of the ***Journal of Transportation Engineering***, Vol. 137, No. 5, May 1, 2011. ©ASCE, ISSN 0733-947X/2011/5-305–310/$25.00.

A vehicle's capability to travel properly on different road pavement conditions is a desirable characteristic that is tuned by vehicle design engineering. Robust active suspensions (Wang et al. 2008) and global motion control technology (Costa 1992) are examples of recent developments. Actually, the traffic engineer is able to quantitatively calculate speed limits only for horizontal curves (Baerwald 1976). This is established from the car's centrifugal inertia force balanced with the transversal tire/road force, which is dependent on the curve radius, superelevation, and friction coefficient. However, it is difficult to establish proper values for straight line driving. The driver expects freedom for his own driving style, and prudence recommends safety in vehicle speed.

The motivation of this work is to contribute scientifically to the complex task of identifying vehicle speed limits, concerning the safety aspects of modern highway systems. The proposed methodology to study this subject is the evaluation of vehicle vertical behavior and relating it to superficial pavement irregularities (Barbosa 1998; Silva et al. 1999; Sun et al. 2001; Sun and Luo 2007), based on a dynamic vehicle/road interaction model. Vehicle safety is the ability to handle adequately the vehicle on the road. Handling quality is a vehicle property that allows a driver to accelerate and stop, to curve and corner, in short, to manage vehicle trajectory through fast and heavily trafficked modern highways. Vehicle driveability is directly related to a vehicle's capability of producing tire horizontal forces. For acceleration and deceleration purposes, longitudinal tire force is required. For lateral maneuvers and curve cornering, lateral tire force is needed. These forces however, are limited to the Coulomb's relationship that correlates vertical tire/road contact forces to tangential forces. This relation is expressed by the tire/road friction coefficient. Therefore, what is desirable is the minimum variation of contact forces that allows the largest horizontal force available, for a given friction coefficient.

To this end, a quarter-car vehicle model was derived, and the vertical elevation of an unpaved road surface was measured. As the road profile roughness is unique to each section, a statistic description was used to qualify this random process. Both functions on the frequency domain were used to statistically define the proneness of vehicle handling capability in a function of the traveling speed.

Vehicle Modeling

The model used in this research is the quarter-car vehicle model (Barbosa 1998). The body and suspension's vertical movements are described by the x_1 and x_2 coordinates. The two degrees of freedom lumped vertical model is shown in Fig. 1. Mass m_2 represents the sprung vehicle body with secondary suspension (k_2 and c_2). Mass m_1 corresponds to the primary suspension composed of tire stiffness and damping (k_1 and c_1).

This model is base-excited by pavement irregularities that induce suspension movements. The vehicle motion equations are obtained by applying Newton's second law to masses m_1 and m_2, resulting in the following differential equations:

$$m_1\ddot{x}_1 + c_1(\dot{x}_1 - \dot{u}) + k_1(x_1 - u) - c_2(\dot{x}_2 - \dot{x}_1) - k_2(x_2 - x_1) = F_1 \quad (1)$$

$$m_2\ddot{x}_2 + c_2(\dot{x}_2 - \dot{x}_1) + k_2(x_2 - x_1) = F_2 \quad (2)$$

Various vehicle frequency response functions may be obtained from this traditional model. For the purpose of this research, the vertical contact force is the objective function to be evaluated.

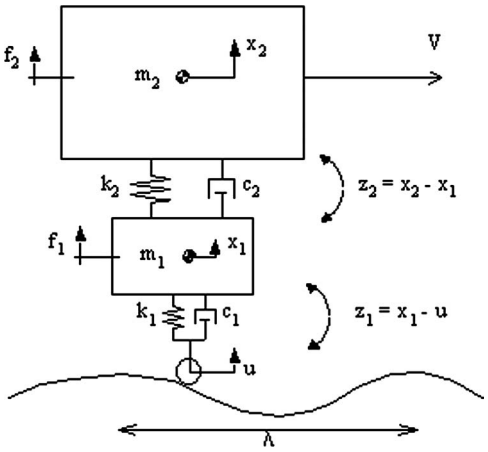

Fig. 1. Quarter-car vehicle model over pavement evenness

The vertical wheel contact force, f_c, between tire and pavement is obtained from the primary suspension deflection and velocity. Considering no external forces acting on the car body and choosing a special pair of coordinates (i.e., $z_1 = x_1 - u$ and $z_2 = x_2 - x_1$), the following can be obtained:

$$m_1(\ddot{z}_1 + \ddot{u}) + c_1\dot{z}_1 + k_1z_1 - c_2\dot{z}_2 - k_2z_2 = 0 \quad (3)$$

$$m_2(\ddot{z}_2 + \ddot{z}_1 + \ddot{u}) + c_2\dot{z}_2 + k_2z_2 = 0 \quad (4)$$

$$c_1\dot{z}_1 + k_1z_1 = fc \quad (5)$$

By taking the Laplace transforms of these differential equations and assuming zero initial conditions, one obtains

$$(m_1s^2 + c_1s + k_1)Z_1(s) - (c_2s + k_2)Z_2(s) = (-m_1s^2)U(s) \quad (6)$$

$$(m_2s^2 + c_2s + k_2)Z_2(s) + (m_2s^2)Z_1(s) = (-m_2s^2)U(s) \quad (7)$$

$$Fc(s) - (c_1s + k_1)Z_1(s) = 0 \quad (8)$$

Eliminating z_1 and z_2 from these equations and after some algebraic manipulation to sort the wheel contact force $Fc(s)$ per displacement excitation $U(s)$ relationship, the vehicle deterministic normalized wheel contact force transfer function, $H(s)$, is obtained

$$\frac{Fc(s)}{U(s)} = \frac{(c_1s + k_1)[(m_2s^2 + c_2s + k_2)(m_1s^2) + (m_2s^2)(c_2s + k_2)]}{[(m_2s^2 + c_2s + k_2)(m_1s^2 + c_1s + k_1) + (m_2s^2)(c_2s + k_2)]} = H(s) \quad (9)$$

The function $H(s)$ has a fifth-order polynomial in the numerator (s^5) and a forth-order denominator (s^4). Analyzing the frequency domain response, replacing s with $i\omega$, and assuming the vehicle properties defined in Table 1, the modal properties are obtained

Table 1. Inertial and Suspension Quarter-Car Characteristics

Characteristics	Vehicle body	Suspension	Proportion (usual)
Mass	375.0 kg	30.0 kg	12% (10 ~ 15%)
Rigidity	18.25 kN/m	146.00 kN/m	8 × (5 ~ 10×)
Damping	1,825 Ns/m	182.50 Ns/m	10%(5 ~ 10%)

Note: Total vehicle normal load N: 4,050 N.

(eigenvalue and eigenvector), and the frequency response curve, $H(\omega)$, normalized by the vehicle normal load, N, can be drawn, as shown in Fig. 2.

The quarter-car model presented in Fig. 1 with two bodies (the vehicle body and the hub/wheel) has a modal behavior with two vibration modes. The first vibration mode occurs when the two bodies moves in the same direction (i.e., the x_1 and x_2 coordinates vary in phase). This vibration mode is associated primarily with large vehicle body movement (a magnitude of the second degree of freedom presented in Table 2 for the first mode). The second vibration mode occurs when the two bodies move in opposite directions (i.e., the system coordinates vary out of phase), which is associated with suspension movements (a large movement of the unsprung mass of the hub and wheel presented in Table 2 for the second mode) (Barbosa 1999; Barbosa and Costa 2001).

The vehicle frequency response function, $H(\omega)$, has two natural damped modes with frequencies 1.1 and 12 Hz, with damping factors of 0.30 and 0.47 for first and second modes, respectively. The normalized eigenvectors obtained from the system matrix, describing the modes proportion and phase angle, are presented in Table 2.

For example, analyzing the wheel contact force transfer function, $H(s)$, presented in Fig. 2 and focusing only into the vehicle's first mode of vibration around 1.1 Hz, a vehicle with a speed of 10 m/s, traveling on a periodic surface with a 10 m wavelength and a 0.01 m amplitude, reveals that the tire contact force will vary $\pm 9\%$ (magnitude of the transfer function $M = 9.5$) around the nominal vertical load. This affects the vehicle's handling properties, reducing its ability to generate guidance tangential forces.

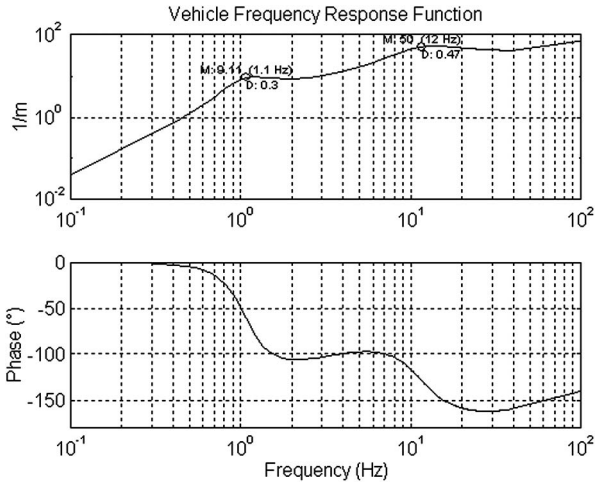

Fig. 2. Vehicle normalized contact force transfer function

Table 2. Modal Eigenvalue and Eigenvector

Vibration mode number	Mode 1 (vehicle)		Mode 2 (wheel/hub)	
Damped natural frequency	1.1 Hz		12.0 Hz	
Damping factor	0.30		0.47	
Degree of freedom	Magnitude	Phase	Magnitude	Phase
x_1	0.1471	−34°	0.9999	0.0°
x_2	0.9999	0.0°	0.0138	−235°

Pavement Roughness Measurements

Road roughness is used as vehicle excitation. An unpaved, 1,400 m long road section of rustic soil pavement with some spread gravel was measured. The surface elevation was measured with a mobile three-point-middle-chord system (Pavimetro Measuring System). This system is composed of a structure and three wheels. The two external wheels are steerable and the central one is movable in relationship to the others. A conventional car pulls the system along the road to measure the track elevation. The central wheel vertical movement is monitored with a precision displacement transducer (LVDT), and elevation is sampled every centimeter. An analog to digital sample board installed in a portable computer acquired the data that are stored in magnetic media for post processing. The vertical unpaved road profile measured is presented in Fig. 3.

The measured roughness data are treated with the measuring system transfer function to obtain the topographic vertical elevation (Pavimetro 2009), as presented in Fig. 3. In this case, 10 points per meter were sampled (i.e., one sample every 0.1 m). A bad roughness shape is shown.

Because road evenness is not a deterministic function (each road section has a different shape) a statistical random process representation was used. The road irregularity described in the space domain was transformed to the frequency domain. The pavement elevation measurements were manipulated to obtain the distribution for the wavelength of periodic irregularities (i.e., an evenness signature). This treatment was performed for 2,048 points at 10^{-2} m intervals. This range allows analyzing the wavelength for 200 m at 0.1 m intervals. The power spectral density function (PSD) between 0.1 and 10 m wavelength of the soil vertical elevation is presented in Fig. 4.

In analyzing the result of the irregularity spectrum distribution, a particular signature was observed with an intensified density magnitude in the wavelength range of 0.5–0.9 m. The spectral density of the measured pavement roughness was equivalent to the ISO quality Level C (ISO 1995) for wavelengths longer than 5 m [2.56×10^{-4} at 10 m wavelength, as shown in Fig. 4].

As discussed by Andrén (2006), the spectral description of surface roughness has a different slope proposition. Despite the ISO standard to qualify pavement roughness with a single slope, in fact, what is really observed in measured pavement roughness

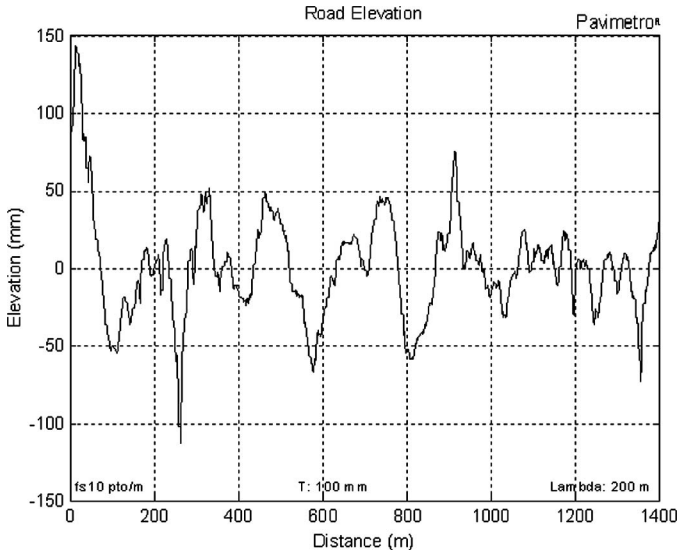

Fig. 3. Surface elevation measurement of the unpaved road

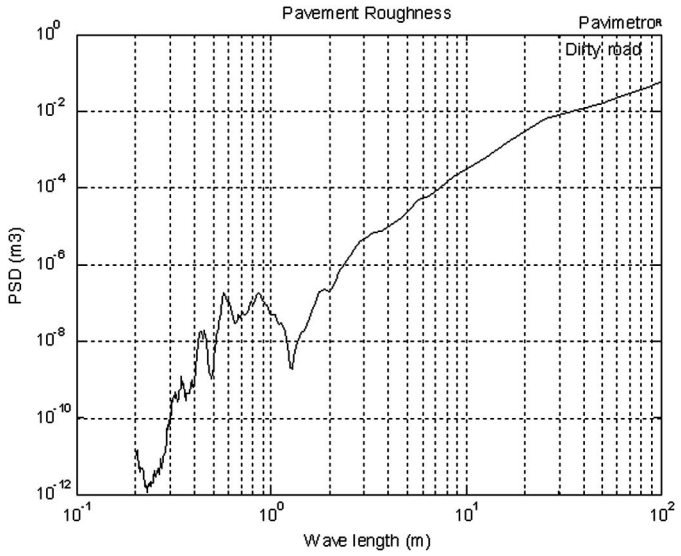

Fig. 4. Power spectral density roughness of the unpaved road

is a content wave number of a density less than 2 dB (decibel) per decade above 0.5×10^1 1/m (or shorter than wavelength 2.0×10^{-1} m) and seems to have two or more slope variations.

Speed Limit Concept

One contribution to establish the safety speed limit can be based on the concept of the loss of vehicle driving abilities. Handling a vehicle is the ability to produce demanded horizontal contact force to control vehicle acceleration and attitude. The maximum tire horizontal contact force is defined by Coulomb's relationship, $F \leq \mu N$. For a small vertical wheel/road contact force, the available tangential guidance force is proportionally affected. The extreme situation is when the wheel/road vertical contact force is null (loss of contact), preventing the possibility of generating tire tangential force. Therefore, the higher and less variable the vertical tire load is, the larger the capacity to generate tangential guidance tire force, ensuring safety.

Vehicle/Road Relationship

To evaluate the vehicle vertical time response attributable to excitation by pavement irregularities, the convolution of the vehicle function with the surface vertical displacement profile can be used (Newland 1984). However, in the frequency domain, the spectral response may be obtained directly only by multiplying the spectrum of the two systems. The resulting function is the inertance magnification of vehicle contact force attributable to spectral pavement roughness. Therefore, considering the vehicle as a time invariant linear system and the pavement roughness as a random input with Gaussian probability distribution, the block diagram presented in Fig. 5 shows function relations in the frequency domain.

Natural vehicle behavior can be expressed as its frequency (1/time) domain function. Pavement irregularities are expressed in spatial frequency (1/space). The relationship between time frequency, ω, and spatial frequency, n, is the vehicle speed, V, simply expressed by

$$\omega = V \cdot n \tag{10}$$

where ω = frequency in hertz; n = spatial frequency in 1/m; and V = vehicle speed in m/s.

Considering pavement irregularity as an ergodic stationary random process (i.e., it has statistical properties obtained from a single, sufficiently long sample) with normal distribution, the evenness density can be expressed through the root mean square (RMS), in units of roughness. According to Perseval's theorem (Oppenheim and Schafer1975), the RMS density of a normally distributed random vertical displacement roughness is the square root of the power spectral density. Transforming $G(n)$ into the frequency domain with the expression 10, the pavement roughness frequency function, $G(\omega)$, is obtained as

$$G(\omega) = V \cdot G(n) \tag{11}$$

Finally, in the frequency domain, the vehicle vertical contact force density function, $I(\omega)$, is obtained from the squared vehicle inertance function weighed by the pavement roughness spectrum (Felício 2007)

$$I(\omega) = |H(\omega)|^2 G(\omega) \tag{12}$$

The results for the inertance function at 25 km/h are presented in Fig. 6.

The pavement roughness spectral density function has been extended at a rate of 5 dB/decade after the maximum acquisition wave number just for length compliance purposes.

The tire/pavement contact force function reveals system characteristics. Considering pavement irregularities as a broadband signal, all vehicle frequencies may be excited at different speeds. Restricting ourselves only to the human perception frequencies range (between 0.1 and 100 Hz), the amplification contact load may be obtained at a given speed. Considering that the input has a Gaussian

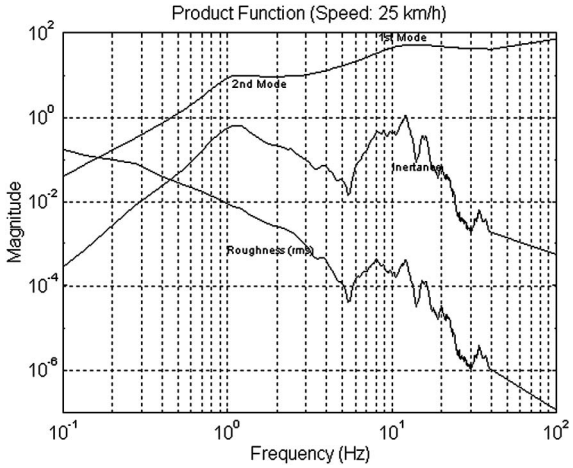

Fig. 6. Inertance function

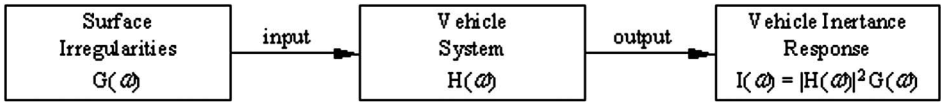

Fig. 5. Flow block diagram

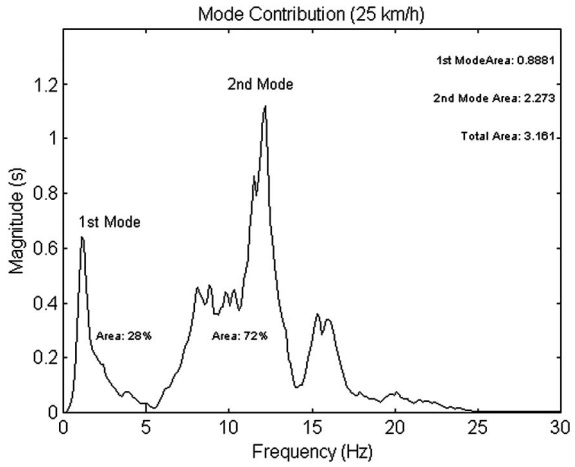

Fig. 7. Mode contribution of the inertance function at 25 km/h

probability distribution (Newland 1984), the density function, $I(\omega)$, can be integrated over all the selected frequency ranges for a given speed, resulting in the contact force probability distribution, Fc, expressed by

$$Fc = \left[\int_{\omega_{\min}}^{\omega_{\max}} I_{(\omega)}\right]^{0.5} \tag{13}$$

As an example, Fig. 7 depicts the modal contribution to the product function, $I(\omega)$, for a vehicle traveling at 25 km/h (6.7 m/s). The first mode contribution represented by the area below the curve reaches 28%, whereas the second mode contribution is almost two and a half times larger (72% of the area below the curve). This fact is assigned to the synchronism of the pavement evenness wavelength (between 0.5 and 0.9 m) at this speed and the second mode natural frequency (approximately 12 hertz). The mode separation is settled in this case to 5 Hz.

In evaluating the function $I(\omega)$ for each speed up to 50 km/h (13.8 m/s), the overall magnitude of the function (i.e., the sum) and the contribution of each mode are determined. The probability of the normalized contact force variation [i.e., the area below the $I(\omega)$ function] as a function of the vehicle speed is presented in Fig. 8.

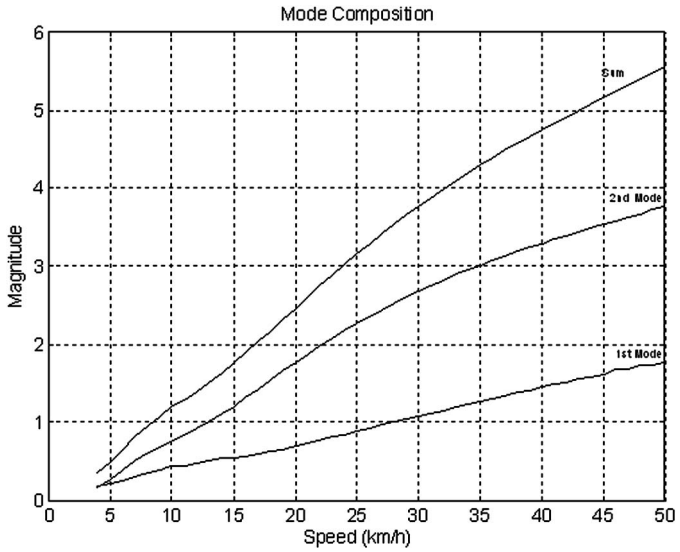

Fig. 8. Vehicle speed and contact force

Considering the measured pavement roughness as a Gaussian process, the likelihood of a wheel to take off with 99.73% confidence (three times the magnitude in the standard deviation scale) is when the vehicle speed is faster than 25 km/h, as shown in Fig. 8. Considering that the loss of vertical contact force is not acceptable (i.e., the magnitude must be less than three) to guarantee the possibility of generating lateral forces (i.e., driveability), and the maximum safe speed limit for this vehicle traveling over this pavement condition is quantified.

Conclusion

In this research, dynamic vehicle behavior and pavement roughness were used to define safety traffic speed limits. The methodology adopted was based on the vehicle vertical wheel contact force frequency response excited by measured pavement irregularities. A quarter-car model was used to identify vehicle dynamic behavior. The vertical elevation of an unpaved road surface was measured. The roughness spectral density was quantified as ISO Level C. Calculations for the vehicle inertance function in the frequency domain with the vertical contact force transfer function were derived with the pavement spectral density roughness function. The statistical contact load variation was obtained from the vehicle inertance density function integration over a frequency range. The vehicle safety behavior concept was based on the ability to generate tangential forces in the wheel/road contact interface. This handling ability was proportional to tire/pavement vertical contact forces. The traffic safety speed limit was obtained from the likelihood of the loss of vehicle driveability. The results showed that faster than 25 km/h the likelihood of contact loss is 99.7% on the measured unpaved road.

Because of vehicle vibration modes, a typical pavement wavelength is harmful for a given traffic speed. This wavelength also makes the worst tire/road load magnification that increases damage to the pavement structure. These irregular wavelength ranges should be minimized or eliminated during pavement maintenance.

The model used restrictions in the analysis of a linear case. A real vehicle suspension has displacement limitations (i.e., it has end stop rubber bushing). This nonlinear characteristic can be incorporated only by using a time integration solution. Additionally, tire diameter, tread size, and internal pressure can soften the contact area, modifying the tire contact length value (typical 0.10 m) and short-wavelength filtering.

A simple two degrees of freedom vertical vehicle model was used for this study. However, on the basis of this methodology, a more detailed model can be employed to access the whole vehicle body movements. Particularly, for vehicle cornering behavior, it would be of interest to access curving speed limits, considering pavement superelevation and irregularities. More than the speed limit indication, this scientific approach may also be useful for the evaluation of passenger comfort, the determination of a vehicle's suspension and structural design, and as a vehicle/road interaction tool to evaluate harmful pavement roughness.

Road irregularities are considered as a single-track patch (i.e., only one tire contact point). Multiple axle/wheel models may be analyzed considering a time delay from the front input of $\Delta t = l/V$ in relation to rear inputs, where l = wheelbase. A complete four wheel independent suspension vehicle model may be employed to access the dynamic behavior provided by a correlation between the irregularities of the left and the right track sides.

Finally, the scientific contribution of this work is the proposition of an objective and quantitative technique to assist the establishment of speed limit on the basis of vehicle/road interaction.

The vehicle dynamic response and the road evenness are analyzed together on the frequency domain, contributing to the identification of safe conditions.

Acknowledgments

The writer would like to thank the Mechanical Engineering Department of the Escola Politécnica da Universidade de São Paulo (EP-USP), for the support to this research.

References

Andrén, P. (2006). "Power spectral density approximations of longitudinal road profiles." *Int. J. Vehicle Des.*, 40(1/2/3), 2–14.

Baerwald, J. E., ed., (1976). *Transportation and traffic engineering handbook*, Institute of Transportation Engineers, Prentice-Hall, Upper Saddle River, NJ, 1080.

Barbosa, R. S. (1998). "Interação veículo/pavimento, conforto e segurança veicular." *Proc., 31a Reunião Anual de Pavimentação, Vol. 2*, Associação Brasileira de Pavimentação (ABPv), Rio de Janeiro, Brazil, 1164–1182 (in Portuguese).

Barbosa, R. S. (1999). "Aplicação de sistemas multicorpos na dinâmica de veículos guiados." Ph.D. thesis, Universidade de São Paulo (USP), Sao Paulo, Brazil, 273 (in Portuguese).

Barbosa, R. S., and Costa, A. (2001). "Safety vehicle traffic speed limit." *Proc., IX Int. Symp. on Dynamic Problems of Mechanics (IX—DINAME)*, Brazilian Society of Mechanical Science (ABCM), Rio de Janeiro, Brazil, 435–443.

Costa, A. (1992). "Application of multibody system (MBS) techniques to automotive vehicle chassis—Simulation for motion control studies, Vol I." Ph.D. thesis, Univ. of Warwick, Warwick, UK, 213.

Elvik, R. (2002). "Optimal speed limits—Limits of optimality models." in Highway safety: Work zones, law enforcement, motorcycles, trucks, older drivers, and pedestrians—Safety and human performance, *Transportation Research Record 1818*, Transportation Research Board, Washington, DC, 32–38.

Felício, L. C. (2007). *Modelagem da dinâmica de sistemas e estudo da resposta*, Editora, Rima, Brazil, 551 (in Portuguese).

Hauer, E. (2009). "Speed and safety." *Transportation Research Record 2103*, Transportation Research Board, Washington, DC, 10–17.

ISO. (1995). "Mechanical vibration road surface profiles—Reporting of measured data." *ISO-8608*, Geneva, 30.

Mannering, F. (2009). "An empirical analysis of driver perceptions of the relationship between speed limits and safety." *Transp. Res. Part F*, 12 (2), 99–106.

Newland, D. E. (1984). *An introduction to random vibrations and spectral analysis*, 2nd Ed., Longman Scientific & Technical, New York, 377.

Oppenheim, A. V., and Schafer, R. W. (1975). *Digital signal processing*, Prentice-Hall, Upper Saddle River, NJ.

Pavimetro. (2009). "Roughness measuring system." ⟨http://www.pavimetro.com.br⟩ (May 25, 2009).

Silva, J. G. S., and Roehl, J. L. P. (1999). "Probabilistic formulation for the analysis of highway bridge decks with irregular pavement surface." *J Braz. Soc. Mech. Sci.*, 21(3), 433–445.

Sun, L., and Luo, F. (2007). "Nonstationary dynamic pavement loads generated by vehicle travelling at varying speed." *J. Transp. Eng.*, 133(4), 252–263.

Sun, L., Zhang, Z., Ruth, J. (2001). "Modelling indirect statistics of surface roughness." *J. Transp. Eng.*, 127(2), 105–111.

Wang, J., Dong, C., Shen, Y., and Wei, J. (2008). "Robust modelling and control of vehicle active suspension with MR damper." *Int. J. Veh. Syst. Dyn.*, 46, Supplement S, 509–520.

8.7 ANEXO G

EXPERIMENTAL INVESTIGATION ON THE DYNAMIC BEHAVIOUR OF A RAILWAY VEHICLE TRAVELLING THROUGH A TURNOUT

Barbosa, R. S.; Santos G. F. M. (2009) Experimental Investigation on the Dynamic Behaviour of a Railway Vehicle Travelling Through a Turnout. International Journal of Heavy Vehicle Systems, DOI: 10.1504/IJHVS.2009.023860, Vol. 16, nº 1-2, pp. 189-206.

Experimental investigation on the dynamic behaviour of a railway vehicle travelling through a turnout

R.S. Barbosa*

Polytechnic School of the University of São Paulo, Brazil
E-mail: spinola@usp.br
*Corresponding author

G.F.M. Santos

Engineer in the Rolling Stock Division of the Companhia Vale do Rio Doce – VALE, Brazil
E-mail: guilherme.fabiano@vale.com

Abstract: Track critical locations with respect to the railway vehicle safety are the passages through the turnouts. The purpose of this investigation is to evaluate the safety of a railway vehicle crossing a turnout. In this study, the topography of a track turnout lay-out has been experimentally measured, and its geometric properties were synthesised. Results show that a constant wavelength vehicle oscillation occurs on the switches in the turnout and that the maximum lateral force at 65 km/h is almost 65% greater than those at low speeds (under 30 km/h).

Keywords: railway; vehicle; dynamic; turnout; safety.

Reference to this paper should be made as follows: Barbosa, R.S. and Santos, G.F.M. (2009) 'Experimental investigation on the dynamic behaviour of a railway vehicle travelling through a turnout', *Int. J. Heavy Vehicle Systems*, Vol. 16, Nos. 1/2, pp.189–206.

Biographical notes: R.S. Barbosa is Professor in the Group of Dynamic and Control of the Mechanical Engineering Department of the Polytechnic School of São Paulo University, Brazil. He worked for 20 years on the Research Institute of Technology of São Paulo in the Transport Division dealing with vibration, comfort and safety on railway vehicles. He received his PhD from the University of São Paulo and DSc from the University of Campinas in São Paulo, Brazil. His research interests are on dynamics of multibody systems, vibration and vehicle dynamics.

G.F.M. Santos is Project Engineer at Rolling Stock Group at Companhia Vale do Rio Doce (CVRD). He received his DSc from the University of Campinas in São Paulo, Brazil.

1 Introduction

Speed and safety are important issues that may affect the efficiency of railway transport systems. Modern railway vehicle tend to increase axle loads and vehicle speed to improve productivity. Higher vehicle speeds may lead to larger dynamic effects that result in increased wearing failures and risks of hazards. According to traffic requirements of the railway system, a double-tracked line is usually provided with a crossing device to allow trains to change lines. The turnout is the device for this purpose. The turnout lay-out is comprised of two successive switches (curves) intercalated with a small straight segment of track. From the vehicle dynamic behaviour point of view, the divergent route of a switch is the geometry responsible for the larger excitations (Andersson and Dahlberg, 1998). In this location, vertical impact forces are observed (Andersson and Dahlberg, 1998; Andersson and Abrahamsson, 2002) because of local track stiffness (Kassa et al., 2006; Ren et al., 2005; Zhu, 2006), rail shape variation between stock rail and switch toes (Bonaventura and Holfeld, 2000; Bugarin and Diaz-de-Villegas, 2002; Klauder, 2001; Oswald and Bishop, 2001) and track irregularities. Additionally, severe lateral contact force needs to be developed to change the vehicle attitude and lateral position (Barbosa, 1999; Ren et al., 2005). The track model as a continuous elastic beam in the vertical direction has been explored in some previous papers (Andersson and Dahlberg, 1998; Andersson and Abrahamsson, 2002; Ren et al., 2005; Zhu, 2006). Despite the importance of the subject, few papers address this issue (Andersson and Dahlberg, 1998), particularly the lateral vehicle/track dynamics and experimental measurements.

Estrada de Ferro Vitória-Minas (EFVM-CVRD) is one of the most productive railway systems in the world, with 65×10^6 TKU (billion net-ton/km in 2005, 80% being iron ore). The company moves 37% of the solid grain in the Brazilian port system. The main line is metric gauge, 25-axle load with 905 km length (being 594 km in double track). It has a fleet of 17,000 wagons and 300 locomotives. It connects iron mines in Minas Gerais State to the exportation port in Vitória. A typical train has a gross weigh of 25,800 tons, with 252 wagons-length and three 4000 Hp locomotives with distributed traction, controlled by a remote system with an average speed of 65 km/h. It has 90 crossing locations where turnouts restrict operational speed. Usually the turnout allowed speed is 55–60 km/h. The increase of these limits will result in travel time reduction and, therefore, the increase of productivity.

This paper presents an experimental study on the dynamic behaviour of a vehicle crossing a turnout with emphasis on the safety limits.

2 Vehicle dynamics passing turnouts

Guided vehicle behaviour is usually investigated based upon the external excitations imposed by the track geometry and the vibration characteristics of the vehicle being considered. Therefore, vehicle/track dynamic interaction is a function of track irregularity inputs and vehicle speed (Andersson and Dahlberg, 1998; Andersson and Abrahamsson, 2002). Vehicle natural frequencies are an important factor with respect to safety issues due to the possibility of magnification of the dynamic response in the resonant region. Since the freight bogie has a non-linear suspension system, characterisation of vehicle's dynamic behaviour appears to be a complex task. The basic turnout geometry is

essentially a tangent track followed by a curved segment. In a circular curve, vehicle body accelerations with respect to a fixed reference frame *Oxyz*, as shown in Figure 1, may be determined by the following expression (França and Matsumura, 2004):

$$\vec{a} = \vec{a}_o + \dot{\vec{\omega}} \wedge (G - O) + \vec{\omega} \wedge [\vec{\omega} \wedge (G - O)]. \tag{1}$$

Figure 1 Turnout lay-out

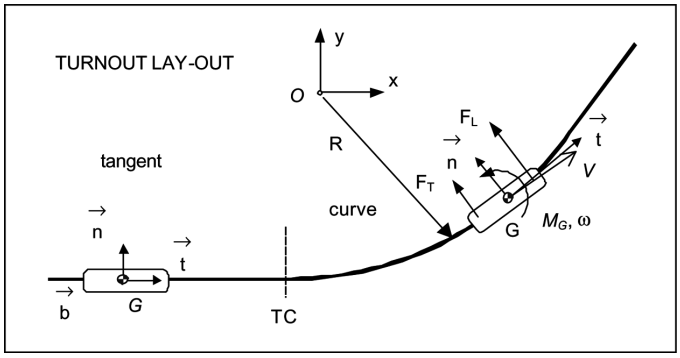

For a constant tangential speed *Vt* and a constant curve radius *R* (therefore $\dot{\omega} = 0$), the body acceleration with respect to the curve centre *O*, is expressed as:

$$\vec{a} = \vec{\omega} \wedge [\vec{\omega} \wedge (G - O)]. \tag{2}$$

Using the relation $\omega = V/R$ for a circular trajectory results in the well-known centripetal formula V^2/R.

. In a turnout, the transition from a tangent segment to the circular curve produces a suddenly change on the track direction. The imposed geometry is discontinuous and changes the vehicle angular speed and centripetal accelerations. In fact, the vehicle takes the curve gradually (leading wheelset of the first bogie, trailing wheelset and so on); therefore, the translational and angular accelerations increase gradually. Additionally, due to the wheel/rail gap and track geometric irregularities, the curvature, as seen by the vehicle, changes smoothly.

Alternatively taking a moving reference frame attached to the vehicle centre of gravity *G* with a vector triad oriented according to the tangential ($\vec{t}$), normal ($\vec{n}$) and binormal directions ($\vec{b} = \vec{t} \wedge \vec{n}$. according to the *Frenet* triad), as also shown in Figure 1, the acceleration is obtained from the time derivative of the tangential vehicle velocity:

$$\vec{a} = \dot{V}\vec{t} + V(\mathrm{d}\vec{t} + \mathrm{d}t) = \dot{V}\vec{t} + (V^2 / \rho)\vec{n}. \tag{3}$$

In the case of constant tangential speed, the acceleration component is only in the normal direction, which is a function of the instantaneous radius of curve (ρ). For a variable trajectory radius along the length, variation of the centripetal acceleration is expected (known as *jerk*, Bugarin and Diaz-de-Villegas, 2002). For a curve with fixed radius, the previous equation becomes similar to the equation (2).

The geometric shape of the transition curve, in which the curvature changes gradually with distance along the curve, results in a spiral form. For a linear curvature variation, the curve shape is generally referred to as *clothoid*. When a vehicle passes a transition curve (spiral or a *clothoid*) its angular speed with respect to the vertical axis increases

gradually to a steady state value (circular curve). The bogies at the vehicle extremities enter and leave the curve in different instants of time, with the vehicle suspension providing some cushioning to the *yaw* accelerations. As a consequence, the bogie axles search for a natural equilibrium position and a compatible attitude to produce the necessary lateral force to generate the necessary vehicle centripetal and angular accelerations. In a transition curve, the imposed vehicle body angular accelerations is obtained using the angular momentum equation:

$$\frac{\mathrm{d}}{\mathrm{d}t}[[J]_O[\vec{\omega}]] + (G-O) \wedge m\vec{a}_O = \vec{M}_O^{\text{ext}}. \tag{4}$$

Choosing the pole O coincident with the body centre of gravity G for a moving reference frame coupled to the vehicle, the above expression can be simplified. The external moment $\vec{M}_G^{\text{ext}}$ due to the leading and trailing bogies wheelset lateral contact forces F_{L} and F_{T} (as shown in Figure 1) necessary to produce the vehicle angular acceleration (*yaw* movement) to align a vehicle trajectory compatible with the geometry of the curve is obtained from:

$$\frac{\mathrm{d}}{\mathrm{d}t}[[J]_G[\vec{\omega}]] = \vec{M}_G^{\text{ext}}. \tag{5}$$

During curve negotiation, an axle angle with respect to the track tangent (angle of attack) is produced to generate the lateral force. Additionally, the wheelset yaw movement misaligns bogie side-frames, loosening bogie orthogonality. The result is the bogie warp phenomenon that induces wheelset misalignment. Both phenomena are relevant to characterise wheel/rail wear (axle misalignment).

Moreover, an angular movement of the body in the longitudinal axis (*roll* movement) is forced due to the vehicle centre of gravity vertical position. This effect suddenly magnifies the vehicle guiding loads that excites natural movements such as *lower sway* (lateral plus roll in phase movements) and *yaw* (angular directioning), which are undesirable from the point of view of wear and safety.

It is known that a three-piece freight bogie, with a side-frame edge dry friction damping system, is a non-linear system with alignment restrictions. Additionally, the suspension static load distribution is a function of track section irregularities. When the lateral contact force is large or oscillating, the tendency of the wheel to climb the rail is magnified (Barbosa, 1999). In this situation, wear may be severe and the safety conditions are at stake, with increasing derailment probability. The metric to measure this tendency is the contact force ratio L/V (lateral contact force divided by the vertical force, Barbosa, 2004). This ratio is known as the safety index (Barbosa, 2005). The body vertical and angular movements influence the vertical wheel force. Vehicle natural movements such as *bounce* and *pitch* (vertical) and *roll* and *yaw* (angular) have a typical resonance frequency. Therefore, variation on vertical load (denominator on the safety index) due to the resonance phenomena needs to be evaluated.

To address these issues, a broad program of experimental measurements on the dynamic behaviour of a railway vehicle passing a turnout with controlled condition was performed. For this task, complete vehicle instrumentation was implemented to quantify the pertinent variables needed to identify the vehicle dynamic behaviour and to perform a safety analysis.

3 Experimental instrumentation

For a safety analysis, the cause-effect for the vehicle movement must be identified. Having the safety formula in mind (L/V), the vertical and lateral mean load values and the oscillation due to the modal movements should be evaluated. For instance, the vertical load variation is quantified from the modal vertical movement (*bounce* and *pitch*), added to the suspension torsional moment effect, caused for instance, on a twisted track. Lateral load effect due to the lateral vehicle translation (*sway*) and the directional rotation (*yaw*) movements are obtained with translational transducers (accelerometers and displacement) and rotational device (*rate-gyro*). The bogie relevant attitude is due to bolster and side-frame misalignment (*warp*) that harms wheelset-track centralisation and inter wheelset angle that induces high angle of attack.

The methodology adopted to investigate the vehicle dynamic behaviour was to pass an instrumented railway wagon through the turnout on a divergent route under controlled conditions. For this purpose, a special train was set-up with a locomotive, a laboratory car and six-loaded iron ore wagons. This composition was driven through the turnout at constant speeds. This test was repeated systematically at different speeds, from 5 km/h to 65 km/h. The vehicle dynamic behaviour was measured with 24 transducers installed at different locations. Wheel loads were measured with two instrumented wheelsets.

The wagon used in the testing program was an iron ore 100-ton gross weight open hopper of the American type (*AAR*). The total wagon length was approximately 10 m long and the bogie distance was 5.5 m. The bogie is composed of three structural pieces: one bolster, where the wagon box is supported in a circular plate, and two side-frames connecting the bolster, through helicoidal springs, and to the axles with roller bearing housings.

The instrumentation set-up was composed of 24 measuring devices, which were distributed according to Figure 2. Four piezo-electric accelerometers were used to identify wagon box translational movements (*bounce* and lateral). Two rate-gyros were used to identify wagon box attitude (*pitch* angular speed and *roll* angular speed). The reason for using an angular speed-measuring device is that it requires only one instrumentation channel for rotational movement and can measure absolute values as required by expression (4). Eight resistive displacement-measuring devices were used for the bogie and the suspension movements. To measure the axle angular movement and bogie *warp* angles, an improved instrumentation set-up with six resistive displacement-measuring devices were used (see Figure 3). Finally, two rotating digital pulse generators were used for distance and speed identification and a synchronisation pulse generated from the events marks along the track.

Data were acquired with a digital acquisition system, installed in a portable personal computer. An analogic to digital 16-bits 32-channel board was used with a sampling rate of 500 samples per second.

Contact forces were measured with two commercial *TTCi-IWS* (*US Transportation Test Center Instrumented Wheelset*) connected to an exclusive digital acquisition system. The instrumentation in the wheel was implemented with several radial *Wheatstone* strain gages bridges, to allow the monitoring of the tri-axial loads with minimised cross-talk effects. This system has proprietary software for signal acquisition and processing (synthesising a variable from multisource measurements) with a rotating device transmission (silver brush slip ring) to synthesise the vertical, lateral and longitudinal

contact wheel loads. For this task, the wheel/rail contact position was needed, which was identified from measurements of the wheel flange bending by means of radial strain gages bridges installed in the wheel. A laboratory calibration process was undertaken for each measured variable, in a tri-axial load machine at every 5° wheelset rotation, to guarantee reliable scale factor.

Figure 2 Wagon instrumentation

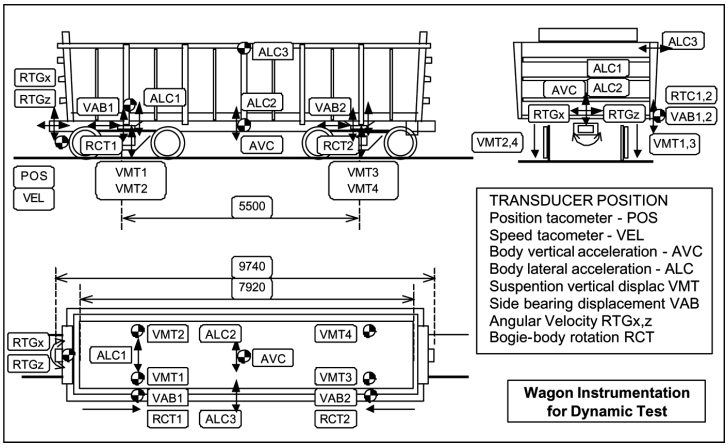

Figure 3 Bogie instrumentation

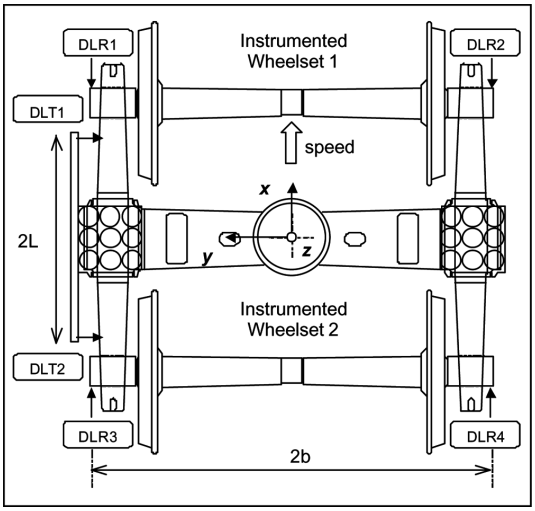

A special transducer combination was proposed to measure the wheelset angle of attack. Four cable potentiometer displacement transducers fixed on the bogie side-frames and connected to the axle roller bearing housing, as shown in Figure 3, comprised this new system. The movements of the two axles, relative to the side-frame, were monitored on each bogie side (transducer identification *DLR* on the *x*-direction shown in Figure 3). In this way, the angle between axles of the bogie can be obtained from arithmetic operations from the acquired signals. This configuration is not affected by the relative longitudinal movement of the side-frames (bogie warp cross-talk free). Additionally,

an angular measuring set-up was used to identify bogie warp, which is composed of two potentiometric displacement transducers, which were fixed between the bolster and the side-frame (see transducer identification DLT on the *y*-direction shown in Figure 3).

4 Turnout geometry

When a vehicle negotiates a curve, the track geometry changes suddenly forward, producing disturbances to the vehicle trajectory. The curved section is generally banked (*super-elevation*) by having the outside curve rail raised relative to the inner rail, to compensate for the centrifugal reaction. The simplest track shape that can provide a reasonably smooth transition between two adjacent sections is a shape with curvature and bank angle at each end that matches those of the neighbouring track section, with a linear variation with distance along the transition.

The turnout is a track deviation with a sequence of curves to change traffic between two adjacent lines. The turnout object of this investigation has two switches with a deviation ratio of 1:20 (50 milliradians), as shown in Figure 4. The switch consists of two tongues and two stock rails, fastening system, with supporting parts and intermediate reinforcements. The track is a double line, 1-m gauge and 4.25 m apart. The switches in the turnout have a curve length of 28 m, with a radius of 548 m, in between a straight track segment of 54 m, resulting in a total crossing length of 110 m, as shown in Figure 4.

Figure 4 Turnout lay-out

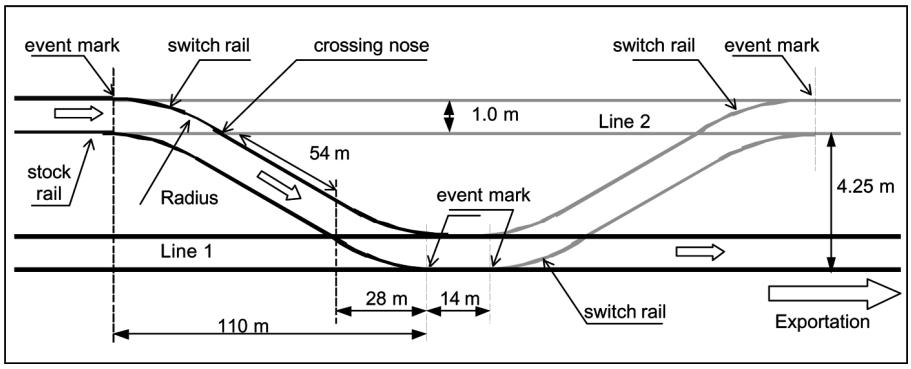

The geometry has to be described in quantitative terms to evaluate vehicle/track relationship. For this purpose, an '*in situ*' topography measuring system was used to extract the geometrical shape from the real track lay-out. The plant view of the turnout, with topographic measurements is shown in Figure 5. The longitudinal position of the track is plotted in the abscissa axis while the latitude of the track profile is in the ordinate.

The track direction variation along its length expressed by the vector $\vec{t}$ of the *Frenet* tri-orthogonal base in the E^3 space (Barbosa, 1999; Nutbourne and Martin, 1988), can be obtained from the curvature κ in the curve center direction $(\vec{n})$ from:

$$\begin{Bmatrix} \vec{t} \\ \vec{n} \\ \vec{b} \end{Bmatrix}' = \begin{bmatrix} 0 & \kappa & 0 \\ -\kappa & 0 & \tau \\ 0 & -\tau & 0 \end{bmatrix} \begin{Bmatrix} \vec{t} \\ \vec{n} \\ \vec{b} \end{Bmatrix}. \tag{6}$$

Figure 5 Turnout lay-out and curvature (see online version for colours)

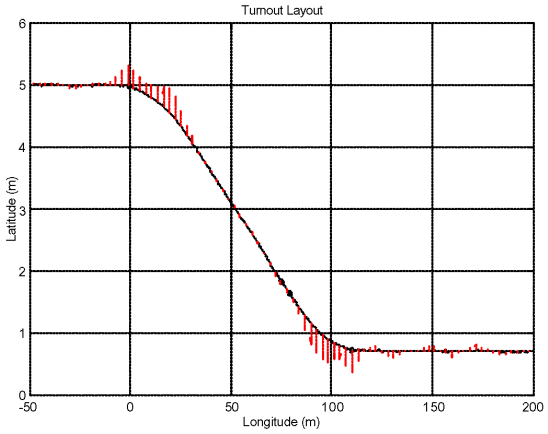

Cartesian coordinates of points along a circular curve, or a *clothoid* spiral, are given by the *Fresnel* integrals, which are well-known mathematical functions (Nutbourne and Martin, 1988). To obtain the curvature (or its reciprocal – the radius) of the track, from topographic-measured points in the *Cartesian* plane (x, y) along trajectory $\boldsymbol{S}$, a higher order derivative expression is used:

$$\kappa = \frac{1}{R} = \frac{(\mathrm{d}^2 y / \mathrm{d}x^2)}{[1 + (\mathrm{d}y / \mathrm{d}x)^2]^{3/2}}. \tag{7}$$

To get a higher order derivative of the *Cartesian* points, for the curvature calculation as given by the early expression, a natural cubic spline interpolation method was used. Owing to measurement uncertainty, a least square smoothing procedure was also used. The results from this calculation are shown in Figure 6. The curvature of the track along its length is shown in the upper graph (unity of curve radius in metres). In the lower graph, the track direction measured in degrees is shown. The local track curvature is also shown as orthogonal vectors in Figure 5 (red lines). Circle marks show the position in which the switch begins, and ends, along the crossing nose.

The treated topographic-measured results show a curvature variation along the switch length with a maximum value of 0.002 (radius of 500 m). The resulting direction result is quite compatible with the switch design (2.86° or 50 milliradians), revealing the confidence of the data processing algorithm. Although nominal switch design gives assurance to a circular curve without transition, the real global curvature varies in a gradual way, probably as a function of the local geometry (*needle*, *frog*, etc.), gauge variation and rail lateral wear and deformations. The employed data processing algorithm consistently recovered the track lay-out geometry. Curvature values obtained were used for correlations with the lateral force in the vehicle dynamic behaviour travelling at a constant speed.

Figure 6 Track curvature and direction along track length (see online version for colours)

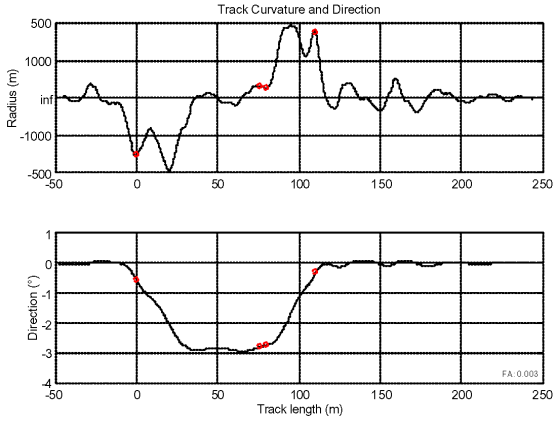

5 Data processing

Special data processing was performed to indirectly synthesise the special variables described earlier. Except for the angular speed device (*rate-gyro*), pairs of translational signals can be combined to obtain a meaningful angular variable. All collected data were previously filtered to avoid aliasing phenomena at the signal conditioning stage.

The vehicle torsion moment was synthesised from the translational measurement of the four suspension deflections (VMT_i, as identified in Figure 2). The difference between adjacent transducers in the same bogie, with respect to the same effect on the other bogie, synthesises the angular torsion τ (mm/m) in the inter bogie distance (5.5 m), by means of:

$$\tau = [(\mathrm{VMT}_1 - \mathrm{VMT}_2) - (\mathrm{VMT}_4 - \mathrm{VMT}_3)] / 5.5. \tag{8}$$

From the product of τ with the suspension stiffness, the suspension torque value can be obtained.

The bogie warp or angle between bolster and side-frame, was measured with two displacement transducers located in the bolster (DLT_i), as shown in Figure 3. This angle can be computed from:

$$warp = (\mathrm{DLT}_1 - \mathrm{DLT}_2) / 2L. \tag{9}$$

The inter-axle angle θ, as shown in Figure 7, was measured with four longitudinal displacement transducers (DLR_i), located between the side-frame extremity and the roller bearing housing (see Figure 3). During vehicle shallow curve negotiation, lateral displacement turns the wheelset due to the wheel tread conicity. The angle between axles is identified with the difference between displacement transducers from:

$$\theta = [(\mathrm{DLR}_1 - \mathrm{DLR}_2) - (\mathrm{DLR}_4 - \mathrm{DLR}_3)] / 2b. \tag{10}$$

Note that this variable is not affected by the *warp* movement due to the cancellation of the opposite variation of the displacement transducers on the same side (DLR_2 and DLR_4).

The lateral wheel force is also influenced by the wheelset angle of attack. As shown in Figure 7, the track tangential angle α is identified with the ratio between the inter-axle distance and the curve radius as:

$$\alpha = br / R. \tag{11}$$

Considering that the leading axle performs the curve inscription (trailing axle tends to the tangent position), the wheelset angle of attack ψ, relative to the track tangent, is the difference between these two angles and given by:

$$\psi = \alpha - \theta. \tag{12}$$

For a turnout 1:20 type (AREMA) with radius of 548 m and bogie inter-axle distance of 1.75 m, the track angle α will be equal to 3.2 milliradians. Therefore, for a measured inter-axle angle θ = 1 milliradians, as shown in the second graph of Figure 8 (deducting 33.5 milliradians offset), one gets an angle of attack ψ of 2.2 milliradians.

Figure 7 Axle angle and bogie curve negotiation

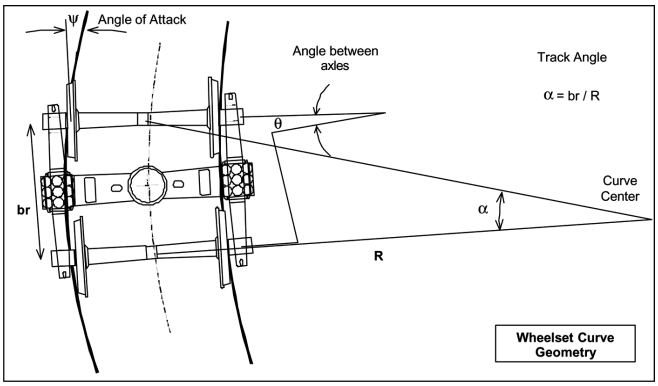

Figure 8 Bogie warp and inter-axle angles (leading bogie, along track distance) (see online version for colours)

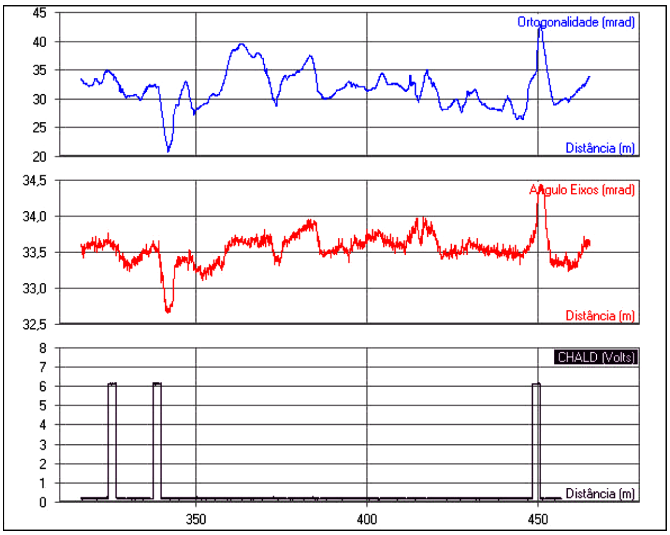

When the axle seeks tangency to the curve, it drags the outer-side side-frame of the bogie, loosening the orthogonality of the three-piece bogie structure, producing the warp angle. This phenomenon can be observed in the upper graph of Figure 8, which shows the front wagon leading bogie warp angle along the track length of the turnout. The lower graph in this figure is the event-mark pulse (*CHALD*) for the switch beginning at position 338 m (*x*-axis is the distance of the vehicle front wheel from the starting point) and switch end at 450-m distance. The middle graph in Figure 8 is the angle between axles. All graphs in this figure are synchronised along the distance travelled by the vehicle, crossing the turnout from line 1 to line 2 (around 110 m) in the same direction characterised in Figure 4.

Figure 8 presents the bogie *warp* (upper graph), inter-axle angles (middle graph) and the eventmark pulse at the switch beginning and end (second and third spikes in the lower graph, with instrumentation channel named *CHALD,* with values in volts as detailed in Figure 4), along the track distance (abscissa of the figure).

Another aspect to be inspected is the ability of the wheelset to negotiate the turnout geometry, appropriately. For this purpose, the inter-axle angle (milliradians), wheel side contact position (millimetres) and front-end right wheel lateral force (kNewton) are presented in Figure 9. This graph is shown from the switch beginning, at position 264 m, the peak of the lateral force inside the curve (70 kN between abscissa 265 and 269 m on the third graph) with almost twice the mean regime value inside the curve (length of 28 m from 264 m to 292 m). This reveals an opportunity for improvement of the wheelset-track negotiation process through better turnout geometry and vehicle suspension properties.

Figure 9 presents the inter-axle angles (upper graph in milliradians), contact lateral position of the wheel with respect to the rail (2nd graph in millimetres) and lateral right wheel force (3rd graph in kN), and the event-mark pulse at the switch beginning (*CHALD* in the lower graph) along the track distance (abscissa of the figure).

Figure 9 Turnout negotiation (inter-axle angle (milliradians), contact lateral position (mm) and lateral right wheel force (kN), along track distance in metres (see online version for colours)

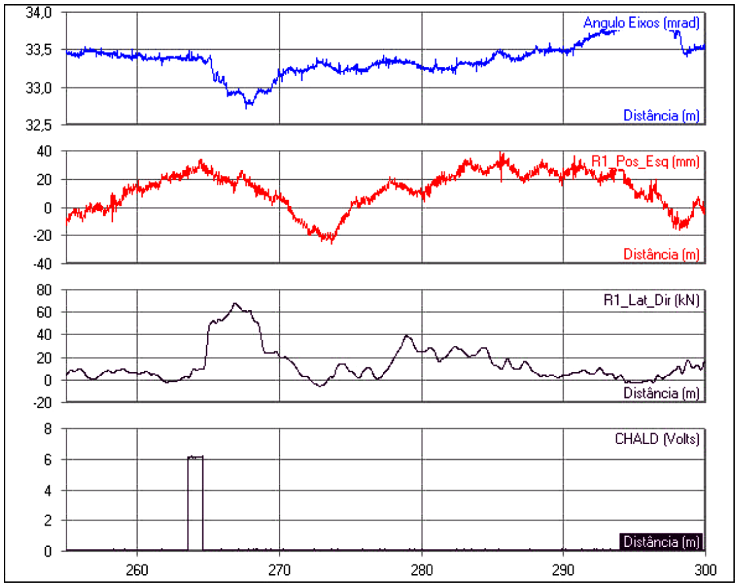

6 Experimental results

The experimental results of the vehicle dynamic behaviour travelling at a constant speed of 60 km/h were selected for analysis. The vehicle was crossing the turnout from line 2 to line 1, as shown in Figure 4. Results of the time history of each variable are presented in the next figures. For comparative purposes, all the results are shown synchronised with the track curvature (as presented in Figure 6). In the bottom graph of each figure, circle marks in the switch begin and end at abscissa 0 and 110 m, respectively.

Maximum lateral force of 92 kN, measured in the leading axle of the front bogie, occurs in the exit of the second switch, as presented in the second graph of Figure 10, at position 110 m (left wheel in the top graph and right wheel in the middle graph). This value is almost twice the oscillating regime peaks. The lateral force on the left wheel is associated with the curvature magnitude for the clockwise sense (negative value) and *vice-versa* for the exit switch. Note the oscillation with a wavelength around 9.5 m. The non-linear aspect of the oscillations in the force magnitude is noticeable, probably due to the damping effect of the dry friction edges of the freight bogie.

The vehicle body attitude is shown in Figure 11. In the upper graph, the middle-vehicle lateral acceleration is presented. The instrument location can be recalled from Figure 2. The circumferential acceleration trend (centripetal) can be observed between positions 0–28 m and 82–110 m. The directioning angular vehicle speed (ω_z), corresponding to the yaw movement, can be observed in the middle graph (*rate-gyro* in the *z*-direction). Note the severe variation near the extreme of switch needle (between 90 m and 110 m).

Figure 10 Lateral contact force and curve radius along track length (see online version for colours)

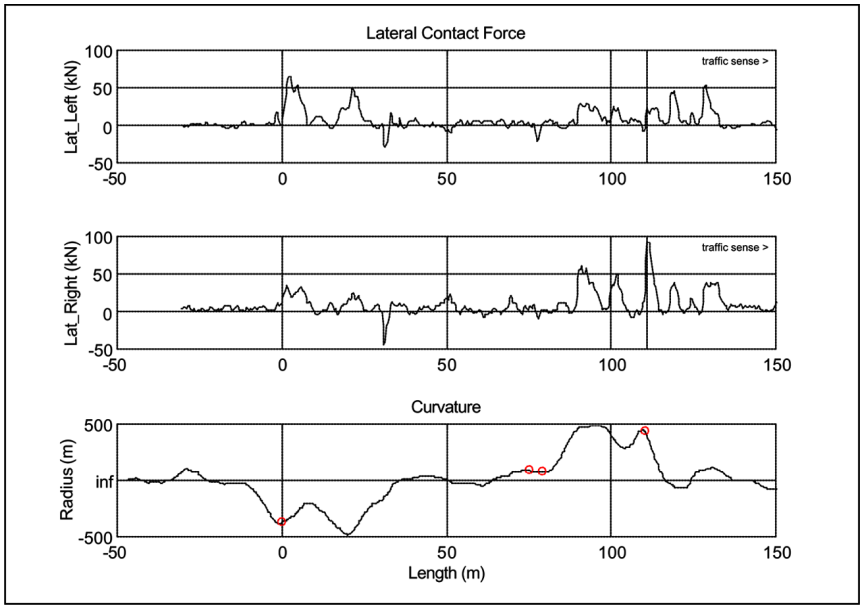

Figure 11 Vehicle lateral acceleration and angular speed along track length (see online version for colours)

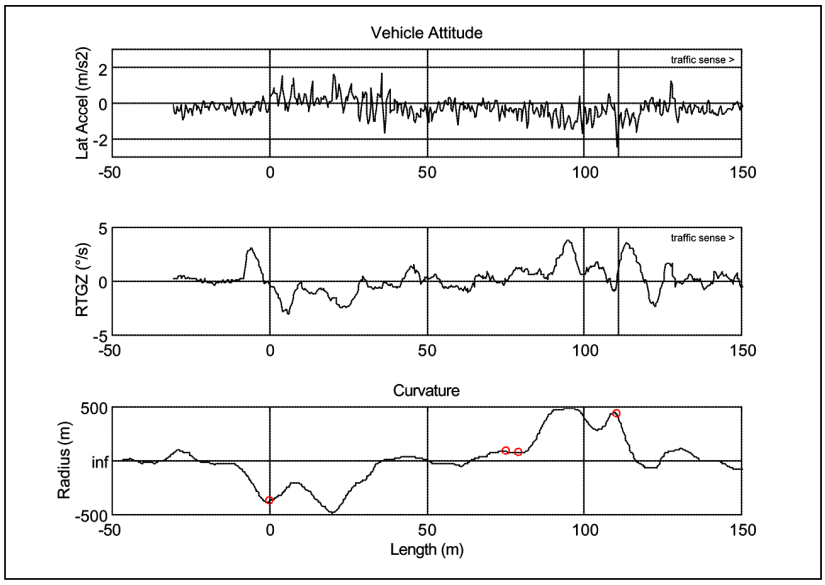

Finally, in Figure 12, the safety index L/V measured with the instrumented wheelset is presented. The maximum L/V value reaches 0.6 for the right wheel, in the exit of the second switch at position 90 m (shown in the middle graph of Figure 12). This value is under the international standards normalised limits. However, a severe oscillation occurs for several metres (between 90–130 m) during and after the vehicle exits the switch. This imposes a periodic stress on the rails and can, therefore, induce a long-wave corrugation wear and a reduced safety margin.

Figure 12 Safety index (L/V) along track length (see online version for colours)

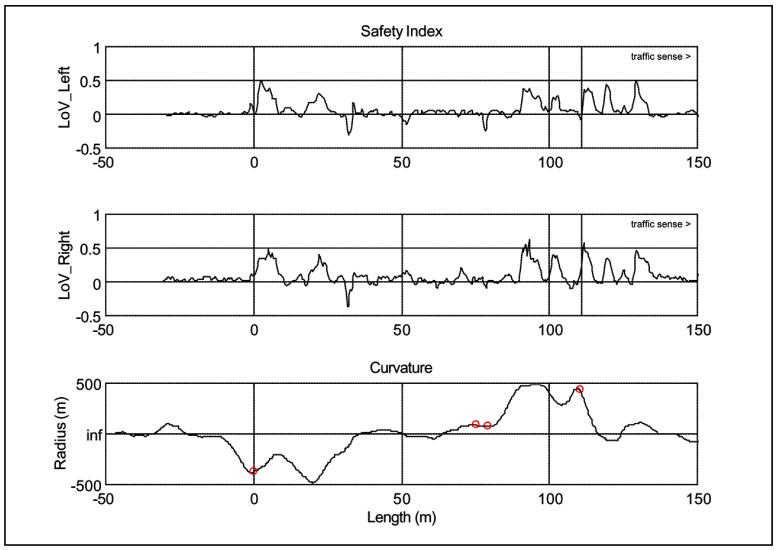

In Figure 10, the lateral contact force of the left wheel (upper graph in kN), the lateral contact force of the right wheel (middle graph in kN), and curvature radius (lower graph in metres), along the track length (abscissa of the figure) are presented.

In Figure 11, the vehicle lateral acceleration (upper graph in m/s^2), the body angular speed in the *z*-direction (middle graph in °/s), and curvature radius (lower graph in meters), along the track length (abscissa of the figure) are presented.

In Figure 12, the safety Index L/V for the left wheel (upper graph), the safety Index L/V for the right wheel (middle graph), and curvature radius (lower graph in meters), along the track length (abscissa of the figure) are presented.

In Figure 13, the vehicle suspension torsion (upper graph in mrad/m), and track twist (lower graph in mrad/m), along the track length (abscissa of the figure) are presented.

The vehicle suspension torsion was identified through the cross difference between bogie springs deflections (see data processing). These results were compared to the track twist in the same length (5.5 m). Results are presented in Figure 13. In the top graph of this figure, the measured suspension torsion is presented in radians per metre (rad/m). This value can be converted to torque unities (Newton × metre), once the suspension stiffness is known. In the bottom graph of the Figure 13, the track twist is presented in the same scale length (abscissa). Although the magnitudes are different, probably due to suspension damping effects and track elasticity, a correlation is noticed between action (track geometry) and reaction (vehicle response).

Figure 13 Suspension torsion along track length (see online version for colours)

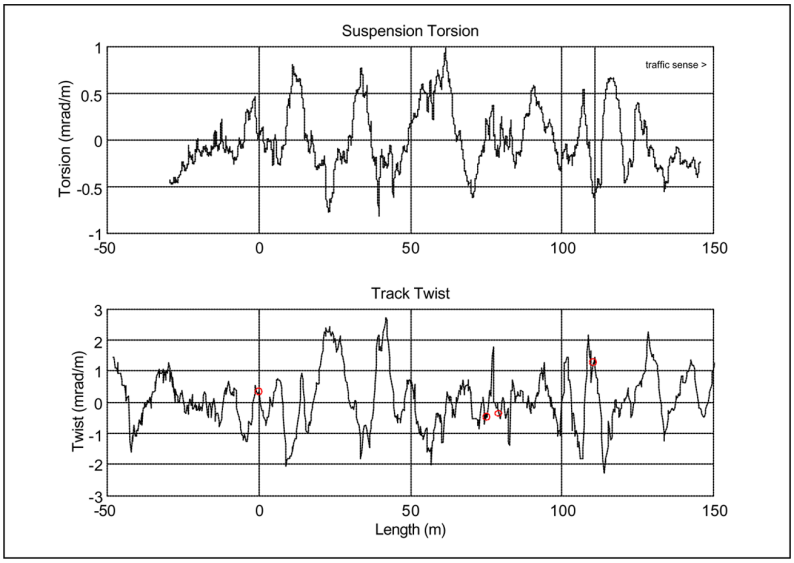

Finally, maximum values measured for different speeds are summarised in the next two figures. Maximum wheel lateral force for different vehicle travelling speed is presented in Figure 14. Greater values can be seen for the right wheel in the exit of the second switch. The maximum wheel lateral force reaches 100 kN for 65 km/h – 65% greater than those at low speeds (under 30 km/h), which has typical value of 60 kN, as shown in Figure 14. Specifically for speed increasing from 50 km/h to 65 km/h, the maximum lateral force changes from 90 kN to 100 kN, reducing the safety margin and increasing

the wear. Peaks are observed at 40 and 55 km/h, which may be associated with resonance of the vehicle modal movements.

Figure 14 Maximum wheel lateral force in function of vehicle speed (see online version for colours)

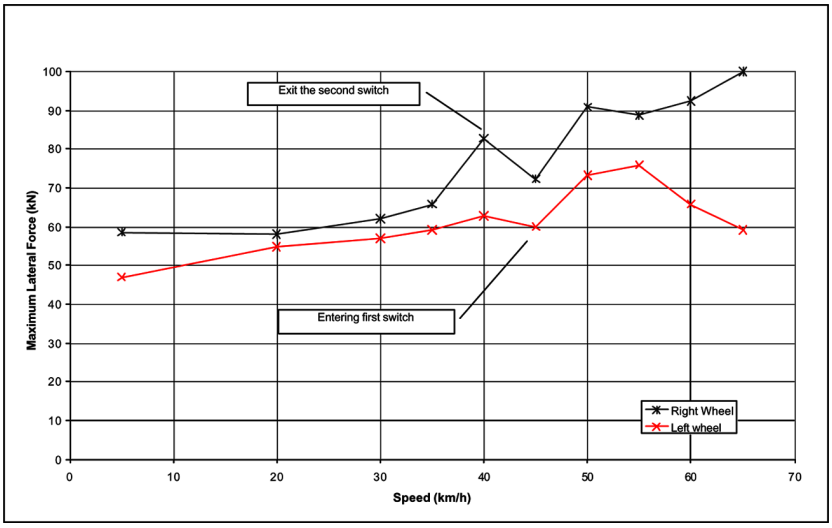

Roll and *yaw* angular speed amplitudes are presented in Figure 15. The expected quadratic tendency is verified, as discussed in Section 2. For each rotational movement reported, a peak is identified as a function of the speed: 35 km/h for the *roll* movement (*RTG*x) and 45 km/h for the *yaw* movement (*RTGz*). The expected cross-talk effect between the *yaw* rotation and *roll* movement, due to the high vehicle centre of gravity, is observed only at 35 km/h.

Figure 15 Angular speed amplitude in the *x* and *z* axis (function of vehicle speed) (see online version for colours)

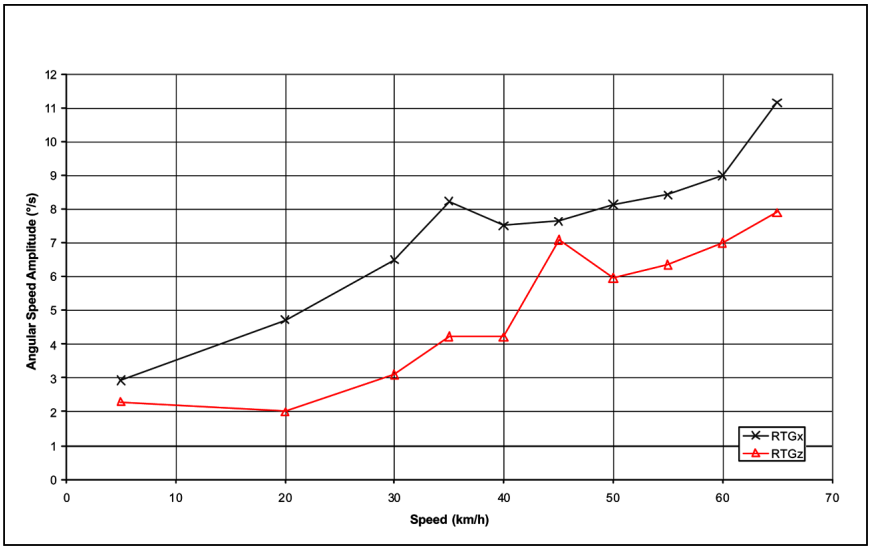

7 Conclusions

An experimental testing program to evaluate the vehicle dynamic behaviour travelling through a turnout on a divergent route was developed. A vehicle was instrumented with accelerometers and angular speed devices to identify its attitude (translation and rotation) in a special train crossing a turnout at different speeds. Vehicle safety was evaluated using the lateral-to-vertical wheel contact force ratio (L/V), known as the safety index, which was measured with two instrumented wheelsets.

Topographic measurements were performed to identify the track geometry. Track properties as curvature and twist were numerically synthesised. Measurements uncertainties were overcome with a least square smoothing data procedure in a cubic spline interpolation process. The employed data processing algorithm consistently recovered the track lay-out geometry.

Vehicle movements, suspension torsion, bogie warp and wheelset angle were identified and the correlation between action (track geometry) and reaction (vehicle response) was observed. The safety index L/V values reach 0.6 (Figure 12) at the exit of the turnout, with the worst safety value. A severe constant wavelength oscillation in the switches was also observed. Maximum lateral force at 65 km/h was 65% greater than those at low speeds (under 30 km/h), which has typical value of 60 kN, as shown in Figure 14. Specifically for speed increasing from 50 km/h to 65 km/h the maximum lateral force changes from 90 kN to 100 kN, reducing the safety margin. This phenomenon is related to the track geometry and vehicle modal movement. A lateral wheel force peak with almost twice the mean regime value inside the curve of the switch was also found, as presented in Figure 9. This reveals an opportunity for improving the wheelset-track negotiation process through better turnout geometry and vehicle suspension properties. Finally, a vehicle modal and safety investigation on new switch geometry is recommended.

Acknowledgements

The authors would like to thank the Mechanical Engineering Department of the Escola Politécnica da Universidade de São Paulo (EP-USP) and Companhia Vale do Rio Doce (VALE) for the support to this research under the VALE-USP scientific cooperation agreement.

References

Andersson, C. and Dahlberg, T. (1998) 'Wheel/rail impacts at a railway turnout crossing', *Proceedings of The Institution of Mechanical Engineers, Part F, Journal of Rail and Rapid Transit*, Vol. 212, No. 2, pp.123–134.

Andersson, C. and Abrahamsson, T. (2002) 'Simulation of interaction between a train in general motion and a track', *Vehicle System Dynamics*, Vol. 38, No. 6, pp.433–455.

Barbosa, R.S. (2004) 'A 3D contact force safety criterion for flange derailment of a railway wheel', *Journal of Vehicle System Dynamics*, Vol. 42, No. 5, pp.289–300.

Barbosa, R.S. (2005) 'Safety criterion for railway vehicle derailment', *Proceedings of the 8th International Heavy Haul Conference*, International Heavy Haul Association – IHHA, Sponsored by CVRD, Rio de Janeiro, Brazil, pp.477–484.

Barbosa, R.S. (1999) *Aplicação de Sistemas Multicorpos na Dinâmica de Veículos Guiados*, PhD Theses at University of São Paulo, São Paulo, Brazil, p.273.

Bonaventura, C.S., Holfeld, D.R., Zarembski, A.M. and Palese, J.P. (2005) 'Test results of a modified turnout designed to increase diverging route speeds without increasing lead length', *2005 AREMA, Annual Conference*, Chicago, IL, USA.

Bugarin, M.R. and Diaz-de-Villegas, J.M.G. (2002) 'Improvements in railway switches', *Proceedings of The Institution of Mechanical Engineers, Part F, Journal of Rail and Rapid Transit*, Vol. 216, No. 4, pp.275–286.

Kassa, E., Andersson, C. and Nielsen, J.C.O. (2006) 'Simulation of dynamic interaction between train and railway turnout', *International Journal of Vehicle System Dynamics*, Vol. 44, No. 3, pp.247–258.

Klauder Jr, L.T., Elkins, J. and Chrismer, S.M. (2002) *Improved Spiral Geometry for High Speed Rail And Predicted Vehicle Response*, Transportation Research Board of the National Academies, TRB meeting, January, pp.17.

Nutbourne, A.W. and Martin, R.R. (1988) *Differential Geometry Applied to Curve and Surface Design*, Ellis Horwood Limited and John Willey & Sons, England, Vol. 1, p.282.

Oswald, J.R. and Bishop, G. (2001) 'Optimisation of turnout layout and contact geometry through dynamic simulation of vehicle-track interaction', *7th International Heavy Haul Conference*, International Heavy Haul Association – IHHA, pp.31–35.

Ren, Z., Sun, S. and Zhai, W. (2005) 'Study on lateral dynamic characteristics of vehicle/turnout system', *Vehicle System Dynamics*, Vol. 43, No. 4, pp.285–303.

Zhu, J.Y. (2006) 'On the effect of varying stiffness under the switch rail on the wheel-rail dynamic characteristics of a high-speed turnout', *Proceedings of The Institution of Mechanical Engineers, Part F, Journal of Rail and Rapid Transit*, Vol. 220, No. 1, pp.69–75.

França, L.N.F. and Matsumura, A.Z. (2004) *Mecânica Geral*, 2nd ed., Edgard Blücher Publisher, Brazil.

Nomenclature

A	Acceleration
Br	Distance between bogie axles
J_o	Inertia matrix with respect to point O
F_L	Leading bogies wheelset lateral contact forces
F_T	Trailing bogies wheelset lateral contact forces
G	Body mass centre
kN	Kilo Newton
M	Metre
M_o	Moment of forces with respect to pole O
N	Newton – force unit
O	Origin of reference frame
Rad	Radians
R	Circular curve radius
Vt	Vehicle tangential speed
α	Tangent track angle
θ	Inter-axle angle
ψ	Axle angle of attack

ρ	Instantaneous radius of curvature
ω_Z	Angular speed on z-direction
$\dot{\omega}$	Angular acceleration
κ	Curvature
τ	Torsion
d/dt	Differential with respect to time
L/V	Ratio between lateral and vertical contact force
RTG	Rate-gyro
$\vec{t}\ \vec{n}\ \vec{b}$	Movable unit vector triad
$Oxyz$	Tri-orthogonal inertial reference frame
AAR	Association of American Railway
AREMA	The American Railway Engineering and Maintenance-of-Way Association
CHALD	Event-mark pulse channel on the graphs
IWS	Instrumented wheelset
TKU	Net-ton/km
TTCi	Transportation Test Center Inc.

8.8 ANEXO H

SAFETY OF A RAILWAY WHEELSET - DERAILMENT SIMULATION WITH INCREASING LATERAL FORCE

Barbosa, R. S. (2009) Safety of a railway wheelset - derailment simulation with increasing lateral force. International Journal of Vehicle System Dynamics, DOI: 10.1080/00423110802650024, pp. 1-18.

Vehicle System Dynamics
Vol. 47, No. 12, December 2009, 1493–1510

Taylor & Francis
Taylor & Francis Group

Safety of a railway wheelset – derailment simulation with increasing lateral force

Roberto Spinola Barbosa*

Escola Politécnica da Universidade de São Paulo – EP-USP, São Paulo, Brasil

(*Received 19 April 2008; final version received 24 November 2008*)

The motivation for this research is to make a comparison between dynamic results of a free railway wheelset derailment and safety limits. For this purpose, a numerical simulation of a wheelset derailment submitted to increasing lateral force is used to compare with the safety limit, using different criteria. A simplified wheelset model is used to simulate derailments with different adhesion conditions. The contact force components, including the longitudinal and spin effects, are identified in a steady-state condition on the verge of a derailment. The contact force ratios are used in a three-dimensional (3D) analytical formula to calculate the safety limits. Simulation results obtained with two contact methods were compared with the published results and the safety limit was identified with the two criteria. Results confirm *Nadal's* conservative aspect and show that safety 3D analytical formula presents slightly higher safety limits for lower friction coefficients and smaller limits for high friction, in comparison with the simulation results with *Fastsim*.

Keywords: safety; railway; derail; vehicle; dynamic; contact

1. Introduction

The fundamental safety requirement for a railway vehicle is that it should be less prone to derailment. The railway derailing process is a very complex dynamic phenomenon. Wheel derailment usually happens when the vehicle negotiates a curve. The external wheel in the curve is subjected to a large lateral force against the high rail. In this situation, the wheelset will seek an equilibrium attitude by oscillating between a lateral displacement and a yaw angle. This equilibrium position will produce a contact force in the wheel/rail contact path that should be enough to avoid the climbing mechanism that produces derailment.

Nadal's traditional treatment for the derailment phenomenon is applied to the wheel transverse section [1]. Despite the supposed second contact point ahead of the contact section, which justifies his proposition, as stated by Gilchrist [2], it is no longer possible in the derailment vicinity, when the wheel flange angle is maximum and the contact becomes punctual again. Another aspect is that Nadal's expression is valid only for the rolling-up mechanism (the wheel transverse contact force is in the upward direction due to rolling without slip mechanism) and

*Email: roberto.barbosa@poli.usp.br

ISSN 0042-3114 print/ISSN 1744-5159 online

DOI: 10.1080/00423110802650024
http://www.informaworld.com

is stated as:

$$\frac{L}{V} \geq \frac{\tan\alpha - \mu}{1 + \mu \tan\alpha}. \tag{1}$$

Conversely, as pointed out by Parena *et al.* [3] and some other authors, the safety formula for another derailment mechanism (referred to here as the lateral sliding mechanism, when the wheel is pushed up, sliding in a lateral movement – wheel transverse contact force is in the downward direction due to the sliding reaction, as seen in Figure 2), should be written alternatively as follows:

$$\frac{L}{V} \leq \frac{\tan\alpha + \mu}{1 - \mu \tan\alpha}. \tag{2}$$

Note that this formula has a singularity when $\mu \tan\alpha = 1$ and the denominator is null and L/V ratio goes to $\pm\infty$. This happens when the adhesion and contact angle is high, which means the wheel flange will stick to the railhead as a wall. Values of derailment limit (L/V) calculated with these two formulae, for different contact angles and friction coefficients, are shown in Figure 1. It is noticeable that both formulae converge to the same results for null adhesion, that is, the tangent of the contact angle.

The search for a simple analytical relationship to identify reliable safety limits is convenient, as the traditional nineteenth century Nadal's safety relationship, known as conservative, is still in use, for example in the *Norme Européenne* NF-EN-14363 [4]. An extensive programme of experimental investigation in railway system safety performed in Europe (DYSAF-Test research) acknowledges the difficulty in obtaining a general multi-parameter safety criterion [5]. Experimental investigation is still being conducted in different countries (*Braghin*, full-scale roller rig, imposed yaw angle, lateral force derailment, Italy [6], and *Ishida*, full-scale roller rig, load transfer, low speed and sharp curve derailment, Japan [7]). The proposition of empirical derailment criteria still appears in 2008 [8], considering only a curve-fitting method of the yaw angle. The motivation for this research is to explore in depth the three-dimensional (3D) aspects of the rolling contact phenomena, which subsidise the dynamic simulation of a railway system and the quantification of safety limits including the longitudinal

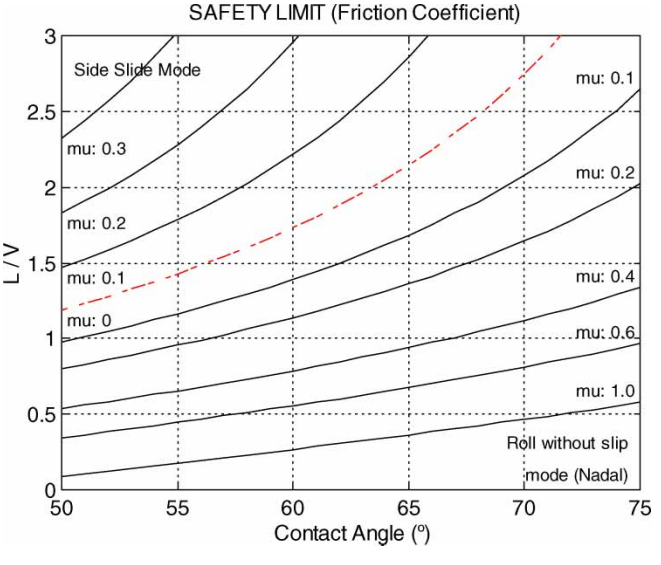

Figure 1. L/V for various contact angles (two mechanisms).

and spin effects. For this purpose, steady-state force contributions on the contact path are identified on the verge of a derailment. The force ratios and wheelset attitude are used in the 3D analytical safety formula proposed by this author [9] to calculate derailment safety limits and to compare them with numeric wheelset dynamic simulations and other available results.

2. Contact forces

During a derailment, a severe external lateral force as well as an external torque are to be sustained by the wheelset. Lateral displacement and yaw rotation is the natural body attitude. When a derailment is bound to happen, contact wheel force is generated, trying to compensate external forces, until the flange overcomes the railhead. On observing the wheel-free body diagram presented in Figure 2, one can identify the wheel–rail contact force $\vec{T}$ and the suspension force $\vec{F} = H\,\vec{I} + L\,\vec{J} + V\,\vec{K}$, expressed in the wheelset reference frame. In the imminence of a derailment, external lateral force L should vanish with a transverse contact force. As the contact plane changes its inclination, the lateral reaction is a combination of normal N and transverse T_y components. The external torque reacts at the contact path level with a moment produced by the longitudinal couple force T_x of each wheel.

For a large lateral displacement, for instance, near the flange, the external wheel (high wheel) contact angle increases suddenly due to the wheel profile. The normal force increases and the transverse force changes its direction due to the significant contribution of the spin effect (large contact angle). Beyond this position, the lateral contact force is produced by the projection of the transverse load in the lateral direction, but chiefly with the contribution of the normal load.

When a tangential force is applied to a body in contact with another, due to local deformation, a resultant reaction force develops in the opposite direction (friction force). This produces a parallel strain field all over the contact zone. When a couple force (or a moment) that is orthogonal to the contact plane is applied through the bodies in contact, a tangential deformation will also be produced. This generates a polar strain field all over the contact zone.

When a circular body subjected to a moment rolls about an axis parallel to a flat surface, due to geometric constraints, the strain grows along the contact zone, until the tangential stress

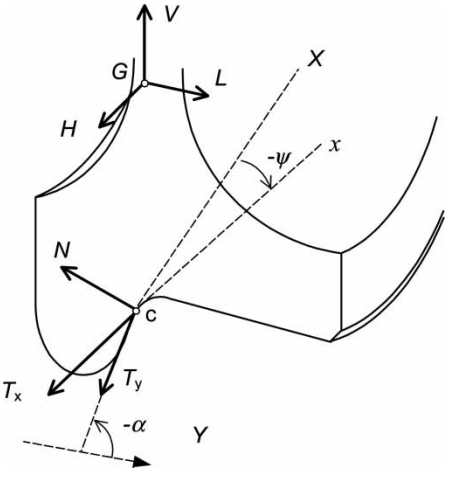

Figure 2. Wheel-free body diagram.

reaches a limit. This limit is a function of the normal stress (usually elliptical distribution) and the friction coefficient between the surfaces in contact (Coulomb relationship). If the rolling axis is not parallel to the surface, a spin effect is added.

Actually, for a conical surface body as the railway wheel tread, the rolling contact process produces a polar strain field in the contact zone. This local strain field is a function of the relative velocity between each body particle in contact. The orientation of this field produces a pole whose location depends on the longitudinal and lateral components of the relative velocity and rotation speed between bodies (spin). This small relative velocity, normalised by the translation speed, is called creepage.

The contact force $\vec{T}$ produced in the contact path is composed of three orthogonal components, expressed in the $C\,\vec{i}\,\vec{j}\,\vec{k}$ moving frame, C being the centre of the contact ellipse, unit vector $\vec{k}$ perpendicular to the contact plane and the unit vector $\vec{j}$, inclined of angle α with respect to the vertical (contact plane is formed by $\vec{i}$ *and* $\vec{j}$), as shown in Figure 4:

$$\vec{T} = T_x\,\vec{i} + T_y\,\vec{j} + N\,\vec{k}. \tag{3}$$

The components of the tangential contact force and spin moment are determined based on the knowledge of the longitudinal, transverse and rotational (*spin*) creepages, as shown in Figure 3. Taking the linear Kalker proposition [10], valid only for infinitesimal creepages, one gets:

$$T_x = -(G\,ab\,C_{11})\,\upsilon_x, \tag{4}$$

$$T_y = -(G\,ab\,C_{22})\,\upsilon_y - (G\,(ab)^{3/2}\,C_{23})\,\phi, \tag{5}$$

$$M_z = -(G\,(ab)^{3/2}C_{32})\,\upsilon_y - (G\,(ab)^2\,C_{33})\,\phi, \tag{6}$$

where terms υ_x, υ_y and ϕ are the longitudinal, transverse and spin creepages, respectively, a, b are the semi-axes of the ellipse dimensions, G is the transverse elasticity modulus and C_{11}, C_{22}, C_{23} and C_{33} are the Kalker creep coefficients [11]. Expression (4) shows that the longitudinal force (T_x) is proportional to the longitudinal creepage (υ_x). The constant of proportionality is the slope at origin (inclination). Expression (5) shows that the lateral force (T_y) is composed of two terms: one due to lateral creepage (υ_y) and the other produced by rotational surface spin creepage (ϕ), which is related to the contact angle. The second term arises from the spin pole location that may be outside the centre of the contact ellipse, depending on the creepage combination. In Kalker's simplified theory [10] based on the elasticity in the contact region,

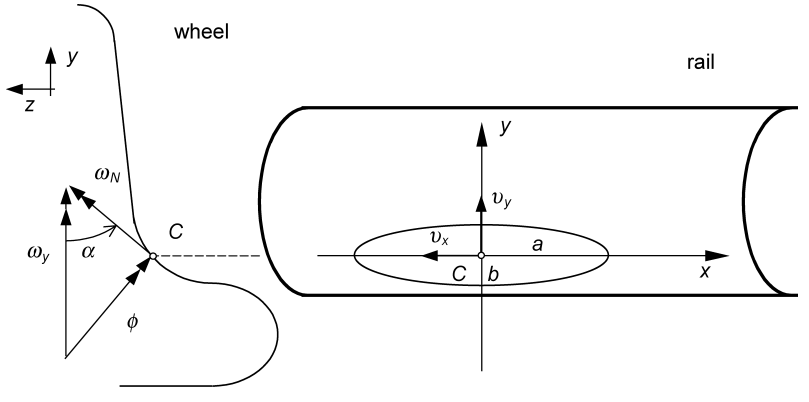

Figure 3. Creepages identification.

an algorithm (FASTSIM) was derived to express the lateral contact force with these creep contributions. Therefore, the deformation field produced by the spin effect will generate a lateral force and a couple moment [10,12]. Considering that the contact dimensions are very small, the contact moment M_z can be neglected.

Adopting the classic kinetic Coulomb's friction relationship, inter-body tangential components $\vec{T} = \vec{T}_x + \vec{T}_y$ in the contact plane will be limited by the normal force as:

$$\vec{T} \leq (\mu\, N)\, \vec{t}, \tag{7}$$

where $\vec{t} = \vec{T}/|\vec{T}|$ is a unit vector towards the tangential force. This means that the capacity to produce tangential force is reached, or saturated, when:

$$|\vec{T}| = \sqrt{T_x^2 + T_y^2} = \mu\, N. \tag{8}$$

It is also possible to represent the tangential force limit with a cone. This cone has a radius base of $\mu\, N$ and a high N, forming an angle β (arc tan μ), as shown in Figure 4 [13]. When the tangential force is greater than the circle radius (friction limit), the bodies will slide against each other into the $\vec{t}$ direction, resulting from the tangential components T_x and T_y proportion ($\tan\theta = T_y/T_x$). Note that now the longitudinal contact force T_x takes part in this limit.

During a severe directioning condition, as entering into a tight curve at a high speed, the external wheel will always produce longitudinal force due to the lateral wheelset displacement and the difference between the rolling radius of each wheel. At the contact path, the maximum contact force available should be partitioned between the longitudinal and transverse components. Longitudinal force will be positive ($T_x > 0$) and increases until saturation occurs. For each direction separately, adhesion limit will be mutually affected by the other force component. To show this effect, one can calculate the normalised lateral force as a function of the normalised lateral creepage (-0.1 to 0.1) for a given ellipse eccentricity. This effect is shown in Figure 5, obtained using the FASTSIM algorithm [10] for longitudinal creepage (υ_x or *nux**100) values varying from 0 to 0.001. For a longitudinal creepage of 1% (*nux* = 1%) and a lateral creepage of -1% (*nuy* = 1%), the adhesion capacity reduces to $\sqrt{2}/2$ (70.7% of the maximum lateral force) for an ellipse eccentricity (a/b) of 3.12, as can be observed in Figure 5.

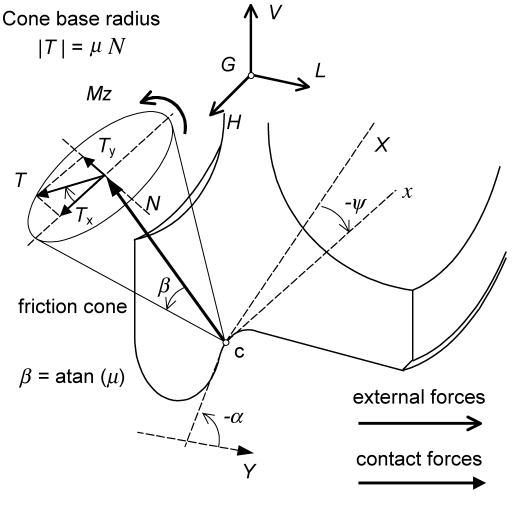

Figure 4. Contact forces and friction cone.

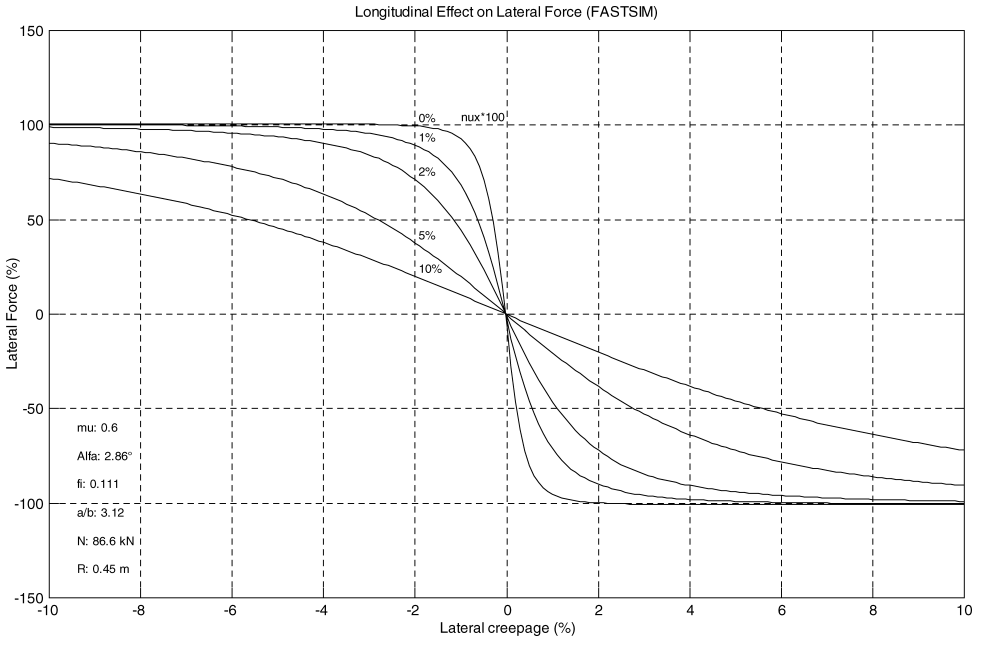

Figure 5. Effect of longitudinal creepage on the lateral force.

The nonlinearity of the curves is due to the gradual saturation of the surface adhesion, which is discretised in the FASTSIM algorithm. Values adopted for this calculation are: $\mu = 0.6$ (or mu), wheel tread angle $\alpha = 2.68$ (conicity of 1:20), spin creepage $\phi = 0.111$ (or phi), ellipse eccentricity $a/b = 3.12$, normal load $N = 86.6$ kN and wheel radius $R = 0.45$ m.

As presented in Equation (5), the total transverse contact force (T_y) is the sum of two terms: one side force term (T_s) related to the lateral creepage and an additional force term (T_ϕ) related to the components of the spin creepage, as stated in Barbosa [9]. For the outer wheel, the term T_ϕ, referred to here as the couple force term, has a lateral direction and an outward sense, and is expressed as:

$$T_y \cong T_s + T_\phi. \tag{9}$$

Therefore, the spin effect also contributes to the transverse direction. This effect is shown in Figure 6, equivalent to a derailment situation, with a high spin creepage due to the maximum contact angle (70° for the wheel profile – see also Gilchrist [2]). For instance, in the same situation described before (1% creepage in each direction), the negative lateral force will decrease to 10% with a spin creepage of -2.1 (typical for the S-1002 wheel profile). The total lateral force is shifted to 50% from the free spin creepage value, at 2% translational creepage values. On the brink of a wheelset derailment, lateral creepage is small, with the dominance of the spin effect. As the contact path is submitted to lateral and spin creeps, the lateral force is a combination of both effects and depends on the instantaneous rotation centre. Difficulties arise when it is necessary to split the lateral creep contribution from the spin effect.

Values adopted for this calculation are: $\mu = 0.6$ (or mu), maximum wheel flange angle $\alpha = -70^\circ$ (contact angle for the S-1002 wheel profile and UIC 60 rail), severe spin creepage $\phi = -2.09$ (or phi), high ellipse eccentricity $a/b = 6.14$, normal load $N = 86.6$ kN and wheel radius $R = 0.45$ m.

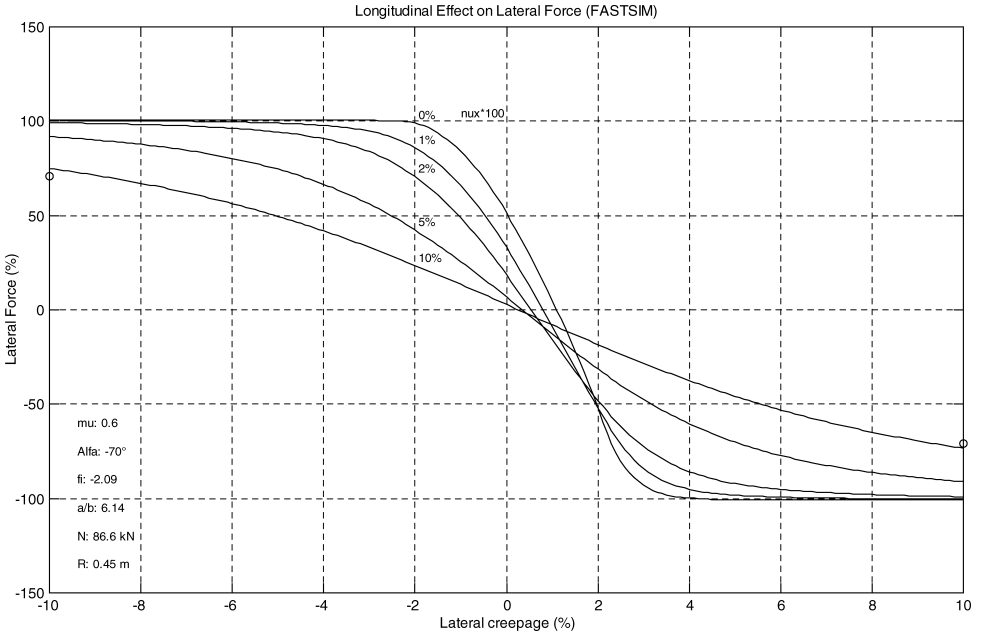

Figure 6. Effect of the spin creepage on the lateral force.

3. Wheelset model and force ratios

A simplified wheelset representation for a dynamic study is a single rigid body planar model with four degrees of freedom in the longitudinal, lateral, vertical and angular directions, as shown in Figure 7. Only the single body model is approached to focus on the wheel–rail contact aspects. Therefore, limitations of this study will be related to the inter-wheelset and bogie effects. The second-order ordinary differential equation for this model, expressed in a matrix form, for a constant translational speed moving reference frame O*XYZ* attached to the bogie frame, $[M]\{\ddot{q}\} + [C]\{q\} = ([T]^* + [F])$ [14], is described as:

$$\begin{bmatrix} m & 0 & 0 & 0 \\ 0 & m & 0 & 0 \\ 0 & 0 & m & 0 \\ 0 & 0 & 0 & J_{Gz} \end{bmatrix} \begin{bmatrix} \ddot{x} \\ \ddot{y} \\ \ddot{z} \\ \ddot{\psi} \end{bmatrix} + \begin{bmatrix} c_x & 0 & 0 & 0 \\ 0 & c_y & 0 & 0 \\ 0 & 0 & c_z & 0 \\ 0 & 0 & 0 & k_{qz} \end{bmatrix} \begin{bmatrix} x \\ y \\ z \\ \psi \end{bmatrix} = \begin{bmatrix} T_x \\ T_y \\ N \\ M_z \end{bmatrix}^* + \begin{bmatrix} F_x \\ F_y \\ F_z \\ M_e \end{bmatrix}. \quad (10)$$

The force vector is composed of the wheel contact force $\boldsymbol{T}$ and yaw moment, both expressed in the wheelset referential frame, and the external lateral load F_y that promotes the derailment. In the vertical direction, Hertizian contact elasticity is neglected and the vertical contact force is assumed to be equal to F_z. The wheels are coupled as a rigid body (no independent rotating movement is allowed) and the wheelset roll is not taken into account. Note that the bogie effects that increase the wheelset yaw angle (ψ) are not included in this simplified model.

The components of the contact force are a function of the creepages. The creepages of the wheel contact path are described in the function of the wheelset attitude (y, ψ). The longitudinal, side and spin creepage components for the wheelset with a constant translational

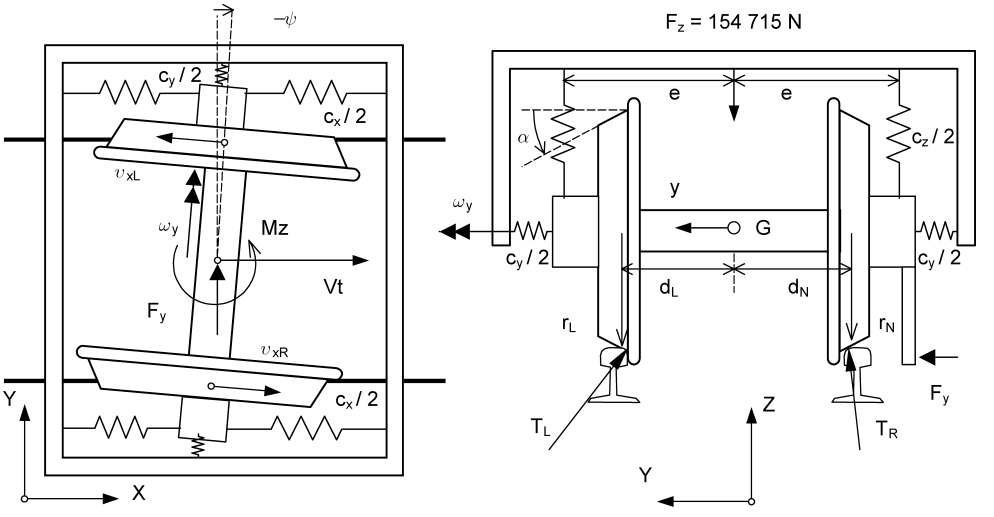

Figure 7. Wheelset model, external forces and creepage.

speed (V_t) are described in the inertial reference frame as:

$$\upsilon_{xL,xR} = \frac{V_t - \omega\, r_{L,R} \cos\psi \mp \dot{\psi}\, d_{L,R}}{V} \rightarrow$$

$$\upsilon_{xL,xR} = \frac{\omega\, r_n - \omega\,(r_n + \Delta r_{L,R}) \cos\psi}{\omega\, r_n} \mp \frac{\dot{\psi}\, d_{L,R}}{V}, \tag{11}$$

$$\upsilon_{sL,sR} = \frac{V_y - \omega\, r_{L,R}\, \sin\psi}{V} \rightarrow \upsilon_{sL,sR} = \frac{\dot{y} - \omega\,(r_n + \Delta r_{L,R})\, \sin\psi}{\omega\, r_n}, \tag{12}$$

$$\phi_{L,R} = \frac{\omega_y\ \sin\alpha_{L,R}}{V} \rightarrow \phi_{L,R} = \frac{\sin\alpha_{L,R}}{r_n}, \tag{13}$$

where r_L, r_R, and d_L, d_R, are the left, right and nominal wheel radii and the corresponding distances from the contact points to the wheel centre. Value r_n is the nominal radius at tape line. Values Δr_L and Δr_R are the left and right wheel instantaneous rolling radii variation in function of the lateral displacement (y) and for a small angle of attack (ψ). The angle of the contact plane (α) and the proportions of the contact ellipses (a/b) are obtained from a table of pre-processed contact properties, in function of the lateral displacement of the wheelset.

When a derailment is bound to occur, at a steady-state condition ($\dot{x}$, $\dot{y}$ and $\dot{\psi}$ are constant, $\ddot{z} = 0$ and $F_x = M_e = 0$), the solution for the system of differential equations can be obtained from the system:

$$\begin{bmatrix} c_x & 0 & 0 & 0 \\ 0 & c_y & 0 & 0 \\ 0 & 0 & c_z & 0 \\ 0 & 0 & 0 & k_{qz} \end{bmatrix} \begin{bmatrix} x \\ y \\ z \\ \psi \end{bmatrix} = \begin{bmatrix} T_x \\ T_y \\ N \\ M_z \end{bmatrix}^{*} + \begin{bmatrix} 0 \\ F_y \\ F_z \\ 0 \end{bmatrix}. \tag{14}$$

The contact forces are a function for the Kalker coefficients and the following creepages:

$$\upsilon_{xL,xR} = \frac{\Delta r_{L,R} \cos\psi}{r_n} \rightarrow \upsilon_{sL,sR} = \frac{\Delta r_{L,R}\, \sin\psi}{r_n} \rightarrow \phi_{L,R} = \frac{\sin\alpha_{L,R}}{r_n}. \tag{15}$$

The moment equilibrium at a steady-state condition is obtained from the longitudinal contact force and allows the identification of the wheelset yaw angle:

$$M_z = T_{xL}\, d_L + T_{xR}\, d_R \rightarrow T_{xL}\, d_L + T_{xR}\, d_R = \psi\, k_{qz} \rightarrow \psi = \frac{T_{xL}\, d_L + T_{xR}\, d_R}{k_{qz}}, \qquad (16)$$

where k_{qz} is the angular stiffness of the suspension ($k_{qz} = c_x e^2$).

The three contact force components (T), expressed in the contact plane moving frame, can be transformed to the wheelset referential frame with the help of the finite rotation matrix [$\boldsymbol{R}$] successively about yaw angles ψ and contact angle α resulting in $\vec{T}^* = [R]\ \vec{T}$. This transformation also projects the external forces $\vec{F}$, producing a nonlinear algebraic equation for the normal contact force (N) needed to calculate the ellipse ration and Kalker coefficients, and is solved using the Newton's interaction method.

$$R = \begin{bmatrix} \cos\psi & -\sin\psi & 0 \\ (\cos\alpha \sin\psi) & (\cos\alpha \cos\psi) & -\sin\alpha \\ (\sin\alpha \sin\psi) & (\sin\alpha \cos\psi) & \cos\alpha \end{bmatrix}. \qquad (17)$$

To solve the contact forces and identify the ratio between the components of the contact force (k_x and k_y) needed for the 3D formula, the formulation proposed by Polach [15] is taken. It expresses each lateral force component through an ellipsoidal to a hemispheric transformation. Polach described the contact force components as:

$$T = \iint_U \tau \, \mathrm{d}x \, \mathrm{d}y, \quad T_x = T\frac{\upsilon_x}{\xi}, \quad T_y = T\frac{\upsilon_y}{\xi}, \qquad (18)$$

where U is the contact area and υ_x, υ_y and ξ are creepages in each direction, and the creep magnitude is described as:

$$\xi = \sqrt{\upsilon_x^2 + \upsilon_y^2}. \qquad (19)$$

The total lateral creepage is composed of two parcels due to the side creepage (υ_s) with the addition of the spin effect (ϕ), which depends on the length $\boldsymbol{a}$ of the contact ellipse and is stated as:

$$\upsilon_y = \upsilon_s + a\phi \rightarrow \upsilon_y = \upsilon_s + a\frac{\sin\alpha}{r_n} \qquad (20)$$

for $a\phi > 0$.

The longitudinal contact force for a given friction coefficient is obtained from:

$$T_x = -\frac{2}{\pi}\mu\, N \left(\frac{\varepsilon_x}{1+\varepsilon_x^2} + \arctan\varepsilon_x\right) \frac{\upsilon_x}{\xi}. \qquad (21)$$

The lateral contact force is then obtained from the two components, due to the sideslip movement and spin effect, stated as:

$$T_y = T_s + T_\phi, \qquad (22)$$

$$T_s = -\frac{9}{16}\mu N K_M \frac{\upsilon_s}{\xi} \text{ and } T_\phi = -\frac{9}{16} a\mu N K_N [1 + 6.3(1 - e^{-a/b})]\frac{\phi}{\xi}, \qquad (23)$$

$$K_{M,N} = |\varepsilon_{s,\phi}| \left(\frac{\delta^3}{3} - \frac{\delta^2}{2} + \frac{1}{6}\right) - \frac{1}{3}\sqrt{(1-\delta^2)^3} \text{ and } \delta = \frac{\varepsilon_{s,\phi}^2 - 1}{\varepsilon_{s,\phi}^2 + 1}, \qquad (24)$$

$$\varepsilon_{x,s} = \frac{1}{4}\frac{\pi GabC_{M,N}}{\mu N}\xi \text{ and } \varepsilon_\phi = \frac{8}{3}\frac{Gb\sqrt{ab}}{\mu N}\frac{C_{23}\upsilon_y}{1 + 6.3(1 - e^{-a/b})}, \qquad (25)$$

Table 1. Wheelset attitude and contact force ratios (ADH algorithm).

Friction	Yaw (mrad)	T_x (kN)	T_y (kN)	N (kN)	F_y (kN)	k_x	k_y
0.1	− 0.151	8.61	0.5	251	235	− 100	− 0.92
0.2	− 0.299	16.8	1.0	248	232	− 48.0	− 4.00
0.3	− 0.446	25.1	5.1	237	221	− 33.7	− 7.82
0.4	− 0.590	33.1	13.1	216	198	− 27.3	− 11.8
0.5	− 0.725	40.7	23.3	188	168	− 24.4	− 15.0
0.6	− 0.835	46.9	33.5	161	139	− 23.2	− 17.5
0.7	− 0.911	51.1	42.6	138	115	− 22.7	− 19.7
0.8	− 0.938	52.8	46.5	97	62.5	− 19.7	− 19.1

where C_M and C_N are:

$$C_M = C_N = \sqrt{\left(C_{11}\frac{\upsilon_x}{\xi}\right)^2 + \left(C_{22}\frac{\upsilon_s}{\xi}\right)^2}. \tag{26}$$

The longitudinal/side force ratio $k_x = T_x/T_s$ is obtained from:

$$\frac{T_x}{T_s} = \frac{9}{8\pi}\frac{1}{K_M}\left(\frac{\varepsilon_x}{1+\varepsilon_x^2} + \arctan\,\varepsilon_x\right)\frac{\upsilon_x}{\upsilon_s}. \tag{27}$$

The couple/side force ratio $k_y = T_\phi/T_s$ is obtained from:

$$\frac{T_\phi}{T_s} = a\frac{K_N}{K_M}[1 + 6.3(1 - e^{-a/b})]\frac{\phi}{\upsilon_s}. \tag{28}$$

Finally, to obtain the wheelset attitude and contact forces for different friction coefficients, one has to solve the rearranged system:

$$[C^*]\{q\} = [F] \rightarrow \{q\} = [C^*]^{-1}[F], \tag{29}$$

where [$\boldsymbol{C}$*] is the rigidity matrix augmented with the contact forces, T*, components that are a function of the system coordinates. The results obtained for the interactive solution of this system are presented in Table 1.

The maximum contact angle ($\alpha = 2.17$ radians or 70°) at the derailment limit corresponds to a wheelset lateral displacement of $y = 6.17$ mm, due to the geometric constraint of the wheel/rail profiles.

Note that the maximum reported value for the yaw angle is always negative (orthogonal line with the wheelset axis pointing inside the track). Contact properties used in the equations are obtained off-line in a geometric algorithm [14] for the wheel–rail profile pair S-1002 and UIC-60.

4. Safety limit

The 3D analytical formula proposed by this author [9] is used to calculate the safety limits. This formulation extends the functionality of the traditional Nadal expression with the inclusion of the longitudinal force and spin effect on it. The safety limit that relates lateral to vertical

Table 2. Safety results for different friction coefficients.

Friction coefficient	Yaw (mrad) FASTSIM	*L/V* FASTSIM	Yaw (mrad) ADH	*L/V* ADH	*L/V* – 3D formula	3D formula/ FASTSIM
0.1	– 0.158	2.51	– 0.151	2.69	2.75	+ 9.6 %
0.2	– 0.310	2.25	– 0.299	2.66	2.65	+ 17.7 %
0.3	– 0.460	1.98	– 0.446	2.53	2.31	+ 16.6 %
0.4	– 0.610	1.76	– 0.590	2.26	1.85	+ 5.1 %
0.5	– 0.758	1.58	– 0.725	1.92	1.48	– 6.4 %
0.6	– 0.904	1.48	– 0.835	1.59	1.22	– 17.5 %
0.7	– 1.040	1.31	– 0.911	1.31	1.04	– 20.7 %
0.8	– 1.180	1.14	– 0.937	0.72	0.89	– 22.0 %

contact force on the wheel is stated as:

$$\frac{L}{V} = \frac{A\mu - B\tan\alpha}{B + A\mu\tan\alpha}, \tag{30}$$

where term A is strongly related to angular wheelset orientation (yaw angle) and term B is connected solely to a force relationship and is described as:

$$A = k_x \sin\psi + (1 + k_y)\cos\psi, \tag{31}$$

$$B = \sqrt{k_x^2 + 1 + 2k_y + k_y^2}, \tag{32}$$

and $k_x = T_x/T_s$ is a longitudinal/side force relation explicitly related to the yaw angle and $k_y = T_\phi/T_s$ is a couple/side ratio explicitly related to the spin effect. The values of the yaw angle and contact force ratio (k_x and k_x) are calculated for a steady-state condition of the wheelset on the verge of a derailment, as described in the previous section. Different from other empirical or curve-fitting methods [5,8], Equation (30) is based on the 3D contact mechanics that includes vertical, lateral, longitudinal and spin contributions. The advantage of this criterion is that the longitudinal and spin effects are explicitly incorporated into the analytical 3D formula, as clearly evidenced in earlier expressions, extending the planar Nadal proposition and better reasoned than other empirical curve-fitting approximations. Values using the ADH algorithm by Polach [15] are presented in Table 1. The safety limits determined with the 3D formula for different values of friction coefficients are presented in Table 2.

5. Typical derailment simulation

For comparative purposes, a lateral force quasi-static derailment simulation was performed with different adherence conditions based on the benchmark proposed by Pascal, in IAVSD [16]. The wheelset differential equation for a validated wheelset model [14] as described in Section 3, running at 30 m/s, is used for simulation purpose. The wheelset mass is 1,887 kg and a vertical load of 154,715 N is applied downwards at the wheelset centre, as shown in Figure 8. The suspension angular rigidity is 8.16×10^7 mN/rad.

The wheelset derailment simulation is performed with a slowly increasing lateral force F_y (at the rate of 50 kN per second) applied to the wheelset at tread level (no vertical load transference to the external wheel is produced). The dynamic simulation is repeated for different values of friction coefficients (μ varying from 0.1 to 0.8). The quasi-static derailment is considered when the maximum contact angle reaches 70° (S-1002 wheel profile). The two contact algorithms are used in the numeric simulations: FASTSIM by Kalker [10] and ADH by Polach [15].

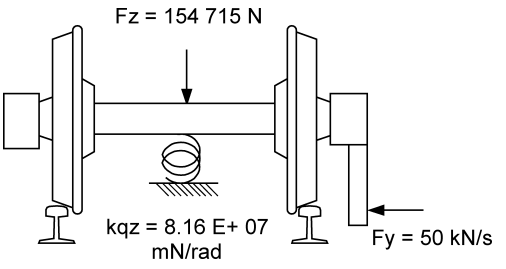

Figure 8. Wheelset model and external force.

A typical simulation result is presented in Figure 9, using the ADH algorithm, performed with a friction coefficient of 0.6. In this figure, the forces described on the contact plane are: longitudinal, transverse and normal (T_x, T_y, N). The projected forces on the wheelset reference frame are: lateral and vertical (L and V). As the external lateral load is applied at the rail level, the reactive vertical load is almost constant (86.6 kN), as can be observed in Figure 9 (no load transfer is present).

The contribution contact forces of the changes suddenly after flanging (before 0.5 s). The longitudinal force (T_x) increases to a stable level. Transverse force (T_y) starts with positive value (due to the wheel tread inclination), changes to negative (lateral creepage) and, after flanging, the transverse force becomes positive again, due to the spin contribution (increase in the contact angle). The normal contact load (N) starts increasing after flanging, absorbing a substantial part of the lateral load. Simulation finishes when the contact angle reaches 1.22 radians (contact angle values presented in Figure 9 are multiplied by 100),

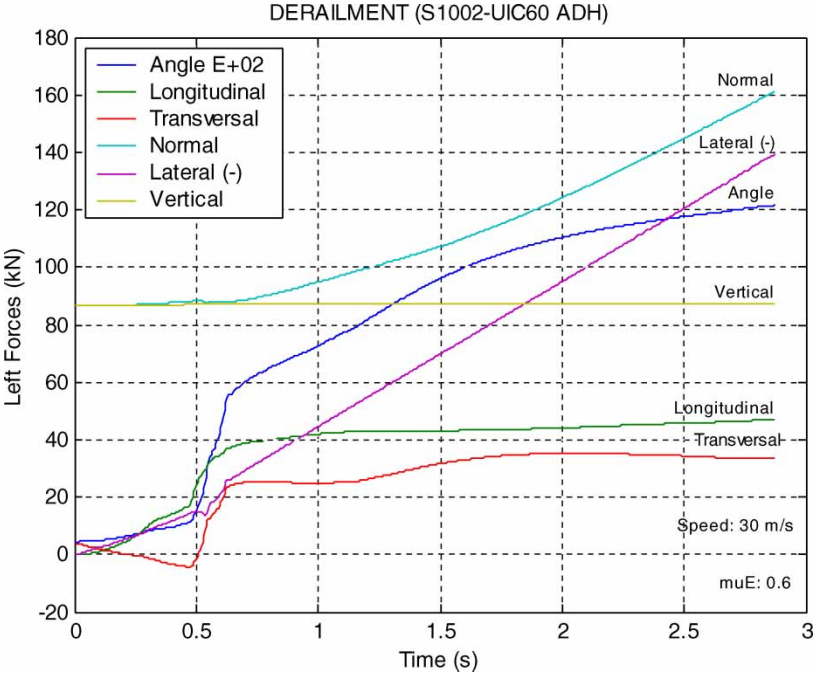

Figure 9. Derailment simulation results (algorithm ADH, $\mu = 0.6$).

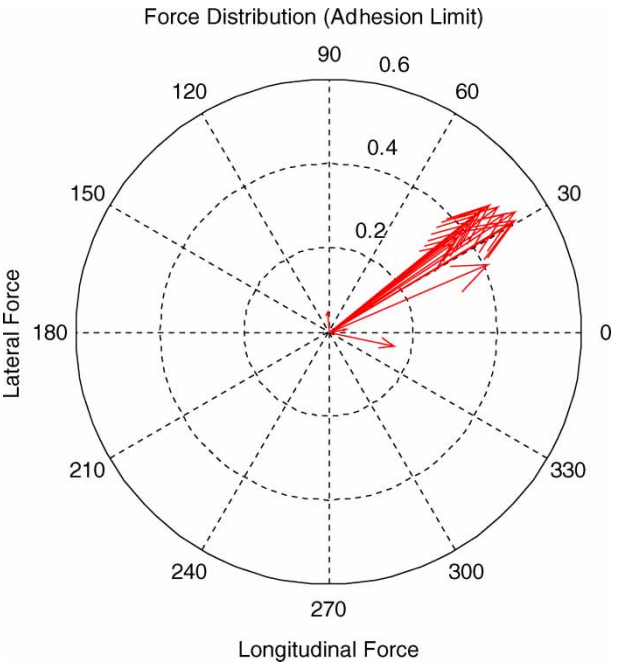

Figure 10. Normalised lateral and longitudinal force distribution (ADH, $\mu = 0.6$).

which is considered a derailment condition (equivalent to the S-1002 maximum wheel profile angle of 70°).

The contact force distribution changes substantially after flanging, when the contact properties modify suddenly, as can be seen in Figure 9. Wheelset oscillations on this region depend on the friction coefficient (contact rigidity and saturation) and travelling speed (creep contact damping).

It can be observed that the maximum longitudinal contact force is around 48 kN and the maximum transverse contact force is 34 kN, resulting in a tangential contact force magnitude of 58.8 kN. The polar graph of Figure 10 shows the magnitude of the tangential contact force (the red vector) normalised by the normal force (N). The external circle is the maximum normalised tangential force corresponding to the selected friction coefficient (in this case, $\mu = 0.6$). The maximum normal force at the derailment is 161 kN and, considering the coefficient of friction of 0.6, the available adherence is 99.6 kN. It is observed that the proportion between lateral and longitudinal forces at the derailment moment is almost constant (between 30° and 40°). Considering a mean angle of 30 between the tangential forces, the maximum lateral force is 50% of the saturation limit.

Similar behaviour is seen for the derailment simulation of the wheelset in the same conditions, but using the FASTSIM algorithm. The results are presented in Figure 11.

Some small differences are observed between results from different contact algorithm (ADH presented in Figure 9 and FASTSIM, in Figure 11). Particularly, the value for the lateral load, which affects the safety value, is 12% smaller than that calculated with the ADH algorithm. The tangential contact forces keep their magnitude and direction around 30° (between 20° and 40°, as presented in Figure 12). This angle can justify some types of railhead defects (head check).

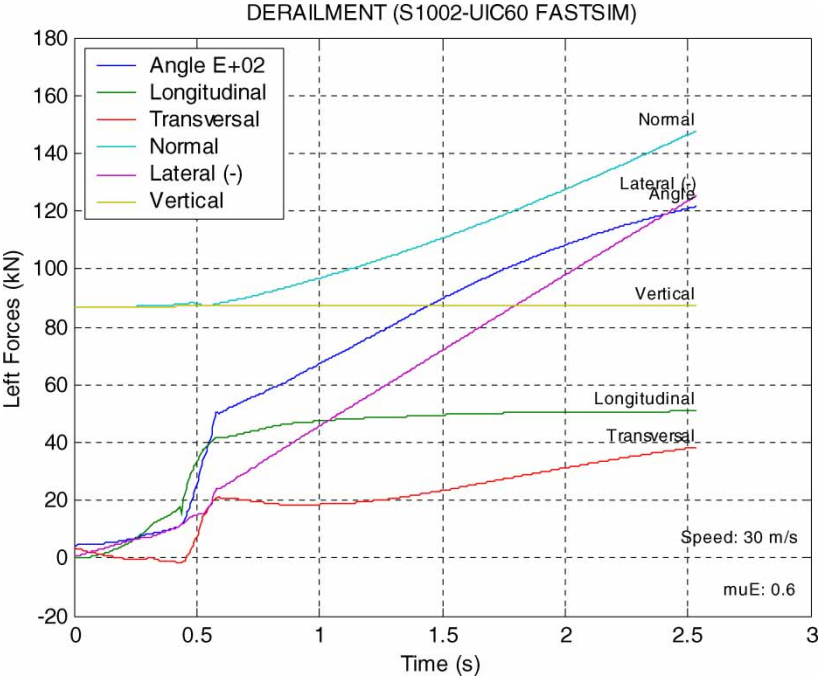

Figure 11. Derailment simulation results (algorithm FASTSIM, $\mu = 0.6$).

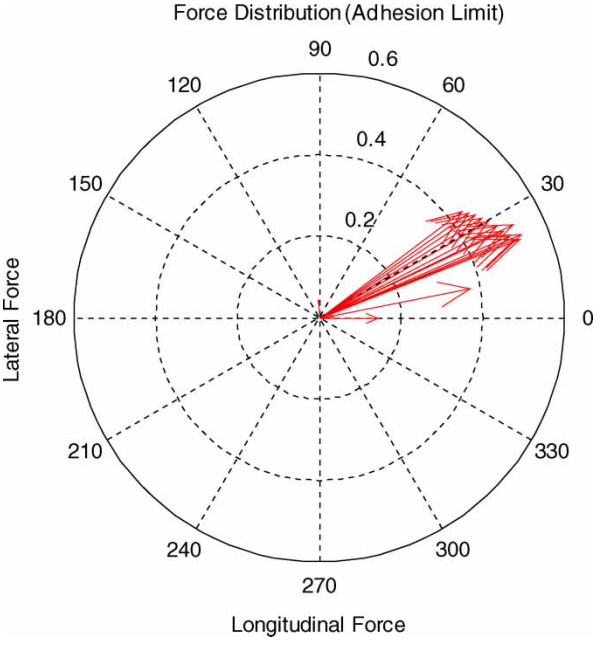

Figure 12. Normalised lateral and longitudinal force distribution (FASTSIM, $\mu = 0.6$).

6. Results comparison and analysis

The derailment (L/V) results obtained for the numeric simulation with the two contact algorithms (ADH and FASTSIM) and the safety limit calculated with Nadal and the 3D formula, for different friction coefficients, are presented in Table 2. In general, all values calculated are greater than the traditional Nadal values (from 40% to 60% greater), confirming the known Nadal conservative aspect.

Figure 13 presents the L/V values, as a function of friction coefficient from the five sources according to Table 2. Three of them are numeric simulation results with ADH and FASTSIM algorithms and the Pascal benchmark results in [16], and two are safety limits obtained from the traditional Nadal formula (rolling without slip formula, from Equation (1)) and the 3D formula (Equation (10) – red line).

It is observed that for high values of friction, the ADH algorithm produces smaller values of L/V during the numeric simulation when compared with the FASTSIM algorithm. This behaviour is also observed in the 3D formula results that are within $\pm 20\%$, when compared with the values of the simulation with FASTSIM (last column of Table 2). These differences seem to be associated to the simplification of the ADH algorithm, which produces deviations of less than 30% for severe creepage condition, when spin is present [15].

Comparison has been made with the results published by Parena [3] (Figure 6a on page 161, European Project – DYSAF). It is observed that the results calculated here are greater than the ones published from other simulation packages (Vampire, Mecano, Medyna). In those papers, results are closer to the Nadal's values, probably due to a forced large angle of attack (15 mrad) produced with an additional external torque and the criteria for characterisation of the point of derailment (the maximum L/V and the maximum first derivative of the wheel profile).

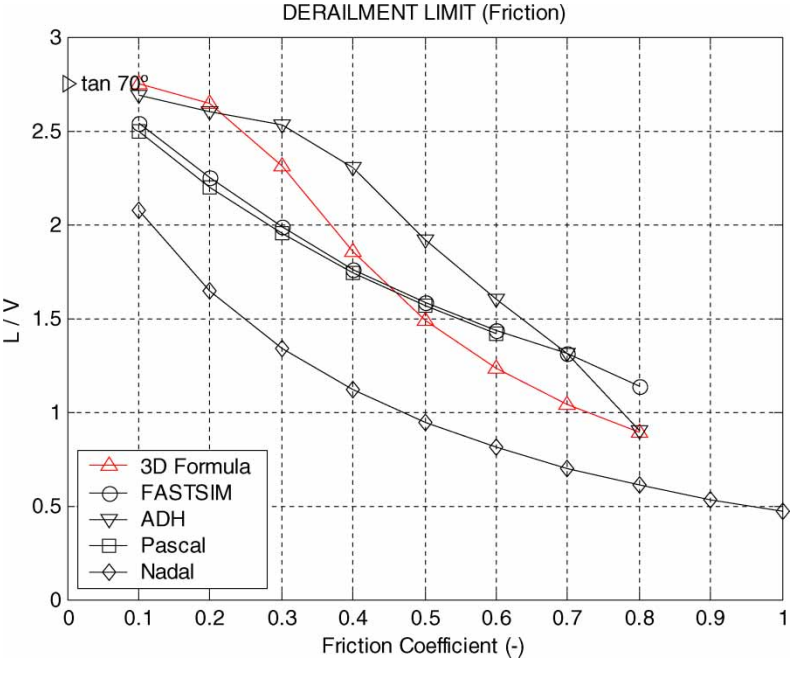

Figure 13. Results of comparison (simulations with FASTSIM, ADH and Pascal; Nadal's safety limits and 3D formula).

Recent publications of experimental data, obtained from full-scale roller rig [6,7] for derailments controlling the yaw angle, lateral force and inter-wheel load transfer, present only results for derailments with variable yaw angle and constant friction coefficients. Although the results presented here are for a small yaw angle, the 3D formula can calculate safety L/V limits for any yaw angle and friction coefficient unrestrictedly, as can be observed in Equations (30) and (31).

7. Discussion

In a large creepage situation, typical for a railway wheelset derailment, a substantial part of the contact patch is subjected to slip due to the tangential adhesion saturation of the surfaces. An algorithm to handle spin effect is strongly recommended for this situation. The ADH algorithm by Polach allows easy separation of the force components and, due to its simplicity, has been used to calculate the force ratios.

Either sustaining lateral force or during a curve segment, longitudinal wheel contact force is always present. This absorbs part of the available adhesion capacity, as shown in Figure 5. Therefore, part of the available lateral force is reduced as well. Note that also for a longitudinal creepage of 1%, the maximum lateral force will be 70%, as expected for a 1% lateral creepage. For longitudinal creepage of 2%, lateral force decreases to 50%.

The contribution of the lateral and spin creepages for the composition of the transverse contact force is presented in Figure 6. A closer look at the composition of transverse force due to the spin creepages reveals that, in the case of small lateral creepage, typical of a steady-state derailment, the lateral force may act in the opposite direction (40% of the maximum adherence). This phenomenon is observed in Figure 9, after wheel flanging.

It is interesting to observe the combination of the longitudinal and transverse contact forces during the simulation. They produce an almost constant angle of 30°, as shown in Figures 10 and 12. The situation presented in Table 2 will change with the introduction of other external effects. For instance, when the bogie negotiates a curve, a suspension moment acts at the wheelset in addition to the lateral force. Therefore, the bogie with stiffer longitudinal suspension and larger wheel spacing in a small radius curve will produce a large angle of attack. Additionally, the angle of direction of the tangential force can justify some types of railhead defects (head check).

In experimental field track tests, vertical and lateral wheel loads are measured with calibrated instrumented wheelset. Usually, the longitudinal force is indirectly measured from the axle torque, and the wheelset angle of attack with respect to the track alignment is very difficult to be measured on-board. The lateral force is measured through several strain-gage *wheatstone* bridges, installed in the wheel plate, and there is no known method or post-processing algorithm with the ability to split the side-and-spin effects of the measured lateral force. However, there is the possibility of composing the side-and-spin effect in the 3D analytical formula to compute a reliable analytical safety limit to confront with the experimental measurements, which is the goal of this research.

As this study is deliberately limited to a single wheelset analysis, the inter-wheelset and bogie suspension effects are not considered. Therefore, a large negative angle of attack is not expected with this model, except in the case of low angular suspension stiffness. An additional case is calculated with the suspension angular stiffness reduced to 3.0×10^6 mN/rad. The friction coefficient is set to 0.5 and the yaw angle results in -10 mrad. Complete results are presented in Table 3 and the safety limit is determined with the 3D formula results in $L/V = 0.979$, close to the Nadal's value.

Finally, it should be pointed out that this study is limited to a single wheelset described with a simplified model (roll and vertical movements are not considered). The complete bogie with

Table 3. Wheelset attitude and contact force ratios (ADH algorithm).

Friction	Yaw (mrad)	T_x (kN)	T_y (kN)	N (kN)	F_y (kN)	k_x	k_y
0.5	− 10.43	32.2	19.2	247	225	− 0.2537	− 1.88

the interaction between wheelsets that will produce large yaw angles in a curve and the entire vehicle suspension system is the next step of this research.

8. Conclusion and final remarks

The fundamentals associated with the dynamic behaviour of a railway wheelset in a severe unsafe condition (derailment) were presented. The contact force components, including the longitudinal and spin effects were identified in a steady-state condition on the verge of a derailment. The contact force ratios were used in the 3D formula to calculate the safety limits. A validated wheelset model was employed to simulate its behaviour in a derailment with different adhesion conditions. The simulation results obtained were compared with the published results and the safety limits for validation purposes.

Simulation results have a reasonable agreement with the numerical results published by Pascal [16] and are greater than the traditional Nadal formula [1], as expected. Results show that the safety limits calculated with the 3D analytical formula present consistent agreement with simulations at medium friction, as can be observed in Figure 13. The results also show a variation within 20% when compared with the simulation results using FASTSIM, for all ranges of friction coefficients. These differences seem to be associated with the simplification of the ADH algorithm, which produces deviations of less than 30% when the spin effect is present [15].

External force substantially changes the wheelset attitude and the contact forces contributions. This fact introduces additional aspects in the traditional formulation, which is exclusively geometric and adhesion-dependent. It is therefore recommended to explore different derailment scenarios, including the bogie (wheelset suspension interaction) and a complete vehicle with two bogies, to get broad credited values for the safety limit (L/V).

Acknowledgements

The author would like to thank the Mechanical Department of the Escola Politécnica da Universidade de São Paulo (EP-USP) in São Paulo, Brasil, and Companhia Vale do Rio Doce – VALE, for support to this research.

References

[1] M.J. Nadal, *Locomotives a Vapeur. Collection Encyclopedie Scientific, Biblioteque de Mechanic Appliquee et Genie*, Paris, 1908, p. 186.

[2] A.O. Gilchrist and B.V. Brickle, *A re-examination of the proneness to derailment of a railway wheel-set*, J. Mech. Eng. Sci. – ImechE 18(3) (1976), pp. 131–141.

[3] D. Parena, W. Kik, N. Kuka, W. Masmoudi, and W. Kik, *Derailment simulation, parametric study*, in *Proceedings of 16th IAVSD Symposium*, Pretoria, South Africa, Vehicle Syst. Dynam. (1999), pp. 155–167.

[4] NF-EN-14363 Norme Européenne, *Essais en vue de l'homologation du comportement dynamique des véhicules ferroviaires, Part E : Railway applications – testing for the acceptance of running characteristics of railway vehicles – testing of running behavior and stationary tests*, AFNOR, France, 2005, p. 110.

[5] W. Kik, R. Menssen, D. Moelle, B. Bergander, and V. Vincent, *Comparison of results of calculations and measurements of DYSAF-test, a research to investigate safety limits of derailment at high speeds*, J. Vehicle Syst. Dynam. 37(Suppl.) (2002), pp. 543–553.

[6] F. Braghin, S. Bruni, and G. Diana, *Experimental and numerical investigation on the derailment of a railway wheelset with solid axle*, Vehicle Syst. Dynam. 44(4) (2006), pp. 305–325.
[7] H. Ishida, T. Miyamoto, E. Maebashi, H. Doi, K. Iida, and A. Furukawa, *Safety assessment for flange climb derailment of trains running at low speed on sharp curves*, Q. Rep. RTRI 47(2) (2006), pp. 65–71.
[8] J. Zeng and Q.H. Guan, *Study on flange climb derailment criteria of a railway wheelset*, J. Vehicle Syst. Dynam. 46(3) (2008), pp. 239–251.
[9] R.S. Barbosa, *A 3D contact force safety criterion for flange derailment of a railway wheel*, J. Vehicle Syst. Dynam. 42(5) (2004), pp. 289–300.
[10] J.J. Kalker, *A fast algorithm for the simplified theory of rolling contact (FASTSIM program)*, Vehicle Syst. Dynam. 11 (1982), pp. 1–13.
[11] J.J. Kalker, *On the rolling contact of two elastic bodies in the presence of dry friction*, PhD Thesis, Deft, The Netherlands, 1967.
[12] Z. Farkas, G. Bartels, T. Unger, and D.E. Wolf, *Frictional coupling between sliding and spinning motion*, Phys. Rev. Lett., Am. Phys. Soc. 90(24) (2003), pp. 1–4.
[13] R.S. Barbosa, *Safety criterion for railway vehicle derailment*, in *Proceedings of the 8th International Heavy Haul Conference, International Heavy Haul Association – IHHA*, CVRD, Rio de Janeiro, Brasil, 2005, pp. 477–484.
[14] R.S. Barbosa, *Aplicação de Sistemas Multicorpos na Dinâmica de Veículos Guiados*, PhD Thesis at University of São Paulo EESC-USP, São Paulo, Brasil, 1999, p. 273.
[15] O. Polach, *A fast wheel-rail forces calculation computer code*, Vehicle Syst. Dynam. 33 (1999), pp. 728–739.
[16] J.P. Pascal, *Benchmarks for multibody simulation software – first railway benchmark*, International Association of Vehicle Systems Dynamics – IAVSD, INRETS, France, 1991.

8.9 ANEXO I

A 3D CONTACT FORCE SAFETY CRITERION FOR
FLANGE CLIMB DERAILMENT OF A RAILWAY WHEEL

Barbosa, R. S. (2004) A 3D Contact Force Safety Criterion for Flange Climb Derailment of a Railway Wheel. International Journal of Vehicle System Dynamics, DOI: 10.1080/0042311042000266711, Vol.: 42, nº 5, p. 289-300.

Vehicle System Dynamics
2004, Vol. 42, No. 5, pp. 289–300

Taylor & Francis
Taylor & Francis Group

A 3D Contact Force Safety Criterion for Flange Climb Derailment of a Railway Wheel

ROBERTO SPINOLA BARBOSA[1]

SUMMARY

A revision on the railway safety criteria evolution has shown that the fundamentals of wheel/rail contact phenomena have not been completely addressed. Limitations encountered on the available criteria for safety against derailment have motivated a deeper analysis on the wheel rolling mechanism. The contact mechanics were completely modelled with two tangential components, lateral and longitudinal forces, including spinning effects. An extended three-dimensional formula for the railway wheel flange climb derailment process is derived. Results show that calculated values agree with the classical formulation, and extend its application. This formulation allows the identification of *L*/*V* limit values for a three-dimensional rolling-contact mechanism. It can help to identify more reliable limits, relocating the safety margin for the dynamic operation of a railway vehicle.

1. INTRODUCTION

A number of different variations of the railway wheel flange climb derailment safety limit [1–4] have been proposed since the elegant Nadal's criterion, stated in 1908 [5]. His well-known *L*/*V* formula is based on the lateral (*L*) and vertical (*V*) contact forces equilibrium in a transversal plane section of the wheel. Experimental measurements on reduced scale laboratorial devices [4], on track with instrumented wheel-set [1, 6] and running with special truck [6–8], have been conducted to validate this criterion for railway vehicles on traffic. Although contested [9] and criticized [10, 11], Nadal's *L*/*V* criterion seems conservative [7–9, 11, 12], and supposedly works well for large angles of attack [1] or large friction coefficients [2]. Many authors have manipulated the *L*/*V* formula introducing different factors to justify unexpected higher values found on experimental measurements. For instance, time of lateral force duration [3, 4, 6], lateral cross effect between wheels [2], angle of attack [1, 8, 9], roll moment and angle [4], and

[1]Address correspondence to: Roberto Spinola Barbosa, Department of Mechanical Engineering of Escola Politécnica da Universidade de São Paulo (EP-USP), Av. Prof. Mello Moraes, 2231, São Paulo 05508-900, SP, Brasil. E-mail: roberto.barbosa@poli.usp.br

Vehicle System Dynamics
ISSN 0042-3114 print; ISSN 1744-5159 online
http://www.tandf.co.uk/journals
DOI: 10.1080/0042311042000266711

friction coefficient [7, 8] have been evaluated, in an attempt to appropriately represent the derailing phenomenon. Revision on the safety criteria evolution has shown that the fundamentals of wheel/rail contact nature have not been completely addressed. Limitations encountered on the available criteria for safety against derailment has motivated a deeper analysis on the rolling contact mechanism, pushing the development of a three-dimensional wheel/rail contact mechanical model, including longitudinal force and spin contact effect, producing a new formulation for the derailment safety limit.

2. NATURE OF THE DERAILMENT

The railway wheel derailing process is a very complex dynamic phenomenon. In a rigid wheel-set, the coned wheel tread performs two main tasks: a) centering the wheel-set on tangent track and b) providing curve inscription. The ability of curve negotiation is related to the tread conicity and the lateral gap between wheel flange and railhead. When a curve is accessed, out-side lateral wheel-set displacement is induced by the natural track geometry and vehicle centrifugal forces. Vehicle inertia and truck suspension forces interact, aiming at an equilibrium position. Assuming a stable steady-state constant speed configuration, a new wheel-set attitude (side displacement and yaw angle) will be reached, producing the necessary wheel/rail contact force for the equilibrium of the lateral centrifugal force. Due to conicity, the out-side wheel will increase its relative longitudinal velocity at contact point, producing a longitudinal force. Even in the absence of longitudinal acceleration, wheel-set lateral displacement is always associated with a couple of longitudinal forces produced by the constraint due to the radius difference between each wheel of a rigid wheel-set.

In the imminence of a derailment, large centrifugal forces have to be reacted through lateral contact forces. Considering a lateral sliding mechanism, vehicle inertial forces have to be retained with contact reaction friction forces to avoid wheel flange to climb the railhead (derailment limit). High contact angle in the outer wheel and consequent spinning between the wheel and rail are expected. Actually, a wheel derailing process is a dynamic combination of tangential forces associated with surface contact saturation. Lateral contact force is composed of a transversal effect and a spinning effect produced by the projection of the wheel rotation in the contact plane. Longitudinal and normal forces are prone to react at the contact surface, also. These effects make up the force scenario at the contact surface to be analysed.

3. PROBLEM FORMULATION

A moving, tri-orthogonal reference frame $O\vec{X}\vec{Y}\vec{Z}$, attached to the wheel-set centre with $\vec{X}$ axis aligned to the velocity vector was selected to describe its position in a

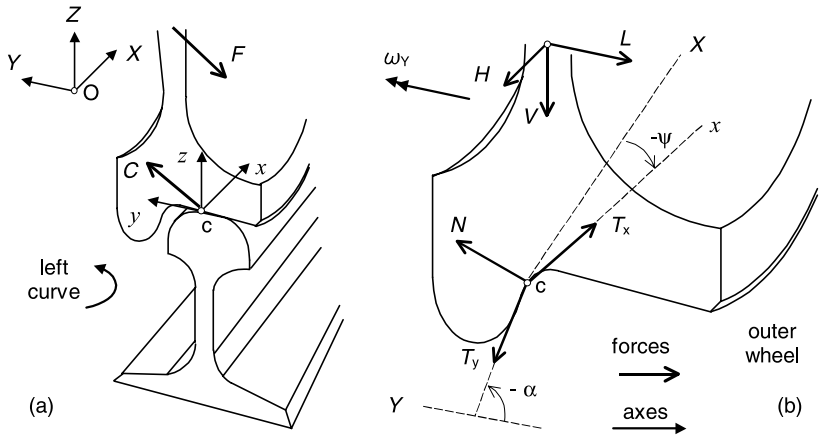

Fig. 1. a) Reference and auxiliary frames, b) external forces, contact and yaw angles.

curve, as shown in Figure 1a. The plane defined by $\vec{Y}\vec{Z}$ axes is vertical and contains the curve centre. Since the selected reference frame is accelerated, Newton's law provides the following expression for the wheel-set,

$$M(\vec{a}_{rel} + \vec{a}_{drag} + \vec{a}_{cor}) = \vec{F}_{ext}, \tag{1}$$

where M is the mass of the wheel-set considered as a rigid body, $\vec{a}_{rel}$ is the relative acceleration, $\vec{a}_{drag}$ the drag acceleration and $\vec{a}_{cor}$ the coriolis acceleration parcels, respectively. External forces $\vec{F}_{ext}$ come mainly from gravitational force $\vec{F}_g$, all wheel-set/suspension links forces $\vec{F}_s$ and wheel/rail contact forces $\vec{C}$. The longitudinal momentum and gyroscopic effects are neglected in the present analysis. Identifying the contact force for each wheel, and considering $\vec{a}$ the absolute acceleration, Equation (1) yields $(M\vec{a} - \vec{F}_s - \vec{F}_g - \vec{C}_{inner}) = \vec{C}_{outer}$, assuming a circular left curve of constant radius and a stable steady-state trajectory at a constant tangential speed. Quasi-static outer wheel equilibrium results in $\vec{F} + \vec{C}_{outer} = \vec{0}$ whose right hand side should vanish (or simply $-\vec{F} = \vec{C}$). The components of the external forces on the wheel, expressed on the $O\vec{X}\vec{Y}\vec{Z}$ reference frame are $\vec{F} = -(H\vec{X} + L\vec{Y} + V\vec{Z})$. Considering only one contact point, contact force components $\vec{C}' = T_x\vec{x} + T_y\vec{y} + N\vec{z}$ are expressed in another tri-orthogonal auxiliary frame $c\vec{x}\,\vec{y}\,\vec{z}$, originating at the contact point c, as shown in Figure 1b. The $\vec{y}\,\vec{z}$ plane is vertical and coincident with the wheel-set axle. The origin c is movable with the contact point. The $\vec{z}$ axis is chosen to be perpendicular to the contact plane. When the contact point moves along the wheel tread on the $\vec{y}\,\vec{z}$ plane, this auxiliary reference frame turns with respect to the $\vec{x}$ axis, changing the contact plane angle α. For a wheel-set rotational movement with respect to the $\vec{Z}$ axis, a yaw angle ψ is produced between $\vec{X}$ and $\vec{x}$ axes. Angles are conventioned positive counter-clockwise, according to the right-hand-rule.

To transform contact force $\vec{C}'$ (expressed in the auxiliary frame) to the wheel-set reference frame, a finite rotation matrix $[R]$ is used, obtained by two successive rotations about contact angle α and yaw angle ψ, expressed by,

$$R = \begin{bmatrix} \cos\psi & -sin\,\psi & 0 \\ (\cos\alpha\, sin\,\psi) & (\cos\alpha\cos\psi) & -sin\,\alpha \\ (sin\,\alpha\, sin\,\psi) & (sin\,\alpha\cos\psi) & \cos\alpha \end{bmatrix}. \tag{2}$$

Wheel-set roll angle is usually very small and is also neglected in this analysis. Taking into account the components of the resultant contact forces $-\vec{F} = [R]\vec{C}'$, three quasi-static equilibrium equations are obtained,

$$H = \cos\psi\, T_x - sin\,\psi\, T_y \tag{3}$$

$$L = (\cos\alpha\, sin\,\psi)T_x + (\cos\alpha\cos\psi)T_y - sin\,\alpha\, N \tag{4}$$

$$V = (sin\,\alpha\, sin\,\psi)T_x + (sin\,\alpha\cos\psi)T_y + \cos\alpha\, N. \tag{5}$$

These equations disclose the influence of the longitudinal contact component (T_x) on its respective projections due to the yaw angle (ψ) and contact angle (α). When the usual *L/V* ratio in a transversal wheel section is performed from Equations (4) and (5), an augmented equation is obtained,

$$\frac{L}{V} = \frac{(\cos\alpha\, sin\,\psi)T_x + (\cos\alpha\cos\psi)T_y - sin\,\alpha\, N}{(sin\,\alpha\, sin\,\psi)T_x + (sin\,\alpha\cos\psi)T_y + \cos\alpha\, N}. \tag{6}$$

Note that for the typical outer wheel profile, angle α between the contact plane and the horizontal plane is negative, according to the counter-clock-wise angle convention.

4. TANGENTIAL CONTACT FORCES OF ROLLING AND SPINNING BODIES

When a tangential force is applied to a body in contact with another body, as a result of local deformation, a reaction resultant force develops in the opposite direction. When a couple force (or a moment) is applied through bodies in contact, a tangential deformation will also be produced. For a cylindrical rolling body, points in contact may stay together inside the contact zone, due to local elastic micro deformation. This produces a parallel strain field in the contact zone. The strain grows along the contact zone until the tangential stress reaches a limit that is a function of the normal stress and the friction coefficient between the surfaces in contact. In fact, for a conical surface body, the rolling contact process simultaneously produces a parallel and a polar strain field in the contact area. This local strain field is a function of the relative

velocity between each particle of the bodies in contact. Orientation of this field produces a pole whose location depends upon the relative lateral velocity and rotation speed between bodies (spin). This small relative velocity, normalized by the translation speed, is called creepage.

Rolling contact mechanics has been extensively studied in the 1970's. From Kalker's linear theory [13], the components of tangential contact force are determined based on the knowledge of the longitudinal, lateral and rotational (spin) creepages,

$$T_x = -(G\,ab\,C_{11})\upsilon_x \tag{7}$$

$$T_y = -(G\,ab\,C_{22})\upsilon_y - (G\,ab^{3/2}\,C_{23})\phi \tag{8}$$

terms υ_x, υ_y and ϕ are the longitudinal, lateral and spin creepages respectively, *ab* are the ellipse dimensions, G is the transversal elasticity modulus and C_{11}, C_{22} and C_{23} are the creep coefficients, respectively. Expression (7) shows that the longitudinal force (T_x) is proportional to the longitudinal creepage (υ_x). Differently, Expression (8), shows that the lateral force (T_y) is composed by two terms: one due to lateral creepage (υ_y) and the other produced by rotational surface spinning creepage (ϕ) which is related to the contact angle. The second term arises from the spin pole location that may be outside the center of the contact ellipse, depending on the creepage combination. Therefore, the deformation field produced by the spinning effect will generate a couple force.

It is assumed in this work that the total lateral contact force (T_y) is the sum of two terms: one transversal force term (T_L) related to the lateral creepage and a force term (T_ω) related to the components of the spin creepage. The term T_ω, here called couple force term, has a lateral direction and an outward sense.

$$T_y \cong T_L + T_\omega. \tag{9}$$

To reinforce this assumption, a tangential stress distribution field was calculated using the well-known and accepted computer code developed by Kalker [14] called FASTSIM. This algorithm computes tangential stress distribution over the contact surface, based on known longitudinal, lateral and rotational (spin) creepages. Surface is discretized and a local strain for each element is determined. Normal stress is an ellipsoidal *hertzian* function and maximum tangential load value is limited by Coulomb's dry friction relationship. Therefore, for a complex deformation state, elements of the surface may be in different adhesion conditions (slip or stick). Figure 2 shows the results of three creepage conditions: a) lateral creepage, b) spinning creepage and c) both effects together. Contact surface was discretized with a 12×15 element mesh. The arrow in each element represents the magnitude and the direction of tangential stress field.

The lateral creepage (Figure 2a) produces a net lateral force around 50% of available saturation ($T_L = 14$ kN, for $\upsilon_y = -0.625 \times 10^{-3}$). Each element of the surface, with

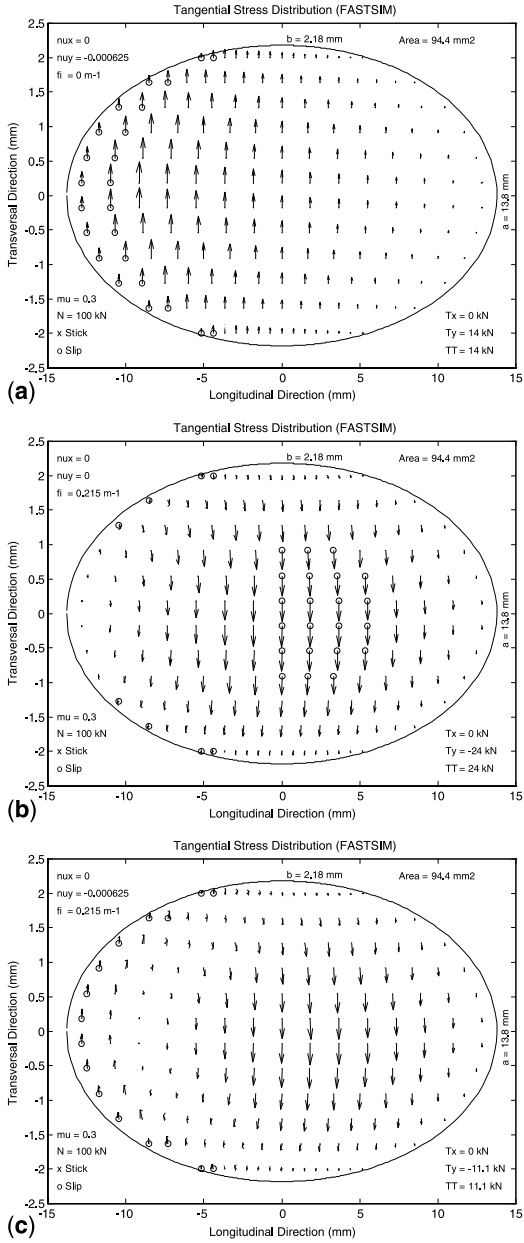

Fig. 2. a) Lateral creepage, b) spin creepage, c) both effects together.

stress lower than the maximum allowable value, will remain stuck. After that, any stress increment will produce slip between elements in contact (a circular symbol is used to indicate slipping element).

Figure 2b presents the spin creepage results. This produces almost all the available lateral couple force ($T_\omega = -24$ kN for $\phi = 0.215$) on the negative axis sense due to the rotation direction. Under these conditions, the spin pole is out of the contact path. Figure 2c shows results for the same lateral and spin creepages together. It can be noted that both effects superimposed produce a resulting total lateral force that is approximately the sum of each effect ($T_y = -11$ kN). The spin pole changes its position into the contact area due to the combined creepages.

A bi-dimensional contact routine [15] based on FASTSIM algorithm was used to identify ellipse size for a particular relative lateral position of the wheel/rail pair, individual element stress (arrow) and slip-stick condition, as shown in Figure 2. This numerical solution considered a 0.472 m wheel radius and a typical rail of 0.080 m head radius (other curvatures are infinite), resulting in an ellipse ratio $a/b = 6.33$ (or $b/a = 0.158$). Also, a normal wheel load of 100 kN, a longitudinal creepage $\upsilon_x = 0.0$ and a friction coefficient $\mu = 0.3$ were adopted.

5. COMPLETE SURFACE FRICTION AND SATURATION

Modelling the contact forces as a macro three-dimensional phenomenon and adopting the classic kinetic Coulomb's friction relationship, inter body tangential components $\vec{T} = T_x\vec{x} + T_y\vec{y}$ of contact force $\vec{C}'$ is a vector quantity limited by normal force $N\vec{z}$, and described by,

$$\vec{T} \leq (\mu N)\vec{t}, \tag{10}$$

where μ is the friction coefficient between surfaces, and $\vec{t} = \vec{T}/|\vec{T}|$ is a unit vector towards tangential force. This means that the capacity of producing tangential force is reached, or saturated, when $|\vec{T}| = \mu N = \sqrt{T_x^2 + T_y^2}$. Above this value, the bodies will slide against each other into $\vec{t}$ direction. Note that longitudinal contact force T_x takes part in this limit. As mentioned before, in the contact plane, lateral force is composed by a transversal component T_L and a couple component T_ω arising from the moment and assuming the linear expression (9) $T_y = T_L + T_\omega$, we obtain,

$$\sqrt{T_x^2 + (T_L + T_\omega)^2} = \mu N. \tag{11}$$

Making use of a contact force ratio k_x related to the longitudinal force and a ratio between lateral force components k_y, Expression (11) can be normalized to,

$$T_L\sqrt{k_x^2 + 1 + 2k_y + k_y^2} = \mu N, \tag{12}$$

where $k_x = T_x/T_L$ is a longitudinal/transversal force relation and $k_y = T_\omega/T_L$ a couple/transversal ratio. Inspecting term k_y carefully, we conclude that this relationship should be negative and greater than unit to promote flange climb. Observe that T_ω is a function of the contact angle (that will have a maximum for a given wheel/rail pair) and angular velocity and ϕ will be constant for a steady state.

6. PROPOSED NEW FLANGE CLIMB CRITERION

Using the three-dimensional contact equilibrium forces depicted earlier in Equations (4) and (5), the normal force N obtained in (12) and introduced in Expression (6) of the L/V ratio, we finally obtain a new extended formula:

$$\frac{L}{V} = \frac{A\mu - B\tan\alpha}{B + A\mu\tan\alpha}, \tag{13}$$

where terms A and B are described by,

$$A = k_x \sin\psi + (1 + k_y)\cos\psi \qquad B = \sqrt{k_x^2 + 1 + 2k_y + k_y^2}. \tag{14}$$

Inspecting these terms, it is found that term A is strongly related to angular wheel-set orientation (yaw angle) and term B is related solely with forces relationship.

Evaluating L/V function behaviour from Equation (13), Figure 3 is obtained for a fixed triad μ, α and ψ. A graph is plotted along k_x variation in the abscissa and the L/V

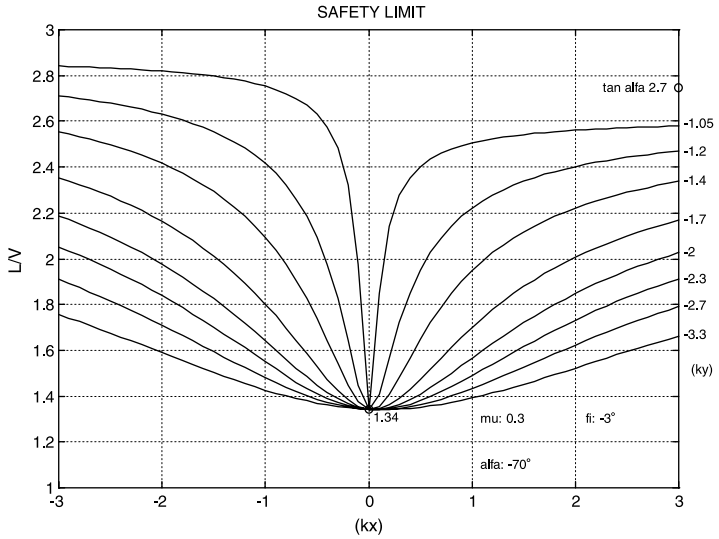

Fig. 3. Safety limit (function of k_x and k_y).

limit in the ordinate. Each line of this graph corresponds to a different value of k_y, identified on the left. Observe that the greater the longitudinal force, the greater the *L/V* limit. The bigger the spin contribution (k_y), the smaller the limit. Values on the left side of this graph are larger than the ones on the right side due to the yaw angle (ψ) adopted. Note that k_y (T_ω/T_L) is negative and bigger than the unit, due to T_ω being opposite and greater than T_L that is positive (against flange climbing process). The adopted friction coefficient is $\mu = 0.3$, contact angle $\alpha = -70^\circ$ and yaw angle $\psi = -3^\circ$ (-52 mrad).

One practical example of application of this formula would be a vehicle whose wheel-set assumes in a curve a yaw angle of -3° due to its suspension characteristics. Due to vehicle dynamics, contact forces produce a longitudinal and lateral ratio of $k_x = 1.0$ and $k_y = -1.2$. In this situation, the *L/V* safety limit will be 2.22 (assuming a wheel/rail profiles with maximum α of -70° and friction coefficient of 0.3).

7. DISCUSSION

If no longitudinal effect is considered $k_x = 0$ and $\psi = 0$, coefficients A and B of Expression (14) are reduced to $A = 1 + k_y$ and $B = \sqrt{(1 + k_y)^2}$. Therefore, for any value of $k_y < (-1)$, due to the square it will produce $B = -A$. Considering this configuration and observing that the contact angle α is negative, Equation (13) assumes the elegant form as described by Nadal [5]. This is the conservative value ($L/V = 1.34$) observed in the ordinate of Figure 3 for a null abscissa ($k_x = 0$), which depends only on μ and α (classical *L/V* limit). If, additionally, the couple effect is neglected, $k_y = 0$ and Expression (14) produces $A = B$. In this case, the denominator of Expression (13) becomes a subtraction since α is negative. This expression was identified in [4, 11, 15, 16] nevertheless, these authors have not explored it in depth. In this situation, when ($\mu \tan \alpha$) tends to unit, *L/V* tends to infinity and bodies will stick. This physically happens because, for a given *V*, the projection of *L* on the contact plane (function of α) increases the normal component (N) and reduces the lateral one (T_y) and contact adhesion will not be saturated. Therefore, sliding will not occur. If, for any reason, surface adhesion becomes saturated (for example, due to a high longitudinal force), no additional tangential force can be sustained. This is equivalent to having an additional adhesion capacity expressed by $\mu_{ad} = 0$, due to which Equation (13) becomes $L/V = \tan \alpha$, as found in [9, 16] confirming asymptotic behavior of curves in Figure 3, increasing the *L/V* limit for high values of $|T_x|(k_x = T_x/T_L)$.

Contact forces are non-linear functions, especially the relations between the transversal effects and the couple moment on the composition of the lateral force. As defined, ratios k_x and k_y relate longitudinal and couple to transversal forces. They are

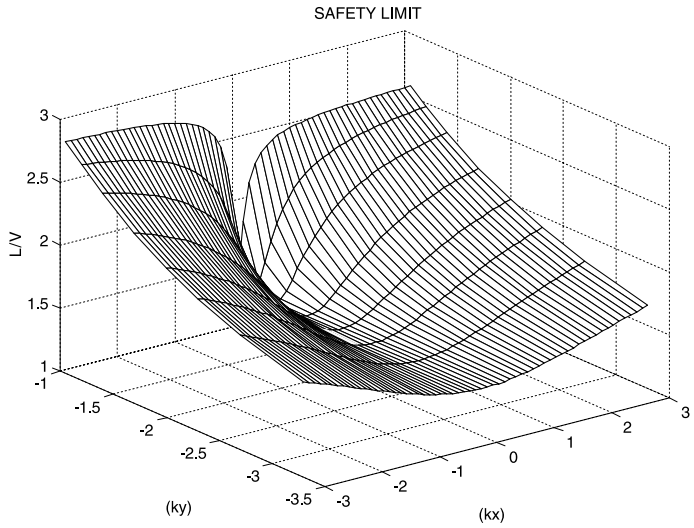

Fig. 4. Three-dimensional surface representation of the safety limit.

not independent functions. A vehicle dynamic behavior will produce a relationship between yaw angle, longitudinal and lateral forces for a boundary derail situation. This will locate a point on the surface shown on the space of Figure 4, defining a *L/V* limit.

The *L/V* Equation (13) may be developed only with the longitudinal effect (k_x). Although the inclusion of the couple and transversal effects (k_y) make the equation more complex, it will reveal the richness of the creep composition on the contact surface, better identifying each contribution.

8. CONCLUDING REMARKS

A review of the evolution on the derailment criteria was performed. Results of experimental measurements published found unexpected higher values for the *L/V* relationship, near the derailment condition. Limitations encountered on the available criteria has motivated a deeper analysis of this mechanism. Rolling contact phenomena were treated in the three-dimensional space including longitudinal forces. The contact mechanics were completely modelled with two tangential components and including spinning effects. This produced a three-dimensional formula for the railway wheel flange climb derailment process.

It is noted that the spinning effect has a decisive contribution to the flange climb-up process in a derailment, dragging wheels up the railhead against transversal retention.

Additionally, longitudinal force reduces the available adhesion capacity on the contact, restricting the climb-up ability and increasing the *L*/*V* limit. Therefore, they must be included in the equilibrium force equations in the complete formulation of derailment proneness. For given wheel/rail profiles and contact properties (α and μ) Equation (13) will produce a particular *L*/*V* surface as in Figure 4. For a given dynamic vehicle scenario (wheel-set properties, suspension configuration, track geometry and vehicle speed), a wheel-set attitude (lateral displacement and yaw angle) will produce a line intersection with this surface outlining a boundary of safety limits.

The new formula range is compatible with the elegant traditional conservative criterion (Nadal) and extends its functionality with three-dimensional parameters. Safety limits obtained are greater than the classical ones, being consistent with experimental measurements published. This formulation allows the determination of *L*/*V* values for a three-dimensional rolling-contact mechanism for a broad class of vehicle dynamic scenarios. It can help to identify more reliable limits, relocating the safety margin for the dynamic operation of a railway vehicle.

ACKNOWLEDGEMENTS

The author would like to thank his colleagues from the Dynamic Group of the Mechanical Department for their generosity in sharing their knowledge, especially Prof. Raul Gonzalez Lima, for patient reading of the manuscript and valuable advice. Thanks to the Escola Politécnica da Universidade de São Paulo (PME-EP-USP) for support provided and also to the Instituto de Pesquisa Tecnológicas do Estado de São Paulo (IPT), Brasil.

REFERENCES

1. Elkins, J. and Wu, H.: Angle of Attack and Distance-Based Criteria for Flange Climb Derailment. *Vehicle Syst. Dyn.* 33(Suppl.) (1999), pp. 293–305.
2. Weinstock, H.: Wheel Climb Derailment for Evaluation of Railway Vehicle Safety. Paper no. 84, WA/RT-1, *ASME*, Winter Annual Meeting, USA, 1984.
3. Matsudaira, T.: Dynamic of a High Speed Rolling Stock. Japan National Railway. *RTRI, Quarterly Reports*, Special Issue, Japan, 1963.
4. Sweet, L.M. and Karmel, A.: Evaluation of Time Duration Dependent Wheel Load Criteria for Wheelclimb Derailment. *J. Dyn. Syst., Meas. Cont.* 103 (1981), pp. 219–227.
5. Nadal, M.J.: Locomotives a Vapeur. Collection Encyclopedie Scientifique. *Biblioteque de Mecanique Appliquee et Genie*, 186, Paris, France, 1908.
6. Kik, W., Menssen, R., Moelle, D., Bergerder, B.: Comparison of Results of Calculations and Measurements of DYSAF-tests, A Research Project to Investigate Safety Limits of Derailment at High Speeds. *Vehicle Syst. Dyn.* 37(Suppl.) (2002), pp. 543–553.

7. Nagase, K., Wakabayashi, Y., Sakahara, H.: A Study of the Phenomenon of Wheel Climb: Results of Basic Experiments Using Model Bogies. In: *Proceedings of the Institution of Mechanical Engineers – ImechE, Part F, London. Journal of Rail and Rapid Transit* 216 (2002), pp. 237–247.
8. Takai, H., Uchida, M., Muramatsu, H., Ishida, H.: *Derail Safety Evaluation by Analytic Equations*. Japan National Railway, RTRI, Quarterly Reports, Japan, 43(3) 2002.
9. Gilchrist, A.O. and Brickle, B.V.: A Re-Examination of the Proneness to Derailment of a Railway Wheel-Set. *J. Mech. Eng. Sci. – ImechE*, 18(3) (1976), pp. 131–141.
10. Elkins, J.A. and Carter, A.: Testing and Analysis Techniques for Safety Assessment of Rail Vehicle: The State-of-the-Art. *Vehicle Syst. Dyn.* 22 (1993), pp. 185–208.
11. Blader, F.B.: Assessing Proximity to Derailment from Wheel/Rail Forces: A Review of State of Art. *ASME*, Winter Annual Meeting, CA, USA, 1989.
12. Pascal, J.P.: First Railway Benchmark to Test Wheel/Rail Contact Forces – Results of *VOCO*. *IAVSD* Benchmarks for Multibody Simulation Software, Paris, France, 1991.
13. Kalker, J.J.: Survey of Wheel-Rail Rolling Contact Theory. *Vehicle Syst. Dyn.* 5 (1979), pp. 317–358.
14. Kalker, J.J.: A Fast Algorithm for the Simplified Theory of Rolling Contact. *Vehicle Syst. Dyn.* 11 (1982), pp. 1–13.
15. Barbosa, R.S.: Aplicação de Sistemas Multicorpos na Dinâmica de Veículos Guiados. Ph.D. theses at University of São Paulo, São Paulo, Brasil, 1999, 273 pp.
16. Parena, D., Kik, W., Kuka, N., Masmoudi, W., Kik, W.: Derailment Simulation, Parametric Study. In: *Proceedings of 16th IAVSD Symposium*. Pretoria, South Africa. *Vehicle Syst. Dyn.* 33(Suppl.) (1999), pp. 155–167.

8.10 ANEXO J

MODELING OF A RAILWAY VEHICLE TRAVELLING THROUGH A TURNOUT

Santos G. F. M.; Barbosa, R. S. (2016) Modeling of a Railway Vehicle Travelling Through a Turnout. Proceedings of the Institution of Mechanical Engineers, Part F: Journal of Rail and Rapid Transit, DOI: 10.1177/0954409715595256, Vol.: 230, Issue nº 4, pp. 1397-1404.

Case Study

Institution of MECHANICAL ENGINEERS
Journal of RAIL AND RAPID TRANSIT

Proc IMechE Part F:
J Rail and Rapid Transit
2016, Vol. 230(4) 1397–1404

DOI: 10.1177/0954409715595256
pif.sagepub.com
SAGE

Modeling of a railway vehicle travelling through a turnout

Guilherme FM dos Santos[1] and Roberto S Barbosa[2]

Abstract

Speed and safety are two key objectives in the operation of a railway. On double-line railways, such as the Estrada de Ferro Vitoria Minas (EFVM), a critical situation occurs when a train changes between lines, this should occur at the maximum allowed speed. However, the iron ore trains consisting of GDE-type wagons that operate on the EFVM perform this operation at 60 km/h, which is 5 km/h less than the maximum speed allowed under normal operating conditions. Thus, the brakes need to be applied over a long distance before the turnout in order to reduce the speed. A number of field tests were conducted in order to determine the actual maximum safe speed for traffic on a crossover (or turnout). This paper presents the results of computer simulations using NUCARS®. The GDE wagons and the characteristics of the track geometry were modeled. Several cases were simulated, with variations of parameters of the wagons, such as side bearing clearance and wheel profile. The results of the computer simulations were compared to the results from the field tests. Good correlation was found between them, indicating that the maximum speed of the GDE wagons running on the turnout might be open to review.

Keywords

Speed limit, railway vehicle, simulation, turnout, safety

Date received: 16 September 2014; accepted: 17 June 2015

Introduction

The Estrada de Ferro Vitória a Minas (EFVM), in southeastern Brazil, has 905 km of track, with 594 km of double-line rack. The nominal gauge is 1000 mm and the distance between the two lines is 4250 mm. At EFVM, the main product transported is iron ore from several mines operating in Minas Gerais. The typical train consists of 240 GDE wagons, and distributed traction with a maximum authorized speed of 65 km/h (empty and loaded), except when travelling through a turnout (changing from one line to another) where the limit is 60 km/h.

In railways around the world, it is common to see multidisciplinary teams (rolling stock, permanent way and operations) addressing wheel and rail contact issues. It is well known that this interaction is a key for the effective management and determination of levels of wear of the two components and safety relating to vehicle dynamics. These groups are still undergoing development in Brazil, with good progress being made.

At Vale, one of the first topics to be covered by the wheel and rail interaction group was to study the possibility of eliminating the speed restriction of the train when at a turnout (Figure 1).

The turnout, as shown in Figure 1, is composed of two successive switches. Due to its small curve radius and track properties[1] (maintenance issues, track stiffness, for example), the contact forces are normally higher than observed in a regular curve.[2,3] This may affect the efficiency of railway transport. Although a higher efficiency and safety are always desired, only a few papers on this topic exist in the published literature.[4] Thus, this paper presents a contribution to the literature, in the form of a case study. It might help other railroad companies to study the optimization of their speed limits.

Currently, the speed limit in turnouts is 60 km/h, whereas on the main track it is 65 km/h. Field tests using appropriate instrumentation have been performed to determine the safe maximum speed that a wagon can travel on a particular region of the railroad. That study is discussed in detail in Barbosa and Santos.[5] Although the results presented in that study were encouraging and indicated that it would be safe to remove the restriction, it was decided by Vale's

[1]Innovation and Development Department, Vale S.A., Brazil
[2]University of São Paulo, São Paulo, Brazil

Corresponding author:
Guilherme FM dos Santos, Innovation and Development Department, Vale S.A., Vitoria, Brazil.
Email: gfmsantos@yahoo.com

engineering team that the restriction would be maintained. The tests were not considered to be statistically valid due to:

- the tests were performed at only a single location on the railroad and thus might not be representative of the entire railway;
- the wagon used during the test could have been in a special maintenance condition;
- the wheel profile variation and side bearing setup were not considered.

These omissions could affect the vehicle dynamics in such a way that the risks were too high to make the decision to increase the maximum speed of the train.

The use of computer simulations would allow the influence of these parameters to be obtained and underpin any decision on to the maximum allowed speed of a GDE wagon travelling through a turnout. A second advantage is that additional on-track testing of vehicles can be avoided. At the EFVM, this is not a simple task, since the track access and time to run test trains is very limited.

Figure 1. A turnout area.

Methodology

NUCARS® computer software was used to simulate a wagon travelling through a turnout. The permanent way was also modeled based on geometrical measurements taken from real track.

Wagon modeling

From the design of the GDE wagon (Figure 2) it is possible to identify and determine the dimensions and positions of bodies based on a reference coordinate system. The suspension, inertia and mass properties are listed in Table 1. In this paper, the wagon was considered to be loaded with a gross weight of 110 tonnes, which was uniformly distributed.

The NUCARS program is based on the generalized nonlinear, multi-body simulation approach. The model assembles the equations of motion for a multi-body system, equations (1), (2) and (3), and solves them to predict a system's response to a deterministic input

$$M\bar{q} = -T^T f(s, \dot{s}) - Dq - \dot{K}q + f \tag{1}$$

Table 1. The parameters of an iron-ore wagon operated on the EFVM.

Parameter	Loaded wagon	Empty wagon
Mass (Tkg)	96.2816	10.0056
Roll inertia (Tkgm^2)	67.7724	10.5593
Pitch inertia (Tkgm^2)	569.430	84.4909
Yaw inertia (Tkgm^2)	610.042	95.8734
Vertical stiffness of a bogie (TN/m)	12,847.5	12,847.5
Lateral stiffness of a bogie (TN/m)	7524.71	2955.20[a]
Center of gravity above top of rail (m)	1.6225	1.082

[a]Theoretical calculation.

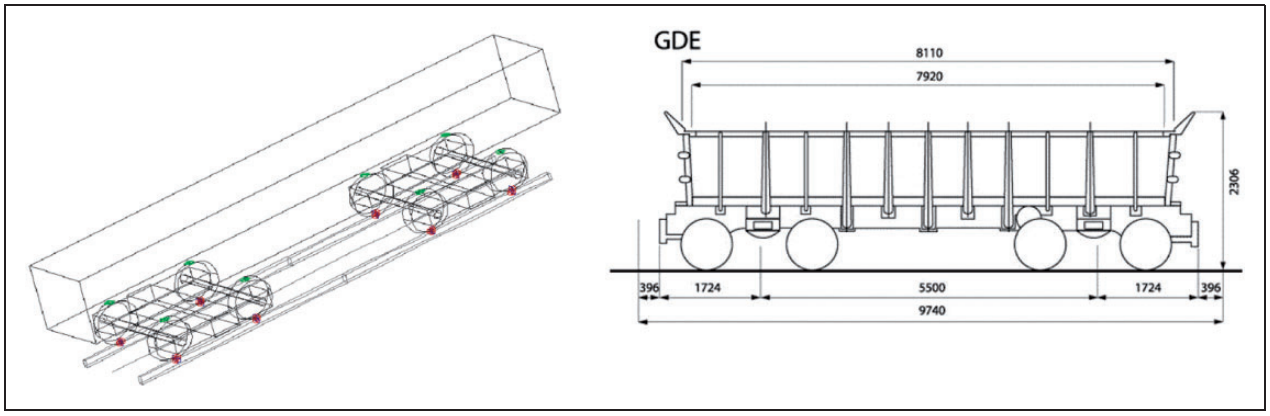

Figure 2. The dimensions (unit: mm) of a GDE wagon.

where

$$s = Tq + T_r r \tag{2}$$

and

$$\dot{s} = T\dot{q} + T_r \dot{r} \tag{3}$$

where M, D and K are the mass, damping and stiffness matrix, respectively. The stroke transformation matrices are T and T_r. The vectors q, $\dot{q}$ and $\bar{q}$ represent the degree-of-freedom displacements, velocities and accelerations. Vectors r and $\dot{r}$ are the inter-body relative displacements and velocities. These displacements and velocities arise from motion along curved or twisted track. Vector f represents the connection forces. These are nonlinear functions of the connection strokes and velocities. Vector F represents the external excitation.

Turnout geometry

A turnout is a track deviation with a sequence of curves that is used to switch traffic between two adjacent lines. The simulated turnout has two switches with a deviation ratio of 1:20 (50 mrad), as shown in Figure 3. Each switch consists of two switch points, two stock rails, and a fastening system, with supporting parts and intermediate reinforcements. The track is a double line, with the tracks being 4.25 m apart with a 1 m gauge. The switches in the turnout have a curve length of 28 m, with a radius of 548 m, in between a straight track segment of 54 m, resulting in a total crossing length of 110 m, as shown in Figure 3. No entry angles were modeled and all rail profiles were modeled as new ones (see Figures 7 to 9).

There are several available ways to measure the geometric properties of track. Results from a survey conducted in 2006 were used in this work. The survey was conducted using a specific procedure designed

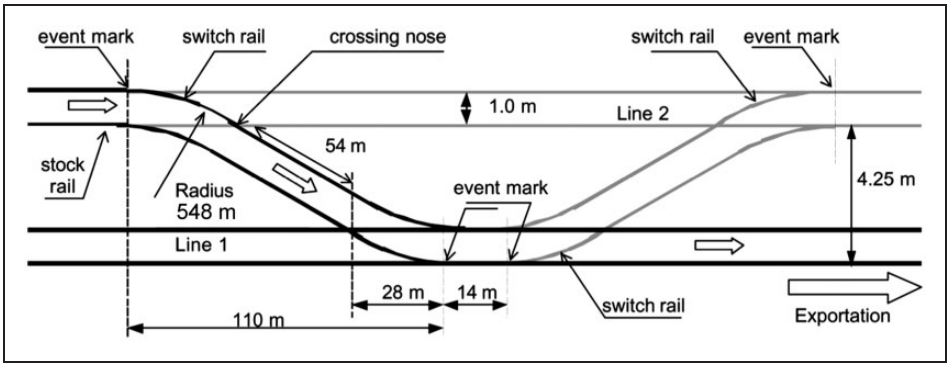

Figure 3. The geometry of a turnout.[5]

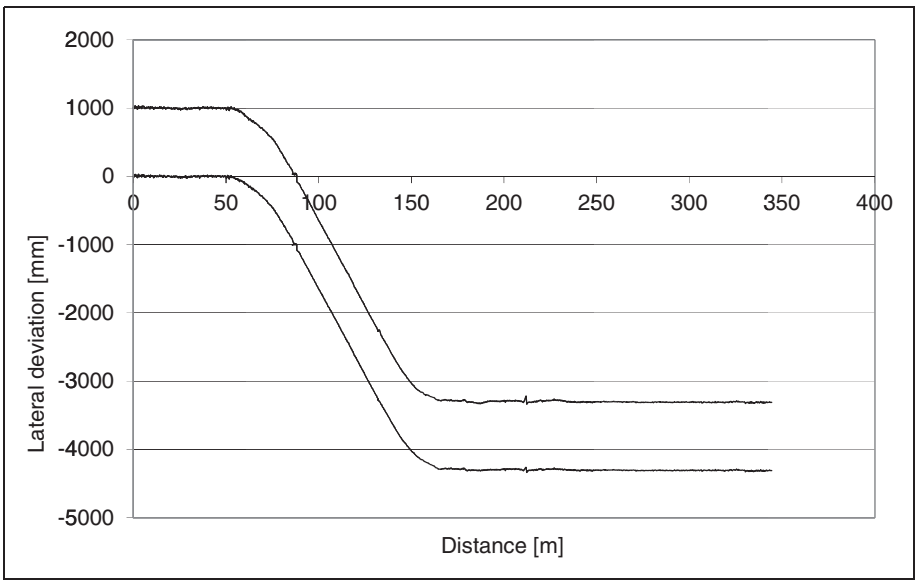

Figure 4. Turnout layout (line 2 to line 1).

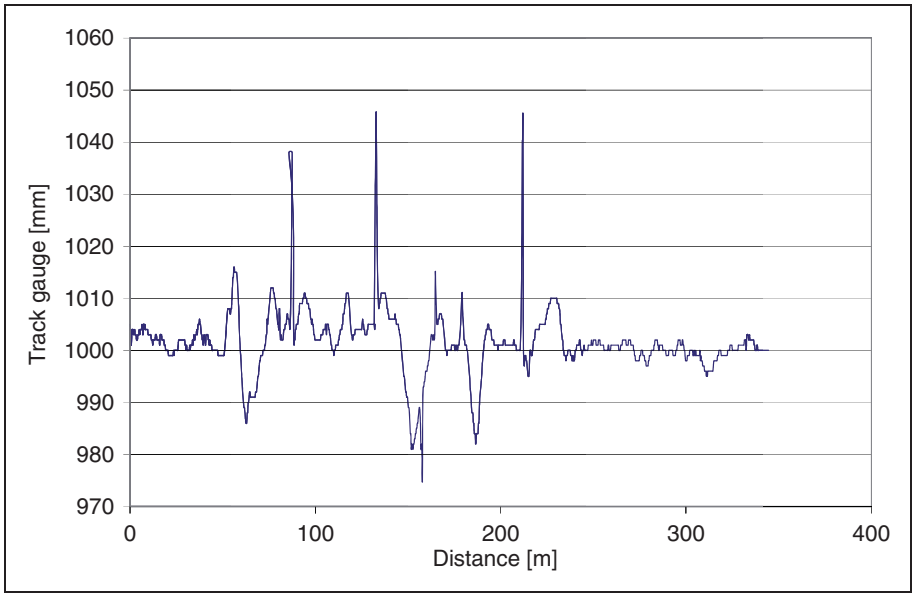

Figure 5. Track gauge.

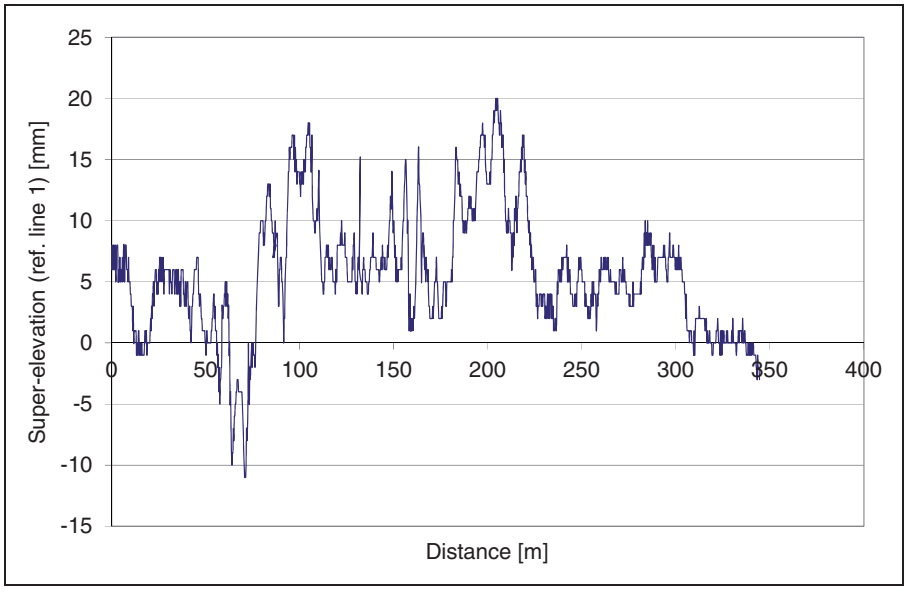

Figure 6. Super-elevation (ref. line 1).

to collect data for this investigation and all data were collected at a particular turnout located 128 km (named Location 22) west from the Port in Vitoria. This location was chosen because it represents a typical turnout of the entire railway in terms of maintenance.

Figures 4 to 6 show the lateral deviation, track gauge and super-elevation at the turnout area starting at line 2 to line 1 (as shown in Figure 4).

Observing the above results, one can highlight the following points regarding the track geometry.

1. The longitudinal length of the turnout of line 2 is approximately 2 m longer than the nominal design.
2. There are points where the super-elevation is up to 20 mm, however, the design says it should be zero.
3. The curvatures are identified to be close to the designed values (about 550 m).
4. The track gauge variation (widening or tightening) may be too high. This affects the dynamic behavior of the vehicle.

Computer simulations

The first step in running the computer simulations was to determine the safety limits;[6] this objective was achieved by the use of Nadal's equation.[7] In order

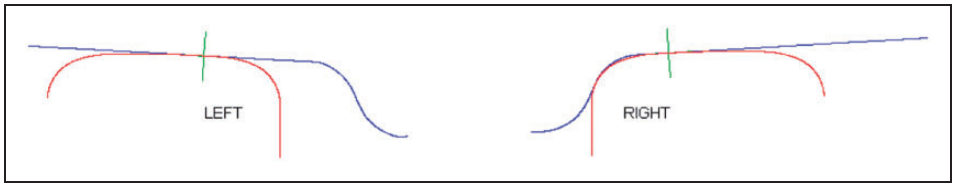

Figure 7. New wheel and new rail profiles.

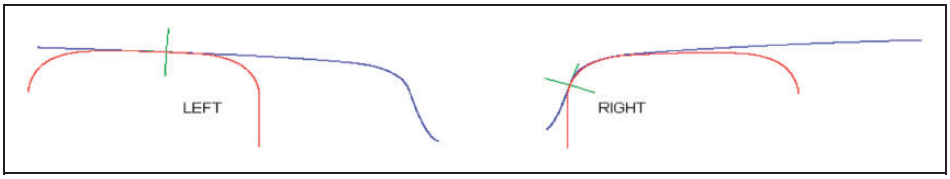

Figure 8. Worn wheel and new rail profiles.

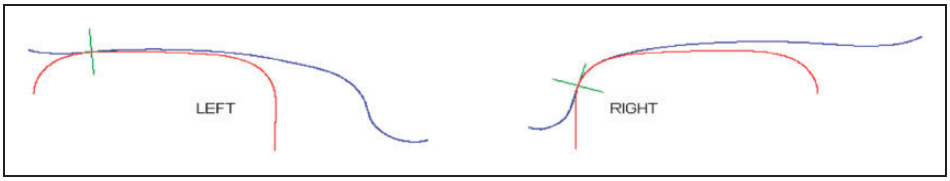

Figure 9. Hollow wheel and new rail profiles.

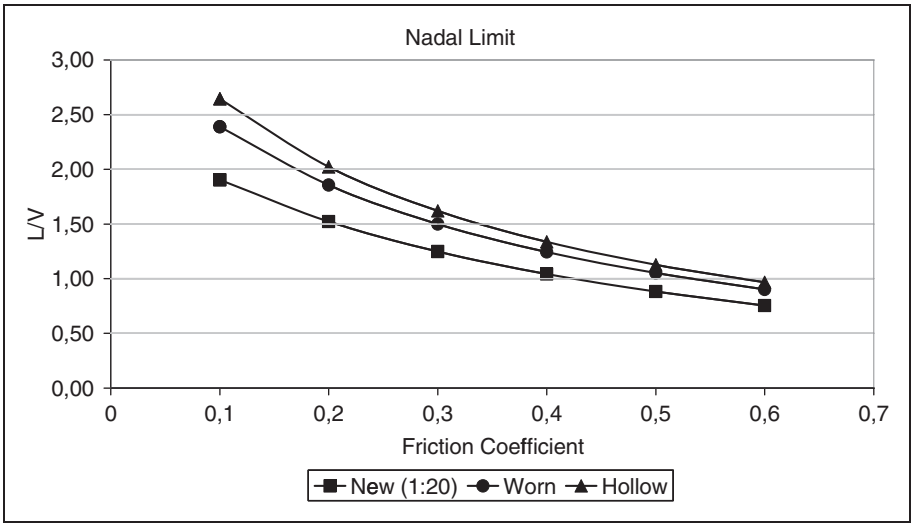

Figure 10. Nadal's limit.

to apply this approach, it is necessary to know the properties at the wheel/rail contact, i.e. the contact angle and the friction coefficient. Three combinations of wheel and rail profiles, as shown in Figures 7 to 9, were chosen for study.

Figure 10 shows the Nadal's limit for each wheel/rail profile combination as a function of the friction coefficient.

After the limits were determined, the GDE wagon and the permanent way models were used in the computer simulations.

In addition to the wheel profiles, the following variations in the wagon model were considered in order to be representative of what could be expected in the field:

- side bearing gap: tight (zero gap) and standard (gap of 6 mm);
- speed: 55, 60 and 65 km/h.

These combinations resulted in 18 cases for investigation. The results in terms of lateral to vertical

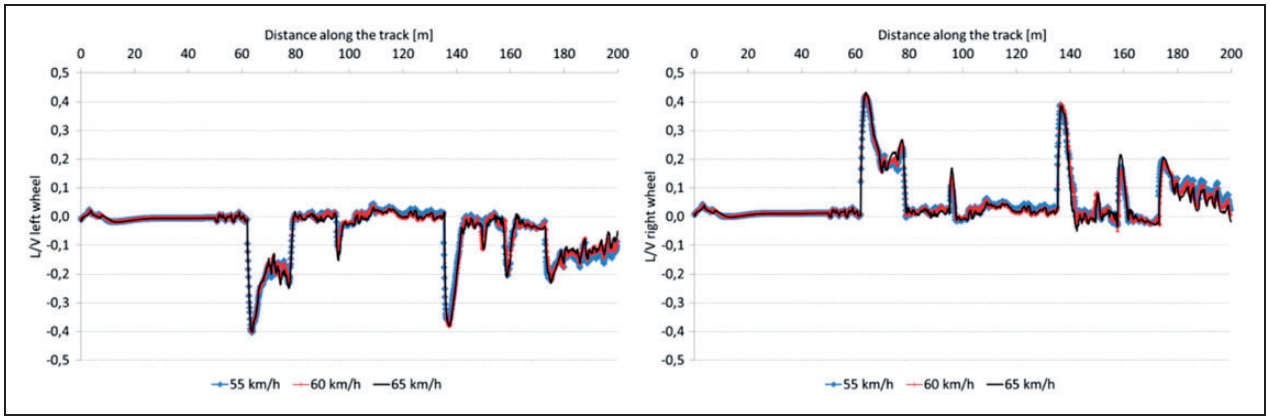

Figure 11. *L/V* for standard side bearing gap and new wheel profile.

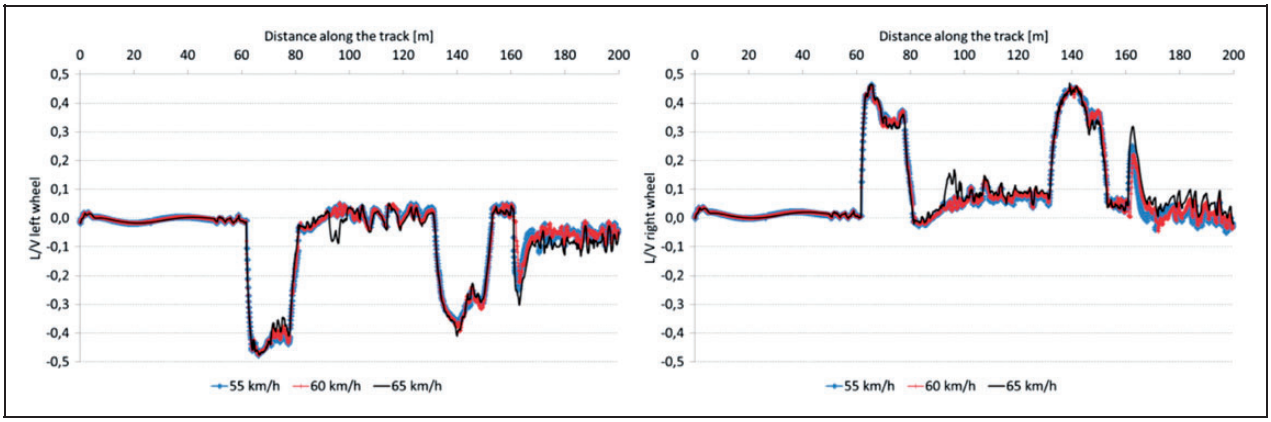

Figure 12. *L/V* for tight side bearing and new wheel profile.

Table 2. Maximum *L/V* based on the wheel profile.

Bearing	Speed (km/h)	Wheel profile		
		Worn	Hollow	New
Standard side bearing	55	0.28	0.13	0.42
	60	0.27	0.11	0.43
	65	0.23	0.16	0.43
Tight side bearing	55	0.41	0.30	0.48
	60	0.38	0.30	0.48
	65	0.40	0.30	0.48

force ratio (L/V) of the first wheelset of the wagon (leading axle) and for the most critical case (highest L/V) are shown in Figures 11 and 12. The obtained results are listed in Table 2. The results in Table 2 are the maximum L/V (absolute value) found at the circular curve of radius 548 m. This curve is shown in the first plot of Figures 11 and 12.

The worst case was the tight side bearing at 65 km/h with wheel new profiles. The L/V for this case was 55% of the limit value for a coefficient of friction of 0.50 (dry rail). These results indicate that, based on the models, safe operation is preserved.

In 2006, Vale performed several tests to verify the operational safety of a GDE wagon travelling through a turnout. A wagon was fully instrumented (including instrumented wheelsets) for the measurement of L/V. Figure 13 shows the summary of results found during the field tests.[8]

There is an acceptable correlation between the results obtained from the computer simulation (Table 2) and the field test (Figure 13), particularly at the speed of 65 km/h. The measured L/V value was about 0.45, whereas the simulated value was 0.43. At speeds of 55 and 60 km/h, the field tests showed L/V values from 0.55 to 0.60 compared with simulated values of 0.42 and 0.43, respectively.

Conclusions

The results from the computer simulation were compared with those recorded in an experimental test conducted in 2006. The simulations used the track geometry measured at the turnout area, three different wheel profiles (new, worn and hollow) and tight

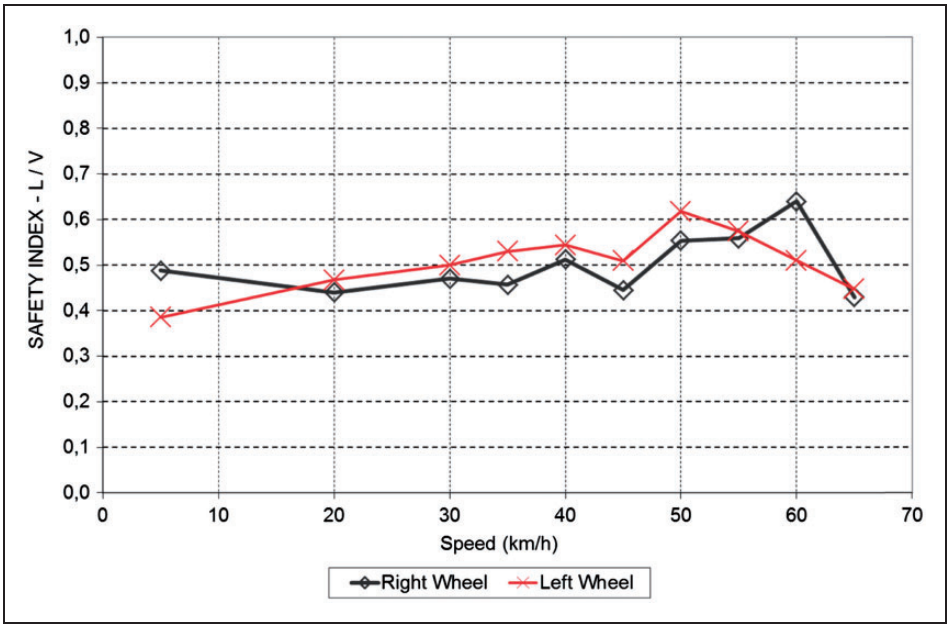

Figure 13. Safety index (L/V) from field testing.[8]

and standard side bearing gap setups. The following conclusions were drawn from the work reported in this paper.

1. The maximum values of the L/V were obtained for the combination of a new wheel profile and tight side bearing gap. The flange thickness of the new wheel profile limits the lateral displacement of the wheel-set, which affects the truck curving.
2. All simulations with a tight side bearing gap resulted in higher L/V values compared with the standard case. It is known that a tight side bearing restricts truck rotation (with respect to the wagon body), which increases the lateral force.
3. The simulations that considered a hollow wheel profile showed the lowest values of L/V. This may be because of the higher conicity of this type of wheels.
4. Very good agreement was found between the measured data and simulated data.
5. The highest L/V values where found when the side bearings were tight.
6. There was no significant variation in terms of L/V with respect to the speed. In addition, in some cases the value found was lower when the speed was higher.
7. Due to the individual properties of each railroad system, such as vehicle design, track gauge, speed etc., it is not possible to directly compare the results with those in the literature. This is the reason why the results were only compared with the field test data.
8. The results indicate an opportunity to increase the maximum authorized speed at the turnout. However, further work needs to be completed before the new allowed speed is set.

The following recommendations are suggested for future work.

1. To use variations of track geometry and lateral and vertical track stiffness values.
2. To perform a parametric study for different conditions of wagon maintenance, such as friction wedges and suspension stiffness characteristics.
3. To include more variations of the rail profile and the friction coefficient, as well as to evaluate if an entry angle affects the results.
4. To repeat the simulation considering the longitudinal dynamics (in-train forces).

Declaration of Conflicting Interests

The author(s) declared no potential conflicts of interest with respect to the research, authorship, and/or publication of this article.

Funding

The author(s) received no financial support for the research, authorship, and/or publication of this article.

References

1. Kassa E, Andersson C and Nielsen JCO. Simulation of dynamic interaction between train and railway turnout. *Int J Veh Syst Dyn* 2006; 44(3): 247–258.
2. Ren Z, Sun S and Zhai W. Study on lateral dynamic characteristics of vehicle/turnout system. *Veh Syst Dyn* 2005; 43(4): 285–303.

3. Zhu JY. On the effect of varying stiffness under the switch rail on the wheel-rail dynamic characteristics of a high-speed turnout. *Proc IMechE, Part F: J Rail Rapid Transit* 2006; 220(1): 69–75.
4. Andersson C and Dahlberg T. Wheel/rail impacts at a railway turnout crossing. *Proc IMechE, Part F: J Rail Rapid Transit* 1998; 212(2): 123–134.
5. Barbosa RS and Santos GFM. Experimental investigation on the dynamic behavior of a railway vehicle traveling through a turnout. *Int J Heavy Veh Syst* 2009; 16: 189–206.
6. Santos GFM, Lopes LAS, Kina EJ and Tunna JM. The influence of wheel profile on safety index. *Proc IMechE, Part F: J Rail Rapid Transit* 2010; 224(5): 429–434.
7. Barbosa RS. A 3D contact force safety criterion for flange derailment of a railway wheel. *J Veh Syst Dyn* 2004; 42(5): 289–300.
8. Babosa RS. *Investigação experimental do comportamento dinâmico de vagão de minério tipo GDE em tráfego na via com travessão* (*EFVM-CVRD*). Technical report 010/2007, 2007. São Paulo, Brazil: University of São Paulo.
9. Sawley KJ. *Initial system investigation and improvement plan report for EFVM CVRD railway*. Technical report P-02-018, 2002. Pueblo, CO: Transportation Technology Center.

8.11 ANEXO K

MONORAIL VEHICLE MODEL TO STUDY INFLUENCE OF TYRE MODELLING ON OVERALL DYNAMIC.

Maciel, G. P. R. Barbosa, R.S. (2016) Monorail vehicle model to study influence of tyre modelling on overall dynamic. International Journal of Heavy Vehicle Systems, DOI: 10.1504/IJHVS.2016.079270, Vol.: 23, nº. 4, pp. 317–332.

Monorail vehicle model to study influence of tyre modelling on overall dynamics

Gabriel P.R. Maciel* and
Roberto Spinola Barbosa

Polytechnic School of the University of São Paulo,
Av. Prof. Mello Moraes, 2231, Sao Paulo, SP,
cep.: 05508-970, Brazil
Email: ga.pe.01@gmail.com
Email: spinola@usp.br
*Corresponding author

Abstract: A mathematical model of a straddle type monorail vehicle has been developed in order to study its stability and the effect of tyre modelling techniques on its dynamic response. An algorithm was developed to build equations of motion using a multi-body systems method, considering deviations of the guideway as forced inputs. Tyre models consider both radial and lateral forces. Four methods to calculate lateral forces were implemented and results were compared. One of the four vehicle models is linear and parameterised with the longitudinal velocity, enabling the stability analysis based on eigenvalues locus. The modal damping decreases with the increase of longitudinal velocity, asymptotically approaching to a stable system. Results show that the influence of tyre radial force on its cornering stiffness can be an important effect to consider in the monorail numerical modelling, increasing the accuracy to predict the vehicle overall dynamics and tyre lateral forces.

Keywords: dynamic; vehicle; monorail; tyre; modelling.

Reference to this paper should be made as follows: Maciel, G.P.R. and Barbosa, R.S. (2016) 'Monorail vehicle model to study influence of tyre modelling on overall dynamics', *Int. J. Heavy Vehicle Systems*, Vol. 23, No. 4, pp.317–332.

Biographical notes: G.P.R. Maciel is postgraduate student in the Group of Dynamic and Control of the Mechanical Engineering Department of the Polytechnic School of São Paulo University, Brazil. His research interests are on dynamics of multibody systems, vibration, vehicle dynamics and structural analysis.

R.S. Barbosa is a Professor in the Group of Dynamic and Control of the Mechanical Engineering Department of the Polytechnic School of São Paulo University, Brazil. He worked for 20 years on the Research Institute of Technology of Sao Paulo, dealing with vibration, comfort and safety on railway vehicles in the Transport Division. He received his PhD from the University of Sao Paulo and DSc from the University of Campinas in Sao Paulo, Brazil. His research interests are on dynamics of multibody systems, vibration and vehicle dynamics.

1 Introduction

With the growth of big cities, the demand to increase the capacity of transport systems has been pushing engineers to develop faster, larger, safer and more comfortable vehicles. In this context, multi-body vehicle dynamics simulation has a major importance in vehicle design, helping the validation of vehicle performance before a prototype is built. Multi-body simulation allows prediction of vehicle stability and safety limits, evaluation of ride quality, determination of design loads for component durability analysis, etc. It is reasonable that the above-mentioned applications require a high degree of trustworthiness and similarity when compared to a real vehicle, since significant deviation of simulation results from real vehicle behaviour may lead to troubleshooting in the late stages of design. Considering this, determination of accurate techniques for building a virtual model is one main challenge in vehicle virtual modelling and simulation.

A review about different techniques for modelling suspension components and the impact of more detailed models in the overall vehicle dynamics was presented by Bruni et al. (2011). Literature indicating that contact forces play an important role in vehicle dynamics is abundant (Cao et al., 2011; Mohajer et al., 2015) while discussions about adequate level of detail for modelling contact forces and its impact on the overall simulation accuracy is limited for applications on straddle type monorail vehicles.

The level of detail of contact forces modelling on road and rail vehicles stability is discussed by Shen et al. (2007) and Polach (2007) respectively.

The necessity of the accurate calculation of tyre forces is discussed by Du et al. (2014), which shows methods to calculate tyre wear on monorail vehicles and how it is influenced by changes in suspension parameters.

In a recent work (Wei and Dorfi, 2014), the influence of tyre transient lateral force on road vehicle dynamics was studied and it was showed that it has a relatively small contribution to vehicle handling performance compared with the tyre steady-state force. This type of study provides important guidelines for the best practices of numerical modelling techniques.

Liu et al. (2014) studied the effect of wheel pressure on vibration of straddle type monorail vehicles. In this paper, it was showed that the influence of vertical, guide and stabilising tyre pressures has a considerable influence on the response of the system, such as at tyre radial forces and car body displacements.

This work intends to review modelling techniques to predict the dynamic behaviour and stability of monorail vehicles and discuss the level of detail of tyre models considering the expected overall accuracy of the virtual vehicle.

There are two types of vehicles used in monorail systems: hanging type and straddle type. The hanging type has its centre of mass under the guideway and runs hanged under it. The straddle type has the vehicle's centre of mass above the guideway and runs on it. The guideway is built using beams that are aligned to each other in order to form a long path of several beams. These beams can be misaligned due to different causes: assembling precision, different radius concordance, curve transitions, thermal expansion, etc. These misalignments will be further simulated in this work in order to evaluate and compare vehicle's transient response.

In this paper, a virtual straddle type monorail vehicle was modelled using different tyre modelling techniques in order to verify the influence of these different approaches on the representation of vehicle dynamics. It is expected that an investment in modelling more detailed components shall add more accuracy to simulation results and vehicle's behaviour. This statement will be used to evaluate the application of modelling techniques due to its

impact on results when compared to less detailed models. Equations of motion were built using multi-body systems (MBS) method, considering deviations of the guideway as forced inputs. Figure 1 shows an example of a straddle type monorail vehicle.

Figure 1 Straddle-type monorail vehicle

2 System description

Figure 2 shows the front view of the model used for dynamic simulation of a monorail vehicle. The model represents half vehicle and is composed by one car body which is assumed to be a rigid body with three degrees of freedom: lateral displacement (y), vertical displacement (z) and roll angle (θ). It is considered that the car body moves forward with a constant velocity V_x.

There are two main Cartesian coordinate systems in the model: one is attached to the car body (Goda et al., 2000; Shabana, 2008) (with centre at point O_c, positioned at car's centre of mass) and another moves along the line at the middle of upper surface of the guideway at the same longitudinal velocity as the car body (with centre at point O_g).

The car body interacts with the guideway trough vertical tyres and horizontal tyres shown in Figure 2. Vertical tyres support the vertical load of the vehicle (indicated by letter p). Guide tyres and stabilising tyres, guide the car body along the guideway (indicated by letters q and r, respectively). The main function of stabilising tyres is to prevent excessive rolling of the car body (Goda et al., 2000). It was considered that each tyre has one point of contact with the guideway surface, defined as ij where i is the corresponding tyre pair letter and j is the tyre number $j = 1, 2$. Each tyre interacts with the guideway with two contact forces: radial and lateral, indicated in Figure 2 as F_{rij} and F_{sij} respectively. All properties and forces are indicated with letters i and j which correspond to the tyre position.

In the virtual model, generalised coordinates are: y for lateral displacement, z for vertical displacement and θ for roll rotation of the car body. Forced inputs x_r are herein representing guideway deviations to a perfectly straight path and are considered small when compared to other displacements.

$$x(t) = \{\, y(t)\; z(t)\; \theta(t) \,\}^T \qquad x_r(t) = \{\, y_r(t)\; z_r(t)\; \theta_r(t) \,\}^T.$$

Figure 2 Dynamic model of monorail car

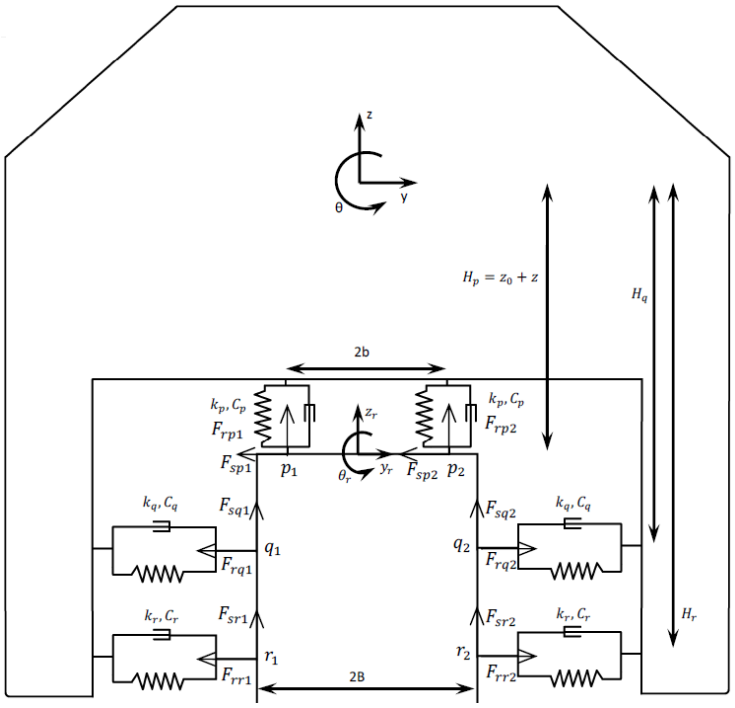

2.1 Tyre forces

Two types of forces are calculated for each tyre: radial and lateral. Radial force is a force reaction of the tyre against the guideway surface in radial direction to the respective tyre acting on the tyre contact point. Lateral forces are generated by lateral slippage in the contact point between tyre and guideway.

2.1.1 Radial forces

The same radial force method was used in all four models in this work. A virtual body is attached to the point of contact of each tyre tread with the guideway. These virtual bodies move along the surface of the guideway and have no mass. A virtual body is connected to the car body through a spring and damper, which causes internal forces at the system when there are relative displacements and/or velocities between virtual bodies and car body.

$$F_{rij} = F^0_{rij} + k_i \Delta S_{rij} + c_i \frac{\partial \Delta S_{rij}}{\partial t}, \tag{1}$$

where F^0_{rij} is the radial preload force and ΔS_{rij} is the relative displacement between virtual body and car body.

2.1.2 Lateral forces

In order to calculate tyre slippage, necessary to calculate lateral forces, a local coordinate system called ‘tyre frame’ was attached at each virtual body and has the same orientation

of guideway coordinate system. Lateral forces due to slip act on virtual bodies when there is a slippage between the corresponding tyre and guideway. It is assumed that longitudinal velocity of car body is constant and tyres roll with constant angular velocity so that there is no longitudinal slippage. Although movements of car body with respect to the guideway can produce lateral slippage at tyres. The direction of lateral slip velocities is parallel to slip forces with opposite orientation.

Figure 3 shows a schematic top view of a tyre (represented with thick lines) with slip forces and velocities oriented in tyre reference frame, where V is the total velocity of contact point, V_{sij} is the lateral slip velocity of tyre ij and lateral slip angle α is the ratio of lateral and longitudinal velocity of tyre. Tyre lateral force is proportional to lateral slip α and cornering stiffness as described in equation (2) (Pacejka, 2005).

$$F_{sij} = \alpha k_{sij}. \tag{2}$$

Later in this work, different methods will be presented as a variation of computing lateral slip velocities and cornering stiffness.

Figure 3 Slip velocities and forces at tyre

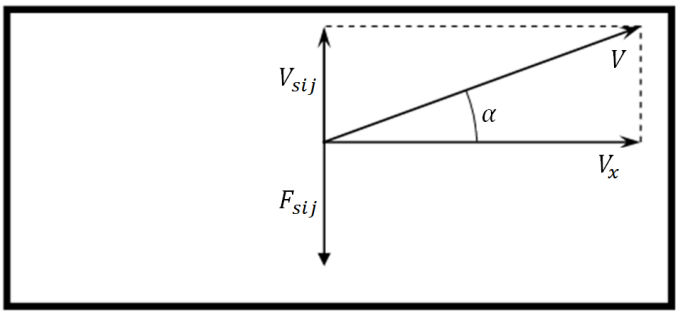

2.2 Equations of motion

Equations of motion are written as function of mass matrix $[M]$, damping matrix $[C]$, stiffness matrix $[K]$ and generalised external forces Q_{ext}, which is composed by tyre lateral slip forces.

$$[M]\ddot{x} + [C]\dot{x} + [K]\,(x - x_r) = Q_{\text{ext}}, \tag{3}$$

where

$$\begin{bmatrix} M & 0 & 0 \\ 0 & M & 0 \\ 0 & 0 & I_x \end{bmatrix} \begin{bmatrix} \ddot{y} \\ \ddot{z} \\ \ddot{\theta} \end{bmatrix} + \begin{bmatrix} 2(c_q + c_r) & 0 & 2(H_q c_q + H_r c_r) \\ 0 & 2c_p & 0 \\ 2(H_q c_q + H_r c_r) & 0 & 2(H_q^2 c_q + H_r^2 c_r + b^2 c_p) \end{bmatrix} \begin{bmatrix} \dot{y} \\ \dot{z} \\ \dot{\theta} \end{bmatrix} +$$

$$\begin{bmatrix} 2(k_q + k_r) & 0 & 2(H_q k_q + H_r k_r) \\ 0 & 2k_p & 0 \\ 2(H_q k_q + H_r k_r) & 0 & 2(H_q^2 k_q + H_r^2 k_r + b^2 k_p) \end{bmatrix} \left(\begin{bmatrix} y \\ z \\ \theta \end{bmatrix} - \begin{bmatrix} y_r \\ z_r \\ \theta_r \end{bmatrix} \right) = \begin{bmatrix} Q_y \\ Q_z \\ Q_\theta \end{bmatrix}.$$

In order to simulate the system of equations in the time domain, equation (3) was rearranged into a first order dynamical system on the state space (Barbosa and Neto, 1996) domain as follows:

$$\dot{X} = \begin{bmatrix} -[M]^{-1}[C] & -[M]^{-1}[K] \\ [I] & [0] \end{bmatrix} X + \begin{bmatrix} [M]^{-1}[K] \\ 0 \end{bmatrix} x_r + \begin{bmatrix} [M]^{-1} \\ 0 \end{bmatrix} Q_{\text{ext}}, \tag{4}$$

where $[I]$ is identity matrix and $X(t) = \{\dot{y}(t), \dot{z}(t), \dot{\theta}(t), y(t), z(t), \theta(t)\}^T$ is the vector that defines the state of the dynamical system at a specified time t.

3 Linearised model (Model 1)

In order to study the influence of tyre modelling on monorail vehicle dynamics, different complexity models were used. System performance was evaluated from a linear model to a complete high order non-linear model.

The first model described is completely linear, with the advantage to perform a stability analysis based on eigenvalues locus in complex plane.

3.1 Cornering stiffness – linear method

In model 1, cornering stiffness k_{sij} was modelled as a constant value.

3.2 Slip velocities – linear method

Taking as an example V_{sp1}, the lateral slip velocity of point P1, aligned to axis Z_r, it's possible to observe that this relation is nonlinearly dependent to the generalised coordinates.

$$V_{sp1} = \dot{y} - \dot{\theta}\left(z_0 + z + \frac{b^2}{z_0 + z}\right). \tag{5}$$

In the linear approach, it was considered that the magnitudes of generalised coordinates at the system are sufficiently small that second order terms were neglected. Using this statement, equation (5) can be linearised leading to linearly dependent slip velocities in respect to generalised coordinates.

$$V_{sp1} = \dot{y} - \dot{\theta}\left(z_0 + \frac{b^2}{z_0}\right). \tag{6}$$

The same approach of equation (6) can be done for all contact points, resulting in a set of linear dependent equations to calculate slip velocities and the resulting relations are called in this work as linear method to calculate slip velocities.

3.3 State space representation

Second order terms are also neglected in order to calculate generalised forces, which are linearly dependent to generalised coordinates.

$$\begin{bmatrix} Q_y \\ Q_z \\ Q_\theta \end{bmatrix} = \begin{bmatrix} F_{sp1} + F_{sp2} \\ F_{sq1} + F_{sq2} + F_{sr1} + F_{sr2} \\ z_0 F_{sp1} + z_0 F_{sp2} - BF_{sq1} + BF_{sq2} - BF_{sr1} + BF_{sr2} \end{bmatrix}. \tag{7}$$

Substituting equation (7) in equation (3), we have:

$$[M]\ddot{x} + \left([C] + \frac{1}{|V_x|}[C_{nc}]\right)\dot{x} + [K](x - x_r) = 0. \tag{8}$$

With

$$[C_{nc}] = \begin{bmatrix} -2k_{sp} & 0 & 2k_{sp}\left(z_0 + \frac{b^2}{z_0}\right) \\ 0 & -2(k_{sq} + k_{sr}) & 0 \\ -2k_{sp}z_0 & 0 & 2k_{sp}(z_0^2 + b^2) - 2k_{sq}(B^2 + H_q^2) - 2k_{sr}(B^2 + H_r^2) \end{bmatrix}.$$

Writing equation (8) in the form of equation (4), it's possible to see that we have a linear dynamic system with the following state space structure:

$$\dot{X} = \begin{bmatrix} -[M]^{-1}[\bar{C}] & -[M]^{-1}[K] \\ [I] & [0] \end{bmatrix} X + \begin{bmatrix} [M]^{-1}[K] \\ 0 \end{bmatrix} x_r, \tag{9}$$

where $[\bar{C}] = [C] + |V_x|^{-1}[C_{nc}]$, $X = \{\dot{x} \quad x\}^T$ and $u = \{x_r \quad 0\}^T$.

4 Complete models

4.1 Cornering stiffness – complete method

The cornering stiffness linear method assumes that cornering stiffness is constant, although linearised modelling can be sufficient in the neighbourhood of design configuration but can have discrepancies if nonlinearities are significant. Moreover it is known that lateral forces are influenced by tyre radial forces (Segel and Ervin, 1981). Using these assumptions, the complete method assumes that the cornering stiffness is influenced by changes in the radial tyre force as described in equation (10) (Pacejka, 2005), where c_{1i} and c_{2i} are constants for each tyre:

$$k_{sij}(F_{rij}) = c_{1i} \sin\left(2 \arctan\left(\frac{F_{rij}}{c_{2i}}\right)\right). \tag{10}$$

4.2 Slip velocities – complete method

The complete method to calculate slip velocities considers that the magnitude of generalised coordinates is not small enough to neglect higher order terms, so slip velocities will be calculated as in equation (5). As a consequence, generalised external forces and moments are calculated as in equation (12) in order to keep consistency with the consideration of higher order terms.

$$\begin{aligned} Q_y &= F_{sp1} + F_{sp2} \\ Q_z &= F_{sq1} + F_{sq2} + F_{sr1} + F_{sr2} \\ Q_\theta &= (z_0 + z)F_{sp1} + (z_0 + z)F_{sp2} - (B + y)F_{sq1} \\ &\quad + (B - y)F_{sq2} - (B + y)F_{sr1} + (B - y)F_{sr2}. \end{aligned} \tag{11}$$

4.3 Preload forces

Tyre cornering stiffness is influenced by radial force and consequently by the radial preload force. The determination of vertical tyres radial preload force can be done based on vehicle's weight, although guiding and stabilising tyres radial preload forces have to be determined as a design parameter that influences vehicles' dynamic response.

Based on equation (10), the maximum value of cornering stiffness is equal to the coefficient c_1. If the cornering stiffness reaches its maximum value, it decreases if the radial force increases. It means that the tyre starts to loose its capacity to generate lateral forces, which is not a desirable behaviour.

Figure 4 shows the variation of the cornering stiffness (normalised by the coefficient c_1) according to radial force (normalised by the coefficient c_2). This relation was calculated using equation (10).

Figure 4 Normalised cornering stiffness in respect to normalised radial force

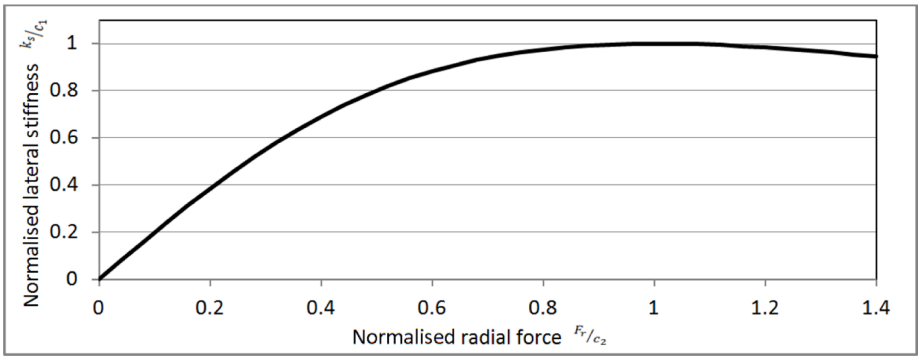

Considering this, the tyre radial force preload has to be specified in a way to produce an initial cornering stiffness not too small but not too close to the maximum value. The authors propose a method to determine the preload radial force by imposing an initial value of cornering stiffness.

Given an arbitrary value of the normalised cornering stiffness, equation (10) can be written as a function of this value. As a contribution to this work, the authors propose a normalised cornering stiffness equals to $\frac{3}{4}c_1$. This means that the preload radial force corresponds to an initial cornering stiffness equal to $\frac{3}{4}$ of the maximum saturation value.

$$F_{rij}^{0} = c_{2i} \tan\left[\tfrac{1}{2} \arcsin\left(\tfrac{3}{4}\right)\right]. \tag{12}$$

4.4 Dynamic models

Four different methodology combinations were evaluated in order to study the effects of tyre modelling techniques. Each one has a different methodology to calculate slip forces at tyres. Table 1 shows the combinations of cornering stiffness and slip velocities methods.

Table 1 Numerical models and corresponding modelling techniques

Model number	*Cornering stiffness*	*Slip velocities*
Model 1	Linear	Linear
Model 2	Linear	Complete
Model 3	Complete	Linear
Model 4	Complete	Complete

5 Results

5.1 Modal analysis and stability

From the linear system (Model 1) described in equation (9), three pairs of complex conjugate eigenvectors can be found, describing three eigenmodes. One eigenmode called lower sway vehicle body movement, determined by the eigenvector, is characterised by phase movement of lateral displacement (y coordinate) and the body angular rolling (θ coordinate) while the vertical displacement (z coordinate) remains in a smaller amplitude (Figure 5 (left)). The eigenmode upper sway is characterised by the opposite phase of y and θ at the eigenvector while z remains in a smaller amplitude (Figure 5 (centre)). At bounce eigenmode, the amplitude of z in the eigenvector is dominant and y and θ are almost imperceptible (Figure 5 (right)).

Figure 5 Eigenmodes of vehicle. (left) lower sway, (centre) upper sway and (right) bounce

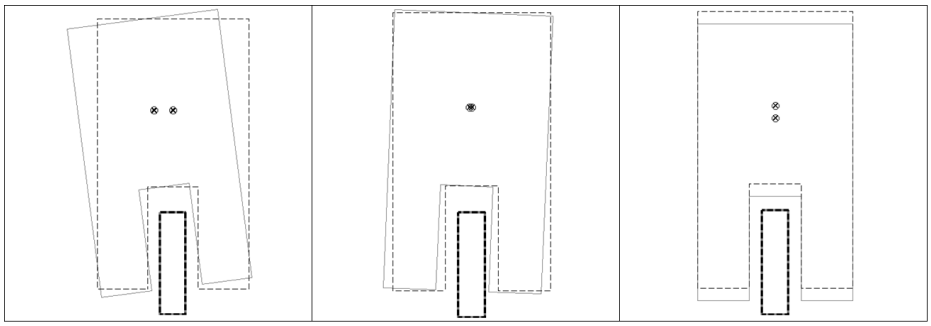

It is possible to verify from the equation (8) that there's a term that depends on the longitudinal velocity of the car body, so the eigenvalues of the system will be influenced by this parameter. Figure 6 shows the location of the system's poles due to a variation of longitudinal velocity V_x from 4 m/s to 30 m/s. Arrows in this figure indicates the path that poles make while longitudinal velocity is increased.

It's also possible to see that in equation (8), the term $1/|V_x|\ [C_{nc}]$ decreases with the increment of the longitudinal velocity, asymptotically approaching to zero. With this statement, it's possible to conclude that $[\bar{C}] \cong [C]$ and the poles of the system at Figure 6

asymptotically approach to the poles of the system described at equation (13) with the increment of longitudinal velocity.

$$\dot{X} = \begin{bmatrix} -[M]^{-1}[C] & -[M]^{-1}[K] \\ [I] & [0] \end{bmatrix} X + \begin{bmatrix} [M]^{-1}[K] \\ 0 \end{bmatrix} x_r. \tag{13}$$

Observing the real part of the eigenvalues in Figure 6, it is possible to conclude that the system is stable in the whole investigated range of speeds up to 108 km/h. Considering that the system in equation (13) is stable, it's also possible to conclude that increasing longitudinal velocity, the monorail vehicle will be stable as well. Figure 7 shows the values of natural frequencies and damping factors of the eigenmodes with the longitudinal velocity increase.

Figure 6 Location of system's poles due to increment of longitudinal velocity (x marks)

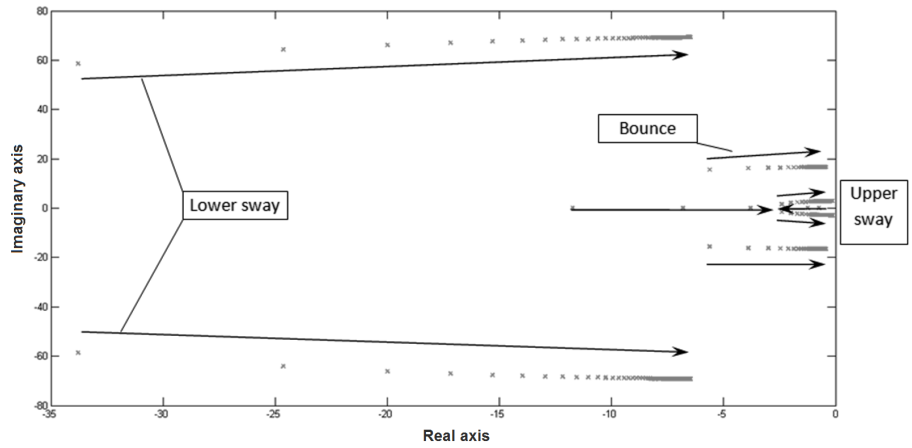

5.2 *Time transient simulations*

In order to evaluate and compare the transient response of the models, two types of forced inputs at the system are proposed. The first input emulates a misalignment between two consecutive beams along the guideway. The first forced input is a lateral misalignment beam transition of 10 mm, which can be modelled as a lateral step input at vector x_r as follows.

$$\begin{cases} x_r(t < 0.1) = \{0 \quad 0 \quad 0\}^T \\ x_r(t \geq 0.1) = \{10 \quad 0 \quad 0\}^T. \end{cases}$$

From Figure 8, it's possible to see that in models 3 and 4, a disturbance in lateral direction leads to a significant displacement in z direction. This behaviour is caused by the variation of the tyre cornering stiffness due to changes in its radial force. When the vehicle is subjected to a lateral step disturbance, tyre forces cause a momentum at car body leading it to start a roll rotation. The roll velocity leads to slippage at guide and stabilising tyres, which are deflected differently by the lateral disturbance. With different radial forces at left and right tyres, different slip forces will be generated at the vertical direction, leading to vertical acceleration (and consequently vertical displacement) of car body.

Figure 7 Natural frequencies and damping factors due to increment of longitudinal velocity

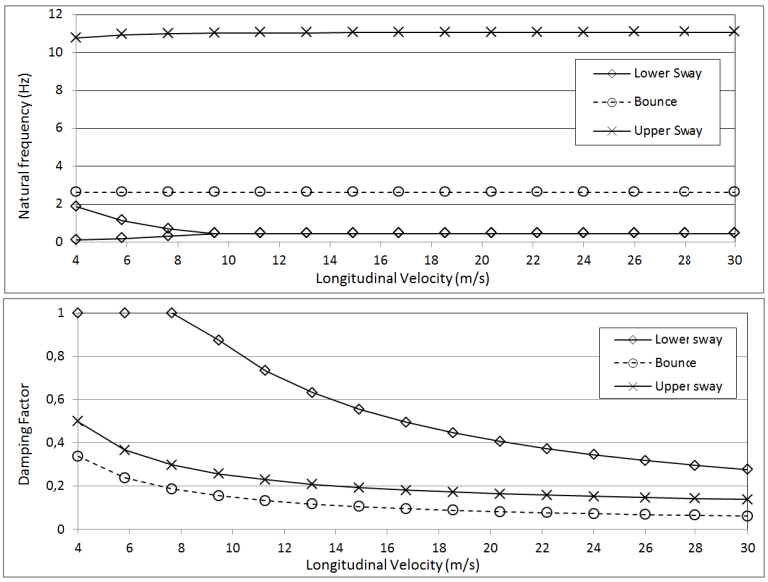

Figure 8 Lateral (top) and vertical (centre) displacements and roll rotation (bottom) – lateral step input (see online version for colours)

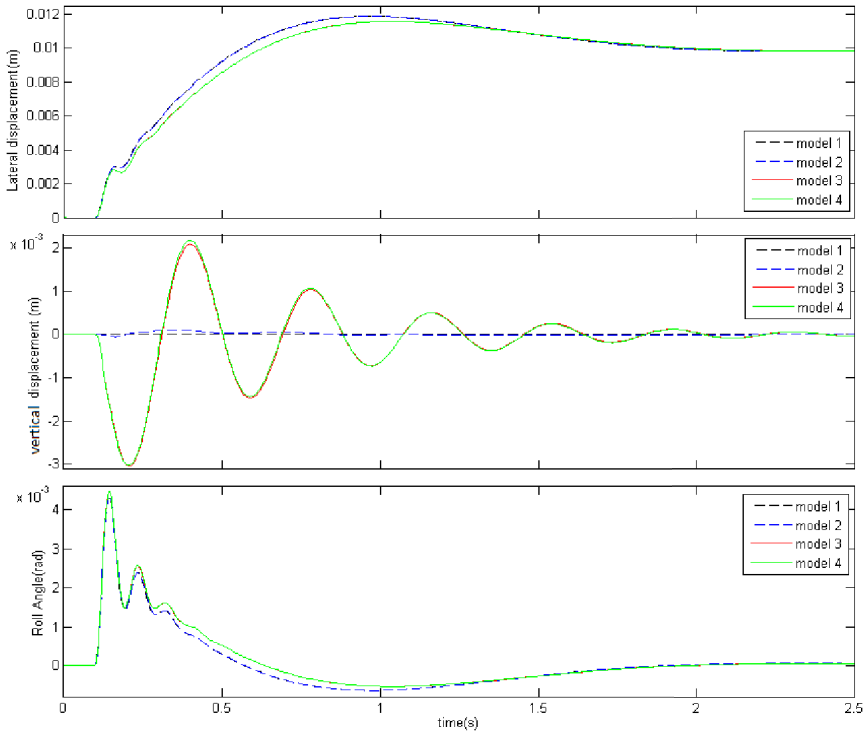

The aforementioned behaviour characterises a nonlinear coupling between lateral and vertical movements of the car body, which is reproduced if the complete cornering stiffness model, described in item 4.1, is adopted. For models where constant cornering stiffness is adopted, this behaviour is non-existent for model 1 and small for model 2.

In order to determine a numerical comparison between models, a parameter e_d was proposed to quantify the relative deviation of the model 4 (with complete methods for cornering stiffness and slip velocities) to the models 1, 2 and 3. Radial and lateral forces at tyres were measured and the maximum value was normalised in respect to the equivalent maximum force at model 4. As stated below for $k = 1, 2, 3$.

$$e_d = \frac{F_k^{\max} - F_4^{\max}}{F_4^{\max}}$$

Figure 9 shows the comparison of lateral force F_{sq1}, which does not increase in models 3 and 4 as fast as it does in models 1 and 2. This effect is caused by the variation of cornering stiffness considered in models 3 and 4 but not considered in models 1 and 2. During transient response, tyre Q_1 radial force decreases, decreasing cornering stiffness and reducing its ability to generate lateral forces.

Figure 9 Lateral force F_{sq1} – lateral step input (see online version for colours)

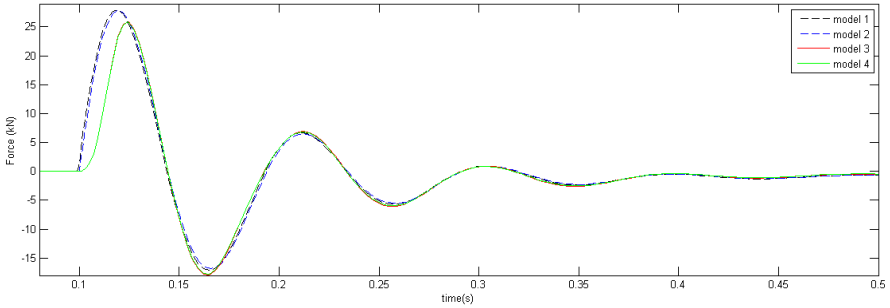

Figure 10 shows the cornering stiffness k_{sq1} value during the lateral step input simulation. The values corresponding to models 1 and 2 are constant as expected. Although in models 3 and 4, there is a variation of approximately 97% and 18% (in respect of the initial value) in $t = 0.1$ s and $t = 0.19$ s respectively.

Figure 10 Cornering stiffness k_{sq1} – lateral step input (see online version for colours)

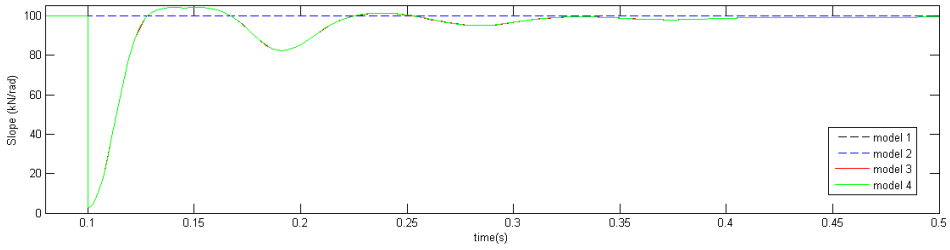

Analysing Table 2, one can observe that the maximum deviation of the radial force predicted with the linear model is –6.8% and the maximum deviation of the slip force is 8.1%.

Table 2 Percentage deviation from the complete model 4 – maximum radial force and maximum absolute lateral force – lateral step

	Unit	*Model 1* (%)	*Model 2* (%)	*Model 3* (%)
Max radial force F_{rp1}	kN	–6.7	–6.7	0.0
Max radial force F_{rp2}	kN	–6.8	–6.8	0.0
Max radial force F_{rq1}	kN	–1.6	–1.6	0.0
Max radial force F_{rq2}	kN	0.0	0.0	0.0
Max radial force F_{rr1}	kN	–1.4	–1.4	0.0
Max radial force F_{rr2}	kN	0.0	0.0	0.0
Max abs lateral force F_{sp1}	kN	–6.6	–6.6	0.0
Max abs lateral force F_{sp2}	kN	–6.1	–6.1	0.0
Max abs lateral force F_{sq1}	kN	8.1	8.1	0.4
Max abs lateral force F_{sq2}	kN	–7.6	–7.3	–0.3
Max abs lateral force F_{sr1}	kN	0.4	0.0	0.4
Max abs lateral force F_{sr2}	kN	–7.7	–7.5	–0.2

The second forced input is a lateral and vertical misalignment beam transition of 10 mm in both lateral and vertical directions, which can be modelled as a lateral step input at vector x_r as follows.

$$\begin{cases} x_r(t < 0.1) = \{0 \quad 0 \quad 0\}^T \\ x_r(t \geq 0.1) = \{10 \quad 10 \quad 0\}^T. \end{cases}$$

Figure 11 shows lateral and vertical displacements and roll rotation angle for the combined vertical and lateral step input. Figure 12 shows the comparison of lateral force F_{sq2}, the maximum values are higher in models 3 and 4.

Analysing Table 3, one can observe that the maximum deviation of the radial force predicted with the linear model is –2.9% and the maximum deviation of the slip force is –10.1%.

Table 3 Percentage deviation from the complete model 4 – maximum radial force and maximum absolute lateral force – combined lateral and vertical step

	Unit	*Model 1* (%)	*Model 2* (%)	*Model 3* (%)
Max radial force F_{rp1}	kN	2.3	2.5	–0.1
Max radial force F_{rp2}	kN	1.6	2.1	–0.6
Max radial force F_{rq1}	kN	–2.9	–2.9	0.0
Max radial force F_{rq2}	kN	–1.2	–1.2	0.0
Max radial force F_{rr1}	kN	0.0	0.0	0.0
Max radial force F_{rr2}	kN	–1.5	–1.5	0.0
Max abs lateral force F_{sp1}	kN	0.0	0.0	0.0
Max abs lateral force F_{sp2}	kN	–1.9	–1.9	0.0
Max abs lateral force F_{sq1}	kN	0.0	0.0	0.0
Max abs lateral force F_{sq2}	kN	–10.1	–10.1	0.0
Max abs lateral force F_{sr1}	kN	–10.1	–10.1	0.0
Max abs lateral force F_{sr2}	kN	7.8	7.5	0.4

Figure 11 Lateral (top) and vertical (centre) displacements and roll rotation (bottom) – lateral and vertical step input (see online version for colours)

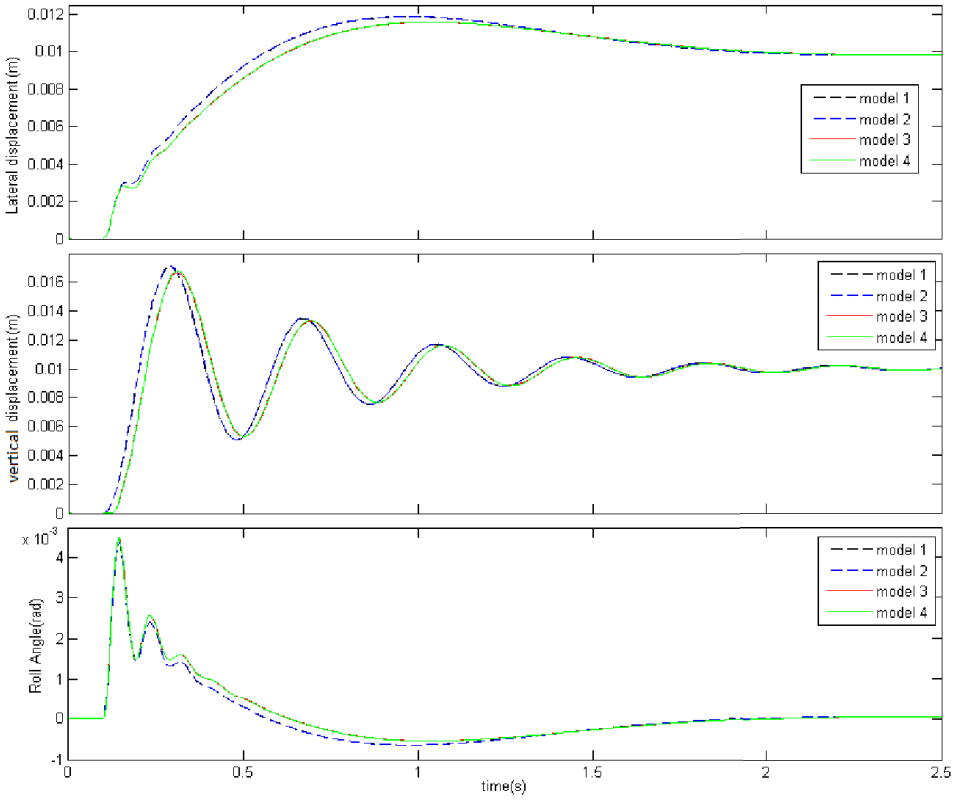

Figure 12 Lateral force F_{sq2} – combined lateral and vertical step input (see online version for colours)

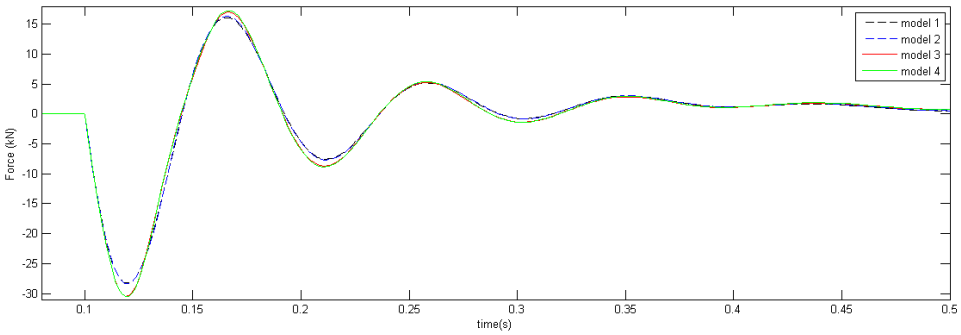

Table 4 shows the properties used in the simulated monorail vehicle models.

Table 4 Model parameters

Parameter name	*Variable*	*Unit*	*Value*
Car body mass (half vehicle)	M	kg	9450
Car body roll inertia (half vehicle)	I_x	kg.m^2	10,000
Stiffness of vertical tyre in radial direction	k_p	N/m	$1.3\dot{1}0^6$
Stiffness of guide tyre in radial direction	k_q	N/m	$1.3\dot{1}0^6$
Stiffness of stabilising tyre in radial direction	k_r	N/m	$1.3\dot{1}0^6$
Damping coefficient of vertical tyre in radial direction	c_p	N.s/m	3180
Damping coefficient of guide tyre in radial direction	c_q	N.s/m	3180
Damping coefficient of stabilising tyre in radial direction	c_r	N.s/m	3180
Tyre cornering stiffness (vertical, guide and stabilising)	$k_{s(p,q,r)}$	N/rad	10^5
Vertical distance of car body centre of mass and guide tyre	H_q	m	2.5
Vertical distance of car body centre of mass and stabilising tyre	H_r	m	3.2
Half of guideway width	B	m	0.25
Half of distance between vertical tyres	b	m	0.185
Initial vertical position of car body centre of mass	z_0	m	2.0
Vertical tyre radial preload force	$F^0_{rp(1,2)}$	N	46,352
Guide tyre radial preload force	$F^0_{rq(1,2)}$	N	13,244
Stabilising tyre radial preload force	$F^0_{rr(1,2)}$	N	13,244
Vertical tyre cornering stiffness coefficient 1	c_{1p}	–	$1.04\dot{1}0^5$
Vertical tyre cornering stiffness coefficient 2	c_{2p}	–	61,803
Guide tyre cornering stiffness coefficient 1	c_{1q}	–	$1.04\dot{1}0^5$
Guide tyre cornering stiffness coefficient 2	c_{2q}	–	17,658
Stabilising tyre cornering stiffness coefficient 1	c_{1r}	–	$1.04\dot{1}0^5$
Stabilising tyre cornering stiffness coefficient 2	c_{2r}	–	17,658

6 Conclusions

A model of a straddle type monorail vehicle was developed with three degrees of freedom representing a frontal half vehicle. As a contribution to this work, the authors introduced a method to determine the guiding and stabilising tyres radial preload forces, based on the tyre properties.

The linear modal behaviour of the vehicle was analysed and the stability based on root locus reveals that the vehicle's pole placement is considerably influenced by its longitudinal velocity. It was showed that lower sway and upper sway vibration modes' natural frequencies and damping factors decrease with the increase of longitudinal velocity, asymptotically approaching to a stable system.

Results show that the tyre modelling technique influences the overall dynamics of a straddle type monorail vehicle numerical model. The influence of tyre radial force on its cornering stiffness has a great effect on the vehicle's overall dynamics. It induces a nonlinear coupling between lateral and vertical movements of the car body, when the vehicle passes through a lateral misalignment at the guideway.

In the simulation of lateral misalignment between two consecutive beams, the maximum deviations of radial and slip forces were –6.8% and 8.1% respectively. In the simulation of

lateral and vertical misalignment beam transition, maximum deviations of radial and slip forces were –2.9% and –10.1% respectively. These differences can be important to develop a virtual model that predicts the real vehicle's behaviour with more accuracy. Moreover, increasing the accuracy to predict tyre lateral and vertical forces can be useful specially to predict tyre durability.

It's also important to notice that the maximum forces are very similar between models 3 and 4 for both simulations. So in the circumstances to which the vehicle was subjected, the implementation of the complete slip velocities contributes very little to the numerical response accuracy of the model.

References

Barbosa, R.S. and Neto, A.C. (1996) 'Dinâmica do rodeiro ferroviário', *Revista Brasileira de Ciências Mecânicas*, Vol. 18, No. 4, pp.318–329.

Bruni, S., Vinolas, J., Berg, M., Polach, O. and Stichel, S. (2011) 'Modelling of suspension components in a rail vehicle dynamics context', *Vehicle System Dynamics: International Journal of Vehicle Mechanics and Mobility*, Vol. 49, No. 7, pp.1021–1072.

Cao, D., Song, X. and Ahmadian, M. (2011) 'Editors' perspectives: road vehicle suspension design, dynamics, and control', *Vehicle System Dynamics: International Journal of Vehicle Mechanics and Mobility*, Vol. 49, pp.3–28.

Du, Z.X., Wen, X.X. and Shen, Z. (2014) 'The impact analysis of tire parameter for tire wear when monorail vehicle curve driving', *Applied Mechanics and Materials*, Vol. 470, pp.529–533.

Goda, K., Nishigaito, T., Hiraishi, M. and Iwasaki, K. (2000) 'A curving simulation for a monorail car', *Proceedings of the 2000 ASME/IEEE Joint Railroad Conference, 2000*, ASME/IEEE Joint, Newark NJ, pp.171–177.

Liu, G. *et al.* (2014) 'Effect of wheel pressure on vibration of straddle monorail transit vehicle-bridge system', *Advanced Materials Research*, Vol. 919, pp.542–546.

Mohajer, N., Abdi, H., Nelson, K. and Nahavandi, S. (2015) 'Vehicle motion simulators, a key step towards road vehicle dynamics improvement', *Vehicle System Dynamics*, Vol. 53, pp.1204–1226.

Pacejka, H.B. (2005) *Tire and Vehicle Dynamics*, Elsevier.

Polach, O. (2007) 'Comparability of the non-linear and linearized stability assessment during railway vehicle design', *Vehicle System Dynamics: International Journal of Vehicle Mechanics and Mobility*, Vol. 44, No. Supp. 1, pp.129–138.

Segel, L. and Ervin, R.D. (1981) 'The influence of tire factors on the stability of trucks and tracktor trailers', *Vehicle System Dynamics*, Vol. 10, No. 1, pp.39–59.

Shabana, A.A. (2008) *Railroad Vehicle Dynamics: A Computational Approach*, CRC Press.

Shen, S., Wang, J., Shi, P. and Premier, G. (2007) 'Nonlinear dynamics and stability analysis of vehicle plane motions', *Vehicle System Dynamics: International Journal of Vehicle Mechanics and Mobility*, Vol. 45, pp.15–35.

Wei, T. and Dorfi, H.R. (2014) 'Tire transient lateral force generation: characterization and contribution to vehicle handling performance', *Tire Science And Technology*, Vol. 42, No. 4, pp.263–289.

8.12 ANEXO L

CHARACTERIZATION AND MODELLING OF A NEW HEAVY AXLE LOAD FREIGHT WAGON FOR WHEEL RAIL WEAR PREDICTION

Santos, G. F. M.; Barbosa, R. S.; Urban, C.; Shu, X.; Joy, R. (2014) Characterization and Modelling of a New Heavy Axle Load Freight Wagon for Wheel Rail Wear Prediction. Journal of Mechanical Engineering and Technology, DOI: 10.18005/JMET0203001, pp. 17-28.

Characterization and Modelling of a New Heavy Axle Load Freight Wagon for Wheel Rail Wear Prediction

Guilherme Fabiano Mendonça dos Santos[*1], Roberto Spinola Barbosa[2], Xinggao Shu[3], Curtis Urban[4], Richard Joy[5]

[1]Innovation and Development Department, Vale S.A, Av. Dante Michelini, 5500, Vitoria, Brazil

[2]Polytechnic School, University of São Paulo, São Paulo, Brazil

[3, 4, 5]Transportation Technology Center, Inc., Pueblo, Colorado, USA

[*1]gfmsantos@yahoo.com; [2]spinola@usp.br; [3]xinggao_shu@aar.com; [4]curtis_urban@aar.com; [5]richard_joy@aar.com

***Abstract*-Vale projects an increase in annual tonnage of more than 120 percent its Estrada de Ferro Carajás between 2012 and 2017. Part of the increase will be accomplished by obtaining new wagons that will be operated at 37.5 tonne axle loads.**

Transportation Technology Center, Inc. (TTCI) and Vale conducted a test of a new wagon to determine secondary suspension stiffness as well as inertial mass moments of inertia of the wagon body. The results were used in conjunction with results from track testing to construct an accurate model of the wagon.

The validated model was used to compare wheel and rail wear at the increased axle loads with the current axle load of 32.5 tonnes. While wheel and rail RCF and wear are predicted to increase with current wheel profiles, implementation of improved wheel profiles may reduce wear and RCF significantly. In addition, the importance of preventive grinding and lubrication is emphasised.

Key words- Rail Wheel Interaction; Rolling Contact Fatigue; Rolling Stock Design; Simulation; Wear

I. INTRODUCTION

Vale's Estrada de Ferro Carajás (EFC) operates an iron ore service in northern Brazil. Vale projects an increase in annual tonnage of more than 120 percent on EFC between 2012 and 2017. Engineering and economic analysis conducted by Vale and the Transportation Technology Center, Inc. (TTCI) indicated that part of the increase in tonnage could be accomplished by increasing the axle loads in two ways: 1.) Increasing the axle loads of the existing fleet of freight wagons to from 31.5 to 32.5 tonnes and 2.) Purchasing new freight wagons capable of 37.5 tonne axle loads. The new freight wagons (designated GDU) are now being put in service with axle loads restricted to 32.5 tonnes because existing infrastructure may not yet be ready for 37.5 tonne axle loads. Vale plans to increase the GDU axle loads to 37.5 tonnes beginning from 2017.

TTCI and Vale conducted a vehicle characterization test of a GDU wagons in 2011 to determine vertical and lateral secondary suspension stiffness as well as inertial mass moment of inertia of the wagon body. The results were used in conjunction with results from track testing conducted in 2010 to construct an accurate model of the wagon. The validated model was then used to predict wagon performance with an emphasis on wheel and rail life. Results will eventually be used to update the economic analysis.

II. BACKGROUND

Vale's ongoing efforts to increase tonnage include double-tracking a majority of the line and doubling the port capacity. TTCI is working with Vale to prepare for the planned increase in axle loads in 2017. This includes:

- Assistance in evaluation of new wagons.
- Implementation of a preventive grinding program – in conjunction with National Research Council Canada Centre for Surface Transportation Technology (NRC-CSTT)
- Optimisation of wheel and rail profiles – in conjunction with NRC-CSTT.

As part of the effort, Vale intends to initiate evaluation of gauge-face and top-of-rail lubrication in late 2012.

Vale conducted a series of acceptance tests on the new GDU wagons as part of the acquisition process [1].

III. OBJECTIVES

The 2008 economic analysis was partly based on estimates of wheel and rail wear from models of the existing wagons (designated GDT) with increased axle loads. Based on these models, it was predicted that increasing axle loads to 37.5 tonnes would increase wheel and rail wear by approximately 16 percent compared to 31.5 tonne axle loads and 11 percent compared to 32.5 tonne axle loads. These results are contained in a report confidential to Vale.

With acquisition of new GDU wagons in progress, it was possible to assemble a more accurate vehicle model to refine the predictions of wheel and rail degradation under increased axle loads.

IV. APPROACH

Simulations were conducted using TTCI's railway multi-body dynamics computer program, NUCARS®, a registered trademark of TTCI. It is designed to simulate the dynamic interaction of any rail vehicle with virtually any track. The user may select any number of bodies, degrees of freedom, and connection elements to describe a vehicle and track system. NUCARS® can be used to analyze the dynamic interaction of rail vehicles and track to predict stability, ride quality, vertical and lateral dynamics, and steady state and dynamic curving response. The program includes detailed nonlinear models of wheel/rail interaction and suspension response, with wheel/rail interaction based on Kalker's complete non-linear creep theory [2]. Simulations of any type of freight, passenger, transit and locomotive rail vehicles are possible. Track simulations may include hypothetical track geometries or measured track supplied by the user, including turnouts and guard rails.

The NUCARS program is a generalized nonlinear, multi-body simulation. A complete description is provided in the NUCARS Help Manual. Briefly, the model assembles the following equations of motion for a multi-body system and solves this set of equations to predict system response to deterministic inputs:

$$M\ddot{q} = -T^T f(s, \dot{s}) - Dq - \dot{K}q + f$$

where

$$s = Tq + T_r r$$

and

$$\dot{s} = T\dot{q} + T_r \dot{r}$$

In the system mass matrix, M, D, and K are the flexible body mode damping and stiffness matrices. The stroke transformation matrices are T and Tr. Vectors q, q̇, and q̈ represent the degree-of-freedom displacements, velocities, and accelerations. Vectors r and ṙ are the inter-body relative displacements and velocities. These displacements and velocities arise from motion along curved or twisted track. Vector f represents the connection forces. These are nonlinear functions of the connection strokes s and velocities. Vector F represents the external forcing inputs.

The NUCARS program has been firmly established as a viable analytical tool. The NUCARS Help Manual describes numerous examples of model validation model beginning with the general method used in calculating wheel/rail forces that originated in work performed by researchers at British Rail in the early 1970's and research conducted by the Association of American Railroads (AAR) and TTCI beginning in the 1980s. A recent project has compared the performance of several different Vehicle Track Interaction software packages, including the NUCARS program. NUCARS was shown to produce comparable results at competitive calculation speeds to the other programs [3], [4].

The success of analytical models relies heavily on the accuracy of the dynamic parameters such as mass, pitch, yaw and roll mass moments of inertia, the centre of gravity location, suspension stiffness, and damping characteristics. Some of these values can be theoretically calculated using data supplied by the wagon builder, truck designer/manufacturer, or other suppliers. However, accurate calculation is often difficult due to variation among rail vehicles of the same type, wear of components, complex vehicle geometry and loading configurations [5].

Parameters for the GDU model were verified in two ways, first through detailed measurements of vehicle response to excitation in a shop environment, and then by comparison of model outputs with vehicle responses measured during testing of bogie configuration.

V. VEHICLE CHARACTERIZATION TEST

An initial phase of work was to conduct a workshop-based vehicle characterization test to determine the stiffness and inertial properties of the GDU wagon. The characterization was conducted at Vale's shops in Sao Luis during the week beginning-on-17 October 2011. Fig. 1 shows the test wagon.

The testing methodology was developed by the Association of American Railroads [5]. The method is cost effective, does not require elaborate equipment and can be executed in most shop environments.

Known rigid body modes of vibration for the rail vehicle - bounce, pitch, yaw, upper centre roll, and lower centre roll were measured. Fig. 2 illustrates these modes.

Fig. 1 Test wagon GDU 191 492 8

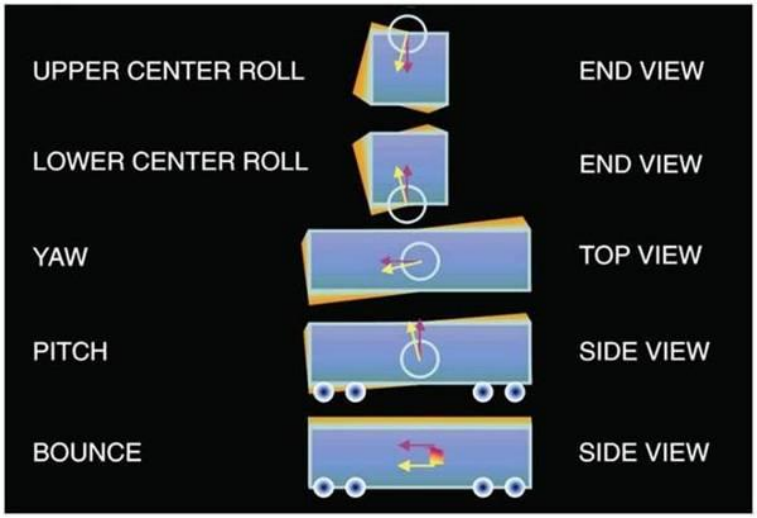

Fig. 2 Rigid body modes

Displacement transducers were placed on the vehicle body at selected key locations. Data was collected from the transducers in the form of time histories that were used to obtain the rigid body resonant frequencies of vibration. Figs. 3 and 4 provide schematic diagrams of the instrumentation setup. Fig. 5 shows displacement transducers installed on the lead bogie, left side for vertical and lateral wagon body displacement.

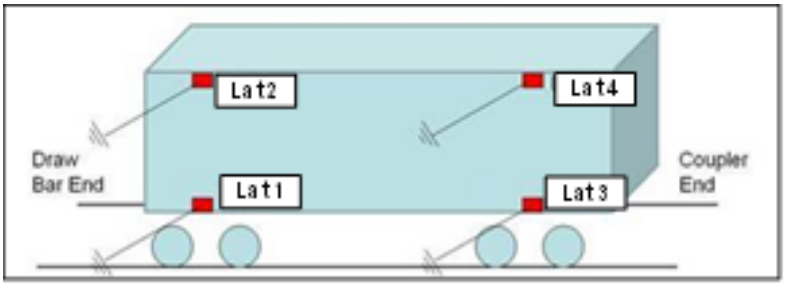

Fig. 3 Instrumentation schematic -- side view

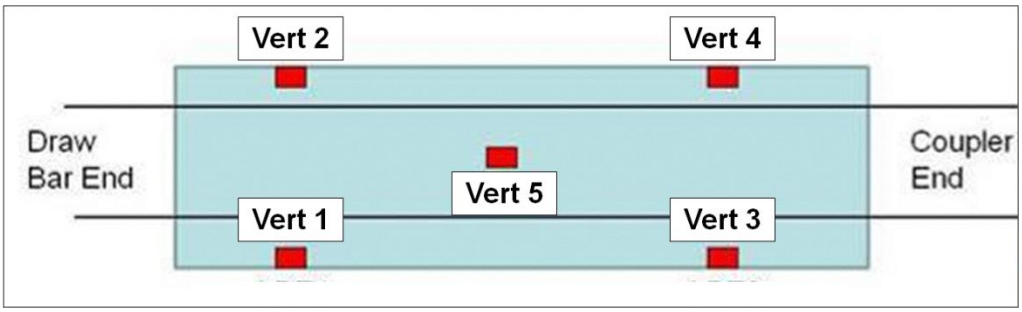

Fig. 4 Instrumentation schematic -- top view

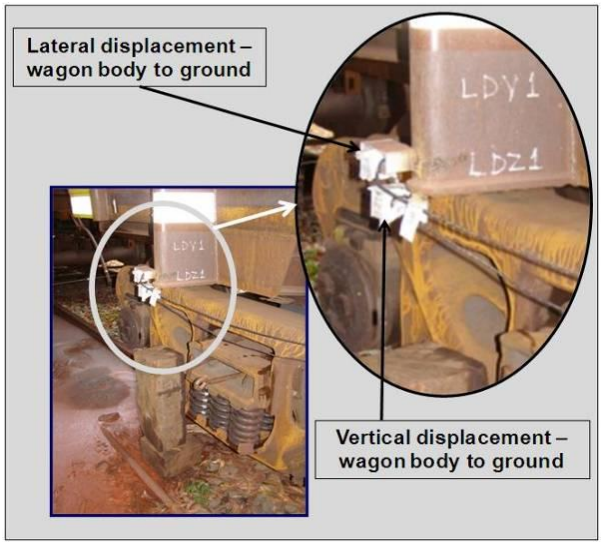

Fig. 5 Displacement transducer installed on the lead bogie, left side

It was necessary to deactivate the damping elements from the suspension system. The friction wedges in the test wagon's bogies were deactivated by pinning them as shown in Fig. 6. All of the main coils for the loaded wagon were retained in the bogie. In addition, the roller side bearings on both bogies were deactivated by blocking / shimming. This effectively created a simple mass spring system that could be excited by hand.

Fig. 6 Pinned Friction Wedges

All modes of vibration were then excited by hand, with assistance of a lever bar and wood block. Bounce mode was excited from the centre of the wagon, pitch mode from either end on the wagon centre line. Yaw and roll modes were excited from the bolster gib locations at either end of the wagon.

Fig. 7 shows an example of time histories - in this case of lateral displacements with the wagon body excited in roll. It is evident that the upper and lower displacements are 180 degrees out of phase, indicating that the wagon is rolling. Fig. 8 shows a frequency domain analysis showing two distinct peaks at approximately 0.9 Hz and at approximately 3.5 Hz. These represent the lower centre roll and upper centre roll frequencies, respectively.

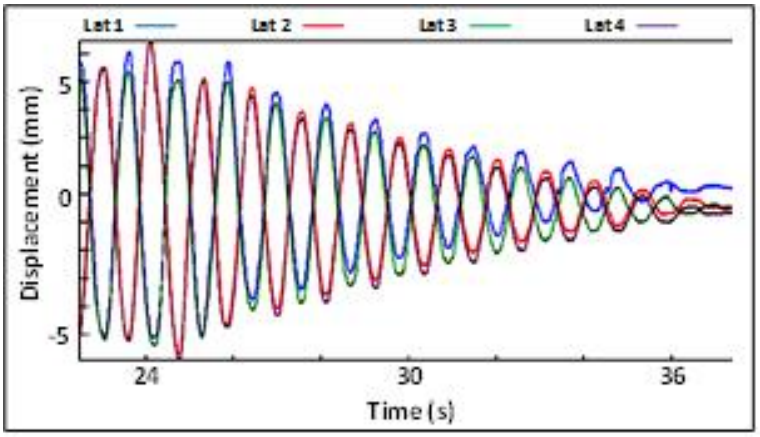

Fig. 7 Time histories – lateral displacements – roll mode

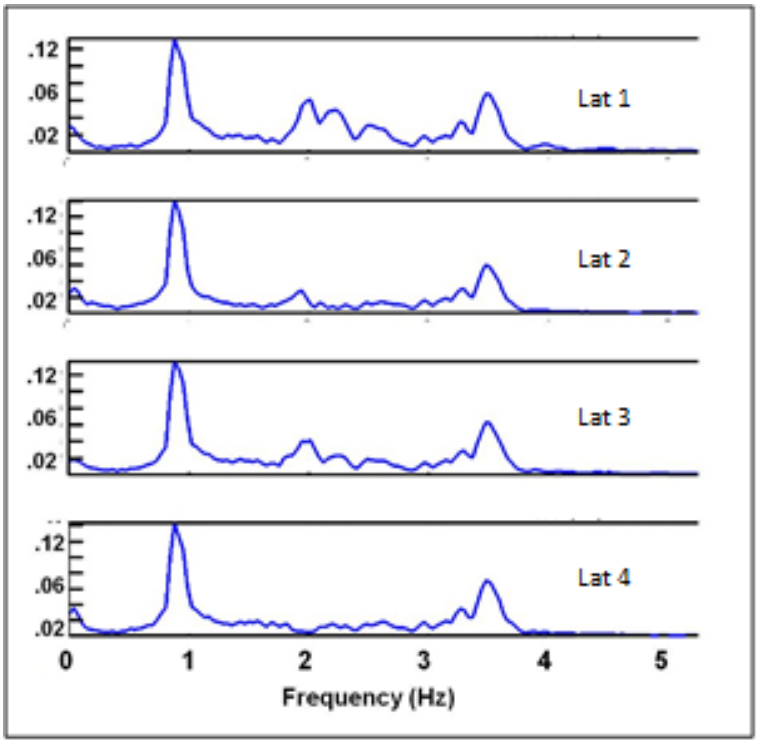

Fig. 8 Power spectral density – roll mode

Equations of motion were used to calculate the vehicle's dynamic parameters. Wilson, et al. [5] described the calculations. Tables 1 to 3 present the measured / calculated parameters.

TABLE 1 RIGID BODY MODES AND CENTRE OF GRAVITY

Mode	Frequency/ Position
Bounce	1.85Hz
Pitch	2.3 Hz
Yaw	1.55 Hz
Upper centre roll	3.09 Hz
Lower centre roll	0.78 Hz
Centre of Gravity	2.345m

TABLE 2 SHOWS THE MEASURED SECONDARY SUSPENSION STIFFNESSES

Property	**Value (**kN/m)
Vertical stiffness (per truck) **(**kN/m)	9,483
Lateral stiffness (per truck) (kN/m)	3,697
Pitch stiffness (kN-m/radian)	138,774
Yaw stiffness (car body to ground) (kN-m/radian)	63,026
Roll stiffness (kN-m/radian)	11,443

TABLE 3 SHOWS THE MASS MOMENTS OF INERTIA THAT WERE CALCULATED BASED ON MEASURED VALUES.

Property	**Value (**kg-m^2)
Car body pitch inertia	6.64E+05
Yaw inertia	6.64E+05
Car body roll inertia	1.20E+05

VI. COMPARISON TO TRACK TESTING

The model was further validated by comparing modelling results with data compiled by Vale during testing, which was conducted on EFC track from Kilometre10 to Kilometre 40 in May 2010. The test data used in this study was collected for the loaded test wagon with Maxion motion control bogies with cross bracing installed to reduce truck warp. Measurements included:

- Position and speed via GPS,
- Wheel / rail forces on the lead bogie via instrumented wheelsets (IWS).
- Vertical and lateral accelerations of the wagon body.
- Rotation and displacement between wagon body and bogies.
- Vertical deflection of the secondary suspension springs.
- Displacement between axles and side frames
- Displacement between side frames and bolsters.

Simulations were conducted through an 873m radius curve (Kilometre 16.525 to 15.415) with 58.7mm super elevation at 70mph running speed. Curvature, super elevation and spiral lengths were used as listed in Vale's track geometry chart. The simulations were of quasi-static curving, i.e. perfect track without perturbations. The simulations were run in the direction of decreasing kilometres (mine to port), beginning on straight track at Kilometre 16.65, Figs. 9 to 13 reflect performance as the vehicle moves from straight track through the transition and into the body of the curve.

Figs. 9 and 10 show a comparison of predicted wheel vertical and lateral forces with those measured with IWS. Since the simulations did not include short-wavelength track geometry, the test data shows a great deal more variation than the forces predicted with the model. It was necessary to slightly scale the mass and inertial values to match the test vehicle. However, the predicted quasi static force trends and average values are generally consistent with the measured data.

The measurement system noise, which also contributes to the discrepancy, was not filtered from the wheel forces in order to demonstrate the dynamic variations in the spiral and curve body.

Fig. 9 shows a shift in measured and simulated vertical force from the inboard to outboard wheel as the vehicle enters the spiral and curve. Fig. 10 shows increased lateral load on both wheels as the vehicle enters the curve.

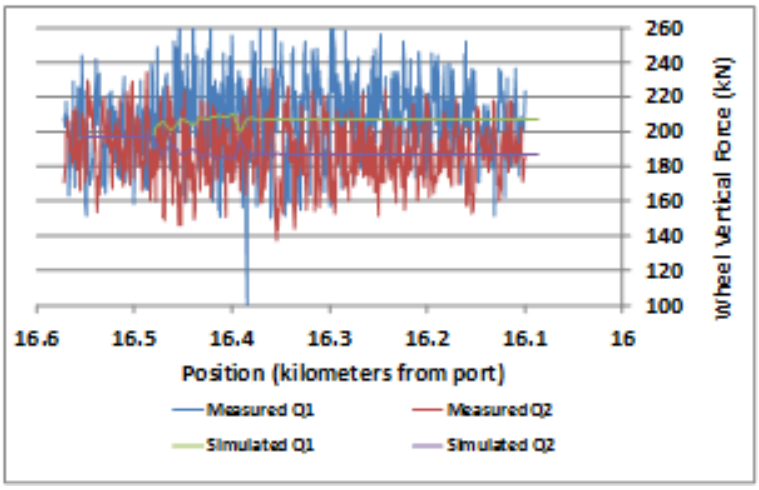

Fig. 9 Wheel vertical force comparison

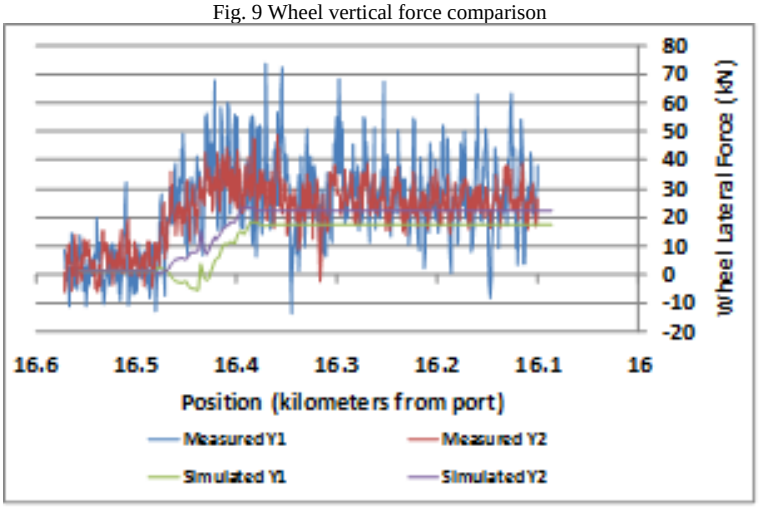

Fig. 10 Wheel lateral force comparison

Figs. 11, 12 and 13 compare predicted and measured displacements from the same curve.

Vertical displacements of the secondary suspension springs, longitudinal displacements between the wagon body and bolster, and lateral displacements between the side frame and bolster are compared. While the measured displacements are complex due to stick-slip action in the suspension, the predicted quasi static displacement trends and average values are generally consistent with the measured data. An exception is the sudden jump in bolster spring displacement VMT2 in Fig. 11 which could be explained by a sticky suspension component that released suddenly in the spiral. Discrepancies on the dynamic peak values are expected since dynamic perturbations were not included in the modelling.

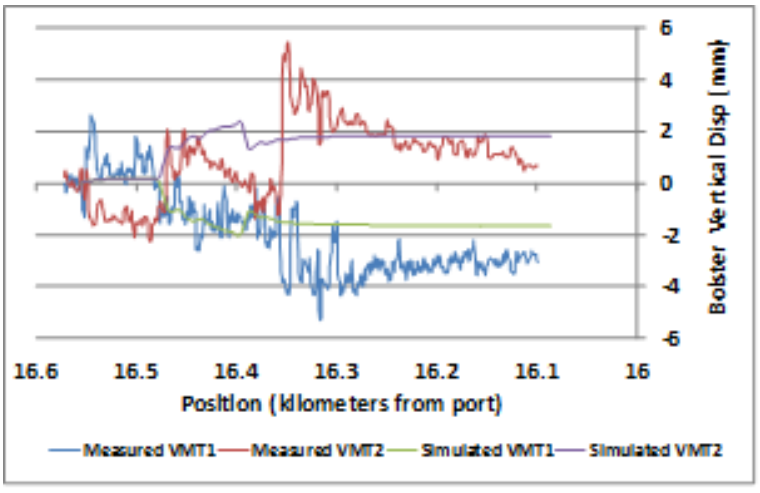

Fig. 11 Bolster spring vertical displacement comparison

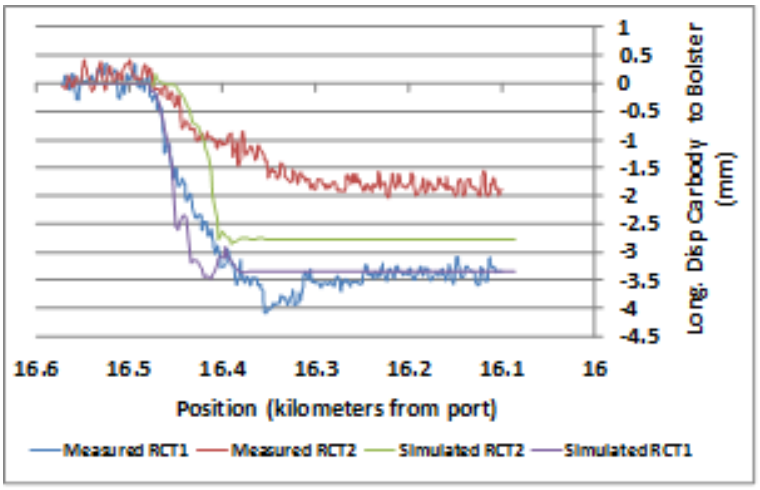

Fig. 12 Comparison of longitudinal displacement between carbody and bolster

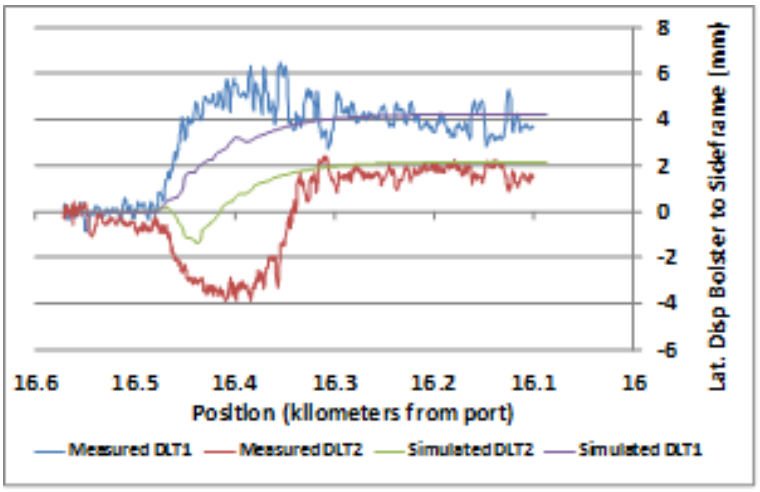

Fig. 13 Comparison of lateral displacement between bolster and side frame

Despite the discrepancies between modelling and test results in peak values of dynamic forces and displacements, the wheel forces and vehicle component displacements predicted from the modelling were generally consistent with the test results both in average values and variation trends on curves. Based on these results the model is considered adequate for quasi static curving simulation and performance evaluation.

VII. MODELLING PARAMETERS

The validated model was used to predict wagon performance with an emphasis on how the GDU wagon with heavier axle load will affect wheel and rail performance.

A GDT and GDU wagon equipped with the same type of cross-braced bogie, but with 32.5 and 37.5 tonnes axle load respectively, were simulated for comparison. The car body mass, moment of inertia, suspension characteristics were updated with values from the vehicle characterization test. Other wagon and cross-braced bogie parameters were adopted from previous investigations.

Simulations were performed using curves with radii of 860m and 1,719 m. The superelevations for these curves were 51mm and 28 mm, respectively. The vehicle running speed was 70 km/hour. The wheel/rail coefficient of friction was 0.5 representing a dry rail condition without lubrication. Table 4 summarizes the data used in the curving simulations.

TABLE 4 CURVING SIMULATION DETAILS

Radius (m)	**860**	**1,719**
Superelevation (mm)	51	28
Speed (km/hour)	70	70

Three different rail profiles were used in the curving simulations:

- New 136 RE with a 10-inch crown radius.

- Grinding templates being implemented as part of the preventive grinding program as recommended by TTCI and NRC-CSTT.
- Worn rail profiles measured on the simulated curves.
- Figs. 14 and 15 show examples of the profiles used.

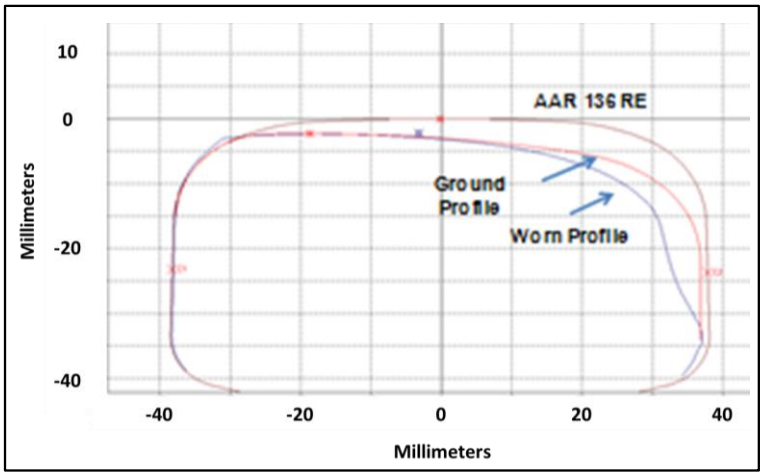

Fig. 14 Profiles used for high rail on 860-metre curve

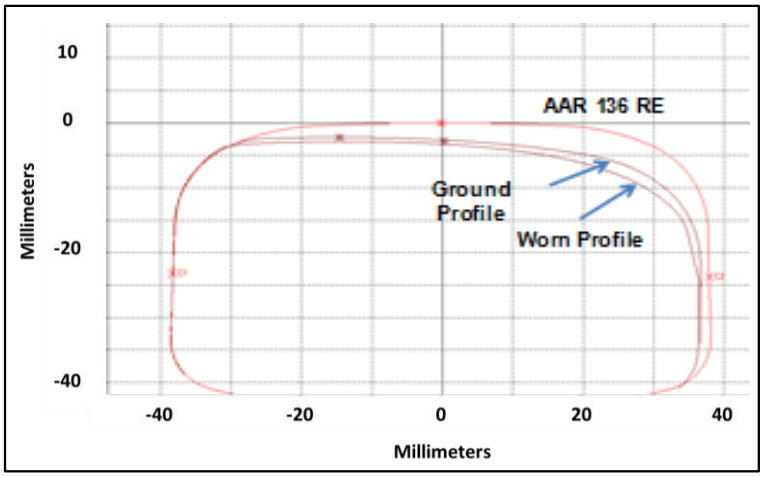

Fig. 15 Profiles used for high rail on 1,719 metre curve

In addition, three wheel profiles were used: the AAR1:20 profile currently used on EFC, and Alternate Designs 2 and 3, recently designed by TTCI and NRC-CSTT that are currently being evaluated on EFC. Alternate Design 1 was initially proposed, but will not be implemented because simulations indicated that Alternate Design 1 would have a lower threshold for the onset of vehicle lateral instability (hunting).

VIII. WHEEL AND RAIL SURFACE DAMAGE MODELS

Wheel and rail wear has been related to the energy transfer through the contact patch. McEwen and Harvey [6] developed relationships between wear and $T\gamma$, where T is the same as the tangential force, and γ is the tangential creepage in the contact patch. Burstow [7] extended this concept to the prediction of RCF. Fig. 16 shows the damage function that was developed by comparing predictions from computer modelling with observations of RCF in service.

The model combines the effects of wear and RCF. For $T\gamma < 15$N-m/m, there is no surface damage on the rail. For 15N-m/m $< T\gamma <$ 65N-m/m, there is RCF that increases linearly with $T\gamma$. For $T\gamma >$ 65N-m/m, wear starts to counteract RCF damage. For $T\gamma >$ 175N-m/m, there is only wear since the wear rate exceeds the rate of propagation of RCF. The y-axis gives rail damage per axle pass. For example, if $T\gamma$ = 65N-m/m the damage per axle = 10^{-5}, and 100,000 axles are required to produce RCF on the rail.

A positive value indicates RCF damage and a negative value indicates wear.

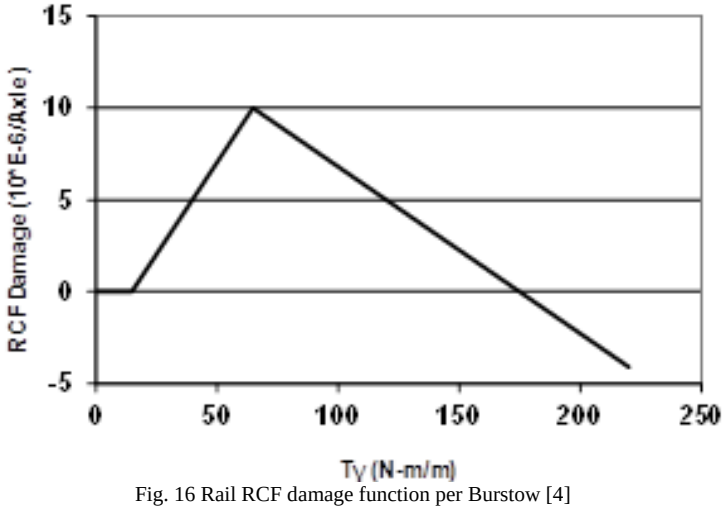

Fig. 16 Rail RCF damage function per Burstow [4]

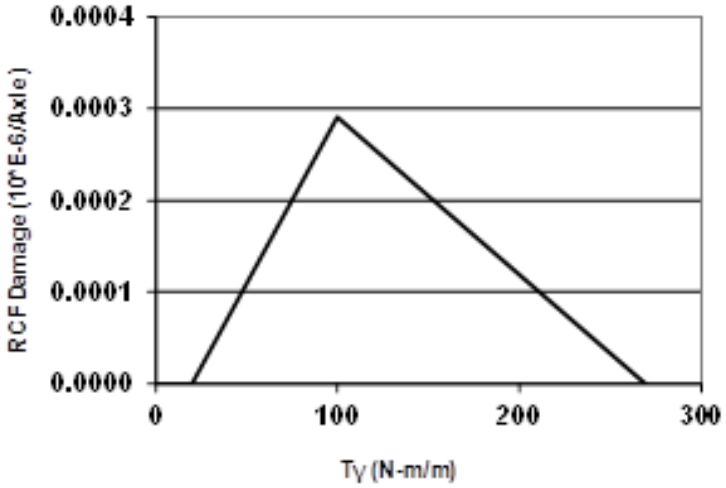

Fig. 17 Wheel RCF damage function per Tunna et al.-[8]

Tunna et al [8] followed a similar method to develop the damage function for wheels shown in Fig. 17.

The y-axis in Fig. 17 gives damage per wheel revolution. For example, if Tγ = 100N-m/m the damage per axle = 0.00029, and 3,448 wheel revolutions are required to produce RCF on the wheel. The breakpoints in Fig. 17 occur at 20 and 100 N-m/m. These are higher than the corresponding values in Fig. 16. This reflects the higher strength of the wheel material compared to that of the rail.

The values quoted here are based on calibration with particular types of wheel and rail materials in service on the British rail system. They have not been calibrated for the axle loads or hardened materials used on EFC. However, they are useful in showing a general relationship between Tγ, RCF and wear.

IX. RESULTS

Fig. 18 shows the predicted Tγ on the high rail and wheel for the cross-braced bogie on the lead axle in the 860-metre curve. The base case is the GDU wagon with AAR 1:20 profiles at 32.5 tonne axle loads. Also shown are results for the GDU wagon at 37.5 tonne axle loads with the AAR1:20 and the two alternate design profiles.

Clearly, increasing axle loads without changing wheel profile results in an increase in Tγ for each of the rail profiles considered.

With the alternate design profiles, the predicted Tγ at 37.5 tonne axle loads is reduced from the base case for new and ground rail and about the same for worn rail.

This is because AAR 1:20 wheel and AREMA 136 rail profile combination generates 2-point contact on the wheel tread and flange, which results in higher lateral force and Tγ. Design 2 and 3 wheel profiles are conformal to the AREMA 136 rail shape and generate 1-point contact on high rail shoulders which generates lower lateral force and Tγ.

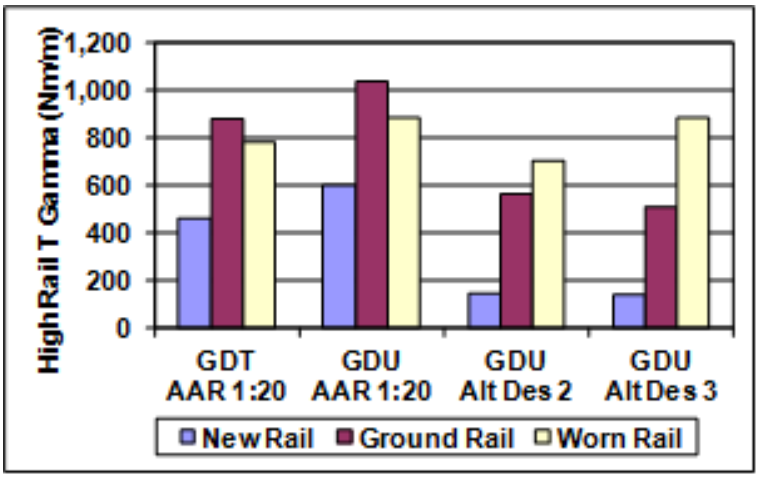

Fig.18 Tγ – 860-metre radius curve high rail

Fig. 19 shows measured rail profiles from a curve similar to the curve simulated after 185 million gross tonnes (MGT) of predominantly GDT traffic. The rail shows heavy wear, calculated to be approximately 0.03 mm/MGT side wear and 0.02 mm/MGT head wear. This indicates that the Tγ for the base case is likely in the wear portion of the rail RCF damage function.

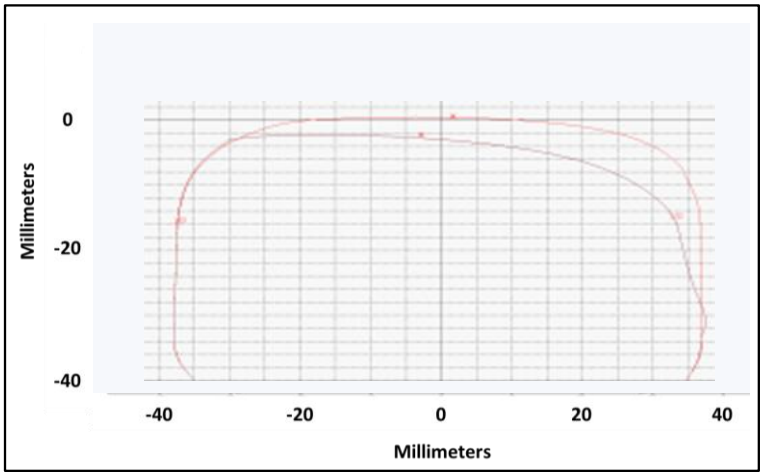

Fig. 19 Rail wear on 869-metre Curve after 185 MGT

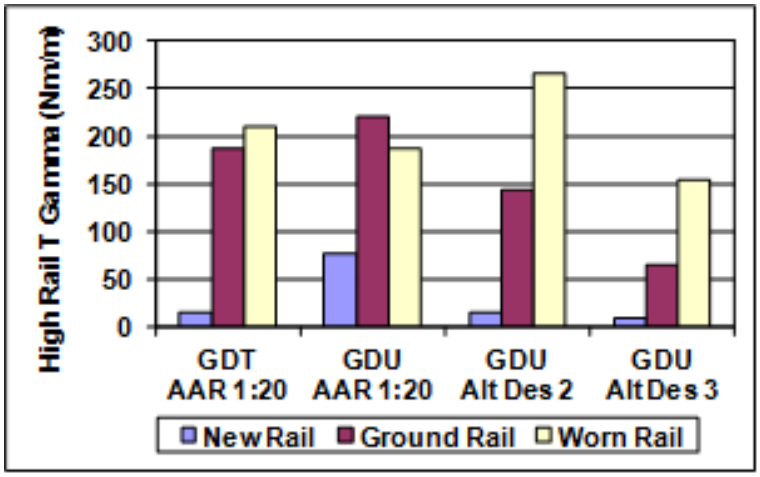

Fig. 20 Tγ – 1,719-metre Radius Curve High Rail

Fig. 20 shows the predicted Tγ on the high rail for the cross-braced bogie on the lead axle in the 1.719-metre curve. The base case is the GDT wagon with AAR 1:20 profiles at 32.5 tonne axle loads. Also shown are results for the GDU wagon at 37.5 tonne axle loads with the AAR1:20 and the two alternate design profiles.

Predicted Tγ is much lower for all cases simulated. GDU wagons with AAR 1:20 wheels are predicted to generate higher Tγ on new and ground rails than GDT wagons with AAR1:20 wheels. However, Tγ levels are about the same or slightly lower

for worn rail.

GDU wagons with Design 2 and 3 wheel profiles generate higher or similar Tγ on worn rails.

These results support implementation of the improved wheel profiles and continued attention to preventive grinding implementation. Work is in progress to better relate Tγ to damage functions for EFC's conditions and provide inputs to Vale's economic models.

X. CONCLUSIONS

A GDU wagon model was set up with updated car body mass, moments of inertia and suspension parameters based on results from a vehicle characterization test. Results were compared with track test data to validate the model.

Simulations were performed of a GDT and GDU wagon equipped with cross-braced bogies, with 32.5 and 37.5 tonnes axle loads respectively. The simulation results were used to investigate the effects of axle load on wheel and rail performance. The following conclusions can be drawn from simulations:

GDU wagons with AAR 1:20 wheel profiles generate higher Tγ values than GDT wagons with the same types of cross-braced bogies and wheels due to axle load increase from 32.5 tonnes to 37.5 tonnes. Correspondingly, GDU wagon wheel life is expected to be shorter than that of GDT wagon under the current operating conditions.

However, in many cases, incorporation of improved wheel profiles currently underway on EFC is predicted to reduce the Tγ values, which will be likely to reduce wear.

When considered in combination with improved wheel profiles, the ground rail profiles generally generate lower Tγ values. This illustrates the importance of continuing implementation of preventive grinding on EFC. However, the rail grinding profiles may need to be adjusted as the axle load is increased [9].

Wheel and rail flange wear is likely to continue on sharp curves. Vale should continue with efforts to implement a lubrication strategy before increasing axle loads to 37.5 tonnes.

Since the simulations did not include short-wavelength track geometry, the track test data shows a great deal more variation than model results. However, results are generally consistent with the test results both in average values and variation trends on curves and are considered adequate for the quasi static curving simulation and performance evaluation reported here.

Work is in progress to improve predictions by including measured track geometry and to better relate Tγ to damage functions for EFC's conditions. Results will provide inputs to Vale's economic models.

ACKNOWLEDGEMENTS

The authors are pleased to acknowledge Amsted Maxion for supporting the test and AimTech Engenharia Ltda. for providing instrumentation and data acquisition services.

REFERENCES

[1] G. Riggal, "Dos Santos GFM. Use of instrumented wheelset to determine best bogie configuration for Vale under 37.5 tonne axle loads," Proceedings: 2011 International Heavy Haul Association Conference, Calgary: International Heavy Haul Association 2011.

[2] J. J. Kalker, "The Computation of Three Dimensional Rolling Contact with Dry Friction," International Journal for Numerical Methods in Engineering, vol. 14, pp. 1293-1307, 1979.

[3] Transportation Technology Center, Inc. "NUCARS® Help Manual 2014.2", Chapter 1, pp. 5-9. [Online]. Available: http://www.ttci.aar.com/nucars/, on 22 October 2014.

[4] Manchester Benchmarks for Rail Vehicle Simulation, Supplement to Vehicle Systems Dynamics, vol. 31, ed. Swets & Zeitlinger B.V., Lisse, The Netherlands, 1999.

[5] N. G. Wilson, C. L. Urban, and M. S. Burnett, "Rail vehicle dynamic parameter identification," Rail Transportation. (Publication) RTD, American Society of Mechanical Engineers, Rail Transportation Division, vol. 13, pp. 83-87, 1997.

[6] I. J. McEwen and R. F. Harvey, "Interpretation of wheel/rail wear numbers TM VDY 004," Derby, UK: British Rail Research, 1986.

[7] M. C. Burstow, "Whole life rail model application and development for RSSB - continued development of an RCF damage parameter," London: Rail Standards and Safety Board, 2004.

[8] J. Tunna, J. Sinclair, and J. Perez, The development of a wheel wear and rolling contact fatigue model, London: Rail Standards and Safety Board, 2007.

[9] P. Sroba, F. Sgavioli, R. Joy, J. R. Santos, A. Pina, and R. Caldwell, "Preventive grinding on Estrada de Ferro Carajás," Proceedings: 2013 International Heavy Haul Association Conference 2013, New Delhi: International Heavy Haul Association, 2013.

8.13 ANEXO M

NUMERICAL OPTIMISATION METHODS APPLIED TO THE CONCURRENT PROBLEM OF VEHICLE RIDE AND HANDLING

Vilela, D.; Barbosa, R. S. (2013) Numerical optimisation methods applied to the concurrent problem of vehicle ride and handling. International Journal of Vehicle Systems Modelling and Testing - IJVSMT, DOI: 10.1504/IJVSMT.2013.057526, Vol. 8, nº 4, pp. 316-334.

Numerical optimisation methods applied to the concurrent problem of vehicle ride and handling

Daniel Vilela*

Vehicle Synthesis, Analysis and Simulation Department,
General Motors do Brasil Ltda.,
GMB VSAS, Av. Goiás, 2769, CT #1, Bairro Barcelona
São Caetano do Sul, SP, CEP: 09550-051, Brazil
E-mail: danvil_br@hotmail.com
*Corresponding author

Roberto Spinola Barbosa

Departamento de Engenharia Mecânica,
Escola Politécnica da Universidade de São Paulo,
Av. Prof. Mello Moraes 2231, Butantã,
São Paulo, SP, CEP: 05508-900, Brazil
E-mail: roberto.barbosa@poli.usp.br

Abstract: This text presents a new proposal for an overall ride and handling metric to be used to optimise vehicle performance through concurrent simulation models. The proposed metric has the intention to cover simultaneously the most relevant aspects of a passenger vehicle dynamic behaviour. The individual models for ride and handling have been validated against physical measurements in order to assure a reliable output. A numerical optimisation method is used to simultaneously evaluate the complete vehicle dynamic performance related to the single overall metric. The results show an effective way to improve the vehicle performance based on this new proposed metric, with gains in terms of reduction in development time and cost for new projects.

Keywords: ride; handling; vehicle dynamics; simulation; optimisation.

Reference to this paper should be made as follows: Vilela, D. and Barbosa, R.S. (2013) 'Numerical optimisation methods applied to the concurrent problem of vehicle ride and handling', *Int. J. Vehicle Systems Modelling and Testing*, Vol. 8, No. 4, pp.316–334.

Biographical notes: Daniel Vilela is an Engineering Technical Manager at General Motors Brazil in the Simulation and Analysis Department. He holds a Doctor's degree in Mechanical Engineering at São Paulo University, São Paulo, Brazil. His research interests include modelling and simulation of ground vehicles for vehicle dynamics and loads analysis, as well as the design and analysis of ground vehicles.

Roberto Spinola Barbosa is a Dr. Professor at the Mechanical Engineering Department of Polytechnic School of the São Paulo University in Brazil. His research interests include multibody systems modelling and simulation with ground vehicles application, developing virtual reality environment on dynamic systems with high performance computation for simulation and training.

1 Introduction

Current literature presents a vast number of models and simulation tools that allow the development engineer to predict the vehicle ride and handling behaviour with very good accuracy. Some of these models are described analytically and covered in the traditional literature for vehicle dynamics, like Milliken and Milliken (1995), Wong (2001) and Pacejka (2002). Other analytical tools are developed with specific purposes, like Gordon et al. (2012) using a quarter-car model to study the influence of the road surface for ride tuning and Talukdar et al. (2012) comparing different simplified models for ride characterisation. These models are simple, therefore extremely efficient in computational terms, making them natural choices to apply numerical optimisation processes. The main drawback in adopting these analytical models from traditional literature is that there is very few data available related to their accuracy against real vehicle measurements. This fact demands additional work to understand the level of model detail necessary to adequately capture the quantities of interest.

Another possibility for the design engineer is to consider a detailed multibody model, making use of commercial multibody software packages, as it has been done using ADAMS® in works by Rongshan et al. (2010), Wu et al. (2009), Vilela (2001) and Prado et al. (2001) – this is currently a widely disseminated approach. By adopting these more complex models the engineer can get very accurate results for the vehicle dynamics response – Rill (2006) and Adamski et al. (1999) describe in more detail how some of these multibody models work, showing the benefits of the flexibility they bring to the design engineer. The issue with this approach is that, as the multibody model gets details in the vehicle construction representation (a common multibody model easily contains more than 100 degrees of freedom), it also becomes less efficient in computational running time. Even with a constantly increasing computational capability available to the design engineer, this non-optimal efficiency might become a bottleneck for numerical optimisation procedures as it demands high number of iterations to get to an optimum design. Besides, these complex models can make it less intuitive for the engineer the understanding of the physics behaviour of the phenomena being studied. These characteristics from the detailed multibody models make the selection of proper tuning variables for the optimisation process more difficult.

The literature for simultaneous analysis of ride and handling is still limited, except for some works using these commercial packages like Rongshan et al. (2010), Yang and Gander (2010) and Wu et al. (2009). Others authors are focused on active control strategies like Liu and Ya (2012), Chen et al. (2011), Rengaraj and Crolla (2011) and Nikzad and Naraghi (2001). Most of these works still propose generic metrics to describe the ride and handling compromise, like Johnston et al. (2010) did by using vertical response spectral profiles for ride quantification and the coefficient of variation of the loads as experienced by the contact patch for handling quantification (what was defined as 'grip' in that work), but these metrics are more difficult to be directly correlated with physical measurements as the authors acknowledge.

This work proposes concurrent use of analytical tools for ride and handling simultaneously through metrics that are current practice for automotive vehicles' development. The handling models used were developed by Vilela and Barbosa (2011a, 2011b) and the numerical tools for ride comfort were developed by Vilela and Gueler (2003) and Vilela and Tamai (2003a, 2003b). These tools present two common key characteristics that make them very suitable for a numerical optimisation process: they

are extremely efficient computationally and, at the same time, they present accurate and consistent results with respect to the physical phenomena they intend to reproduce. This aspect has been confirmed by means of direct correlation with experimental measurements. It is also applied the response surface method (RSM) [as presented by Myers and Montgomery (2002) and Myers et al. (2004)] to the concurrent model proposed in order to understand the potential benefits of this tool for the automotive industry.

2 Objective metrics

The main roadblock that needs to be surpassed to consider a numerical optimisation process for any given problem is to obtain quantitative metrics that represent well the phenomenon studied. In the case of the ride and handling optimisation, these metrics need to meet the following criteria:

- *Be objective:* it is mandatory to consider objective metrics to be used with the optimisation process during the suspension set-up phases, even though ride and handling are areas where a good subjective impression by the final user is the ultimate goal during the vehicle development. These objective metrics must also be quantifiable.
- *Present good objective-subjective correlation:* the objective metrics considered must capture adequately the subjective impressions from the human drivers. At the same time however, these metrics must be independent of human judgement (i.e., it should be possible to measure/calculate the final value of the metric directly from physical variables like accelerations, displacements and forces) in order to make them effective for an automatic optimisation process.
- *Present good numerical-physical correlation:* for a complete optimisation process, the metrics considered must be calculated by computer simulation (analytical formulation or interactive analysis) and the results obtained by these numerical formulations must be consistent with the experimental results measured in physical vehicles.

In the sequence the various metrics considered for the numerical optimisation study are presented.

2.1 Ride comfort metrics

The ride comfort metrics considered are related with the vehicle's capacity to filter vertical road inputs and are described in the sequence. A detailed work with the proving ground expert drivers has been performed in order to determine the kind of road input where each one of the metrics defined is more evident and, as much as possible, isolated from the others. The metrics herein shown were initially described by Vilela et al. (2002).

- *Harshness:* capacity of the vehicle suspension to filter high frequency irregularities with low amplitude road inputs. *Road input:* Belgium blocks track.
- *Absorption capability:* capacity of the vehicle suspension in absorbing the impact with medium size obstacles on the road surface, small size wavelength perturbation

like cats' eyes or little parts of stone. *Road input:* one side of the vehicle upon cats' eyes (50 mm high) and the other on a smooth paved road.

- *Jounce bumper:* evaluates the vehicle behaviour when passing through pot holes, concerning the bump impact felt by the driver (medium size wavelength input). This metric uses the same name of the suspension component in order to keep the common terminology used by the proving ground evaluators, which is related to the fact that the typical pot hole inputs usually excite the jounce bumper component. *Road input:* series of pot holes in both sides of the track.
- *Ride balance:* evaluates the vehicle behaviour when passing through cross ditches or similar obstacles on the road (long wavelength roughness), concerning the pitch stability of the vehicle. *Road input:* cross ditch followed by a flat road.

Finally, the dynamic variables were correlated to each ride comfort parameter. The following parameters were taken into consideration:

- vertical acceleration at the driver position
- front and rear forces for the spring, shock absorbers and bumpers
- body pitch and roll accelerations.

The variables above were calculated by means of a simplified multibody model illustrated in Figure 1 and with general state equations described in equations (1) to (3). These variables were then combined by means of a weight matrix, resulting in values that were correlated with the subjective grades given by the expert drivers at the experimental proving ground. This methodology was developed to correlate the dynamic ride comfort variables from the simulation with the subjective grades from the expert drivers. It presented good correlation, allowing its usage with the upcoming numerical optimisation process – more details about the correlation results are presented in Vilela et al. (2002), Vilela and Gueler (2003) and Vilela and Tamai (2003a, 2003b).

Figure 1 Sketch of the vertical vehicle model for ride comfort metrics calculation (see online version for colours)

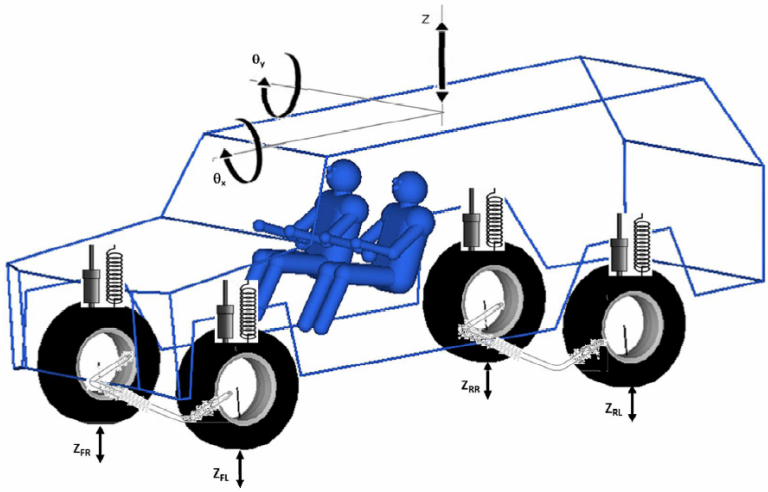

$$\Delta x[i] = \sum_{j=1}^{N_M+N_I+N_{EX}} \left(Inf[i,\ j].x[j] \right) \tag{1}$$

$$\Delta \dot{x}[i] = \sum_{j=1}^{N_M+N_I+N_{EX}} \left(Inf[i,\ j].\dot{x}[j] \right) \tag{2}$$

$$F[k] = \sum_{l=1}^{N_{Link}} \left[-Inf[l,\ k].\left(F_{Stiff}[l] + F_{Damp}[l] \right) \right] \tag{3}$$

2.2 Handling metrics

The handling metrics are related to the capacity of the vehicle to generate tangential contact loads with minimum variation of vertical contact loads. Based on common development practice, the following metrics were considered:

- roll gradient
- understeer gradient
- steering sensitivity
- lateral acceleration response
- roll response.

2.2.1 Roll gradient metric

The roll gradient is defined as the derivative of the vehicle body roll angle with respect to the lateral acceleration acting at its centre of gravity (CG), as indicated in Figure 2 (curve point highlighted by red line represents the lateral acceleration level where this metric is being calculated for the current work). The curve itself is generated by a series of points where the steady-state condition is observed. This value can be experimentally measured through a constant radius circular manoeuvre with small steps of increase in the longitudinal velocity (and therefore the lateral acceleration), keeping as close as possible of a steady-state condition.

An analytical model, described by equation (4), has been developed for this metric and correlated against experimental results as shown in Figure 3. Experimental data was acquired for a passenger vehicle with instrumented steering wheel angle, longitudinal velocity, lateral acceleration (accelerometers at vehicle's CG position) and roll angle with respect to the ground. The manoeuvre performed for the data acquisition was a slowly increasing longitudinal velocity over a constant radius and it has been repeated three times to assure that measurement results were consistent. The details of the measurements and correlation results are presented by Vilela and Barbosa (2011a).

$$K_{roll} = \frac{\partial \theta}{\partial a_L} = \frac{MgH_r}{K_T} \tag{4}$$

Figure 2 Roll gradient definition (see online version for colours)

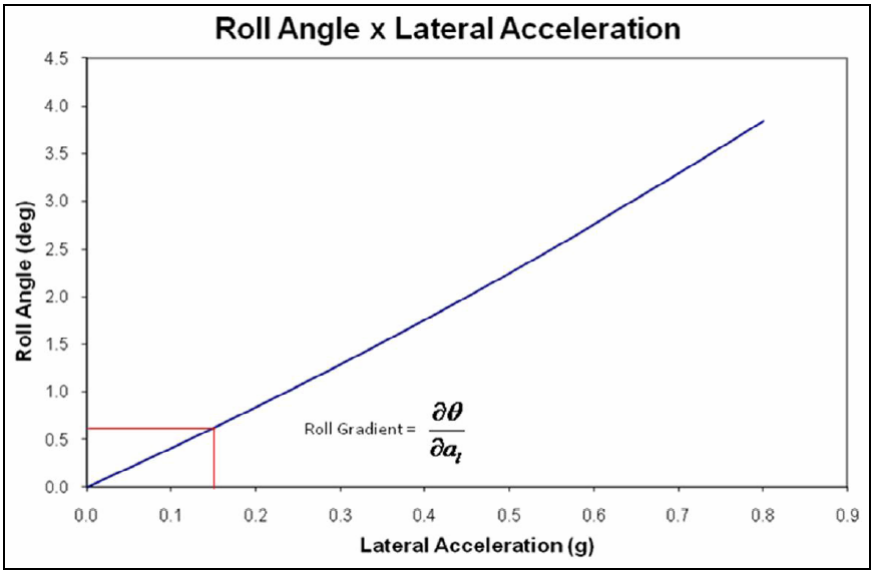

Figure 3 Roll gradient correlation results against experimental measurements (see online version for colours)

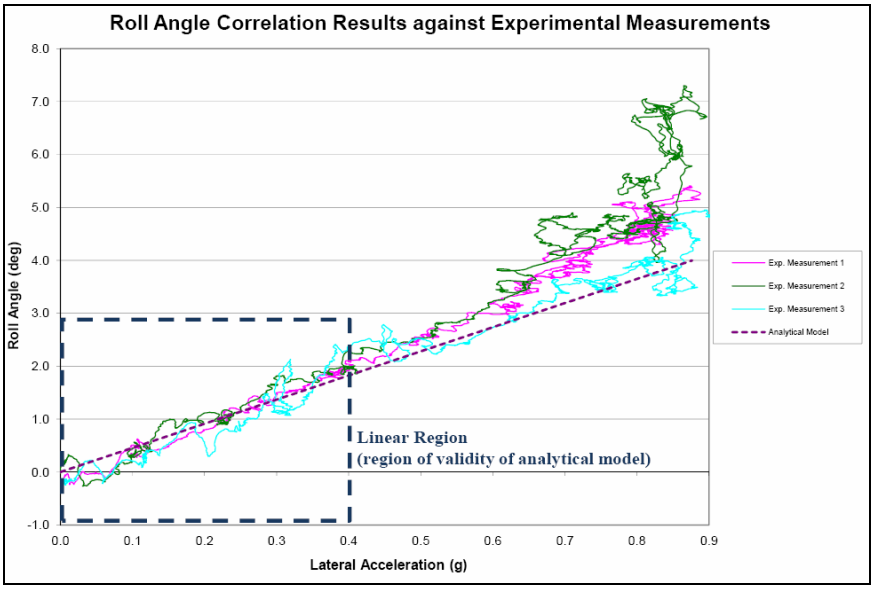

2.2.2 Understeer gradient metric

The understeer gradient is defined as the derivative of the front tyres average steer angle with respect to the lateral acceleration imposed to the vehicle at its centre of gravity in a steady-state condition, as indicated in Figure 4.

Figure 4 Understeer gradient definition (see online version for colours)

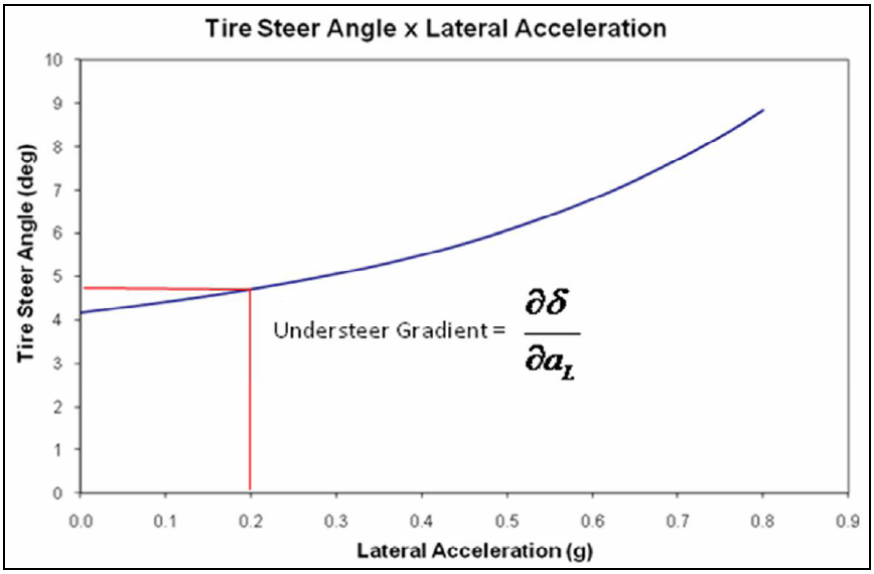

This parameter evaluates the tendency of the vehicle to be understeer when in a steady-state curve manoeuvre (understeer gradient > 0 → vehicle demands higher steering angles to keep the same curve radius at higher speeds) or oversteer (understeer gradient < 0 → vehicle demands lower steering angles to keep the same curve radius at higher speeds). The vehicle is said to be neutral when the steering angle to keep a curve trajectory is dependant only on the curve radius and not on the vehicle speed (understeer gradient null).

An analytical model capable of reproducing the experimental results with good accuracy was developed by Vilela and Barbosa (2011a). The development starts from a simple bicycle model that was gradually implemented with the effects of tyre self-align torque, lateral load transfer, vehicle's suspension and steering system compliances and suspension kinematic variation with vertical suspension travel. This analytical model is described by equations (5) to (7) and its development and correlation against experimental results is detailed by Vilela and Barbosa (2011a).

$$K = \frac{\partial \delta}{\partial a_L} = \left(\frac{c}{C'_{\alpha f}} - \frac{b}{C'_{\alpha r}} \right) \frac{M}{2L} \tag{5}$$

$$C'_{\alpha f} = \frac{C_{\alpha f,llt} c}{B_f B_{f,rs} c'} \tag{6}$$

$$C'_{\alpha r} = \frac{C_{\alpha r,llt} b}{B_r B_{r,rs} b'}. \tag{7}$$

2.2.3 Steering sensitivity metric

The steering sensitivity is defined as the derivative of the lateral acceleration with respect to the steering wheel angle imposed to the vehicle's centre of gravity, as indicated in Figure 5.

Figure 5 Steering sensitivity definition (see online version for colours)

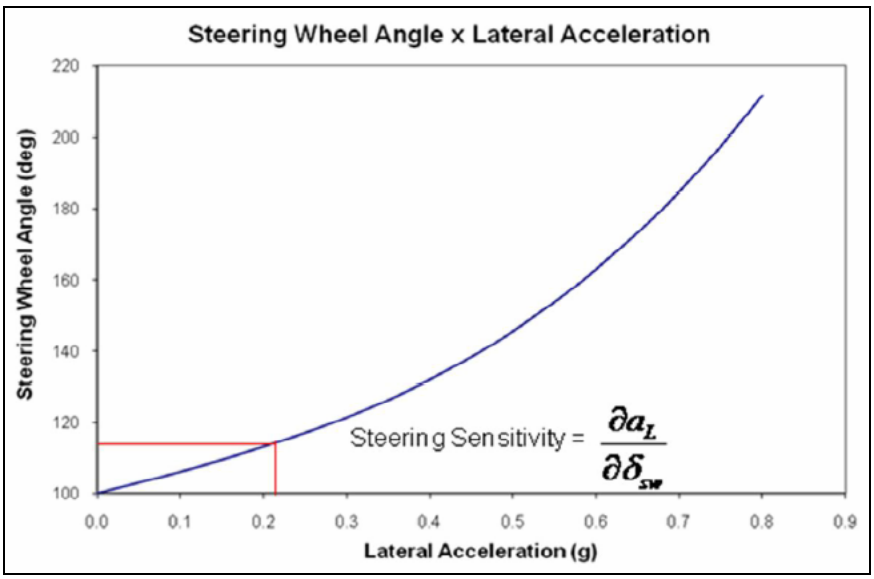

This parameter evaluates the responsiveness of the vehicle with respect to the driver inputs at the steering wheel. Low steering sensitivity values disclose a subjective feeling to the driver of a slow response or lack of response from the vehicle. High values instead are associated with very fast vehicle response that is more difficult to control. In this case, a small disturbance in the steering wheel produces a reasonable amount of lateral acceleration, changing significantly the vehicle trajectory. The steering sensitivity is closely related to the understeer gradient, being inversely proportional to that metric and to the overall steering ratio of the vehicle. The reason that makes it relevant to consider this metric independently is that many projects are limited to use the same steering system for a wide range of vehicles. This fact makes the compromise between understeer gradient and steering sensitivity more difficult to be achieved. Besides that, there is also a compromise between this metric and the steering effort, as the steering sensitivity is inversely proportional to the overall steering ratio of the vehicle, what is especially critical for non-assisted (manual) steering systems. This analytical model is summarised by equation (8) and its development and correlation against experimental results is also detailed by Vilela and Barbosa (2011a).

$$K_s = \frac{\partial a_L}{\partial \delta_{vol}} = \frac{\partial a_L}{\partial \delta}\frac{\partial \delta}{\partial \delta_{vol}} = \frac{1}{K}\frac{1}{r_{dir}}. \tag{8}$$

2.2.4 Lateral acceleration response metrics for periodic excitation

The lateral acceleration response of the vehicle with respect to the excitation frequency of the steering wheel (harmonic response to a sinusoidal excitation type) presents a decreasing behaviour at the beginning of the response curve. Eventually it achieves a minimum response value for a specific frequency. This is called *null gain frequency*, as the gain value at this frequency is very close to zero. Another metric that can be taken from this response is the so-called *lateral acceleration bandwidth* – it is defined as the frequency value where a reduction in the lateral acceleration response is noticed by most users. The reduction in 3 dB gain for this metric proposed by Kunkel and Leffert (1998) is adopted in this work. Figure 6 shows these concepts at the lateral acceleration response graphic.

Figure 6 Lateral acceleration bandwidth and null gain frequency definition (see online version for colours)

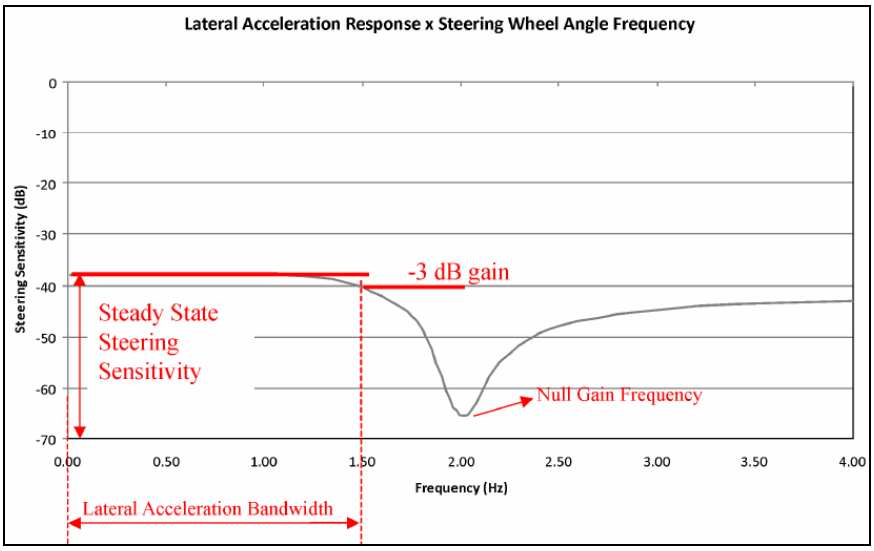

Vilela and Barbosa (2011b) detail the development and correlation of an analytical model capable of replicating the behaviour of the lateral acceleration response as presented in Figure 6, with results compared against a detailed multibody model and a simpler analytical model proposed by Pacejka (2002). This model is summarised by equation (9).

$$\left[\frac{\left(M+\frac{2}{V_x^2}\left(C_{\alpha f}b-C_{\alpha r}c\right)\right)}{2\left(C_{\alpha f}+C_{\alpha r}\right)}J_z\right]\ddot{a}_L+\left[\frac{1}{V_x}J_z\right]\dot{a}_L$$
$$+\left[\frac{2}{V_x^2}\left(b^2C_{\alpha f}+c^2C_{\alpha r}\right)-\frac{\left(M+\frac{2}{V^2}\left(C_{\alpha f}b-C_{\alpha r}c\right)\right)\left(2\left(bC_{\alpha f}-cC_{\alpha r}\right)\right)}{2\left(C_{\alpha f}+C_{\alpha r}\right)}\right]a_L \tag{9}$$
$$=\left[2C_{\alpha f}\left(b-\frac{\left(2\left(bC_{\alpha f}-cC_{\alpha r}\right)+J_z\omega^2\right)}{2\left(C_{\alpha f}+C_{\alpha r}\right)}\right)\right]\delta$$

2.2.5 Roll response metric for periodic excitation

The vehicle body roll angle behaviour with respect to the excitation frequency of the steering wheel (harmonic response to a sinusoidal excitation type) presents a typical second order system behaviour as depicted in Figure 7. The main metric that can be taken here is the dimensional measure defined by the peak roll gradient response divided by the response at steady-state condition ($\omega \rightarrow 0$), which is called *roll gradient peak/steady-state ratio*. This metric indicates how much the vehicle roll response varies with respect to the steering wheel excitation frequency. Lower values (close to 1.0) are better perceived by the users, as it reflects a more homogeneous response, independent of the steering wheel excitation frequency. Higher values can bring a strong non-linearity feeling to the users with respect to the roll response and extreme cases might affect the safety of the vehicle with respect to rollover. This metric is strongly affected by the suspension damping properties. Usually there is a compromise between the roll dynamic response and the vehicle ride comfort.

Figure 7 Roll gradient peak/steady-state ratio definition (see online version for colours)

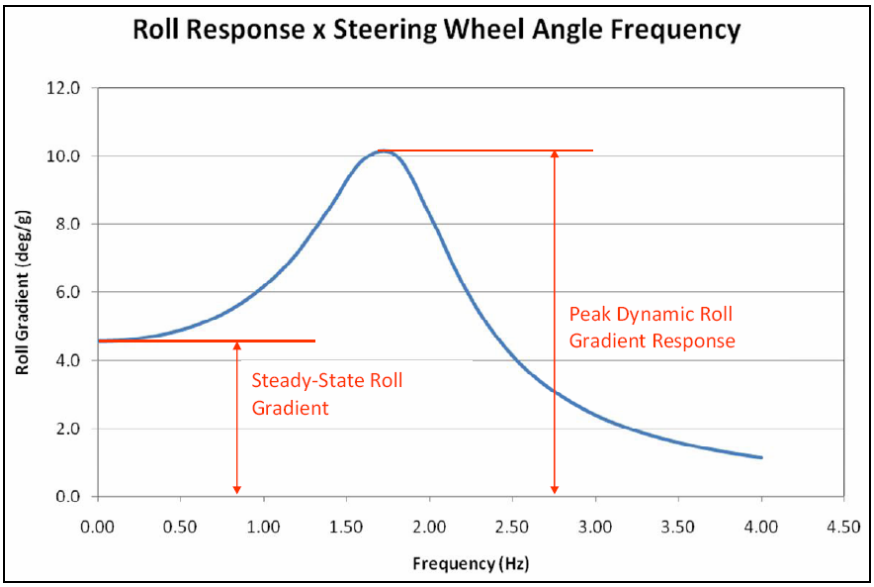

Vilela (2010) developed an analytical model, described by equation (10), that is capable of replicating the behaviour of the roll angle response as presented in Figure 7 and the correlation results against a detailed multibody model is detailed in that work.

$$J_x\ddot{\theta} - C_T\dot{\theta} - K_T\theta = -MH_r a_L \tag{10}$$

All handling metrics considered in this work were proposed by Vilela and Barbosa (2011a, 2011b). Table 1 presents the correlation results of the proposed numerical models for a passenger vehicle, with the correlation level calculated as per definition from equation (11). The steady-state metrics (roll gradient, understeer gradient and steering sensitivity) reference values were experimentally measured in the vehicle performing a constant radius manoeuvre. The frequency response metrics reference values were

obtained from a detailed multibody model of the same vehicle. Correlation is defined as 100% when proposed analytical model results matches reference results from experimental measurements and/or detailed multibody model.

$$\text{Correlation level} = \frac{\min(\text{Experimental result, Proposed model result})}{\max(\text{Experimental result, Proposed model result})} \tag{11}$$

Table 1 Handling metrics correlation results

Metric	*Unit*	*Reference value*		*Proposed model result*	*Correlation level (%)*
		Experimental result	*Detailed multibody model result*		
Roll gradient	deg/g	4.93	4.59	4.56	92.5%
Understeer gradient	deg/g	3.85	3.54	3.92	98.2%
Steering sensitivity	g/100 deg SWA	1.55	1.66	1.50	96.8%
Lateral acceleration bandwidth	Hz	N/A	1.35	1.53	88.2%
Null gain frequency	Hz	N/A	2.09	2.04	97.6%
Roll gradient peak/steady-state ratio	-	N/A	2.24	2.24	100.0%

2.3 Overall ride and handling metric

The application of the numerical optimisation tools herein considered demands a single combined metric. The intention is to propose a combined metric to optimise ride and handling metrics simultaneously.

Figure 8 Nominal-the-better metrics normalisation (see online version for colours)

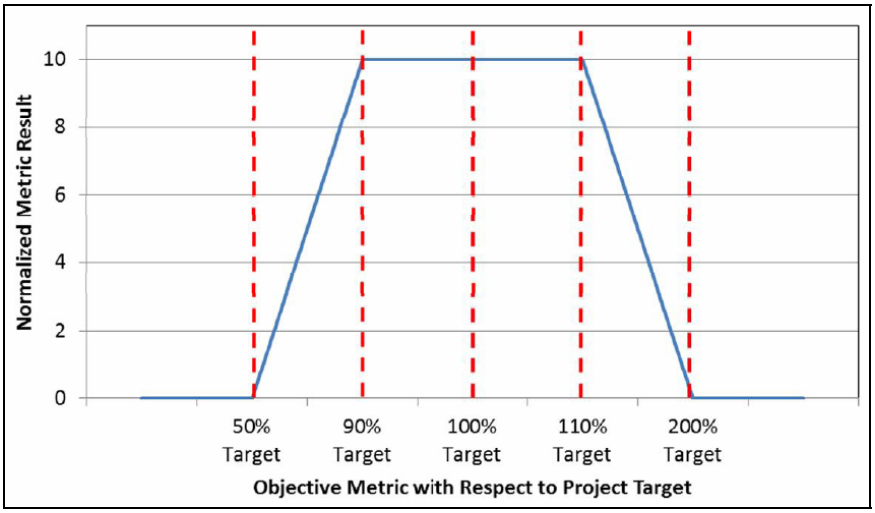

Figure 9 Higher-the-better metrics normalisation (see online version for colours)

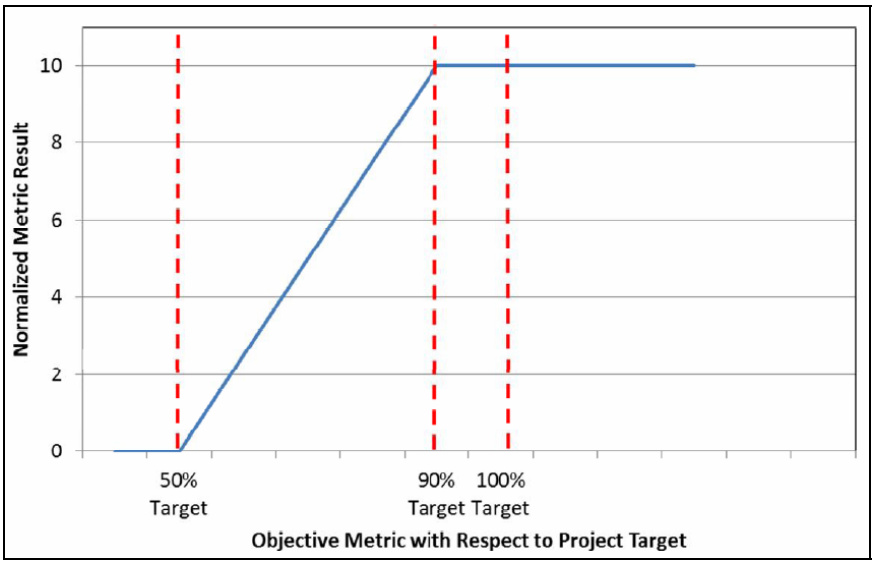

Figure 10 Lower-the-better metrics normalisation (see online version for colours)

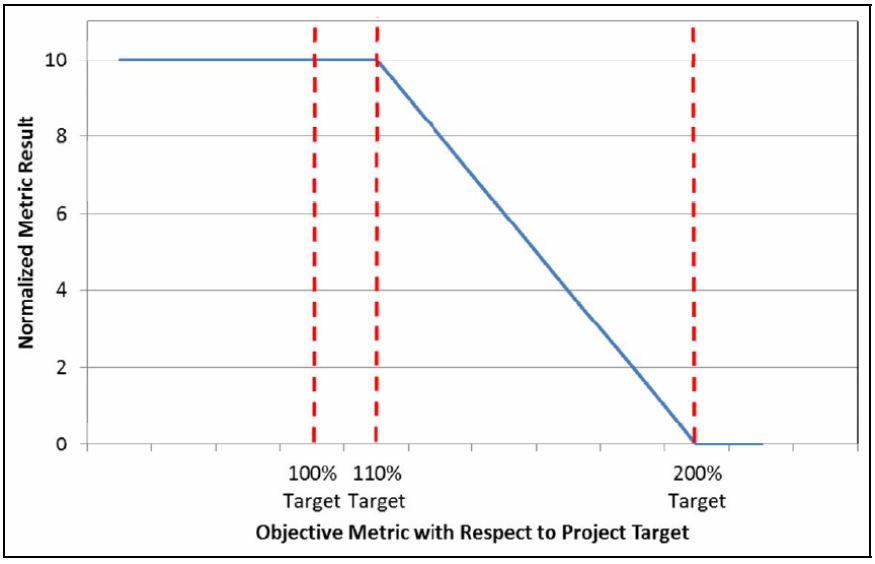

The ride comfort metrics previously described already present a 'higher-the-better' characteristic (i.e., higher values of the metric imply in a better behaviour of the vehicle with respect to that metric) and are already normalised to produce results between 0 and 10. On the other hand, the handling metrics described demand some manipulation for the final metric combination. A specific vehicle project has clearly defined targets for each handling metric considered. These metrics present either a nominal-the-better characteristic (understeer gradient and steering sensitivity), a higher-the-better characteristic (lateral acceleration bandwidth) or a lower-the-better characteristic (roll

gradient and roll gradient peak/steady state ratio). Mathematical manipulation through linear functions can be then applied to normalise the result to a value between 0 and 10, as described in Figures 8 to 10 in the sequence.

The overall handling metric can be then defined as a weighted average of the individual metrics, with each individual weight factor defined based on the vehicle project specific goals, which are dependent on its application (a vehicle can be sportive, family-oriented or off-road for example) and expected user behaviour (one vehicle might be designed to younger drivers, while another might be oriented to families and/or senior public). In this sense, with weight factors defined as p_1 until p_5:

$$f(handling) = \frac{p_1 f(K_{roll}) + p_2 f(K) + p_3 f(K_s) + p_4 f(R_{roll}) + p_5 f(\omega_{plane})}{\sum_{i=1}^{5} p_i} \tag{12}$$

Finally, the combined ride and handling metric can be also defined as a weighted sum between *f*(*ride*) and *f*(*handling*). Once more, the weight factors must be defined according to the specific project needs.

$$f(optimisation) = \frac{p_{ride} f(ride) + p_{handling} f(handling)}{p_{ride} + p_{handling}} \tag{13}$$

The metric defined by equation (13) is also normalised between 0 and 10 and is suitable for the numerical optimisation procedures proposed.

Besides these properties, it is very important that the numerical optimisation does not seek for solutions that emphasise too much a subset of the metrics despite bad results for others. Among available empirical adjustments, the hyperbolic function described in Figure 11 has been chosen. This additional factor increases the relative weight of the metrics with lower values, forcing thus the optimisation procedure to seek for more balanced results among the various metrics.

Figure 11 Additional weight factor proposed (see online version for colours)

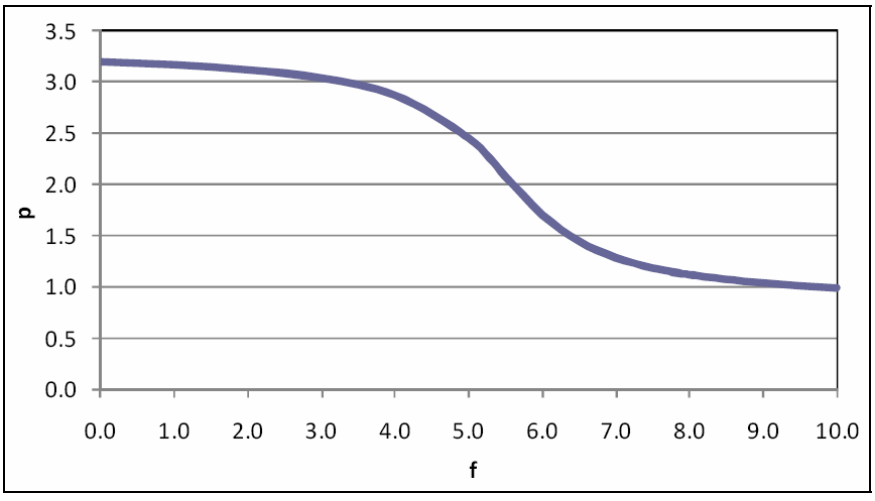

3 Application of numerical optimisation

As the ride comfort model is an interactive multibody model, a direct regression for the optimisation study is not possible. For this reason, the RSM as described by Myers and Montgomery (2002) and considered by Vilela and Tamai (2005) is explored in this work in order to understand the effectiveness of the proposed metric for numerical optimisation purposes. The objective of the optimisation is to maximise the function defined by equation (13), what is equivalent to minimise the same function with opposite sign as described in equation (14), considering the variables x within the limits of the considered admissible set A. The variables and limits considered for this study are presented in Table 2. Specifically for the tyres, the various inflation pressures were considered by adopting the equivalent radial stiffness (used in the ride and roll models) and cornering stiffness (lateral force vs. slip and align torque vs. slip coefficients for the handling models).

$$\underset{x \in A}{Min}\left(-f(x)\right) \tag{14}$$

Table 2 Optimisation variables and limits considered

Variable	*Minimum*	*Maximum*	*Unity*
x_1 – rear axle antiroll bar stiffness	0 (no bar)	10	N/mm
x_2 – front spring stiffness	18	22	N/mm
x_3 – rear spring stiffness	18	22	N/mm
x_4 – front antiroll bar diameter	18	22	mm
x_5 – front tyre inflation pressure	26	34	psi
x_6 – rear tyre inflation pressure	26	34	psi
x_7 – front shock damping	–20% over nominal	+20% over nominal	N/(m/s)
x_8 – rear shock damping	–20% over nominal	+20% over nominal	N/(m/s)

The noise factor considered was the vehicle ballast condition, with the ride and handling metrics calculated at ballast = kerb + two front passengers and at ballast = gross vehicle mass (GVM). Table 3 shows the handling metric targets that were considered along with the normalisation presented in Figures 8, 9 and 10.

Table 3 Targets for handling metrics

Metric	*Unity*	*Criteria*
Roll gradient	deg/g	5.0
Understeer gradient	deg/g	2.5
Steering sensitivity	g/100 deg SWA	1.5
Roll gradient peak/steady-state ratio	-	1.5
Lateral acceleration bandwidth	Hz	1.2

For this study, the project-related weight factors are all kept equal to unity, so as to make this study a completely balanced ride and handling optimisation with respect to the metrics considered. The additional weight factors presented in Figure 11 are maintained as defined (i.e., dependant on the metric result) so as to help the numeric optimisation routine to find a balanced optimum point.

A fractional factorial matrix as detailed by Vilela (2010) has been considered for this work. Considering the backward elimination method it is possible to obtain the most significant regressors as shown in Table 4.

Table 4 RSM most significant regressors

Factor	*Partial regression coefficient*
Intersection	+7.068
Ballast condition (noise factor)	–0.501
Front shock damping	–0.365
Front antiroll bar stiffness	+0.171
Front tyre inflation pressure	–0.152
Interaction between ballast condition and rear tyre inflation pressure	+0.107
Rear axle torsional stiffness	+0.094
Interaction between ballast condition and front antiroll bar stiffness	+0.085
Interaction between rear axle torsional stiffness and front antiroll bar stiffness	–0.076
Interaction between ballast condition and front shock damping	+0.066
Interaction between ballast condition and rear axle torsional stiffness	+0.046
Rear spring stiffness	+0.041
Interaction between rear spring stiffness and front antiroll bar stiffness	–0.040

One possible way to quantify the accuracy of the RSM regression models is to compare their results directly with the original results from the fractional factorial matrix, as shown in Table 5.

Table 5 RSM models accuracy check

	RSM regressors
Average difference between fractional factorial results and RSM model	0.08
Maximum positive difference (RSM model > original result)	+0.37
Maximum negative difference (RSM model < original result)	–0.24

Table 6 Ballast condition variability study using RSM model

Factor	*Initial configuration*	*Minimum variability*	*Maximum metric value*
	Metric = 7.27 Var = 0.43	*Metric = 7.81 Var = 0.15*	*Metric = 7.88 Var = 0.29*
Rear axle torsional stiffness	0.00	+1.00	+1.00
Front antiroll bar stiffness	0.00	+1.00	+1.00
Front tyre inflation pressure	0.00	–1.00	–1.00
Rear tyre inflation pressure	0.00	+1.00	–0.35
Front shock damping	0.00	–1.00	–1.00

As the RSM obtains simple linear equations with the regressors, it is possible to use these equations with common linear quadratic optimisation routines readily available in

software packages like MatLab® and SciLab®, allowing the design engineer to understand how the global ride and handling optimisation metric varies as function of the optimisation variables and the ballast condition (variability as function of noise considered). Table 6 presents some results considering this aspect.

The RSM results bring a series of extremely useful information to the design engineer. As example, from the partial regression coefficients from Table 3, the following observations can be done:

- Within the range of this study, the vehicle ballast condition presents the highest regressor. That means that the noise produced by the ballast condition has more influence in the global ride and handling metric than any of the optimisation variables alone (shocks, springs, tyres, etc.). The fact that the coefficient is negative means that the metric is reduced when the variable value increases, i.e., the global ride and handling metric considered is degraded as the vehicle ballast increases, what is aligned with passenger vehicles usual response.
- The interaction between the ballast and the rear tyre inflation pressure is positive: that means that for higher ballasts (positive values for variable), it is interesting to increase the rear tyre inflation pressure to improve the vehicle ride and handling. This conclusion is also very much aligned with the common practice to consider different tyre inflation pressures for the tyres with different ballast conditions (especially true for the rear tyre).
- The interaction between the vehicle ballast and the front antiroll bar torsional stiffness is also positive: that means that the heavier ballasted vehicle will perform better with a stiffer front bar for the ride and handling global metric considered. This kind of information can help the design engineer to idealise different solutions for the project – in this example, it might be feasible to study an antiroll bar whose stiffness increases as function of the ballast or, alternatively, a front spring with progressive rate that will end up increasing the effective roll stiffness of the front axle as the ballast increases.

Besides these points, a direct conclusion can be obtained by a comparison of the partial regression coefficients' magnitude, what can help the design teams to put more effort in the components/variables that affect most the results.

The goal of improving the initial design has been achieved: in the example described here this improvement was in the range of 8% (around 0.6 points over initial 7.3 in a scale from 0 to 10) only with the application of the numerical optimisation process over regular suspension tuning components (springs, tyres, shock absorbers and antiroll bars), meaning that this gain was obtained at no extra cost to the product.

4 Conclusions

A new unified concurrent ride and handling metric is proposed to be used with numerical tools to optimise vehicle suspension design. The models developed include the relevant aspects to represent the physical phenomena involved, having at the same time a simple structure and providing good numerical efficiency. The models were validated against experimental values and more detailed and complex multibody models.

The RSM has been applied to this new unified ride and handling metric and the goal of improving the initial design has been achieved. Along with the application of the RSM optimisation process with the proposed model, significant insightful information about the interactions among the variables was obtained.

These points indicate that the proposed model and the optimisation methodology aid the design engineer and bring a significant contribution to the automotive companies. Their application can ultimately accelerate the development process through the usage of numerical methods over traditional hardware work in the initial phases of their projects, reducing associated costs and timing demands at the same time.

References

Adamski, D., Schuster, C. and Hiller, M. (1999) 'Advances in modelling of mechatronic systems: the toolset FASIM_C++ for the simulation of vehicle dynamics', *Journal of the Brazilian Society of Mechanical Sciences*, Vol. 21, No. 4, pp.683–698.

Chen, S., Zong, C., He, L. and Yin, G. (2011) 'An integrated control strategy towards improvement of vehicle ride and handling via active suspension', *Commercial Vehicle Engineering Congress*, September, Chicago, IL, USA, SAE Paper 2011-01-2161.

Gordon, T., Chaturvedi, B. and Karamihas, S. (2012) 'The influence of road surface properties on vehicle suspension parameters optimized for ride – design trends for global markets', *SAE 2012 World Congress & Exhibition*, April, Detroit, MI, USA, SAE Paper 2012-01-0521.

Johnston, M., Rieveley, R., Johrendt, J. and Minaker, B. (2010) 'Metrics for evaluating the ride handling compromise', *SAE 2010 World Congress & Exhibition*, April, Detroit, MI, USA, SAE Paper 2010-01-1139.

Kunkel, D.T. and Leffert, R.L. (1988) 'Objective directional response testing', *22nd FISITA Congress*, Dearborn (MI), USA, SAE Paper 885008

Liu, W. and Ya, H. (2012) 'Cooperative optimization of vehicle ride comfort and handling stability by integrated control strategy', *SAE 2012 World Congress & Exhibition*, April, Detroit, MI, USA, SAE Paper 2012-01-0247.

Milliken, W.F. and Milliken, D.L. (1995) *Race Car Vehicle Dynamics*, SAE, Warrendale, USA.

Myers, R.H. and Montgomery, D.C. (2002) *Response Surface Methodology*, 2nd ed., Wiley-Interscience, New York, NY, USA.

Myers, R.H. et al. (2004) 'Response surface methodology: a retrospective and literature survey', *Journal of Quality Engineering*, Vol. 36, No. 1, pp.53–77.

Nikzad, S.V. and Naraghi, M. (2001) 'Optimizing vehicle response in a combined ride and handling full car model by optimal control strategies', *Noise and Vibration Conference & Exposition*, April, Traverse City, MI, USA, SAE Paper 2001-01-1581.

Pacejka, H.B. (2002) *Tire and Vehicle Dynamics*, SAE, Warrendale, USA.

Prado, M., Cunha, R.H., Costa Neto, A., Costa, A., Mancosu, F., Savi, C. and Délboux, J.E. (2001) 'Bus handling analysis and experimental validation using the multibody system technique', *SAE Brazil 2001 Congress and Exhibit*, São Paulo, SP, SAE Paper 2001-01-3966.

Rengaraj, C. and Crolla, D. (2011) 'Integrated chassis control to improve vehicle handling dynamics performance', *SAE 2011 World Congress & Exhibition*, April, Detroit, MI, USA, SAE Paper 2011-01-0958.

Rill, G. (2006) 'Vehicle modeling by subsystems', *Journal of the Brazilian Society of Mechanical Sciences*, Vol. 28, No. 4, pp.430–442.

Rongshan, Y., Huang, X. and Kegang, Z. (2010) 'Investigation of vehicle handling and ride comfort oriented cooperative optimization', *SAE 2010 World Congress & Exhibition*, April, Detroit, MI, USA, SAE Paper 2010-01-0722.

Talukdar, S., Mazumdar, A., Mullasseril, M. and Kalita, K. (2012) 'Mathematical modeling in vehicle ride dynamics', *SAE 2012 World Congress & Exhibition*, April, Detroit, MI, USA, SAE Paper 2012-01-0056.

Vilela, D. (2001) 'Vehicle dynamics simulation correlation with field maneuvers', *SAE Brazil 2001 Congress and Exhibit*, São Paulo, SP, SAE Paper 2001-01-3799.

Vilela, D. (2010) *Aplicação de Métodos Numéricos de Otimização ao Problema Conjunto da Dirigibilidade e Conforto Veicular*, Doctorate thesis, Mechanical Engineering Department, Polytechnic School of the São Paulo University [online] http://www.teses.usp.br/teses/disponiveis/3/3152/tde-20082010-153319/pt-br.php.

Vilela, D. and Barbosa, R.S. (2011a) 'Analytical models correlation for vehicle dynamic handling properties', *Journal of the Brazilian Society of Mechanical Sciences and Engineering*, Vol. 33, No. 4, pp.437–444.

Vilela, D. and Barbosa, R.S. (2011b) 'Analytical solution proposal to vehicle dynamic handling properties', *International Journal of Vehicle Systems Modelling and Testing*, Vol. 6, No. 1, pp.56–71.

Vilela, D. and Gueler, G.F. (2003) 'Simulation applied to ride comfort suspension optimization', *SAE Brazil 2003 Congress and Exhibit*, São Paulo, SP, SAE Paper 2000-01-4021.

Vilela, D. and Tamai, E.H. (2003a) 'Ride comfort suspension optimization with simulation tools', *IASTED International Conference on Modeling, Identification and Control*, Innsbruck (Austria), Proceedings, Acta Press, Anaheim.

Vilela, D. and Tamai, E.H. (2003b) 'Simulation applied to ride comfort suspension optimization', *17th International Congress of Mechanical Engineering*, São Paulo, *Proceedings of the 17th Internacional Congress of Mechanical Engineering*, ABCM, São Paulo.

Vilela, D. and Tamai, E.H. (2005) 'Optimization of vehicle suspension using robust engineering method and response surface methodology', *International Symposium on Dynamic Problems DINAME*, Ouro Preto, MG, *Proceedings of The International Symposium on Dynamic Problems of Mechanics*, ABCM, São Paulo.

Vilela, D., Franceschini, F.H. and Mesquita, V. (2002) 'Automotive suspension calibration', *X Mobility Technology Conference & Exhibit – SAE BRASIL 2002*, São Paulo, SP, SAE Paper 2002-01-3393.

Wong, J.Y. (2001) *Theory of Ground Vehicles*, John Wiley & Sons Inc., New York, USA.

Wu, S., Hou, Y., Li, L., Zhang, Y. and Chen, L. (2009) 'Special analytical target cascading for handling performance and ride quality based on conceptual suspension model and multi-body model', *SAE World Congress & Exhibition*, April, Detroit, MI, USA, SAE Paper 2009-01-1455.

Yang, X. and Gander, J. (2010) 'Handling and ride performance sensitivity analysis for a truck-trailer combination', *SAE 2010 World Congress & Exhibition*, April, Detroit, MI, USA, SAE Paper 2010-01-0642.

Appendix

Definitions, acronyms and abbreviations

a_L	Lateral acceleration
b / c	Distance between CG and front/rear axle
b' / c'	Adjusted distance between CG and front/rear axle considering tire self-align torque
B_f, B_r	Front/rear suspension/steering system compliance term
$B_{f,rs}$, $B_{r,rs}$	Front/rear roll steer term
$C_{\alpha f,llt}$, $C_{\alpha r,llt}$,	Front/rear tire cornering stiffness with lateral load transfer effect
$C'_{\alpha f}$, $C'_{\alpha r}$	Equivalent front/rear tire cornering stiffness
C_T	Vehicle total roll damping
$F[k]$	Total force acting on link system [k]
$F_{Stiff}[l]$	Force acting on link system [k] due to stiffness components
$F_{Damp}[l]$	Force acting on link system [k] due to damping components
g	Gravity acceleration (9.81 m/s^2)
H_r	Effective roll arm
$Inf[i,j]$	Influence matrix component relating link system [i] to link system [j]
Jx	Vehicle roll moment of inertia (x axis)
Jz	Vehicle yaw moment of inertia (z axis)
K	Understeer gradient
K_{roll}	Roll gradient
K_s	Steering sensitivity
K_T	Vehicle total roll stiffness
L	Wheelbase
M	Vehicle mass
r_{dir}	Steering ratio
Vx	Vehicle longitudinal velocity
$x[i]$	Position of link system [i] in ride multibody model
$\dot{x}[j]$	Velocity of link system [i] in ride multibody model
δ	Front wheel steer angle
δ_{vol}	Steering wheel angle
θ	Vehicle roll angle
ω	Frequency of steering wheel excitation

8.14 ANEXO N

ANALYTICAL MODELS CORRELATION FOR VEHICLE DYNAMIC HANDLING PROPERTIES

Vilela, D.; Barbosa, R. S. (2011A) Analytical models correlation for vehicle dynamic handling properties. Journal of the Brazilian Society of Mechanical Sciences and Engineering, DOI: 10.1590/S1678-58782011000400007, Vol. 33, nº 4, pp. 437-444.

Analytical Models Correlation for Vehicle Dynamic Handling Properties

Daniel Vilela
danvil_br@hotmail.com
General Motors do Brasil Ltda.
Vehicle Synthesis
Analysis and Simulation Dept.
Sao Caetano do Sul
09550-051 SP, Brazil

Roberto Spinola Barbosa
roberto.barbosa@poli.usp.br
Escola Politécnica da Universidade de São Paulo
Departamento de Engenharia Mecânica
Sao Paulo
05508-900 SP, Brazil

Analytical models to evaluate vehicle dynamic handling properties are extremely interesting to the project engineer, as these can provide a deeper understanding of the underlying physical phenomena being studied. It brings more simplicity to the overall solution at the same time, making them very good choices for tasks involving large amounts of calculation iterations, like numerical optimization processes. This paper studies in detail the roll gradient, understeer gradient and steering sensitivity vehicle dynamics metrics, starting with analytical solutions available in the literature for these metrics and evaluating how the results from these simplified models compare against real vehicle measurements and more detailed multibody simulation models. Enhancements for these available analytical formulations are being proposed for the cases where the initial results do not present satisfactory correlation with measured values, obtaining improved analytical solutions capable of reproducing real vehicle results with good accuracy.
Keywords: *handling, vehicle dynamics, analytical solution, simulation*

Nomenclature

a_L	= lateral acceleration, m/s^2
b / c	= distance between CG and front/rear axle, m
F_{yf}, F_{yr}	= front and rear centrifugal force per axle, N
H_r	= effective roll arm, m
H_{CG}	= CG height to the ground, m
H_{rf}, H_{rr}, H_{rcg}	= vehicle roll center height at front axle, rear axle and CG position, m
K	= understeer gradient, rad/(m/s^2)
K_{bf}, K_{br}	= front and rear roll stiffness due to stabilizer bars, (Nm)/rad
K_{fyf}, K_{fyr}	= front and rear wheel steer angle stiffness with respect to tire lateral force, rad/N
K_{mzf}, K_{mzr}	= front and rear wheel steer angle stiffness with respect to tire align torque, rad/(Nm)
K_{roll}	= roll gradient, rad/(m/s^2)
K_s	= steering sensitivity, (m/s^2)/rad
K_{sf}, K_{sr}	= front and rear wheel roll stiffness due to springs, (Nm)/rad
K_T	= vehicle's total roll stiffness, (Nm)/rad
K_{tirf}, K_{tirr}	= front and rear wheel roll stiffness due to tires, (Nm)/rad
L	= wheelbase, m
M	= vehicle mass, Kg
$M_{ext,zf}$, $M_{ext,zr}$	= front and rear tire align torque, Nm
r_{dir}	= steering ratio, dimensionless
V_f, V_r	= front and rear tire velocity vector, m/s
T_{roll}	= roll moment, Nm

Greek Symbols

α_f, α_r	= front and rear tire slip angle, rad
δ	= front wheel steer angle, rad
θ	= vehicle roll angle, rad
$C_{\alpha f}$, $C_{\alpha r}$	= front and rear tire cornering stiffness, N/rad

Introduction

The most important vehicle dynamics steady state metrics, including roll gradient, understeer gradient and steering sensitivity, are covered in the traditional literature for vehicle dynamics, like Milliken (1995), Wong (2001) and Pacejka (2002). Each of these authors proposes analytical formulations to quantify these metrics, being these analytical solutions very important tools to the development engineer, who is able to have a very good understanding of the underlying phenomena and how the tuning variables affect each of these metrics. Besides that, the analytical solutions are extremely efficient in terms of computation time, allowing their usage for quick studies and very early assessments, as well as their linkage to numerical optimisation processes that take the advantage of their computational efficiency. Although these authors present simple analytical solutions to the metrics mentioned, none of them goes to the point of effectively comparing the results of their proposed analytical equations against real measurements to verify the accuracy of these formulations. Although the literature on the topic already presents analytical formulations for many of the usual vehicle dynamics metrics, few has been done in order to quantify the accuracy of these analytical models against real vehicle measurements and to understand the level of detail necessary to adequately capture the quantities of interest with such models.

On the other extreme, there are papers in the literature that present the comparison of physical measurements with the results of much more complex multibody models for non-linear dynamic manoeuvres, making usage of commercial multibody software packages, as it has been done using ADAMS® in previous works by Vilela (2001) and Prado et al. (2001). Rill (2006) and Adamski et al. (1999) describe in more details how some of these more complex multibody models work, showing the benefits of the flexibility that these models allow to the design engineer. By adopting these more complex models the engineer can get very accurate results for the vehicle dynamics response, including the steady-state metrics previously mentioned. The main drawback of this approach is that the more the multibody model gets details in the vehicle construction representation (a common multibody model easily contains more than 100 degrees of freedom – see example in Fig. 1), the more difficult and less intuitive is for the engineer the understanding of the basic dynamic phenomena being studied. Besides that, as these models usually contain lots of details in their construction, it is more difficult for the engineer to correctly guess which of the tuning variables affects more the metric of interest. Finally, the computational running time of such models is not as efficient as an analytical solution and, while this might not be a big problem for the normal development cycle in the industry with the current computing capabilities available, it might become a bottleneck for numerical optimisation procedures that demand a very high number of iterations to get to an optimum design. In a similar way, the application of active control systems for innovative active suspensions demands simpler models for its implementation, as presented by Shirahatt et al. (2008), where genetic algorithm optimization techniques and LQR control systems are applied to a model with 8 degrees of freedom.

Paper received 4 March 2010. Paper accepted 8 August 2011.
Technical Editor: Domingos Rade

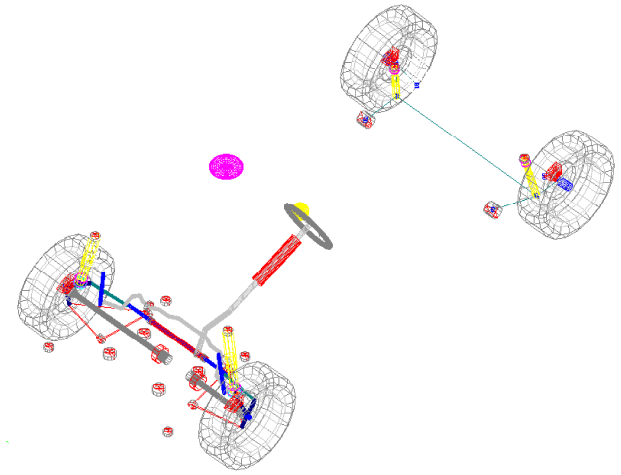

Figure 1. Graphical Representation of a Detailed Multibody Model (ADAMS®).

Following the idea that there is a need to understand better how these simple analytical formulations' results compare to real vehicle values and at which extent they can be applied for the vehicle development, the purpose of this paper is to present the analytical solutions available in the literature for roll gradient, understeer gradient and steering sensitivity metrics, comparing in the sequence the results from these simplified models against real vehicle measurements and more detailed multibody simulation models. In the cases where the initially calculated results do not present satisfactory correlation with measured values, enhancements for these analytical formulations are proposed, being the ultimate goal of this work to achieve/propose analytical solutions capable of reproducing real vehicle results with good enough accuracy that allow their usage for development purposes.

Roll Gradient Metric

The roll gradient is defined as the derivative of the vehicle body roll angle with respect to the lateral acceleration acting at its centre of gravity (CG), as indicated in Fig. 2. This value is usually evaluated in unities of degrees/g of lateral acceleration and can be physically measured through a constant radius circular manoeuvre with slow increase of the longitudinal velocity (and, therefore, the lateral acceleration), keeping as close as possible to a steady-state condition.

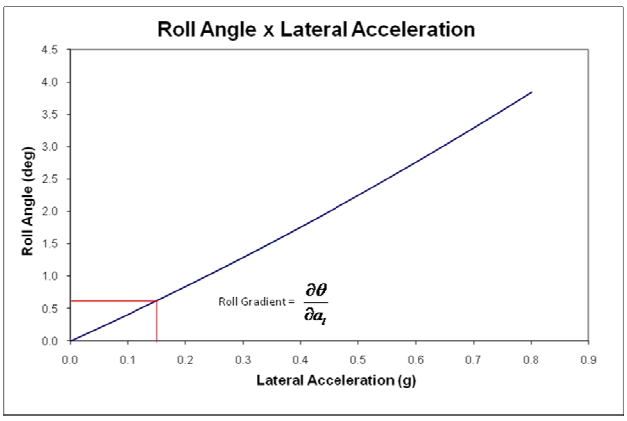

Figure 2. Definition of Roll Gradient.

Figure 3. Vehicle Rolling in a Curve.

This parameter quantifies in a very straightforward way how much a vehicle rolls during a curve manoeuvre, as illustrated in Fig. 3. In general, vehicles that roll less (i.e., present lower roll gradient values), are better evaluated in subjective terms by the drivers.

In order to analytically calculate the roll gradient, one has first to calculate the vehicle rolling stiffness K_T, in terms of torque per degree of body relative roll to the ground. The total rolling stiffness of the vehicle is calculated as the sum of the front and rear suspensions individual rolling stiffness and, in a first approach, this value can be calculated based only on the spring stiffness values, stabilizer bar stiffness values and tire radial stiffness values, as illustrated in Fig. 4.

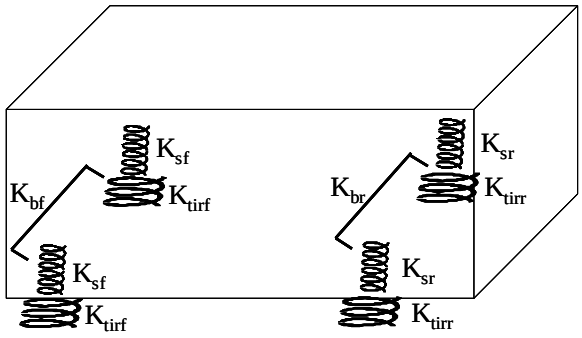

Figure 4. Main Elements for Roll Stiffness Calculation.

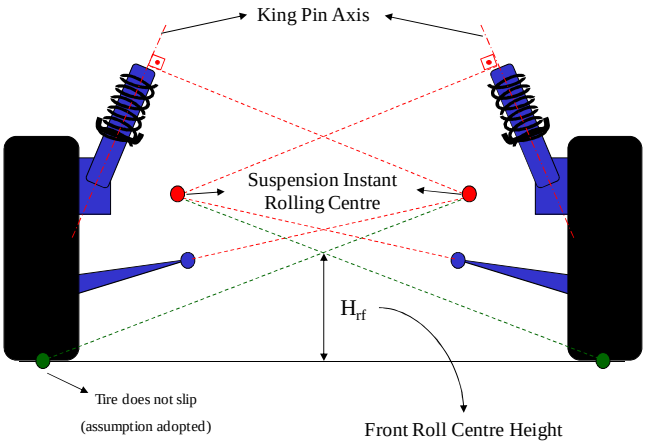

Figure 5. Front McPherson Suspension Roll Centre Height Calculation.

After this step, it is necessary to define the effective rolling arm H_r of the vehicle. Calculating the front and rear suspensions instant rolling centres, it is possible to join these points with the centre of the tire contact patch to the ground. Adopting the simplification that the tire contact patch to the ground does not move with respect to the local vehicle coordinates (i.e., there is no slip in the tires), the distance to the ground of the point in this line that crosses the centre plane of the vehicle is the front or rear suspension roll centre height. Figure 5 illustrates the calculation of the roll centre height for a McPherson front suspension type.

Following the same process for the front and rear suspensions, it is then possible to have a roll axis line in the vehicle's side view, and the distance between this line and the vehicle's CG is then defined as the effective rolling arm H_r, as illustrated in Fig. 6.

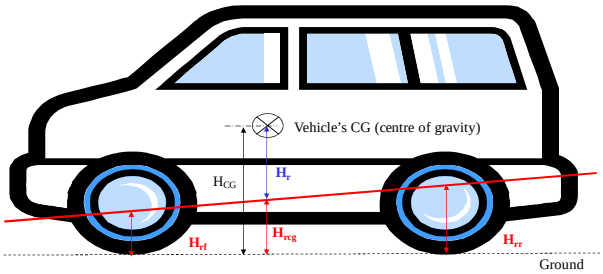

Figure 6. Vehicle's Roll Axis and Effective Rolling Arm.

With the effective rolling arm H_r defined, it is possible to calculate the roll moment T_{roll} applied to the vehicle due to the lateral acceleration imposed:

$$T_{roll} = M\, a_L H_r \tag{1}$$

The roll gradient K_{roll} is then calculated by the reaction between the roll moment T_{roll} and the vehicle's total roll stiffness K_T, as follows:

$$K_{roll} = \frac{T_{roll}}{\mathrm{K_T}} \tag{2}$$

Finally, using K_T in units of Nm/deg and normalizing the results for 1g of lateral acceleration in order to have the roll gradient results in the usual deg/g unit:

$$K_{roll} = \frac{\partial\theta}{\partial \mathrm{a_L}} = \frac{M\, g\, H_r}{K_T} \tag{3}$$

In order to understand the accuracy of the results from Eq. (3), these have been compared against physical measurements and a detailed multibody model (Fig. 1) for two different vehicles, here named vehicle 1 and vehicle 2. The physical measurements have been repeated in order to observe measurement variability and average results were considered for the comparison purposes. Data was acquired for the steering wheel angle, longitudinal velocity, lateral acceleration (accelerometers at vehicle's CG position) and roll angle with respect to the ground. The manoeuvre performed for the data acquisition was a slowly increasing longitudinal velocity over a constant radius in order to keep as close as possible to a steady-state condition. Figure 7 illustrates the test condition.

Figure 7. Vehicle Physical Test Condition.

The multibody model was simulated using the software ADAMS® and considering a fairly detailed description of the vehicle. The main characteristics of this detailed multibody model (depicted in Fig. 1) are:

- 256 degrees of freedom;
- Separate subsystem description for front suspension, rear suspension, steering system, front stabilizer bar, tires, body, powertrain and brakes;
- All masses, rotational inertia and joints between parts detailed;
- Non-linear representation of springs, shock absorbers and jounce bumpers;
- All suspension and steering compliant bushings represented by their non-linear stiffness characterization in all directions;
- Tires modelled with Magic Formula 5.2;
- Rear axle modelled as flexible body (finite element representation) and other bodies considered rigid.

The results are summarized in Table 1, demonstrating that the analytical model for the roll gradient metric herein presented provides good results compared to the physical measurements, and also in a similar level of accuracy compared to the detailed multibody model.

Table 1. Roll Gradient Results Comparison.

	K_{roll} (deg/g)	
	Vehicle 1	Vehicle 2
Experimental Measurements	4.93	6.62
Analytical Model Results	4.56	6.67
Detailed Multibody Model Results	4.59	5.99

Understeer Gradient Metric

The understeer gradient is defined as the derivative of the front tires average steer angle with respect to the lateral acceleration imposed to the vehicle at its centre of gravity, as indicated in Fig. 8. This value is usually evaluated in unities of degrees/g of lateral acceleration and, similarly to the roll gradient, can be physically measured through a constant radius circular manoeuvre with slow

increase of the longitudinal velocity (and, therefore, the lateral acceleration), keeping as close as possible to a steady-state condition.

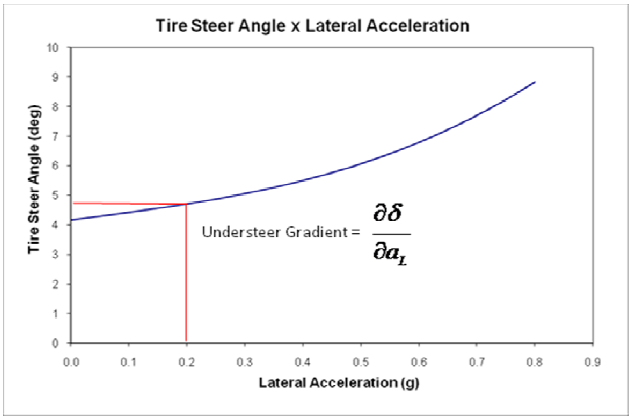

Figure 8. Understeer Gradient Definition.

This parameter evaluates the tendency of the vehicle, when in a steady-state curve manoeuvre, to be understeer (vehicle demands higher steering angles to keep the same curve radius at higher speeds) or oversteer (vehicle demands lower steering angles to keep the same curve radius at higher speeds). The vehicle is said to be neutral when the steering angle to keep a curve trajectory is dependant only on the curve radius and not on the vehicle speed. This definition is illustrated in Fig. 9.

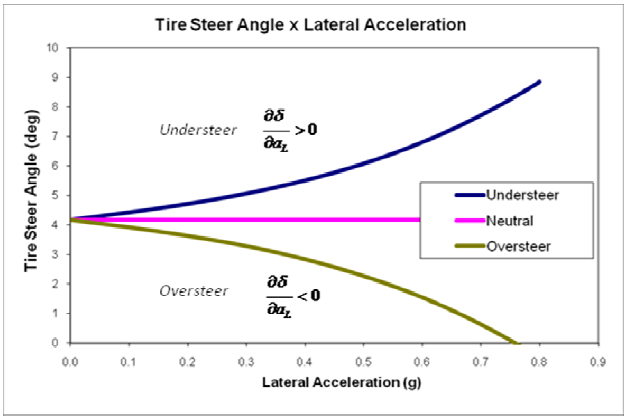

Figure 9. Understeer and Oversteer Definition.

A widely adopted simplified model to represent the vehicle for lateral dynamics is the bicycle model, where both right hand and left hand tires are grouped in a single entity and the vehicle is assumed to have its mass distributed along its centre line. This model is represented in Fig. 10 for a steady-state curve manoeuvre.

The centrifugal forces per axle can be calculated as follows:

$$F_{yf} = \frac{c}{L} M a_L \tag{4}$$

$$F_{yr} = \frac{b}{L} M a_L \tag{5}$$

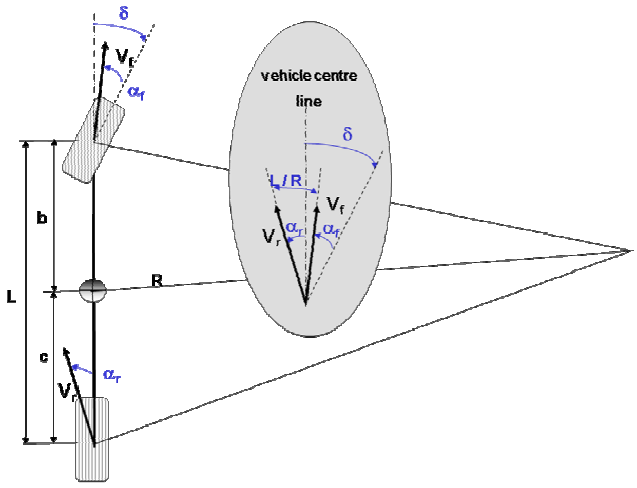

Figure 10. Bicycle Model for Steady-State Curve Manoeuvre.

Considering that the only external forces applied to the model are generated by the tire, and the tire forces can be calculated by a linear relationship between the slip angle and its cornering stiffness C_α, the following relationships are achieved (remembering there are 2 tires per axle in the bicycle model adopted):

$$F_{ext,yf} = 2C_{\alpha f}\alpha_f \tag{6}$$

$$F_{ext,yr} = 2C_{\alpha r}\alpha_r \tag{7}$$

Grouping Eqs. (4) to (7):

$$\alpha_f = \frac{F_{yf}}{2C_{\alpha f}} = \frac{M c a_L}{2LC_{\alpha f}} \tag{8}$$

$$\alpha_r = \frac{F_{yr}}{2C_{\alpha r}} = \frac{M b a_L}{2LC_{\alpha r}} \tag{9}$$

Finally, using the relationships shown in Fig. 9, the understeer gradient K can be calculated, as follows:

$$\delta = \frac{L}{R} + \left(\frac{c}{C_{\alpha f}} - \frac{b}{C_{\alpha r}}\right)\frac{M}{2L}a_L \tag{10}$$

$$K = \frac{\partial \delta}{\partial a_L} = \left(\frac{c}{C_{\alpha f}} - \frac{b}{C_{\alpha r}}\right)\frac{M}{2L} \tag{11}$$

Similarly to the roll gradient results, the understeer gradient values obtained with the Eq. (9) have been compared against physical measurements and a detailed multibody model. The results are summarized in Table 2.

Table 2. Understeer Gradient Results Comparison.

	K (deg/g)	
	Vehicle 1	Vehicle 2
Experimental Measurements	3.85	4.03
Analytical Model Results	0.53	1.16
Detailed Multibody Model Results	3.54	3.63

As it can be seen in the results from Table 2, this initial analytical model for the understeer gradient does not provide accurate results when compared to the physical measurements and the detailed multibody models. This difference can be explained by the factors that are not considered in this initial analytical formulation that considers only mass and tire properties. In order to improve the accuracy of the analytical model, the proposal of this work is to exchange of the terms $C_{\alpha f}$ and $C_{\alpha r}$ by equivalent terms $C'_{\alpha f}$ and $C'_{\alpha r}$ in the formulation previously described, which will take into consideration the following effects:

Additional effect 1 (e1): tire self-align torque effect

The tire self-align torque comes from the fact that the resultant lateral force generated by the tire is not coincident with the tire geometric centre, but rather located in a different point in the longitudinal axis of the tire. This distance is known as pneumatic trail t, and effectively changes the distances b and c between the lateral force application points and the CG of the vehicle as follows:

$$b' = b + t_f \tag{12}$$

$$c' = c + t_r \tag{13}$$

Additional effect 2 (e2): lateral load transfer

The lateral load transfer is a dynamic effect of the vehicle body under lateral acceleration, where there is a vertical (normal) load shift from the inner wheels to the outer wheels of the vehicle that is linearly proportional to the lateral acceleration that the vehicle is subject to and also the roll center height of the front/rear suspensions – more details about roll center height definition are shown by Milliken (1995) in the chapter 17.

The effect in the equations herein developed is that the front and rear individual tire cornering stiffness values $C_{\alpha f}$ and $C_{\alpha r}$ are dependent on the tire normal load. In this case, when the equations developed consider that the total cornering stiffness per axle is equal to 2 times the individual tire cornering stiffness at static normal load, the correct consideration to take into account in the lateral load transfer effect is to sum the inner and outer tire cornering stiffness individually. This can be done by adopting the average of the inner and outer tire values for the $C_{\alpha f}$ and $C_{\alpha r}$, as follows:

$$C_{\alpha f,llt} = \frac{C_{\alpha f,inner} + C_{\alpha f,outer}}{2} \tag{14}$$

$$C_{\alpha r,llt} = \frac{C_{\alpha r,inner} + C_{\alpha r,outer}}{2} \tag{15}$$

In general, for low lateral acceleration values (that is the range of interest of this study), this effect is not as much important as the ones previously described in the appendix section.

Additional effect 3 (e3): vehicle's suspension and steering system compliances

The forces and moments generated by the tires cause deformations in the suspension and steering systems of the vehicle, as illustrated in Fig. 11.

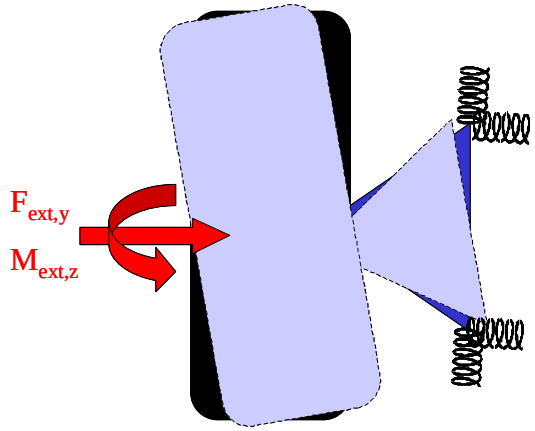

Figure 11. Effect of Vehicle's Suspension and Steering System Compliances.

Assuming that there is a linear relationship between the tire lateral force and align torque with the angle generated in the front/rear wheels due to the suspension and steering system compliance, the front/rear slip angles can be redefined as:

$$\alpha'_f = \alpha_f - F_{ext,yf} K_{fyf} - M_{ext,zf} K_{mzf} \tag{16}$$

$$\alpha'_r = \alpha_r - F_{ext,yr} K_{fyr} - M_{ext,zr} K_{mzr} \tag{17}$$

Same as the lateral force, the front/rear tire align torque is also assumed to be linear with respect to the tire slip angle as follows:

$$M_{ext,zf} = 2 C_{mz\alpha f} \alpha_f \tag{18}$$

$$M_{ext,zr} = 2 C_{mz\alpha r} \alpha_r \tag{19}$$

It is possible to define then new auxiliary terms B_f and B_r:

$$B_f = 1 + 2C_{\alpha f} K_{fyf} + 2C_{mz\alpha f} K_{mzf} \tag{20}$$

$$B_r = 1 + 2C_{\alpha r} K_{fyr} + 2C_{mz\alpha r} K_{mzr} \tag{21}$$

And the slip angles adjusted by the suspension and steering system compliances can be then defined as:

$$B_f \alpha'_f = \alpha_f \tag{22}$$

$$B_r \alpha'_r = \alpha_r \tag{23}$$

Additional effect 4 (e4): kinematic steering variation with vertical suspension travel

The wheels also steer due to the vertical travel of the suspension, being this variation a function of the vehicle's specific suspension/steering geometry. This effect is shown in more detail by Milliken (1995) in the chapter 19 and is also known in the literature as roll steer.

Considering that the vehicle is on a plane road, the vertical travel of the suspension is only a function of the vehicle roll angle θ, and the later can be considered linearly related to the lateral acceleration through the roll stiffness of the vehicle in the range of interest for this work (less than 0.4 g's of lateral acceleration). In this sense, following the same rationale previously described for the suspension and steering compliances, the kinematic steering variation with vertical suspension travel can be described through auxiliary terms $B_{f,rs}$ and $B_{r,rs}$, where the index **rs** refers to the roll steer effect. It is also interesting to mention that, in most cases, the front steered suspension is more sensitive to this effect than the rear suspension.

Summation of additional effects

The consideration of the effects previously described for the tire self-align torque, vehicle's suspension and steering system compliances, kinematic steering variation with vertical suspension travel and lateral load transfer can be implemented in the analytical solution through the substitution of the terms $C_{\alpha f}$ and $C_{\alpha r}$ by the equivalent terms $C'_{\alpha f}$ and $C'_{\alpha r}$ in the formulation previously described, as follows:

$$C'_{\alpha f} = \frac{C_{\alpha f,llt}\, c}{B_f\, B_{f,rs}\, c'} \tag{24}$$

$$C'_{\alpha r} = \frac{C_{\alpha r,llt}\, b}{B_r\, B_{r,rs}\, b'} \tag{25}$$

The results of adding each of the previously described effects (e1, e2, e3 and e4) are summarized in Table 3. A graphical representation intended to help the visualization of the individual contributions is shown in Figs. 12 and 13.

Table 3. Understeer Gradient Results Comparison – Additional Effects.

		K (deg/g)	
		Vehicle 1	Vehicle 2
	Experimental Measurements	3.85	4.03
Base Model	Initial Analytical Model Results	0.53	1.16
e1	e0 + Tire Self-Align Torque	0.66	1.37
e2	e1 + Lateral Load Transfer	0.76	1.49
e3	e2 + Vehicle's Suspension and Steering System Compliances	2.71	3.73
e4	e3 + Kinematic Steering Variation with Vertical Suspension Travel	3.92	4.04
Multibody	Detailed Multibody Model Results	3.54	3.63

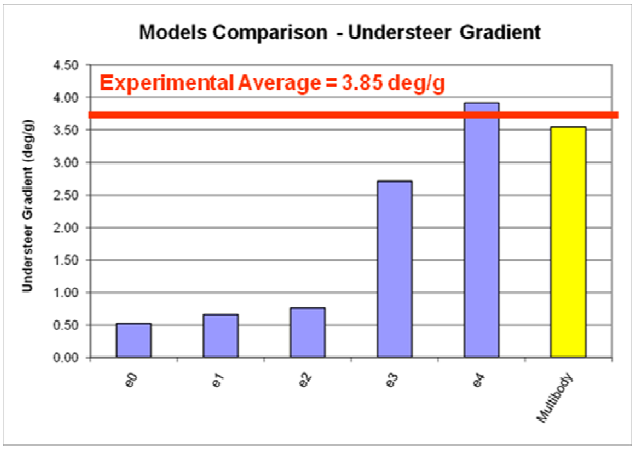

Figure 12. Vehicle 1 Understeer Gradient Results Comparison – Additional Effects.

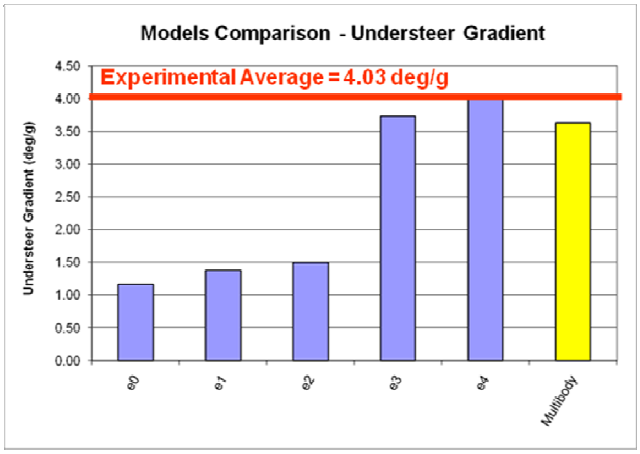

Figure 13. Vehicle 2 Understeer Gradient Results Comparison – Additional Effects.

Steering Sensitivity Metric

The steering sensitivity is defined as the derivative of the lateral acceleration with respect to the steering wheel angle imposed to the vehicle at its centre of gravity, as indicated in Fig. 14. This value is usually evaluated in unities of g/100 degrees of steering wheel angle (SWA) – the multiplication of the unit by a 100 times factor is intended to get numerical values in the range of 1.0, making them easier to work with. Analogous to the previous metric, the steering sensitivity can be physically measured through a constant radius circular manoeuvre with slow increase of the longitudinal velocity (and, therefore, the lateral acceleration), keeping as close as possible to a steady-state condition.

This parameter evaluates the responsiveness of the vehicle with respect to the driver inputs at the steering wheel, where low values can bring a subjective feeling of a slow response or lack of response from the vehicle and, at the same time, values too high are associated with the subjective feeling of a very fast response more difficult to control, as small disturbances in the steering wheel already produce a reasonable amount of lateral acceleration, changing its trajectory. The steering sensitivity is closely related to the understeer gradient, being inversely proportional to that one and to the overall steering ratio of the vehicle. Some of the reasons that make it important to consider this metric independently of the

understeer gradient are that many projects are limited to use the same steering system for a wide range of vehicles, making the compromise between understeer gradient and steering sensitivity more difficult to be achieved. Besides that, as the steering sensitivity is inversely proportional to the overall steering ratio of the vehicle, there is also a compromise between this metric and the steering effort of the vehicle, what is especially critical for non-assisted (manual) steering systems.

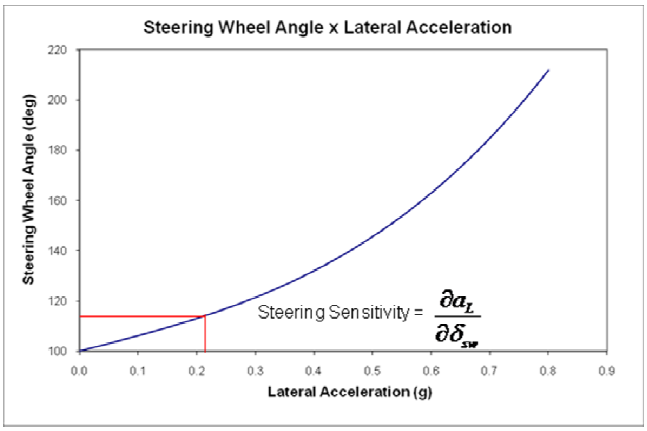

Figure 14. Steering Sensitivity Definition.

The steering sensitivity K_s is defined by the Eq. (27), where K is the understeer gradient as previously defined and r_{dir} is the on-center overall steering ratio, i.e. the ratio between steering wheel angle and average front wheels steer angle, which can be described by the derivative of the relationship between both values, as indicated in Eq. (26).

$$r_{dir} = \frac{\partial \delta_{vol}}{\partial \delta} \tag{26}$$

$$K_s = \frac{\partial a_L}{\partial \delta_{vol}} = \frac{\partial a_L}{\partial \delta}\frac{\partial \delta}{\partial \delta_{vol}} = \frac{1}{\mathrm{K}}\frac{1}{r_{dir}} \tag{27}$$

Table 4. Steering Sensitivity Results Comparison.

		Steering Sensitivity (g/100° SWA)	
		Vehicle 1	Vehicle 2
	Experimental Measurements	1.55	1.59
Base Model	Initial Analytical Model Results	11.17	5.49
e1	e0 + Tire Self-Align Torque	8.95	4.63
e2	e1 + Lateral Load Transfer	7.75	4.26
e3	e2 + Vehicle's Suspension and Steering System Compliances	2.17	1.71
e4	e3 + Kinematic Steering Variation with Vertical Suspension Travel	1.50	1.58
Multibody	Detailed Multibody Model Results	1.66	1.76

In a similar way to what has been done in the case of the understeer gradient, the steering sensitivity analytical model has been improved by the inclusion of additional effects, and the experimental results and comparison between the analytical models for each improvement step are shown in Table 4. A graphical representation intended to help the visualization of the individual contributions is shown in Figs. 15 and 16.

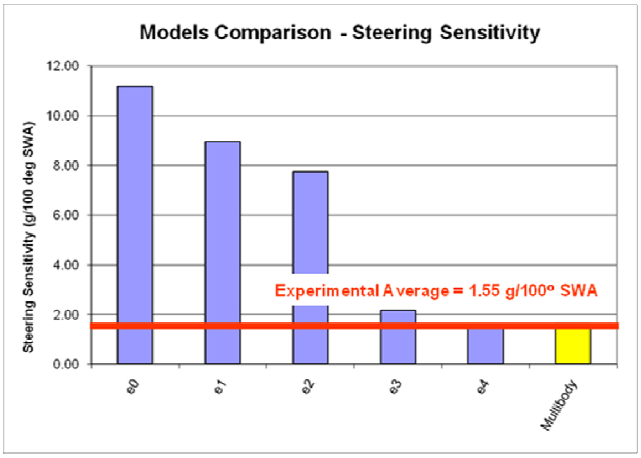

Figure 15. Vehicle 1 Steering Sensitivity Results Comparison.

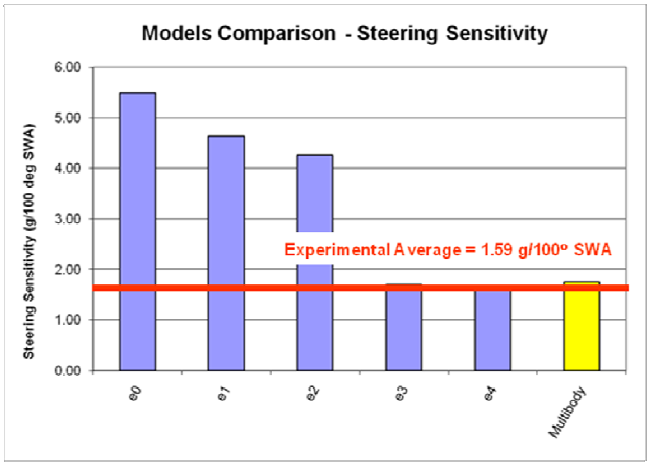

Figure 16. Vehicle 2 Steering Sensitivity Results Comparison.

Conclusions

This paper has described the analytical model for the roll gradient, understeer gradient and steering sensitivity metrics. The results of each of these analytical solutions have been compared against physical measurements and more detailed multibody models.

The comparison has shown that the analytical solutions presented in the commonly known literature (Milliken, 1995; Wong, 2001 and Pacejka, 2002) are accurate enough to represent the roll gradient, but the initial results for the understeer gradient and steering sensitivity are not enough accurate. The paper has then described the inclusion of additional effects in these analytical formulations that affect the phenomena related to these metrics: namely steer compliance and steer angle variation due to suspension vertical travelling. The comparative results against the

physical measurements indicate that these additional effects are indeed very important to adequately represent these metrics, and the accuracy improvements obtained for each additional effect have been presented. This make possible for the engineer or analyst to have a quantitative idea of the importance of each of these additional effects.

The results of the final analytical models achieved are considered to have enough accuracy to allow their usage for development purposes. The fact that these analytical models are much more efficient in terms of computational time compared to the more detailed multibody models makes them excellent options to be used with numerical optimization routines. These advantages are especially interesting in the early development phases of a new project. Additionally, the analytical models can give much more insight of the underlying phenomena to the engineer compared to the more detailed models, letting it very clear how the tuning variables affect each of these metrics.

Finally, future developments of this work might include additional metrics and their validation against physical measurements following the same process, making it possible the extension of the analytical modelling usage for vehicle dynamics characterization.

References

Adamski, D., Schuster, C., Hiller, M., 1999, "Advances in Modelling of Mechatronic Systems: The Toolset FASIM_C++ for the Simulation of Vehicle Dynamics", *Journal of the Brazilian Society of Mechanical Sciences and Engineering*, Vol. 21, No. 4.

Milliken, W.F., Milliken, D.L., 1995, "Race Car Vehicle Dynamics", SAE, Warrendale, USA.

Pacejka, H.B., 2002, "Tire and Vehicle Dynamics", SAE, Warrendale, USA.

Prado, M., Cunha, R.H., Costa Neto, A., Costa, A., Mancosu, F., Savi C., Délboux, J.E., 2001, "Bus Handling Analysis and Experimental Validation Using the Multibody System Technique", In: SAE Brazil 2001 Congress and Exhibit, 2001, São Paulo, SP, SAE Paper 2001-01-3966.

Rill, G., 2006, "Vehicle Modeling by Subsystems", *Journal of the Brazilian Society of Mechanical Sciences and Engineering*, Vol. 28, No. 4.

Shirahatt, A., Prasad, P.S.S., Panzade, P., Kulkarni, M.M., 2008, "Optimal Design of Passenger Car Suspension for Ride and Road Holding". *Journal of the Brazilian Society of Mechanical Sciences and Engineering*, Vol. 30, No. 1.

Vilela, D., 2001, "Vehicle Dynamics Simulation Correlation with Field Maneuvers", In: SAE Brazil 2001 Congress and Exhibit, 2001, São Paulo, SP, SAE Paper 2001-01-3799.

Wong, J.Y., 2001, "Theory of Ground Vehicles", John Wiley & Sons Inc., New York, USA.

8.15 ANEXO O

ANALYTICAL SOLUTION PROPOSAL TO VEHICLE DYNAMIC HANDLING PROPERTIES

Vilela, D.; Barbosa, R. S.; (2011B) Analytical solution proposal to vehicle dynamic handling properties. International Journal of Vehicle Systems Modelling and Testing - IJVSMT, DOI: 10.1504/IJVSMT.2011.039831, Vol. 6, nº 1, pp. 56-71.

Analytical solution proposal to vehicle dynamic handling properties

Daniel Vilela*

Vehicle Synthesis, Analysis and Simulation Department,
General Motors do Brasil Ltda., São Caetano do Sul,
GMB VSAS – Av. Goiás, 2769 – CT #1 – Bairro Barcelona,
São Caetano do Sul – SP, CEP: 09550-051, Brazil
E-mail: danvil_br@hotmail.com
*Corresponding author

Roberto Spinola Barbosa

Departamento de Engenharia Mecânica,
Escola Politécnica da Universidade de São Paulo,
Av. Prof. Mello Moraes 2231 – Butantã,
São Paulo – SP, CEP: 05508-900, Brazil
E-mail: roberto.barbosa@poli.usp.br

Abstract: One very important aspect of the vehicle handling behaviour is how it reacts to dynamic inputs from the driver. While much has been done in the analytical realm to describe the vehicle steady state handling properties, the transient and dynamic behaviour of the vehicle have been studied mostly through multibody software packages, as the analytical solution is usually more difficult to be achieved. Taking into consideration that the analytical approach provides the engineer a deeper understanding of the underlying physical phenomena being studied, bringing more simplicity to the overall solution at the same time, this paper proposes an analytical solution for the vehicle lateral acceleration response to periodic excitation at the steering wheel. In the sequence, a comparison of the results between this analytical model and a detailed multibody model is performed, showing that the proposed analytical model is capable of reproducing the more detailed multibody model with good accuracy.

Keywords: handling; analytical solution; frequency response; simulation; vehicle dynamics.

Reference to this paper should be made as follows: Vilela, D. and Barbosa, R.S. (2011) 'Analytical solution proposal to vehicle dynamic handling properties', *Int. J. Vehicle Systems Modelling and Testing*, Vol. 6, No. 1, pp.56–71.

Biographical notes: Daniel Vilela is a Senior Mechanical Engineer at General Motors Brazil in the Simulation and Analysis Department. He received his PhD in Mechanical Engineering at São Paulo University, São Paulo, Brazil. His research interests include modelling and simulation of ground vehicles for vehicle dynamics and loads analysis, as well as the design and analysis of ground vehicles.

Roberto Spinola Barbosa is a PhD Professor at the Mechanical Engineering Department of Polytechnic School of the São Paulo University in Brazil. His research interests include multibody systems modelling and simulation with ground vehicles application, developing virtual reality environment on dynamic systems with high performance computation for simulation and training.

1 Introduction

Traditional literature for vehicle dynamics, like Milliken and Milliken (1995), Wong (2001) and Pacejka (2002), covers in detail the analytical description of the vehicle handling for steady state measures, defining very important metrics like understeer gradient, steering sensitivity and roll gradient among others. The analytical solutions to these metrics are very important tools to the development engineer that is able to have a very good understanding of the underlying phenomena and how the tuning variables affect each of these metrics. Besides that, the analytical solutions are extremely efficient in terms of computation time, allowing their usage for quick studies and very early assessments, as well as their linkage to numerical optimisation processes that take the advantage of their computational efficiency.

If for one side there is no question that these steady state parameters are very good indicators of vehicle handling performance and of fundamental importance for vehicle development in this regard, on the other hand, they are not complete, in the sense that they do not capture dynamic variations with the frequency of the inputs by the driver and the transients before achieving the steady state condition.

To be able to simulate these dynamic effects, the engineer usually considers the usage of multibody software packages, as it has been done using ADAMS® in previous works by Vilela (2001) and Prado et al. (2001). By doing so, the engineer can get very accurate results for these dynamics conditions through detailed models of the vehicle and a common multibody model easily contains more than 100 degrees of freedom (see example in Figure 1). The main drawback of this approach is that the more the multibody model gets details in the vehicle construction representation, the more difficult and less intuitive is for the engineer the understanding of the basic dynamic phenomena being studied. Besides that, as these models usually contain lots of details in their construction, it is more difficult for the engineer to correctly guess which of the tuning variables affects more the metric of interest. Finally, the computational running time of such models is not as efficient as an analytical solution and, while this might not be a big problem for the normal development cycle in the industry with the current computing capabilities available, it might become a bottleneck for numerical optimisation procedures that demand a very high number of iterations to get to an optimum design.

For the dynamic handling performance, a very important class of metrics is related to how the steady state responses of the vehicle vary as a function of the frequency of steering wheel input by the driver. Kunkel and Leffert (1988) demonstrate how this class of parameters is objectively evaluated through the so-called ‘frequency response test’ where, among other metrics, the variation of the steering sensitivity (lateral acceleration response of the vehicle) with the steering wheel input frequency is evaluated. This same characteristic is evaluated through a detailed multibody model by Prado et al. (2001) for a passenger bus.

Figure 1 Graphical representation of a detailed multibody model (ADAMS®) (see online version for colours)

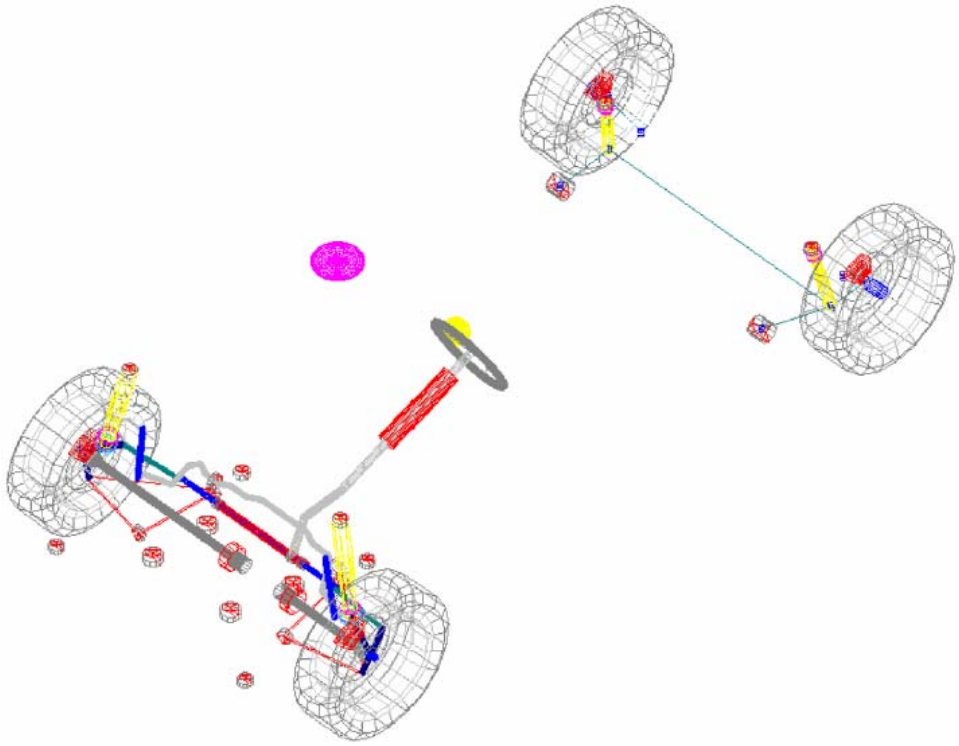

Understanding that this is an important dynamic characteristic of the vehicle that is not satisfactorily studied through the analytical approach in the literature, the purpose of this paper is to propose an analytical model for the vehicle lateral acceleration response to periodic excitation at the steering wheel by the driver, comparing the results with a much more detailed multibody model, so as to help in quantifying the accuracy of the results of the proposed analytical model.

The analytical solution herein proposed is analogous to a simple angular mass-spring-damper system, allowing to the engineer the adoption of other analogies from this simple mass-spring-damper system resolution that can be very helpful during the vehicle development phase. In this sense, this analogy allows the engineer to study the response of the vehicle for inputs other than sinusoidal, like step steer inputs or impulse inputs.

2 Lateral acceleration response metrics for periodic excitation

When evaluating the lateral acceleration response of the vehicle varying the excitation frequency of the steering wheel (harmonic response to a sinusoidal excitation type), it can be noticed that this lateral acceleration response to the steering wheel input starts with a decreasing behaviour in regard to the excitation input frequency, eventually achieving a minimum response value for a specific frequency, which will be used here as a metric

and named as *null gain frequency*, as the gain value at this frequency is very close to zero (it is indeed null for the analytical model proposed, as will be demonstrated further). Besides this metric, this work will consider the *lateral acceleration bandwidth*, which is defined as the frequency value at which there is a reduction in the lateral acceleration response that is noticed by most users. Here, the definition of 3 dB gain reduction proposed by Kunkle and Leffert (1988) will be adopted. Figure 2 shows these definitions at the lateral acceleration response graphic.

Figure 2 Definition of lateral acceleration bandwidth and null gain frequency (see online version for colours)

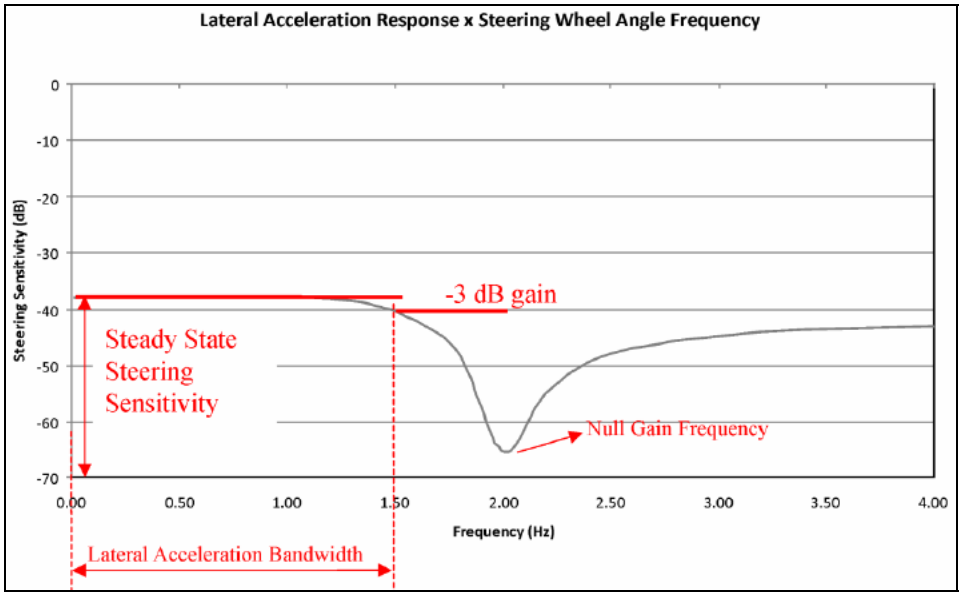

3 Analytical formulation of the lateral acceleration response to periodic excitation

The objective of this chapter is to present the deduction of the analytical equations for the lateral acceleration response to periodic excitation. Some simplifications are introduced to allow the usage of analytical expressions – the simplifications are explained, and their overall validation verified by the comparison with the results of a detailed multibody model. Figure 3 and Figure 4 show the sketch of the vehicle on a curved path in the XY (top view) and YZ (front view) planes respectively:

The application of Newton's second law to the lateral direction implies in the following:

$$Ma_y = \sum F_y + MR\Omega^2 + 2M\dot{\theta}\dot{z} - 2M\Omega\dot{x} \tag{1}$$

In order to simplify the analytical expression obtained from (1), the following points were considered:

- the vehicle longitudinal velocity $\dot{x}$ is a constant value V_x
- $\dot{z}$ is only a function of the roll angle θ (consideration of flat road without irregularities)
- for the range of interest of the expression obtained (low lateral acceleration limits – from steady state until –0.4 g), θ has a small absolute value, so that $\sin(\theta) \approx \theta$ and $\cos(\theta) \approx \theta$
- the higher order terms in β, θ e Ω are neglected, what is a reasonable assumption as these higher order terms tend to have a much smaller influence compared to the main terms (this simplification will be checked along with the others in the comparison with the detailed multibody model results).

The equation (1) can be then re-written as:

$$\sum F_y = Ma_L \tag{2}$$

$$\text{with } a_L = \frac{V_x^2}{R} \tag{3}$$

Differently from the steady state condition, the derivative of the sideslip angle β is not null. Considering the relative angular velocity $\dot{\beta}$ and the drag angular velocity Ω, for a circular movement with instantaneous radius R, as presented in Figure 5, the kinematic of a rigid body provides the following absolute velocity:

$$V_x = R\left(\dot{\beta} + \Omega\right) \text{ or } \frac{1}{R} = \frac{\left(\dot{\beta} + \Omega\right)}{V_x} \tag{4}$$

The lateral acceleration a_L can then be re-written:

$$a_L = \frac{V_x^2}{R} = V_x^2 \frac{\left(\dot{\beta} + \Omega\right)}{V_x} = V_x\left(\dot{\beta} + \Omega\right) \tag{5}$$

Figure 5 shows the vehicle bicycle model with the consideration of the derivative of the sideslip angle β as shown in equation (4).

Figure 3 Vehicle on a curved path – top view (see online version for colours)

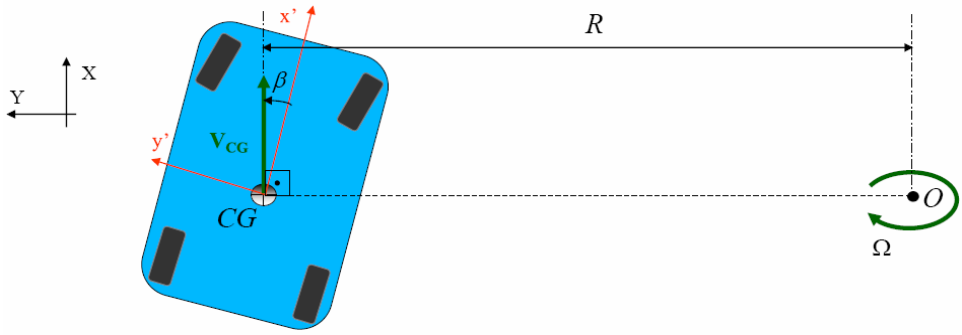

Figure 4 Vehicle on a curved path – front view (see online version for colours)

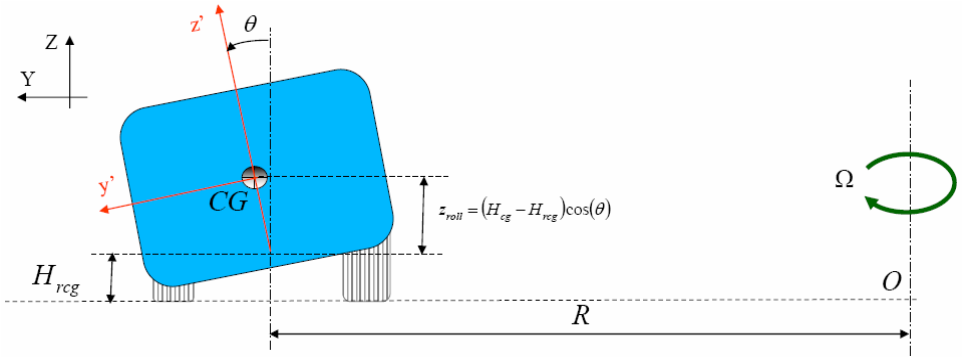

Figure 5 Vehicle bicycle model (see online version for colours)

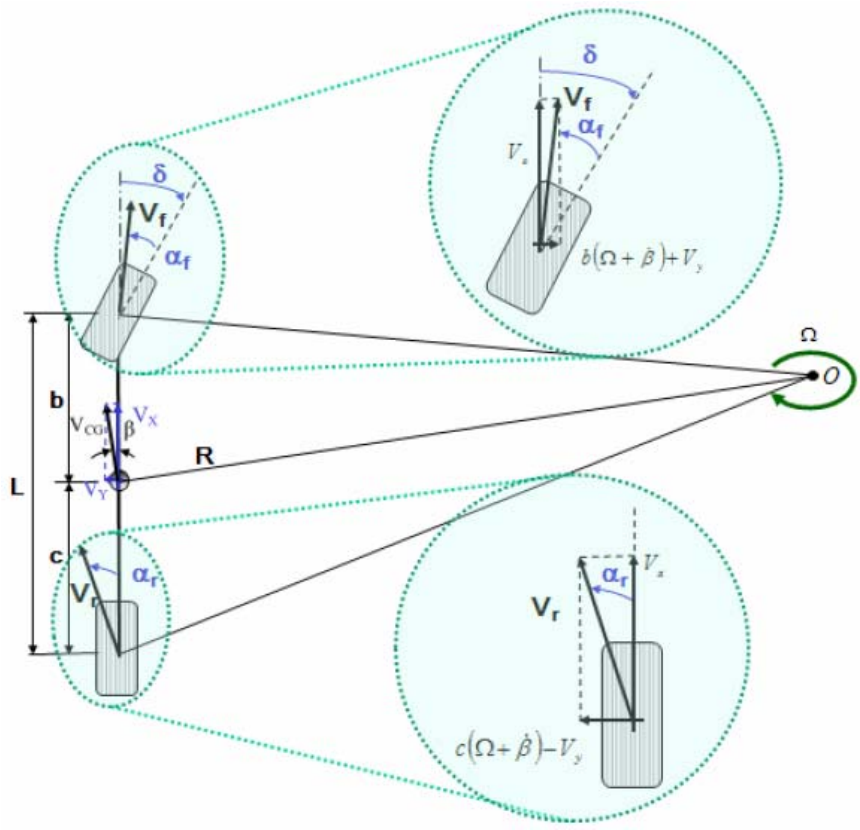

Figure 5 can be applied to determine the front and rear tyre slip angles for a general situation (non-steady state), as long as the curve radius R is considered to be varying with time (not constant). Applying the results from (4) and (5), the slip angles are then calculated:

$$\alpha_f = \delta - \frac{\left\lfloor b\left(\dot{\beta}+\Omega\right)+V_y \right\rfloor}{V_x} \rightarrow \alpha_f = -\beta + \delta - \frac{b\left(\dot{\beta}+\Omega\right)}{V_x} \rightarrow \alpha_f = -\beta + \delta - \frac{b}{V_x^2} a_L \quad (6)$$

$$\alpha_r = \frac{\left\lfloor c\left(\dot{\beta}+\Omega\right)+V_y \right\rfloor}{V_x} \rightarrow \alpha_r = -\beta + \frac{c\left(\dot{\beta}+\Omega\right)}{V_x} \rightarrow \alpha_r = -\beta + \frac{c}{V_x^2} a_L \quad (7)$$

For low lateral acceleration levels (range of interest for the final analytical expression), it is reasonable to assume that the tyres are working within their linear range, so that the external lateral force produced by them is proportional to the tyre cornering stiffness C_α, as follows (2 tyres per axle):

$$F_{ext,yf} = 2C_{\alpha f}\alpha_f = 2C_{\alpha f}\left(-\beta + \delta - \frac{b}{V_x^2} a_L\right) \quad (8)$$

$$F_{ext,yr} = 2C_{\alpha r}\alpha_r = 2C_{\alpha r}\left(-\beta + \frac{c}{V_x^2} a_L\right) \quad (9)$$

$$Ma_L = 2C_{\alpha f}\left(-\beta + \delta - \frac{b}{V_x^2} a_L\right) + 2C_{\alpha r}\left(-\beta + \frac{c}{V_x^2} a_L\right) \quad (10)$$

It is possible then to define auxiliary terms A_1 and A_2, isolating the sideslip angle β in the sequence:

$$A_1 = M + \frac{2}{V_x^2}\left(C_{\alpha f} b - C_{\alpha r} c\right) \quad (11)$$

$$A_2 = 2\left(C_{\alpha f} + C_{\alpha r}\right) \quad (12)$$

$$A_1 a_L + A_2 \beta = 2C_{\alpha f}\delta \rightarrow \beta = \frac{2C_{\alpha f}\delta - A_1 a_L}{A_2} \quad (13)$$

The equation (5) can have the angular velocity Ω isolated and its derivative with respect to time calculated in the sequence:

$$\Omega = \frac{a_L}{V_x} - \beta \rightarrow \dot{\Omega} = \frac{\dot{a}_L}{\dot{V}_x} - \dot{\beta} \quad (14)$$

The application of the angular momentum theorem in conjunction with the equation (14) leads to the following:

$$\sum M_{CG,z}^{ext} = J_z \dot{\Omega} \rightarrow J_z\left(\frac{\dot{a}_L}{V_x} - \ddot{\beta}\right) = bF_{yf} - cF_{yr} \quad (15)$$

Applying the results from (8) and (9) in (15):

$$J_z\left(\frac{\dot{a}_L}{V_x}-\ddot{\beta}\right)=2\left(cC_{\alpha r}-bC_{\alpha f}\right)\beta-\frac{2}{V_x^2}\left(b^2C_{\alpha f}-c^2C_{\alpha r}\right)a_L+2bC_{\alpha f}\delta \tag{16}$$

Once more, it is possible to define auxiliary terms A_3 and A_4 to help with the solution:

$$A_3=\frac{2}{V_x^2}\left(b^2C_{\alpha f}+c^2C_{\alpha r}\right) \tag{17}$$

$$A_4=2\left(bC_{\alpha f}+cC_{\alpha r}\right) \tag{18}$$

$$\frac{J_z}{V_x}\dot{a}_L+A_3a_L-J_z\ddot{\beta}+A_4\beta=2bC_{\alpha f}\delta \tag{19}$$

The equation (13) can also have its derivatives with respect to time calculated:

$$\beta=\frac{2C_{\alpha f}\delta-A_1a_L}{A_2}\rightarrow\dot{\beta}=\frac{2C_{\alpha f}\dot{\delta}-A_1\dot{a}_L}{A_2}\rightarrow\ddot{\beta}\frac{2C_{\alpha f}\ddot{\delta}-A_1\ddot{a}_L}{A_2} \tag{20}$$

Applying the results above in (19), it is then possible to obtain the following:

$$\begin{aligned}&\frac{J_z}{V_x}\dot{a}_L+A_3a_L-J_z\left(\frac{2C_{\alpha f}\ddot{\delta}-A_1\ddot{a}_L}{A_2}\right)+A_4\left(\frac{2C_{\alpha f}\delta-A_1a_L}{A_2}\right)=2bC_{\alpha f}\delta\\&\rightarrow\frac{A_1}{A_2}J_z\ddot{a}_L+\frac{J_z}{V_x}\dot{a}_L+\left(A_3-\frac{A_1A_4}{A_2}\right)a_L=2C_{\alpha f}\left(b-\frac{A_4}{A_2}\right)\delta+\frac{2C_{\alpha f}J_z}{A_2}\ddot{\delta}\end{aligned} \tag{21}$$

Taking into consideration that the steering wheel excitation studied is periodic in this case, it is possible to take its derivative with respect to time:

$$\ddot{\delta}=-\omega^2\delta \tag{22}$$

Finally, with the help of additional auxiliary variables A_5 to A_8, the following results are obtained:

$$A_5=\frac{A_1}{A_2}J_z \tag{23}$$

$$A_6=\frac{1}{V_x}J_z \tag{24}$$

$$A_7=A_3-\frac{A_1A_4}{A_2} \tag{25}$$

$$A_8=2C_{\alpha f}\left(b-\frac{\left(A_4+J_z\omega^2\right)}{A_2}\right) \tag{26}$$

$$A_5\ddot{a}_L+A_6\dot{a}_L+A_1a_L=A_2\delta \tag{27}$$

It is possible to notice that the equation (27) obtained for the lateral acceleration response of the vehicle to periodic steering wheel excitation is completely analogous to a simple mass-spring-damper linear system, with the difference that the term A_5 has units of kg ms^2, A_6 has units of kg ms, A_7 has units of kg m and A_8 has units of Nm. Keeping these differences in mind, it is possible to obtain the analogue terms for natural frequency ω_n, damping coefficient ζ and frequency ratio r:

$$\omega_n = \sqrt{\frac{A_7}{A_5}} \tag{28}$$

$$\zeta = \frac{A_6}{2\sqrt{A_7 A_5}} \tag{29}$$

$$r = \frac{\omega}{\omega_n} \tag{30}$$

The definition of the frequency response of a dynamic system states that $G(\omega) = \dfrac{output(\omega)}{input(\omega)}$. In this sense, using the steer angle as input and the lateral acceleration at the CG of the vehicle as the output for the system being considered and the known solution for the mass-spring-damper system, it is possible to obtain:

$$\begin{aligned} G_s(\omega) &= \left|\frac{A_8}{A_7}\right| \frac{1}{\sqrt{\left(1-r^2\right)^2 + (2\zeta r)^2}} \\ &= \left| \frac{2C_{\alpha f}\left(b - \dfrac{\left(A_4 \_ J_z\omega^2\right)}{A_2} \right)}{A_7} \right| \frac{1}{\sqrt{\left(1-\left(\dfrac{\omega}{\omega_n}\right)^2\right)^2 + \left(2\zeta\dfrac{\omega}{\omega_n}\right)^2}} \end{aligned} \tag{31}$$

The result of the equation (31) has units of $\dfrac{\text{m/s}^2}{\text{rad}}$ and corresponds to the behaviour of the lateral acceleration response to periodic excitation as shown in Figure 2.

From the equations obtained, the null gain frequency happens when the term $A_8 = 0$, as follows:

$$b - \frac{\left(A_4 + J_z\omega_{null}^2\right)}{A_2} = 0 \rightarrow \omega_{null} = \sqrt{\frac{bA_2 - A_4}{J_z}} \tag{32}$$

From the lateral acceleration bandwidth definition:

$$-3dB = 20\log_{10}\left(\frac{G_s}{G_s|_{\omega=0}}\right) \tag{33}$$

After some algebraic manipulations and the definition of additional auxiliary variables A_9 to A_{11}, the frequency of the lateral acceleration bandwidth is then defined as:

$$A_9 = \left[\frac{10^{0,3} J_z^2}{\left(A_2 b - A_4\right)^2} - \frac{1}{\omega_n^4} \right] \tag{34}$$

$$A_{10} = \left[\frac{\left(2 - 4\zeta^2\right)}{\omega_n^2} - \frac{2.10^{0,3} J_z}{\left(A_2 b - A_4\right)} \right] \tag{35}$$

$$A_{11} = 10^{0,3} - 1 \tag{36}$$

$$\omega_{band}^2 = \frac{-A_{10} - \sqrt{A_{10}^2 - 4 A_9 A_{11}}}{2 A_9} \tag{37}$$

4 Analytical model results comparison

In order to quantify the accuracy of the proposed analytical model and the validity of the adopted simplifications, its results are compared against a detailed multibody model with 256 degrees of freedom like the model depicted in Figure 1 and the analytical solution proposed by Pacejka (2002) in the equation (1.78) from that work. This comparison has been performed for a passenger vehicle and the results are shown in Figure 6.

Figure 6 Lateral acceleration response × frequency comparison – dB scale (see online version for colours)

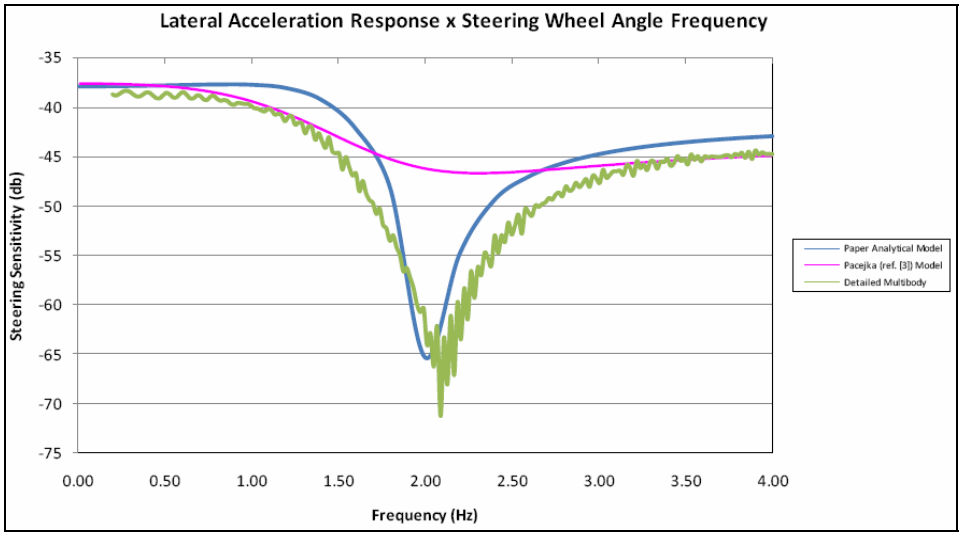

Note: Proposed analytical model results in blue and detailed multibody model results in purple.

The results of the proposed analytical model are similar to the results obtained by Prado et al. (2001). All models analysed capture well the lateral acceleration bandwidth, which is the range where there is no significant variation from the steady state lateral acceleration response value. Ideally, this range would be as wide as possible, i.e., the vehicle has a response similar to the steady state response in a wide range of steering wheel frequency input. The results of the vehicle studied represent a regular passenger vehicle response, with the bandwidth between 1.0 Hz and 1.5 Hz.

However, compared to the analytical model proposed by Pacejka (2002), it is understood that the inclusion of the derivative of the sideslip angle β as shown in equation (4) in the proposed model leads to a better accuracy in capturing the null gain frequency effect. This null gain frequency effect may affect important aspects of the vehicle handling, as it represents a frequency value where the steering wheel input does not produce any lateral acceleration at all. The value around 2.0 Hz is also typical for passenger vehicles and the analytical model proposed here could capture this effect in a satisfactory way.

Finally, the Table 1 shows the comparison of the null gain frequency and lateral acceleration bandwidth metrics between the proposed analytical model and the detailed multibody model.

Table 1 Lateral acceleration frequency response metrics results comparison

	Analytical model	*Detailed multibody*	*Absolute difference*	*% difference*
Lateral acceleration bandwidth (Hz)	1.53	1.35	0.18	13.5%
Null gain frequency (Hz)	2.04	2.09	–0.05	–2.4%

It is important to mention that the results herein shown already take into consideration the following effects:

$$e1 = f(\text{tyre self-align torque}) \tag{38}$$

$$e2 = f(\text{vehicle's suspension and streering system compliances}) \tag{39}$$

$$e3 = f(\text{kinematic streering variation with vertical suspension travel}) \tag{40}$$

$$e4 = f(\text{lateral load transfer}) \tag{41}$$

All these effects already affect the steady state lateral acceleration response results (known as steering sensitivity in the literature) and their implementation in the analytical formulation proposed here can be done very straightforwardly through the substitution of the terms $C_{\alpha f}$ and $C_{\alpha r}$ by the equivalent terms $C'_{\alpha f}$ and $C'_{\alpha r}$ in the formulation previously described, which will include these effects in the final results, as follows:

$$C'_{\alpha f} = f\left(C_{\alpha f}, e1, e2, e3, e4\right) \tag{42}$$

$$C'_{\alpha r} = f\left(C_{\alpha r}, e1, e2, e3, e4\right) \tag{43}$$

These effects are described in more detail in the Appendix 1.

5 Conclusions

This paper has proposed a new analytical solution to the lateral acceleration response of a vehicle submitted to a periodic input at the steering wheel. The proposed method presents better accuracy than previously available analytical solutions (Pacejka, 2002) for the same problem.

The metrics related to the lateral acceleration response to periodic excitation have been presented and the results obtained through the proposed analytical model have been compared to a much more detailed multibody model. Small difference has been observed, showing that the proposed analytical model is capable of reproducing with good accuracy the more detailed multibody model. This allows its utilisation for development purposes, especially during early development phases for conceptual designs. It can be also used in numerical optimisation procedures, where the gains in computational running time are very interesting.

A future development proposal is the extension of the model herein proposed for inputs other than periodic steering variation, like step steering inputs and impulse steering inputs. For linear systems these responses can be simply derived through transformations of the frequency response functions. The analogy with a mass-spring-damper system used in the proposed approach might be of great interest for the design engineer, as this kind of simple mechanical system has easy dynamic understanding and classic analytical solution. Following the same steps, outputs other than lateral acceleration, like roll angle or yaw velocity, could also be calculated analytically for dynamic manoeuvres.

Finally, an experimental investigation to compare the results of a physical vehicle against the analytical model and the detailed multibody model is recommended in order to have a more complete understanding of correlation level for each modelling technique.

References

Kunkel, D.T. and Leffert, R.L. (1988) 'Objective directional response testing', in *22nd FISITA Congress, 1988*, Dearborn (MI), USA, SAE Paper 885008.

Milliken, W.F. and Milliken, D.L. (1995) *Race Car Vehicle Dynamics*, SAE, Warrendale, USA.

Pacejka, H.B. (2002) *Tire and Vehicle Dynamics*, SAE, Warrendale, USA.

Prado, M., Cunha, R.H., Costa Neto, A., Costa, A., Mancosu, F., Savi, C. and Délboux, J.E. (2001) 'Bus handling analysis and experimental validation using the multibody system technique', in *SAE Brazil 2001 Congress and Exhibit, 2001*, São Paulo, SP, SAE Paper 2001-01-3966.

Vilela, D. (2001) 'Vehicle dynamics simulation correlation with field maneuvers', *SAE Brazil 2001 Congress and Exhibit*, SAE Paper 2001-01-3799, São Paulo, SP.

Wong, J.Y. (2001) *Theory of Ground Vehicles*, John Wiley & Sons Inc., New York, USA.

Appendix 1

Definitions, acronyms and abbreviations

X, Y, Z	absolute coordinate system (inertial)
x', y', z'	vehicle coordinate system (non-inertial)
CG	vehicle centre of gravity
O	centre of curve
R	curve radius
V_x	vehicle longitudinal velocity
V_y	vehicle lateral velocity
V_{CG}	vehicle CG total velocity
β	vehicle sideslip angle
Ω	turning angular velocity
H_{cg}	centre of gravity height to the ground
H_{rcg}	roll centre at CG position
θ	vehicle roll angle
z_{roll}	roll moment arm
δ	front wheel steer angle
α_f / α_r	front/rear tyre slip angle
V_f / V_r	front/rear tyre velocity vector
L	wheelbase
b/c	distance between CG and front/rear axle

Appendix 2

Additional considerations for the lateral acceleration results

e1 Tyre self-align torque effect

The tyre self-align torque comes from the fact that the resultant lateral force generated by the tyre is not coincident with the tyre geometric centre, but rather located in a different point in the longitudinal axis of the tyre. This distance is known as pneumatic trail t, and effectively changes the distances b and c between the lateral force application points and the CG of the vehicle as follows:

$$b' = b + t_f \tag{A1}$$

$$c' = c + t_r \tag{A2}$$

e2 Vehicle's suspension and steering system compliances

The forces and moments generated by the tyres cause deformations in the suspension and steering systems of the vehicle, as illustrated in Figure A1.

Figure A1 Effect of vehicle's suspension and steering system compliances (see online version for colours)

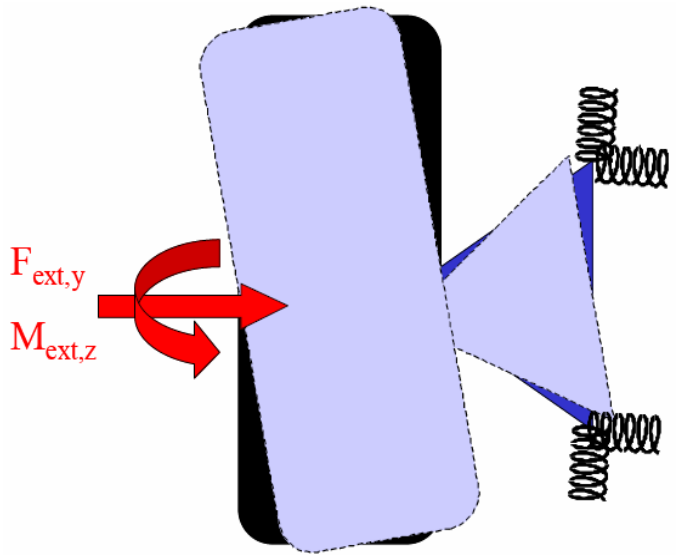

Assuming that there is a linear relationship between the tyre lateral force and align torque with the angle generated in the front/rear wheels due to the suspension and steering system compliance, the front/rear slip angles can be redefined as:

$$\alpha'_f = \alpha_f - F_{ext,yf} K_{fyf} - M_{ext,zf} K_{mzf} \tag{A3}$$

$$\alpha'_r = \alpha_r - F_{ext,yr} K_{fyr} - M_{ext,zr} K_{mzr} \tag{A4}$$

where the following definitions apply:

K_{fyf}, K_{fyr} front and rear wheel steer angle stiffness with respect to tyre lateral force

K_{mzf}, K_{mzr} front and rear wheel steer angle stiffness with respect to tyre align torque

$M_{ext,zf}$, $M_{ext,zr}$ front and rear tyre align torque.

Same as the lateral force, the front/rear tyre align torque is also assumed to be linear with respect to the tyre slip angle as follows:

$$M_{ext,zf} = 2C_{mz\alpha f}\alpha_f \tag{A5}$$

$$M_{ext,zr} = 2C_{mz\alpha r}\alpha_r \tag{A6}$$

It is possible to define then new auxiliary terms B_f and B_r:

$$B_f = 1 + 2C_{\alpha f} K_{fyf} + 2C_{mz\alpha f} K_{mzf} \tag{A7}$$

$$B_r = 1 + 2C_{\alpha r} K_{fyr} + 2C_{mz\alpha r} K_{mzr} \tag{A8}$$

And the slip angles adjusted by the suspension and steering system compliances can be then defined as:

$$B_f \alpha'_f = \alpha_f \tag{A9}$$

$$B_r \alpha'_r = \alpha_r \tag{A10}$$

e3 Kinematic steering variation with vertical suspension travel

The wheels also steer due to the vertical travel of the suspension, being this variation a function of the vehicle's specific suspension/steering geometry. This effect is shown in more detail by Milliken and Milliken (1995) in the chapter 19 and is also known in the literature as roll steer.

Considering that the vehicle is on a plane road, the vertical travel of the suspension is only a function of the vehicle roll angle θ, and the later can be considered linearly related to the lateral acceleration through the roll stiffness of the vehicle in the range of interest for this work (less than 0.4 g's of lateral acceleration). In this sense, following the same rationale previously described for the suspension and steering compliances, the kinematic steering variation with vertical suspension travel can be described through auxiliary terms $B_{f,rs}$ and $B_{r,rs}$, where the index **rs** refers to the roll steer effect. It is also interesting to mention that, in most cases, the front steered suspension is more sensitive to this effect than the rear suspension.

e4 Lateral load transfer

The lateral load transfer is a dynamic effect of the vehicle body under lateral acceleration, where there is a vertical (normal) load shift from the inner wheels to the outer wheels of the vehicle that is linearly proportional to the lateral acceleration that the vehicle is subject to and also the roll centre height of the front/rear suspensions (more details about roll centre height definition are shown by Milliken and Milliken (1995) in the chapter 17).

The effect in the equations herein developed is that the front and rear individual tyre cornering stiffness values $C_{\alpha f}$ and $C_{\alpha r}$ are dependent on the tyre normal load. In this case, where the equations developed consider that the total cornering stiffness per axle is equal to two times the individual tyre cornering stiffness at static normal load, the correct consideration to take into account the lateral load transfer effect is to sum the inner and outer tyre cornering stiffness individually. This can be done by adopting the average of the inner and outer tyre values for the $C_{\alpha f}$ and $C_{\alpha r}$, as follows:

$$C_{\alpha f,llt} = \frac{C_{\alpha f,inner} + C_{\alpha f,outer}}{2} \tag{A11}$$

$$C_{\alpha r,llt} = \frac{C_{\alpha r,inner} + C_{\alpha r,outer}}{2} \tag{A12}$$

In general, for low lateral acceleration values (that is the range of interest of this study), this effect is not as much important as the ones previously described in the Appendix section.

Summation of additional effects

The consideration of the effects previously described in the Appendix 1 for the tyre self-align torque, vehicle's suspension and steering system compliances, kinematic steering variation with vertical suspension travel and lateral load transfer can be implemented in the analytical solution proposed in the paper through the substitution of the terms $C_{\alpha f}$ and $C_{\alpha r}$ by the equivalent terms $C'_{\alpha f}$ and $C'_{\alpha r}$ in the formulation previously described, as follows:

$$C'_{\alpha f} = \frac{C_{\alpha f,llt} c}{B_f B_{f,rs} c'} \tag{A13}$$

$$C'_{\alpha r} = \frac{C_{\alpha r,llt} b}{B_r B_{r,rs} b'} \tag{A14}$$

8.16 ANEXO P

A STABILITY STUDY OF A THREE-POINT AND A FOUR-POINT SECONDARY SUSPENSION CONFIGURATION FOR A RAIL PASSENGER CAR

Prado, M.; Costa Neto, A.; Barbosa, R. S.; Grando, D. (2011) A stability study of a three-point and a four-point secondary suspension configuration for a rail passenger car. International Journal of Vehicle System Dynamics, XIV IAVSD Symposium. DOI: 10.13140/2.1.2595.7126, Vol. 1, pp. 6.

A STABILITY STUDY OF A THREE-POINT AND A FOUR-POINT SECONDARY SUSPENSION CONFIGURATION FOR A RAIL PASSENGER CAR

Marcelo Prado, Januário Vieira, Denilson Grando, Fabio Kanizawa
Multicorpos Engenharia
São Carlos - SP, Brazil

Álvaro Costa Neto
Department of Materials, Aeronautic and Automotive, University of São Paulo
São Carlos - SP, Brazil

Roberto Spinola Barbosa
Department of Mechanical Engineer, University of São Paulo
São Paulo - SP, Brazil

marcelo@multicorpos.com

Abstract

A dynamic analysis of a rail passenger car study was performed in order to evaluate the differences between a secondary air suspension bogie with three-point and a four-point control system. Dynamical analyses with different conditions of turning radius and velocities were performed and the L/V coefficients were calculated. The results have shown that there was not a best configuration for all conditions of velocities. The magnitudes of the L/V coefficients in the three-point configuration depend on the direction of the movement of the rail car. The four-point configuration showed an intermediate performance in all velocities. The best performance could be achieved with the development of a switch system that changes the configuration of the three-point system according to the direction of movement and velocity of the rail passenger car.

1. INTRODUCTION

A comparison study was performed in order to evaluate the dynamic behavior of a secondary suspension of a rail car using the three-point and a four-point leveling control system. In the industry there is not a consensus about which type of configuration is the best for safety

This project was sponsored by a Sao Paulo transportation company in Brazil (CPTM) which is responsible for the maintenance of the rail passenger cars in the city of Sao Paulo. Because safety issues CPTM asked for a study to determine if the three-point configuration is better than four-point configuration. Most of the rail passenger cars running in the city have a four-point leveling control system.

In the four-point configuration the vehicle is supported by two pneumatic bellows at each truck to form a four-point suspension in which each of the bellows is individually controlled by its own control leveling valve (two point at each truck). In the case of three-point configuration one of the trucks the two bellows are connected pneumatically to each other and are controlled by only one leveling valve (one truck with two points and the other with a single point).

The four-point configuration can create imbalance between vertical loads and this is more prominent at slow velocities. This disadvantage apparently does not appear in a three-point suspension system since the connection between the two bellows absorb the sway motion of the vehicle body. But the results have shown that the 3-point suspension system had different performance according to the direction of the movement and velocity.

2. METHODS

In order to study the behavior of the rail car using a three-point and a four-point suspension leveling control valves a complete multibody model of the rail car was developed using a multibody software MSC.Adams/Rail (Figure 1). A central role in this project is the thermodynamic model of the suspension air springs (bellows) and a correct

pneumatic model of control leveling valves.

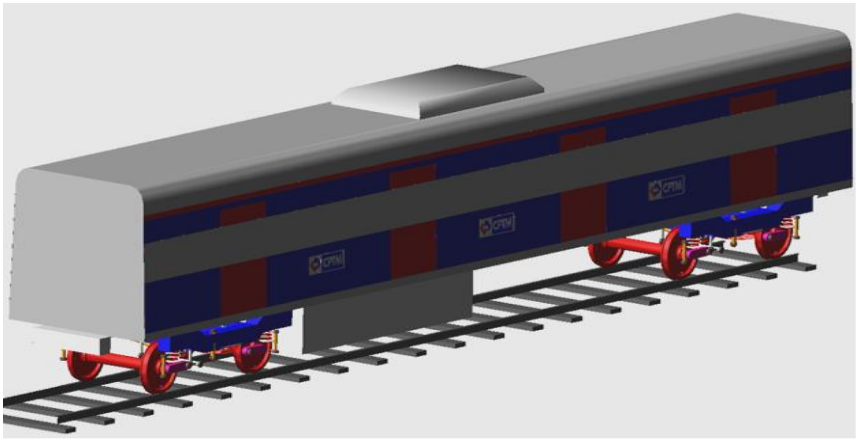

Figure 1: A complete multibody model of a rail passenger car in MSC.Adams/Rail 2005R2

The multibody model of the bogie developed for this project can be seen in Figure 2. As can be seen in the figure, the bogie has four primary helicoidal springs, with four vertical shock absorbers. The secondary suspension is composed of two air springs, vertical and yaw shock absorbers.

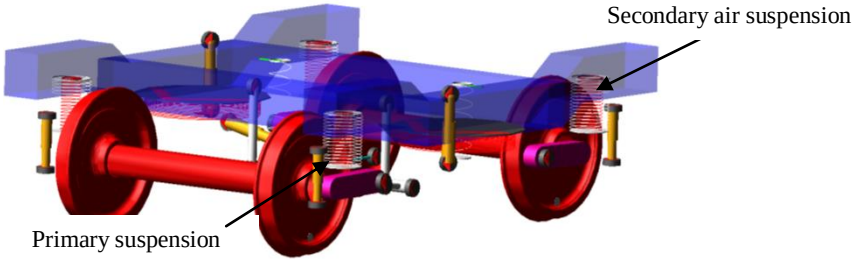

Figure 2: Bogie model in MSC.Adams/Rail 2005

The main characteristics of the rail can be seen in Table 1 below.

Track Width (m)	1.6
Track Type	TR-57
Wagon mass unladen (without passenger) (Kg)	25700
Wagon mass Laden (385 passengers) (Kg)	52650

Table 1: Rail Characteristics CPTM Série 2000

Two models of the rail passenger car were built: one model with four-point control leveling valves and one model with 3 point control leveling valves.

In the 4 point configuration, each air suspension has a unique control leveling valve. Also there is a compensator valve with cracking pressure of 1,47 bar (the valve opens when the difference of pressure between the air springs is higher than 1,47 bar).

In the 3-point configuration two air springs are controlled by one leveling valve and the two air springs are connected by means a tube and the pressures inside the elastic chamber are equal.

The analyses were performed in three different configuration (see Figure 3). The three point-configuration analyses were performed in both directions, in order to study the dynamic behavior and the influence of the pneumatic control in L/V coefficient for the front wheelset.

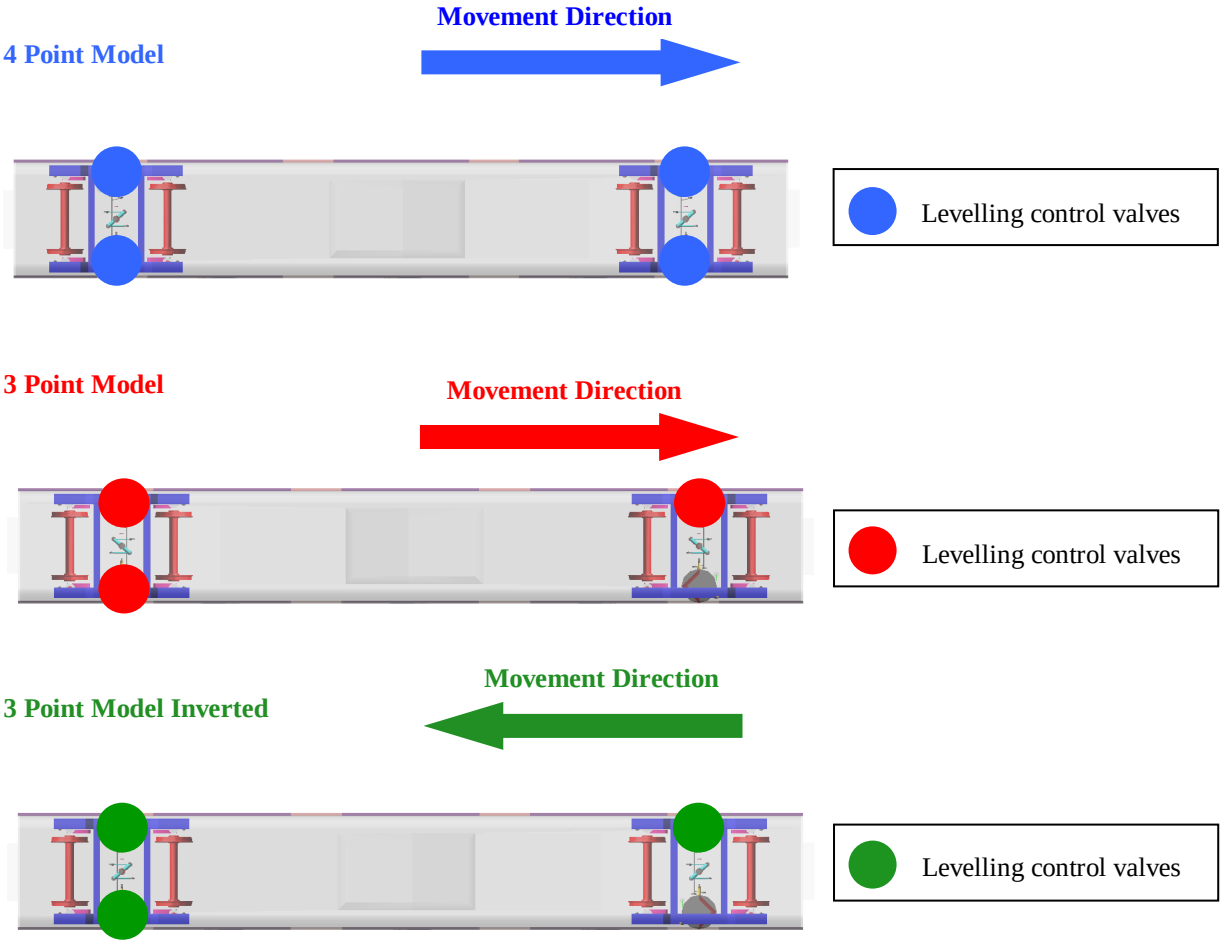

Figure 3: Scheme of control levelling valves of air suspension for 4 point and 3 point configurations

A thermodynamic model of air springs was developed in the MSC.Adams/Rail, using the Krettek air spring model, which is based on the energy and mass balance. The control leveling valve was modeled using the calibration curve of flow versus angle of the valve and the pneumatic circuit of the air suspension, taking into account the losses due to the geometry of the pipeline of the pneumatic circuit.

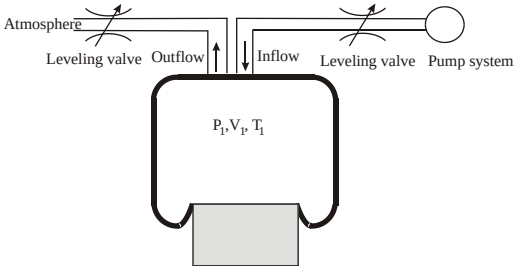

Figure 4. Scheme of an air spring system

The work process into the elastic chamber depends upon the speed of compression and expansion of the air. A rapid process (rapid spring deflection) is an adiabatic process, resulting in a high pressure and stiffness. On the other hand, slow deflection results in an isothermal process and low pressure and stiffness.

In practice, air spring operates in a process between adiabatic and isothermal. This process is called polytropic process and it is closer to an adiabatic process.

The thermodynamics equations that describe the behaviour of the elastic chamber is based on the energy and mass balance.

The ideal gas law gives:

$$P_1 V_1 = mRT_1 \tag{1}$$

Differentiating with respect to time:

$$\dot{P}_1 V_1 + P_1 \dot{V}_1 = \dot{m}RT_1 + mR\dot{T}_1 \tag{2}$$

Isolating the term $\dot{P}_1$, the rate of change of pressure in the above equation, we can write:

$$\dot{P}_1 = \frac{\dot{m}RT_1}{V_1} + \frac{P_1 \dot{T}_1}{T_1} - \frac{P_1 \dot{V}_1}{V_1} \tag{3}$$

Writing the equation of energy conservation we obtain:

$$\partial W = -\partial U + \partial Q \tag{4}$$

Where *W* is the total energy, *U* is the internal energy and *Q* is the heat exchange. Each term in equation (4) can be written as:

$$\partial W = P_1 \dot{V}_1 \tag{5}$$

$$\partial U = \dot{m}c_v T_1 + mc_v \dot{T}_1 \tag{6}$$

$$\partial Q = \dot{m}c_p T_2 + K_h A(T_{env} - T_1) \tag{7}$$

The term $K_h A(T_{env} - T_1)$ is the heat exchange with the environment. Substituting equations (5), (6) and (7) into equation (3) and isolating the term $\dot{T}_1$:

$$\dot{T}_1 = \frac{T_1(k-1)}{P_1 V_1}\left[-P_1 \dot{V}_1 - \dot{m}c_v T_1 + \dot{m}c_p T_2 - K_h A(T_1 - T_{env})\right] \tag{8}$$

The air spring force is the pressure times the effective area. This can be written as:

$$F_{air} = P_1 A_e \tag{9}$$

Supposing a laminar flow, it can be shown that the air mass flow through the pipe into chamber is:

$$\dot{m} = \rho(T_1, P_1) C_d A_p \sqrt{\frac{2}{\rho(T_1, P_1)}(P_{feed} - P_1)} \tag{10}$$

The air mass ouflow from the chamber is given by:

$$\dot{m} = \rho(T_1, P_1) C_d A_p \sqrt{\frac{2}{\rho(T_1, P_1)}(P_1 - P_{atm})} \tag{11}$$

At high temperatures and pressures the air density is not linear. The following equation gives the air density based on temperature and pressure:

$$\rho(T_1, P_1) = 1.2929\left(\frac{27313}{T_1}\right)\left(\frac{P_1 - 0.38783e}{760}\right) \tag{12}$$

3. DYNAMIC ANALYSES

Analyses were performed with two velocities, 20 Km/h and 70 Km/h and with different turning radius and super elevation of the track. Table 2 shows the maneuver conditions for the analysis.

In the Table 2 Maneuver 1 was the physical condition of the track, Maneuver 2 was the proposed modification of the track in order to decrease the L/V coefficient and increase the safety condition at low velocities. Maneuver 3 was performed in order to evaluate the 4-point and 3-point configuration at higher speed (70 Km/h).

	Maneuver 1	Maneuver 2	Maneuver 3
Superelevation (mm)	190.0	160.0	50.0
Transition (m)	50.0	80.0	50.0
Curve lenght (m)	100.0	210.0	400.0
Miminum curve radius (m)	217.0	217.0	400.0
Operation velocity (Km/h)	20.0	20.0	70.0

Table 2: Maneuver parameters for dynamic analysis

The L/V coefficients for the outside wheel at the leading truck for maneuvers shown in Table 2 can be seen in Figure 5. The lowest L/V coefficient was obtained in the 3-point configuration with the front truck with one control valve. But in the 3-point configuration when the two-point truck is the leading truck the L/V coefficient increases significantly (green line in the graphics).

For higher velocities (70Km/h) the L/V of the 3-point configuration with the leading truck with two valves was the best configuration, with the lowest L/V coefficient.

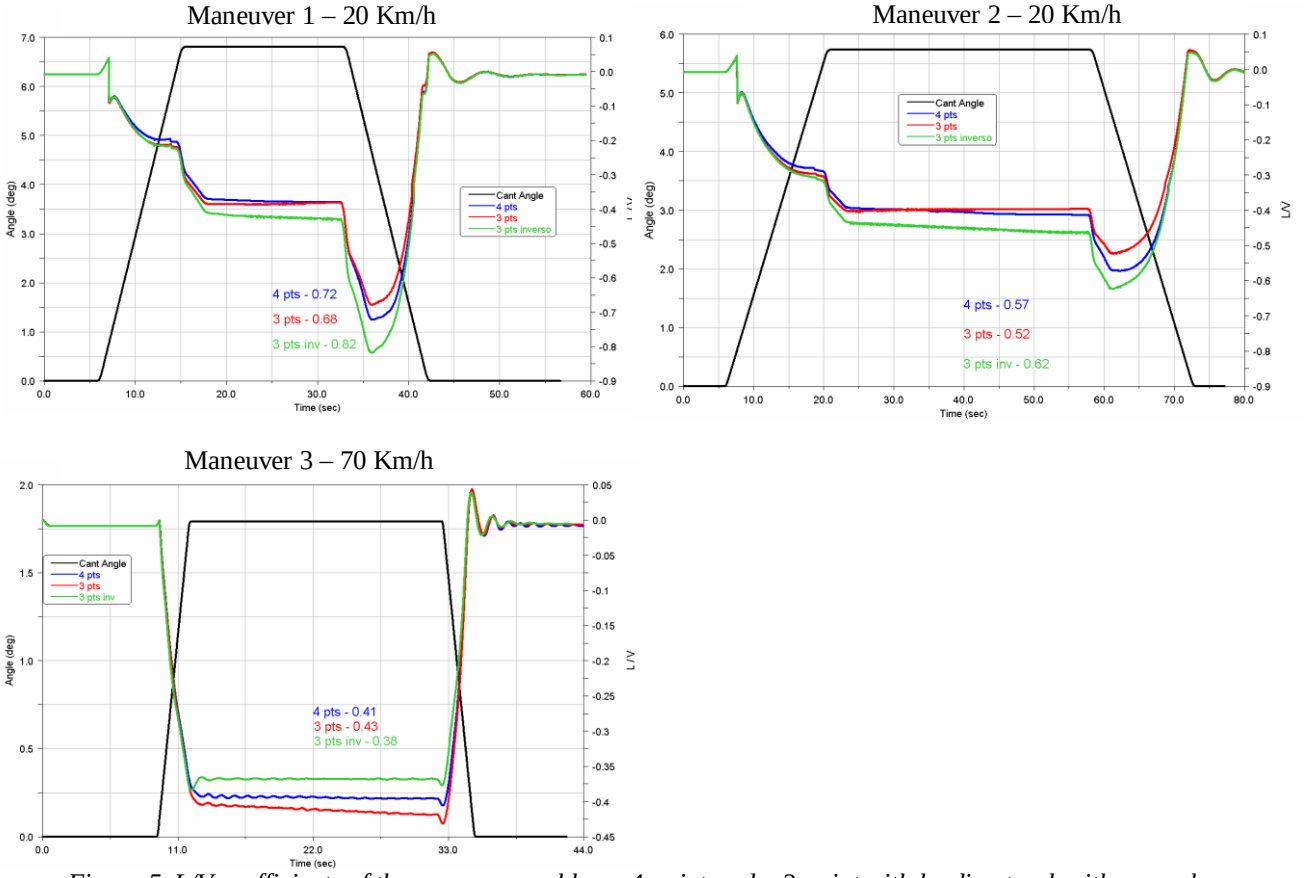

Figure 5. L/V coefficients of the maneuvers – blue – 4-point, red – 3-point with leading truck with one valve, green – 3-point with leading truck with two-valves.

Table 3 shows a summary of the highest value of the L/V coefficients obtained in each maneuver. As can be seen in Table 3 there is not a best configuration for all conditions of speed. The 4-point configuration has an intermediate performance in both low and high speeds.

	Maneuver 1 20 Km/h	Maneuver 2 20 Km/h	Maneuver 3 70 Km/h
4 point	**0.72**	**0.57**	**0.41**
3 point	**0.68**	**0.52**	**0.43**
3 point inverted	**0.82**	**0.62**	**0.38**

Table 3:Summary of L/V coefficients of the maneuvers

4. CONCLUSIONS

The results have shown that at low velocities the three-point configuration has a better performance than four-point configuration, but only in one direction, when the single point truck is the leading truck. In the three-point configuration when the truck with single point is in the rear (with two-point truck in the leading truck) the three-point has a poor performance at the low speed velocity .

In the case of high velocities the 3-point configuration with the leading truck with two valves showed the best performance. Analyzing the data the conclusion is that the 4-point configuration has the intermediate performance for all the velocity conditions.

As a suggestion for future work is the development of a switch system for the 3-point configuration, changing the leading truck control leveling system based on the direction of movement and velocity, changing the one and two valves configuration according to the direction of the movement and velocity of the rail passenger car. In this case we could reach the best performance for all velocities.

Acknowledgements

We want to acknowledge the CPTM (Companhia Paulista de Trens Metropolitanos – São Paulo Metropolitan Rail Company), which help this work supplying the technical data and giving the permission for publication.

References

[1] Garg, V. K. & Dukkipati, R. V., Dynamics of Railway Vehicle Systems. USA, Academic Press, 1984.

[2]Wickens, A.H., Fundamentals of Rail Vehicle Dynamics – Guidance and Stability. The Netherlands, Swets & Zeitlinger. ISBN 902651946. 2003.

[3] EN14363:2005 – Railway applications – Testing for the acceptance of running characteristics of railway vehicles – Testing of running behavior and stationary tests.

PÁGINA EM BRANCO